CONOR J. SHEIL

MODELLING ACCOMMODATION AND AGEING OF THE CRYSTALLINE LENS IN THE HUMAN EYE

MODELLING ACCOMMODATION AND AGEING OF THE CRYSTALLINE LENS IN THE HUMAN EYE

CONOR J. SHEIL

UNDER THE SUPERVISION OF

DR. ALEXANDER V. GONCHAROV

A Thesis Towards Understanding the Optics of the Human Eye

Submitted in Partial Fulfillment of the Requirements for the Degree of Doctor of Philosophy (Ph.D.)

Applied Optics Group
School of Physics
National University of Ireland, Galway

June 2016

" 'When I was a boy my grandfather died, and he was a sculptor. He was also a very kind man who had a lot of love to give the world, and he helped clean up the slum in our town; and he made toys for us and he did a million things in his lifetime; he was always busy with his hands. And when he died, I suddenly realized I wasn't crying for him at all, but for the things he did. I cried because he would never do them again, he would never carve another piece of wood or help us raise doves and pigeons in the back yard or play the violin the way he did, or tell us jokes the way he did. He was part of us and when he died, all the actions stopped dead and there was no one to do them just the way he did. He was individual. He was an important man. I've never gotten over his death. Often I think, what wonderful carvings never came to birth because he died. How many jokes are missing from the world, and how many homing pigeons untouched by his hands. He shaped the world. He did things to the world. The world was bankrupted of ten million fine actions the night he passed on.'

. . . 'Everyone must leave something behind when he dies, my grandfather said. A child or a book or a painting or a house or a wall built or a pair of shoes made. Or a garden planted. Something your hand touched some way so your soul has somewhere to go when you die, and when people look at that tree or that flower you planted, you're there. It doesn't matter what you do, he said, so long as you change something from the way it was before you touched it into something that's like you after you take your hands away. The difference between the man who just cuts lawns and a real gardener is in the touching, he said. The lawn-cutter might just as well not have been there at all; the gardener will be there a lifetime.' "

— Ray Bradbury, *Fahrenheit 451*.

Dedicated to the loving memory of "Granny" Rita Sheil.

ABSTRACT

This thesis is a study on the optical properties of the human eye; specifically, optical modelling of the human lens with accommodation and ageing. The idiosyncratic nature of the human eye provides a hindrance to modelling efforts in terms of model construction and verification. For this reason, generic data—while lacking useful individual information—prove very useful. Hence, a comprehensive review of the literature on age-related changes in spherical aberration was performed, with the goal of using spherical aberration as an important constraint for developing more realistic generic optical eye models.

An analytical method to describe the accommodative changes in the human crystalline lens has been proposed. The method is based on the geometry-invariant lens model, in which the Gradient Refractive INdex (GRIN) iso-indicial contours are coupled to the external shape. This coupling enables definition of the GRIN structure if the radii and asphericities of the external lens surfaces are known. As an example, the accommodative changes in lenticular radii and central thickness were taken from the literature, while the asphericities of the external surfaces were derived analytically by adhering to the basic physical conditions of constant lens volume and its axial position. The resulting changes in lens geometry are consistent with experimental data, and the optical properties are in line with expected values for optical power and spherical aberration. This provides an anatomically and optically accurate lens model that is valid for 3 mm pupils and can be used as a new tool for better understanding of accommodation.

Second, a new age-dependent model of the human lens is proposed, with two GRIN power distributions (axial and radial) which, together with a logarithmic model of the lens core, allow decoupling of three fundamental optical characteristics of the lens, namely axial optical path length, optical power and third-order spherical aberration, without changing the external shape of the lens. The spherical aberration calculated by exact raytracing is shown to be in line with experimental data. Conversely, the near-surface GRIN structure conforms to the external shape of the lens, which is necessary for accommodation modelling. The proposed model is compared to previous GRIN models from the literature, and it is concluded that the features of the new model will be useful for GRIN reconstruction in future experimental studies; in particular, studies of the accommodation-dependent properties of the ageing human eye. The extra flexibility of this model is highlighted in the concluding section, where the lens paradox is examined.

The requirement of a smooth equatorial join of the anterior and posterior lens surfaces imparts anatomical relevance to the models. While importantly allowing volume specification, this formulation has many more applications, purely because of its physical significance. This will form the basis for a joined optical and bio-mechanical model of the lens using finite element methods.

PUBLICATIONS

Some ideas and figures have appeared previously in the following publications, reproduced wholly or in part with kind permission from The Optical Society.

1. C. Sheil and A. V. Goncharov, "Characterisation and comparison of ophthalmic instrument quality using a model eye with reverse ray-tracing," in "SPIE Optical Metrology 2013," (International Society for Optics and Photonics, 2013), pp. 87890C-1–87890C-9.

2. C. J. Sheil, M. Bahrami, and A. V. Goncharov, "An analytical method for predicting the geometrical and optical properties of the human lens under accommodation," Biomed. Opt. Express **5**, 1649–1663 (2014).

3. C. J. Sheil and A. V. Goncharov, "Accommodating volume-constant age-dependent optical (AVOCADO) model of the crystalline GRIN lens," Biomed. Opt. Express **7**, 1985–1999 (2016).

I now warn the reader not to mock me and my mental daze. It is easy for him and me to decipher now a past destiny; but a destiny in the making is, believe me, not one of those honest mystery stories where all you have to do is keep an eye on the clues. In my youth I once read a French detective tale where the clues were actually in italics; but that is not McFate's way—even if one does learn to recognize certain obscure indications.

— Vladimir Nabokov, *Lolita*

ACKNOWLEDGEMENTS

First, I would like to thank my supervisor, Sasha, who has been so generous with his time over the past four years, particularly when I was under time pressure to submit to my first conference, and revise my peer-reviewed papers. I don't think I ever had a question that he couldn't answer. Not only is he a genius in my estimation, he's an incredibly friendly person and general life-coach, with whom I hope to remain friends indefinitely.

Second, I want to thank my parents for their continued support in their trusting and unobtrusive way. I owe them everything. I also want to thank Brian for encouraging me to start a PhD and for his enthusiasm, too. He is always very proud of my accomplishments and generous with his time when I ask him to look something over.

Third, I want to thank my friends, with whom I'm glad to have a laugh over good food or questionable drinks. I would like to thank Adam and Colm for providing a well-rounded friendship; my friendly office-mate Niamh; the rest of Applied Optics, Ken, Lettie and Mark; the other physics postgrads; and Aisling for her companionship.

Last, I remember Wil van der Putten, who did so much for medical physics in Galway. Whenever I bumped into Wil, he would ask me good-naturedly when would I finish. Wil, here is the finished product. Thank you for your support.

This research was funded in part by the Irish Research Council.

CONTENTS

LIST OF FIGURES

LIST OF TABLES

LISTINGS

ACRONYMS

AIS Adjustable Internal Structure

AVOCADO Accommodating VOlume-Constant Age-Dependent Optical

BFL Back Focal Length

GIGL Geometry-Invariant Gradient refractive index Lens

GRIN Gradient Refractive INdex

HOA Higher Order Aberrations

HSWFS Hartmann-Shack WaveFront Sensor

LSA Longitudinal Spherical Aberration

MRI Magnetic Resonance Imaging

OCT Optical Coherence Tomography

OPL Optical Path Length

RK Runge-Kutta

RMS Root Mean Square

SA Spherical Aberration

TSA Total Spherical Aberration

Part I

BACKGROUND

1

INTRODUCTION

Understanding the optics of the human eye has importance beyond basic human curiosity and appetite for knowledge. For example, one of the basic human requirements for good quality of life is reasonable eyesight. If a patient's eyesight has been jeopardised, its restoration might require successful treatment of ocular abnormalities or successful outcome of ocular surgery—both of which depend on knowledge of the optical system of the eye.

A number of societal factors are leading to the general requirement for better understanding of the human eye. For example, the combination of an ever-ageing population with higher and differing expectations of personalised surgical procedures is placing demands on physicians to predict the outcome of cataract surgery. Traditionally, ocular surgeries such as cataract surgery are based on simplified eye models. The simplified eye model is constructed with population-averaged biometric data and based on this, the required surgical procedure is determined for a particular patient. This model works well for normal patients, since the population-averaged data will form a normal statistical distribution. However, for patients with abnormal eyes, this procedure tends to provide unsatisfactory outcomes. Historically, an abnormal eye would be one that was simply different due to disease, abnormal growth patterns, or other relatively rare condition. Human eyes can also be rendered abnormal by corneal refractive surgery. That is, if you take a normal eye and change the corneal shape, then that eye becomes abnormal in terms of population statistics. So, ocular abnormality is no longer something that occurs relatively rarely; in recent years, corneal refractive surgery has seen a large uptake, and the amount of patients presenting for cataract surgery who have previously undergone corneal surgery will continue to grow as the current generations age. Since corneal refractive surgery is customised, the resulting ocular abnormality will be highly idiosyncratic; hence, a statistical analysis of post corneal refractive surgery eyes has no real significance. This means that the outcomes of cataract surgery will continue to worsen, and the fact that patients are expecting better

outcomes as time progresses means that the discrepancy between expectation and outcome is two-fold.

The easiest way to improve prediction of surgical outcome and hence patient satisfaction is to depart from traditional statistical, simplified models of the human eye. The first step in doing so is to use models that more closely represent the real human eye—for example, using a GRIN lens structure instead of a homogeneous refractive index. It could be argued that even a very simple thin-lens and a complex GRIN lens have the same paraxial properties. While this is true, it becomes clear that the two models are similar in this regard only. There are many important discrepancies between the models, just one of which is the observation that GRIN models have both an average refractive index and an equivalent refractive index. This aspect of the lens is studied in further detail in Chapter 5.

The suitability and complexity of ocular models has increased over the years. The first model eyes of Gullstrand and variations by Le Grand and Emsley consisted of regions of homogeneous refractive index and spherical refracting surfaces—Lotmar and Kooijman later introduced aspheric surfaces.[1] Generally speaking, these models were used to match some property of a generic human eye; for example, a power of sixty dipotres. According to Smith [1], Blaker was the first to introduce a GRIN structure for the lens. Most recent models have adopted the GRIN description proposed by Pierscionek [2]. The use of more realistic models together with a GRIN medium allows customised model design in addition to specification of the average and equivalent refractive indices.

Aside from the basic requirement that cataract surgery restores the correct paraxial refractive power in the patient's eye, a new trend of customised aberration correction is emerging. For aberration calculation, we obviously require more advanced models of the human lens. For example, the shape of the lens surfaces in the model must represent the real lens, and the axial position of the lens equator might have an influence on the post-operative position of the intraocular lens. The need for a model with a GRIN structure and anatomical accuracy rules out earlier schematic models with spherical or conic surfaces and homogeneous refractive indices. To date, no model has been proposed that contains a mathematical formulation capable of accommodating with realistic volume changes, and capable

1 For further information on the history of early schematic eyes, including references, see the 1995 paper by George Smith [1].

of accounting for age-related changes in the lens GRIN structure. In this thesis, we propose a new model capable of doing so.

With the advancement of lens models, the method used to raytrace through the lens must progress at the same rate—for the purposes of aberration analysis, there is little benefit in using complex GRIN models if the raytracing procedure is not accurate. One attempt at simplifying the raytracing procedure involves splitting the GRIN structure into a series of shells, each with a constant refractive index. Some of the first to perform this were Pomerantzeff and co-workers, who generated a lens with up to 398 layers. Recently, Bahrami and Goncharov [3] introduced the Geometry-Invariant Gradient refractive index Lens (GIGL) model. The mathematical formulation of this model allowed the development of a series of equations for analysing the third-order aberrations of the lens. The particular advantage of this analytical basis is in its ability to very easily calculate lenticular aberrations for modest pupil heights and field angles. However, this third-order analysis is not entirely accurate, and becomes less so for increasing pupil sizes and field angles. In 2014, Bahrami and Goncharov [4] compared this analytical method with a shell method of exact raytracing, where the GRIN medium is split into discrete layers of homogeneous refractive index. They found that the percentage difference between the third-order and shell methods was as large as 91% for a full field angle of 8° and a pupil diameter of 4 mm. Hence, we can see that the third-order theory, while very convenient, is not entirely suitable for aberration analysis outside the paraxial region.

Furthermore, it can be shown that techniques involving division of the GRIN into discrete shells are erroneous. The discrete nature of these shells is detrimental to exact raytracing since, at certain stages, the propagating light ray will "miss" a shell. When a ray misses a shell, it is the same as if the ray traverses a significantly different optical path. The significance can be clearly seen in lenticular longitudinal aberration plots, where the plots are highly irregular, even if 100,000 shells or so are used. Moreover, "padding" of the problematic region with many extra shells does not seem to rectify the problem. For this reason, we must solve the differential ray equation for light rays travelling in the lens GRIN medium; this method is introduced in Chapter 3.

The goal is to develop an optical model of the human lens with anatomical accuracy that allows study of its accommodative and ageing properties. The model will include a realistic GRIN structure with sufficient degrees of freedom to match

experimentally observed values of important lens characteristics, such as power or Spherical Aberration (SA). In addition, the properties of the model will be studied using comprehensive numerical methods so that historical sources of confusion in data interpretation can be revisited.

While accurate models of the lens require relatively complex models with a large number of parameters, it is important that there not be too many degrees of freedom in the model. With too many degrees of freedom relative to the number of constraints, the problem of generating a customised lens model becomes over-determined. In an over-determined system, there is an infinite number of possible solutions. To limit the number of solutions, certain physical properties of the lens can be used—for example, the constancy of lens volume can be used as a constraint during accommodation. It can be shown that this basic physical constraint is very useful for predicting the changes in conic constants of the lens external surface under accommodation; this is discussed in Chapter 4.

In addition to generating a lens model with a GRIN medium and anatomically accurate surface representations, it is also necessary to formulate the GRIN in a way that represents the real ageing eye. This involves qualitatively replicating the shape of the iso-indicial contours of the lens bulk, as well as matching experimentally measured optical properties such as refractive power, SA and average and equivalent refractive indices. This forms the basis of our new Accommodating VOlume-Constant Age-Dependent Optical (AVOCADO) model in Chapter 5.

Already mentioned is the requirement for models that provide a more realistic representation of the real human lens and contain, conversely, the fewest unknown parameters. The large inter-subject variability in human ocular geometry means that, within the modelling process, convergence to a sensible solution can be difficult. While personalised ocular modelling is the ultimate goal, any new model must first be verified against sensible data. Ideal for use in this exercise are generic, averaged data. Because generic data are averaged across many eyes, it is true that the valuable individuality of the data is lost; however, the generic data can provide usefully representative values for the population and provide a starting point on which modelling can be based or verified. One such datum is SA. Studies have shown that SA has a non-zero population average, and its rotational symmetry makes its measurement relatively robust against instrument and intraocular component misalignment. In addition, age-related changes in SA can provide extra information for the modelling process. With this in mind, a compre-

hensive review of the literature on age-related changes in internal and total ocular SA is given in Chapter 2.

With numerical methods to study an anatomically accurate lens model containing a sensible number of degrees of freedom, one could revisit areas of optical modelling that have traditionally caused confusion. One such source of confusion is the so-called "lens paradox", resulting from the inability of early lens models to account for experimentally measured age-related changes in refractive error. In Chapter 6, we revisit some of these areas in an attempt to discover their aetiology.

2

A LITERATURE REVIEW OF SPHERICAL ABERRATION

The optical performance of the human eye has been studied quantitatively for close to a century, with several hundred studies published on ocular Higher Order Aberrations (HOA) in the last twenty years alone. Our wish is to have good agreement between many studies, across all subjects, with a clear age-related trend. However, as already outlined, the peculiarities of individual eyes make this ideal average non-feasible. Instead, a generic average forms a good compromise.

In what follows, a selection of salient studies on SA of the human eye will be outlined, with particular emphasis on SA of the ageing human eye. Of the primary and higher-order aberrations, SA in particular is found to have a non-zero average for the population and, due to its rotational symmetry, SA is relatively insensitive to instrument misalignment and inter-ocular component tilt. Several studies from the literature, the main emphases of which are say comparison of SA between groups of different refractive errors, are also included in this chapter, as they can provide information on the ageing eye. In Section 2.2, studies that have given values for SA of the internal optics of the eye are summarised. While the majority of such studies assume that the SA of the lens is given by a simple subtraction of the single-surface corneal power from total power, they are nonetheless included here for completeness. In Section 2.3 and Section 2.4, studies that report explicit data on the age-related changes in SA are reviewed—these studies provide linear or higher-order polynomial fits to the data, for example. Studies that do not provide explicit age-related changes are reviewed in Section 2.6. In Section 2.5, the relationship between SA and refractive error of the ageing eye is reviewed. The findings are summarised in the tables or figures at the end of each section. Studies that do not clearly state the SA calculation convention or, for example, those that calculate Total Spherical Aberration (TSA) are omitted from the tables and figures.

2.1 SPHERICAL ABERRATION AND ITS MEASUREMENT IN DIOPTRES

Spherical aberration manifests in an optical system as a change in Back Focal Length (BFL). For positive (undercorrected) SA, rays passing through the marginal region of a lens will focus closer to the lens. That is, the marginal zones have a shorter BFL. This effect is shown for a spherical mirror in Fig. 1. If BFL is plotted as

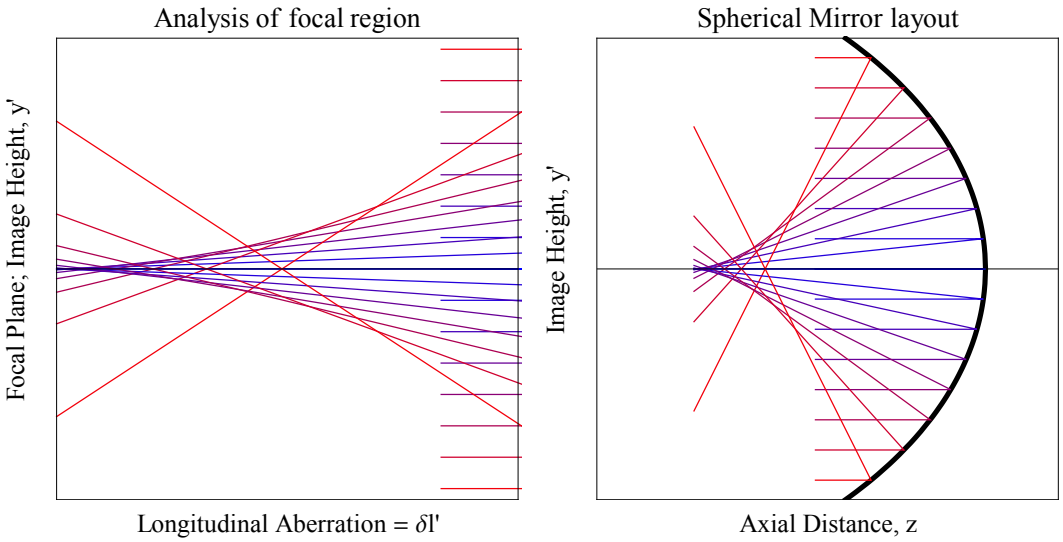

Figure 1: Schematic diagram of SA in a spherical mirror.

a function of pupil height, this gives rise to the concept of Longitudinal Spherical Aberration (LSA), shown in Fig. 2.

In some older studies of ocular aberrations, SA was presented as LSA in dioptres. The reasoning behind this is as follows. For positive SA in a lens, for example, the marginal rays form a focus closer to the lens than the paraxial rays; and, because of this, it appears that the marginal region of the lens has a larger "power". The amount of SA is hence given as the difference in power between the marginal and paraxial zones. Since SA depends on pupil height to the fourth power (in terms of wavefront), it is clear that the "power" of the peripheral zone increases with increasing pupil height. For this reason, if SA is to be represented in terms of power, the marginal ray height must be specified.

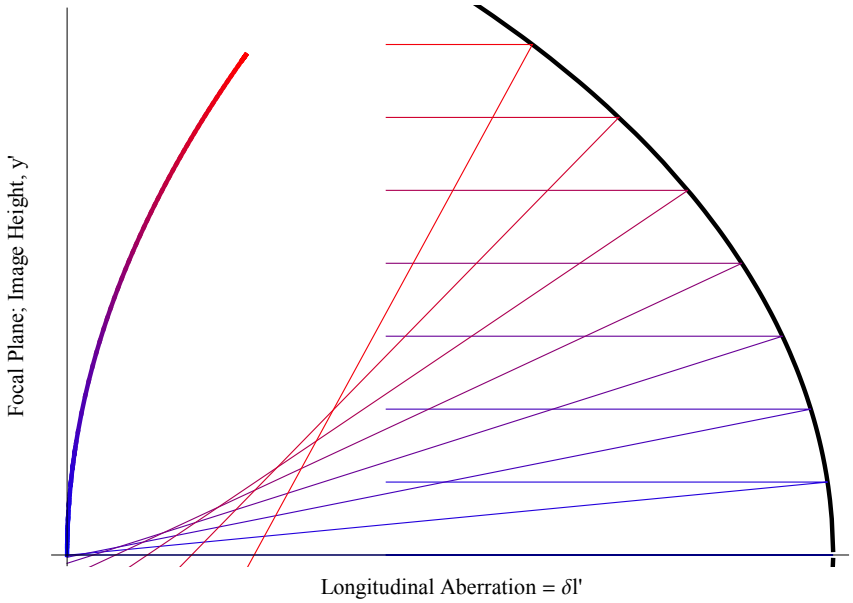

Figure 2: Schematic diagram of LSA in a spherical mirror.

In an optical system, if the distance from the back principal plane to paraxial image point is denoted l', then the power of that system is $F = n'/l'$, where n' is the image-space refractive index. If the system contains aberrations such that the longitudinal aberration is $\delta l'$, then the aberrations can be expressed in terms of the power difference they produce, as:

$$\Delta F = \frac{n'}{l' + \delta l'} - \frac{n'}{l'},$$

where ΔF is in dioptres if l' is in metres. Some confusion may arise when this formula is used in optometry, say, where aberrations are quantified in terms of the spectacle power required for their correction. In this case, the spectacle power is $-\Delta F$. For a rotationally symmetric system containing only primary aberrations, the power error is given by [5]:

$$\Delta F = br^2.$$

The variable b has units of D/mm².

In 2001, Atchison and Smith [5] summarised several historical measurements of SA in dioptric form. The mean weighted value of b was found to be:

$$b = 0.076 \pm 0.035 \text{ D/mm}^2;$$

hence, for a pupil diameter of 6 mm, say, $\Delta F = 0.684$ D.

In, 2007 Radhakrishnan and Charman [6] give the formula for calculating b from the 4th-order Zernike SA term C_4^0:

$$b(\text{D/mm}^2) = \frac{24\sqrt{5}}{r^4} C_4^0,$$

where C_4^0 is in µm and r is in mm. They extracted the values of b from several studies [7–11]. The average value of these studies is $b = 0.078$ D/mm², with each study showing a large standard deviation—some standard deviations have the same magnitude as b. For a pupil diameter of 6 mm, this gives a defocus term of $\Delta F = 0.706$ D. In this 2007 study, the three-dimensional relationship between aberrations, age and accommodation was assessed. They imaged the right eye of 47 healthy individuals, ranging in age from 17 to 56 yr. These were split into four age-dependent groups: < 20, 20–29, 30–39 and > 39 yr.

Their Fig. 4 shows the values for SA and coma in D/mm² and D/mm, respectively. While the measurements were taken at natural pupils, this method normalises the data to 1 mm pupil size. The average value for b was 0.073 D/mm², which, for a pupil diameter of 6 mm, gives a defocus of $\Delta F = 0.657$ D. Both coma and SA can be seen to increase with age, but only SA was statistically significant, with a linear regression of:

$$y = -0.0433 + 0.0047 \times \text{age } (\text{D/mm}^2).$$

There is a slight misconception in the representation of SA as a change in power with pupil height. This arises because SA is a change in BFL, as opposed to a change in *focal length*. BFL is the distance from the intersection of the last surface with the optical axis, to the intersection of the ray with the optical axis. Focal length, on the other hand, is related to the distance from the intersection of the ray with the optical axis, and the principal surface. For non-paraxial systems, the focal length of a marginal ray is given as $-h_0/\sin(u')$, where h_0 is the initial entrance ray

height to the system and u' is the angle between the exitant ray and the optical axis. If SA is a change in BFL with pupil height, *coma* is a change in power with pupil height.

To see the difference between the two aberrations SA and coma, we can consider two simple system examples. The first example is a spherical mirror. It is well known that spherical mirrors contain on-axis aberrations, shown in Fig. 1. Aside from the observation that, according to third-order theory, strictly speaking coma is absent on-axis, the spherical mirror appears to have a larger power in the marginal zones. This is not true, because the sphere has the same curvature at all ray heights; hence, the power of each marginal zone is the same. As a result, the power of the mirror does not change with marginal ray height. It can therefore be concluded that the aberration is caused by a change in BFL with pupil height—this is SA. The second example is that of a parabolic mirror, where all on-axis non-paraxial rays form the same focus; that is, BFL is constant across the pupil. To look at this mirror, one might therefore think that the power of the surface does not change with pupil height; however, this is not the case. If we were to calculate the curvature of the surface at each marginal zone, we would see that it is not constant. In addition, we could look at the power in terms of focal length, since power is inversely proportional to focal length. For the power to be constant, the focal length therefore must be constant. Since for the parabolic mirror all rays form the same focus, if the focal length were to be constant, this would mean that the focal lengths would form the radial lines of a circle, centred at the paraxial focal point. In other words, the principal surface would be a perfect sphere centred on the paraxial focal point. If we were to plot the principal surface of a parabolic mirror, we would clearly see that it is not a sphere. Hence, the power changes but the BFL does not.

The two preceding examples highlight the difference between SA and coma. The first example is a system containing SA but zero coma; the second contains zero SA but does contain coma. While the method of representing SA in dioptres provides a convenient single number, particularly useful for comparing older studies, we can see that the value of ΔF refers to one pupil size only; hence, the useful information on changes with pupil height are lost. Furthermore, the assumption that only primary aberration terms are present in the eye reduces the applicability of the method, particularly for measurements on eyes with large pupils and large

amounts of higher-order aberrations. For this reason, the Zernike term Z_4^0 is more useful, which is summarised in the following sections.

2.2 INTERNAL SPHERICAL ABERRATION OF THE HUMAN EYE

One of the earliest quantitative reports on ocular HOA was given in 1993 by Tomlinson *et al.* [12]. They used measurements of the contrast sensitivity function and modulation transfer function to deduce SA of the lens. These results were excerpted in 2001 by Smith *et al.* [13], who converted the values to the wavefront aberration polynomial $W_{4,0}$. An average of the two values of SA gives $W_{4,0} = 0.025 \pm 0.019\ \mu m/mm^4$.

The main aim of a 2004 study by Llorente *et al.* [14] was to examine the similarities in aberrations and geometrical features of both hyperopes and myopes—aberrations were measured using the laser raytracing technique and were calculated for 6.5 mm pupils. The authors took care to ensure that both groups were of the same age, with an average of 30.5 ± 3.8 yr for the myopic group of 24 eyes and 30.3 ± 5.2 yr for the hyperopic group of 22 eyes. Furthermore, both groups had similar amounts of refractive ametropia. In the case of internal aberrations, these values were found by subtracting corneal aberrations from total ocular aberrations. They found that aberrations of the internal optics did not differ significantly between the two groups, while internal SA became significantly less negative with age in the hyperopes. Shown in their Fig. 2D is the mean SA of the internal optics: $-0.12 \pm 0.14\ \mu m$ for hyperopes and $-0.14 \pm 0.09\ \mu m$ for myopes.

This manuscript includes some references to previous studies where no correlation was found between degree of ametropia and aberrations [7, 9], or differences in the amount of aberrations [9]; and to studies where myopes were found to have larger amounts of aberrations than emmetropes [15–18]. In the particular case of SA, they cite Collins *et al.* [15] as having found SA and myopia to be significantly correlated, while Carkeet *et al.* [19] found significant disparity between highly myopic individuals compared to hyperopes, emmetropes or even low myopes; some investigators did not report that SA and ametropia were significantly correlated for a wide range of myopia [17].

They also cite some of the literature dealing with the age-related trends in aberrations of the eye. The age-related increase of aberrations found by some authors

[13, 20–22] backs up the findings of Artal *et al.* [20], who showed that the balance of corneal and internal aberrations in young eyes is adversely affected by ageing [23]. It has been proposed that the lens is largely responsible for this, since its SA becomes less negative (more positive) with age [24]. Interstingly, Llorente *et al.* [14] found that "Occasionally it may happen that the internal SA overcompensates for the corneal aberration, resulting in a slightly negative total SA (for myopes)", as evidenced by their subject #M4.

In Fig. 4 of this paper, shown respectively in green, red and blue are the total, cornal and internal SA for each eye of the study, where the eyes are sorted by age. While only eyes $\leqslant 40$ yr were used in the study, and the results appear to be scattered, the authors found a marginally significant age-related trend in internal and total SA of the hyperopes. The slope of total ocular SA vs age is larger than that traditionally reported by previous investigators. No age-related trends were found in the myopes. As a summary, their Fig. 5 reports data from several previous investigations [13, 20–22] indicating the age-related increase of ocular SA, due to SA of the lens becoming more positive (less negative) with age. We can see from this figure that, for their own data, myopes appear to have a slope of SA vs age equal to 0.005 μm/yr, whereas for hyperopes it is 0.013 μm/yr. There may be an error on the y-axis label of that Fig. 5.

In 2005, 72 eyes of 72 subjects (26 male) with a large range of ages were studied by Alió *et al.* [25]. The age range was 8–80 yr, with a mean of 41 ± 21 yr. Aberrations were measured using a Hartmann-Shack WaveFront Sensor (HSWFS) after pupil dilation and cycloplegia, and calculated for 4 and 6 mm pupils. In Fig. 8 of this manuscript, a plot of ocular and corneal total HOA is shown, together with linear regression fits. From the figure, we can see that HOA in the whole eye are lower than the cornea—this indicates some sort of internal aberration compensation. Ocular and corneal HOA have the same size at the age of approximately 40 yr. Shown in Fig. 10 is a plot of internal SA (Z_4^0) for a 6 mm pupil, with an equation of approximately $y = -0.19 + 0.003 \times \text{age}$, where y is Z_4^0 in μm and age is in years. If corneal Z_4^0 is constant with age, then the slope of the equation above could be indicative of the age-related change in ocular Z_4^0. Note that the Zernike polynomials used in Refs. [21, 22, 26, 27] differ from those analysed in this study.

In 2006, Artal *et al.* [28] examined HOA in 73 eyes of 57 myopes with a mean age of 29.7 ± 7.1 yr, and 16 hyperopes with a mean age of 33 ± 7.9 yr. Aberrations

were measured for 6 mm pupil size with a HSWFS, and were reported as Zernikes in Noll's format. The lens aberrations were found by subtracting the corneal values from the total ocular values. Fig. 5 of this manuscript shows that myopes had a mean value of internal SA of -0.131 ± 0.113 μm, while hyperopes had a mean of -0.172 ± 0.152 μm.

In 2009, Athaide *et al.* [29] examined HOA in 630 eyes of 315 subjects, of which 155 were male. Mean subject age was 31 ± 16 yr, with a range of 5–64 yr. Patients were sub-divided into four age-dependent groups: 68 aged 5–14 yr; 55 aged 15–24 yr; 116 aged 25–44 yr; and 76 aged 45–67 yr. Aberrations were measured using the LADARWave® instrument (Alcon Laboratories Inc, Orlando, FLA, USA), based on the HSWFS, up to 6th-order for 6.5 mm pupil. It is unclear whether HOA data were obtained before or after cycloplegia. Ocular SA was found to increase with age, due to the contribution of the internal optics. 50% of children showed negative SA values, with a median of 0.02 μm. The median value of SA increased to 0.26 μm in the middle-aged adult group. For the internal optics, SA was found to increase significantly with age, with a mediam of -0.01 μm in children and 0.22 μm in mid-age adults. The results for SA of the internal optics, cornea and total eye are summarised in their Fig. 4, and are compared to the work of Kirwan *et al.* who, in 2006, reported that 84.6% of children had negative SA [30]. The data in this study are presented in graph form only; hence, exact values are difficult to find. For this reason, this study is omitted from Table 1.

A highly-cited large-scale aberration study of 675 adolescents was published by Philip *et al.* [31] in 2012. The population was grouped into myopes, emmetropes and hyperopes aged between 16 and 19 yr, with a mean of 16.9 ± 0.7 yr. Measurements were performed on 5 mm pupils after administering cycloplegic agent, and using the HSWFS-based COAS aberrometer. Aberrations were calculated as Zernikes up to 6th-order in OSA format. In this study, the lenticular aberrations were the same as the internal aberrations, and were given by subtracting corneal from ocular aberrations. Both internal and total SA were found to correlate with degree of ametropia, summarised in Table 1.

In summary, there appears to be no general consensus on the numerical value of internal SA for the middle-aged eye, highlighting the inter-study variability in addition to the inter-subject variability seen from the individual standard deviations. We can conclude that the internal optics have negative SA. According to the

2005 study of Alió *et al.* [25], the slope of internal SA vs age is 0.003 μm/yr for a 6 mm pupil which, scaled to a 5 mm pupil is 0.001 μm/yr—this is similar to the slope of total ocular SA vs age, which will be reviewed in the following sections.

2.3 AGEING CHANGES IN SPHERICAL ABERRATION OF THE YOUNG EYE

In this section, studies providing explicit age-dependent SA data for young eyes are reviewed. This area is not well-explored due to the limited number of studies on the ageing young eye. The findings are summarised in Fig. 3. A review of age-dependent changes in SA of the mid to old age eye is given in the following Section 2.4.

Children in Northern Ireland were assessed regarding the relationship between HOA and ametropia in 2014 by Little *et al.* [32]. They examined two groups: one aged 9–10 yr and another aged 15–16 yr. The young group consisted of 170 children (79 female) with an average age of 10.09 ± 0.39 yr, 166 of which had HOA measurements taken. The older group consisted of 148 children (83 female) with an average age of 16.06 ± 0.31 yr, 147 of which had HOA measurements taken. Aberrations were measured after cycloplegia with cyclopentolate 1% using the irx3 aberrometer (irx3; Imagine Eyes, Orsay, France), which is based on the HSWFS; the results were given for 5 mm pupils as 3rd- to 6th-order Zernike polynomials in the OSA standard. Data from right eyes were used for analysis. The children were further split into refraction-dependent groups for HOA analysis. The median value of SA (Z_4^0) was found not to be statistically different in the two age-groups, with both groups having a median of 0.07 μm. The young group had an interquartile range of 0.04–0.12 μm, while the older group had a range of 0.02–0.11 μm. Furthermore, SA was also found to be similar between the different refractive groups i.e. SA did not appear to depend on the amount of ametropia.

A longitudinal report of HOA in 166 emmetropic right eyes was performed in 2014 by Philip *et al.* [33]. Zernike aberration coefficients were calculated up to 6th-order in OSA format, for 5 mm pupils, using the HSWFS technique after cycloplegia. Anaesthetic (1% amethocaine hydrochloride) was followed by cyclopentolate 1% and tropicamide 1%. The purpose of this study was to compare equivalent refraction and SA ($C[4,0]$) in the 166 eyes in an initial baseline study (in the years 2004–2005) and the follow-up study (years 2009–2010). At the baseline study, av-

Table 1: Summary of studies reporting internal SA

Study/Method	Number of Eyes	Mean Age or Range (yr)	Internal Z_4^0 (μm)	±S.D. (μm)	Ocular Z_4^0 (μm)	±S.D. (μm)	Pupil Dia. (mm)
Tomlinson *et al.* [12]/CS (1993)	20	20–56	−0.030	0.023	—	—	4
Llorente *et al.* [14]/LR (2004)							
hyperopes	22	30	−0.12	0.14	0.22	0.17	6.5
myopes	24	31	−0.14	0.09	0.10	0.13	6.5
Alió et al. [25]/HS (2005)	72	41	$(-0.19 + 0.003\text{age})$			—	6
Artal *et al.* [28]/HS (2006)							
hyperopes	16	33	−0.17	0.15	0.01	0.11	6
myopes	57	30	−0.13	0.11	0.07	0.10	6
Philip *et al.* [31]/HS (2012)	1350	17					
low hyperopes	706	—	−0.038	0.05	0.083	0.05	5
emmetropes	394	—	−0.081	0.04	0.036	0.04	5
low myopes	200	—	−0.088	0.04	0.038	0.05	5
moderate myopes	50	—	−0.095	0.05	0.026	0.06	5

[a]CS, contrast sensitivity; LR, Laser raytracing; PM, psychophysical methods; HS, Hartmann-Shack.

erage subject age was 12.63 ± 0.48 yr and in follow-up was 17.08 ± 0.67 yr. The average of all subjects' baseline value of SA ($C[4,0]$) was 0.035 ± 0.047 μm with a range of -0.070 to 0.190 μm.

The subjects were assessed to see if their equivalent refraction changed during the two measurements. 41 eyes (25%) underwent a myopic shift in refraction, with the remaining 125 showing no change. For the 41 subjects that underwent a myopic shift, SA was significantly lower (less positive) in the follow-up. At baseline and follow-up the respective values were 0.049 ± 0.062, range -0.070 to 0.280 μm; and 0.024 ± 0.050, range -0.060 to 0.130 μm. SA Root Mean Square (RMS) also decreased in the follow-up. For the 125 subjects showing no change in refraction, SA was significantly higher (more positive) in the follow-up. At baseline and follow-up the respective values were 0.033 ± 0.046, range -0.050 to 0.190 μm; and 0.047 ± 0.046, range -0.060 to 0.170 μm. SA RMS also increased in the follow-up. Figure 1 of that manuscript summarises the SA findings.

The aberrations of a relatively large sample of 557 children, ageing from 10 to 15 yr, were measured in 2015 by Papamastorakis *et al.* [34]. The mean age of all children was 12.8 ± 0.1 yr, of which 291 were male. The children were split into 3 age-dependent groups, the averages and standard deviations of which were: group 1, 10.7 ± 0.5 yr; group 2, 12.4 ± 0.5 yr and group 3, 14.5 ± 0.5 yr. The aberrations were measured with a HSWFS, and statistical analysis of the aberrations in OSA format was carried out on the right eye only, for pupils of 5 mm. In agreement with previous studies in the literature, most individual aberration terms averaged to zero. Spherical aberration was significantly different from zero with a mean of 0.018 μm. Spherical aberration also showed the largest change between the groups, with an increase from 0.007 ± 0.005 μm in group 1, to 0.011 ± 0.004 μm in group 2, to 0.030 ± 0.004 μm in group 3. As with previous studies, the authors found a relatively large degree of inter-subject variability in HOA. Interestingly, their Table 1 shows that the actual sign of SA had large variability between subjects—for example, in the youngest group, as little as 54% of subjects had positive SA, while 46% had negative SA.

For each study in Fig. 3, the pupil diameter for the original measurement, ρ_0 is given in the legends. The value of SA from each study has been scaled to a 5 mm pupil diameter for comparison, using the factor $(5/\rho_0)^4$. Shown also in Fig. 3, for comparison, are the polynomial fits of Salmon and van de Pol [35] and Brunette

et al. [26]. Those two studies performed measurements on a large range of subject ages. Considering the majority of their subjects were older than the young children summarised in this section, the significance of these fits for such a low age range is questionable. However, they are shown here for completeness.

To summarise, younger eyes have less positive SA than older eyes in general. There is an interesting trend of decreasing SA in the majority of studies presented in this section. However, as stated, the polynomial fits of Salmon and van de Pol, and Brunette *et al.* might not be relevant, especially considering the significance of fitting a polynomial to a cloud of data points and extrapolating to young ages. The 2014 study of Philip *et al.* raises some interesting questions on the cross-sectional study of ocular aberrations. In this longitudinal study, we can see that the subjects undergoing no age-related shift in refraction show an increase in SA. This would mean that the young emmetropic eye grows to an old emmetropic eye and in this scenario, SA is found to increase. This increase in SA is also found in cross-sectional studies where young emmetropic eyes are compared to old emmetropic eyes. However, for the subjects undergoing a myopic age-related shift in refraction, SA decreases. This means that the young emmetropic eye grows to an older myopic eye. Hence, for these subjects, it would not be correct for cross-sectional studies to compare young emmetropic eyes to older emmetropic eyes. This could be one reason for the large inter-subject variability of cross-sectional studies in both SA and age-related changes therein.

2.4 AGEING CHANGES IN SPHERICAL ABERRATION OF THE MID–OLD EYE

In this section, the age-related changes in ocular SA of the mid- to old-age eye are summarised and presented in Fig. 4 below.

In 2001, McLellan *et al.* [22] published a commonly-cited study of 38 individuals aged 22.9–64.5 yr showing that, for a 7.32 mm pupil diameter, ocular Zernike RMS SA increases at a rate of 0.0043 µm/yr. They measured aberrations using the spatially resolved refractometer method after dilation with tropicamide 0.5%, and calculated the aberrations as Zernikes up to 7th-order in the OSA format.

Brunette *et al.* published a highly-cited paper in 2003 [26], being perhaps the first paper to demonstrate that aberrations of the human eye tend to decline until middle-aged adult life, after which they increase. Their introduction provides a

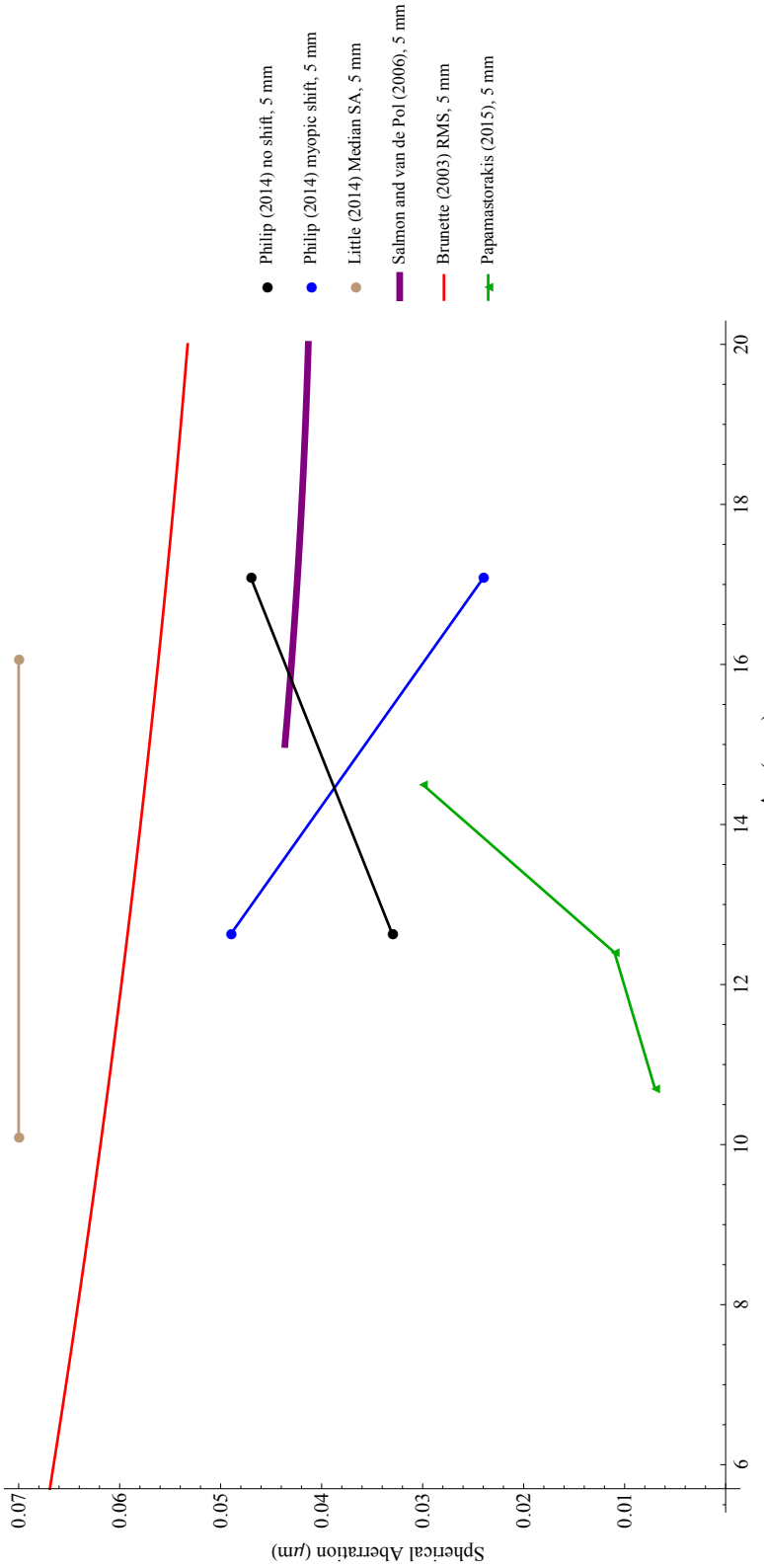

Figure 3: Summary of ageing changes in SA of younger eyes. All values have been scaled to a 5 mm pupil.

good summary of previous aberration measurements. They measured 114 subjects (mean 43.2 ± 24.5 yr; range 5.7–82.3 yr), with a HSWFS. Aberrations were measured after pupil dilation and cycloplegia and were calculated for 5 and 7 mm pupils as Zernikes up to 7th-order in the OSA format.

Plotted in their Fig. 8 are age-related changes in RMS wavefront error for SA (4th- and 6th-order Zernike) for a 5 mm pupil. They fitted a second-order polynomial regression curve, giving the polynomial: $(y = 0.07477 - 0.0015x + 2.125 \times 10^{-5}x^2$, where x is age in years. They also plot mean RMS for a 5 mm pupil in their three age groups, for 4th- and 6th-order aberrations. In line with other studies [36, 37], an increase in variance as a function of pupil size was found. Their study found the general pattern that while the young adult's eye produces a higher-quality retinal image than the older eye at 5 mm pupils, the child's eye is suboptimal and, in terms of RMS, its retinal image quality can be compared to that of the older eye. In their Fig. 11, they compare results with other studies.

Also in 2003, Wang and Koch [10] outlined their awareness of only four peer-reviewed publications on ocular aberration [7, 22, 38, 39]. They intended to expand upon these previous experimental endeavours by measuring 532 eyes of 306 subjects (mean age 41 ± 10 yr; range 20–71), with 6.0 mm pupils. Aberrations were measured without pupil dilation using the HSWFS-based WaveScan® (AMO, USA), and the ocular HOA were examined from 3rd–6th-orders. Their population included a relatively high proportion of myopes, with fewer emmetropes than that found in a normal population [40]. Furthermore, the young individuals were far more myopic compared to the older individuals. However, the authors defended this by referencing a 2003 study of Cheng *et al.* [9] showing that refractive error and wavefront aberration were not correlated in a sample of 200 normal eyes.

Consistent with previous findings [7, 39, 41–43], the wavefront aberrations of the whole eye differed greatly between individuals, with an average SD of roughly 0.10 µm for the total HOA. The RMS of SA, given by the square root of the sum of the squared coefficients of Zernike components Z_4^0 and Z_6^0, came out as 0.128 ± 0.074 µm. The mean values of the individual Zernike components were: $Z_4^0 = 0.101 \pm 0.103$ µm, range: -0.266 to 0.355 µm; and $Z_6^0 = 0.011 \pm 0.029$ µm, range: -0.081 to 0.120 µm.

For each of the 306 subjects, one eye was measured to study the age-related changes in ocular aberrations; the results are given in their Table 6. Of the higher-

order aberrations, 4th-order SA Z_4^0 and 5th-order vertical coma Z_5^{-1} showed a slight age-related increase, the results of which are shown in their Figs. 4–6. However, the statistical significance of these results, given by the r^2 value, was $\leqslant 0.1$, hinting that ageing causes only $\leqslant 10\%$ of the variation in results. In Fig. 5 of that manuscript, the authors reveal the linear fit of RMS SA (RMS of Z_4^0 and Z_6^0) versus age: $y = 0.002x + 0.046$ μm, where x is age in years.

There is a useful discussion contained in this paper of Wang and Koch [10]. They cite Porter *et al.* 's 2001 investigation [7] of 2nd–5th-order ocular aberrations for 5.7 mm pupil size in 109 normal individuals. They found that approximately 7% of the total aberrations were contained within the 3rd–5th-order, showing large inter-subject variability. Porter et al. [7] report a moderately larger average 4th-order SA coefficient (0.138 μm across 5.7 mm pupils); interestingly, the SD was the equivalent (0.103 μm). The work of Castejón-Mochón *et al.* [39] also shows large inter-subject variability for aberrations of the whole eye, in the 2nd–5th-order with 5 mm pupil in 59 younger students. The negative average 4th-order SA coefficient reported may be because their sampled consisted only of younger subjects (age range 20–30 yr). The studies of Porter *et al.* and Castejón-Mochón *et al.* did not report total HOA RMS or assess any age-related changes in aberrations.

In 2004, Amano *et al.* [44] measured HOA in 75 eyes of 75 normal patients ranging in ages from 18 to 69 yr, with a mean of 43.5 ± 11.7 yr. Aberrations were measured using a HSWFS for natural pupils of 6 mm, and were reported as Zernikes up to 6th-order. In addition to the Z_4^0 Zernike term, the authors calculated RMS SA as the square root of the sum of the squared coefficients of Z_4^0 and Z_6^0. They found that both Z_4^0 and RMS SA correlated positively with age. Shown in their Fig. 7 is the age-related change in Z_4^0; judging by this figure, ocular SA had a value of zero at approximately 10 years of age, and the slope is 0.004 μm/yr.

These results agree with previous studies by reporting an increase in SA of the whole eye [20–22, 45], with no ageing changes of corneal SA [27]. From this, they conclude that the positive corneal SA is compensated by the lens in younger eyes, and total ocular SA becomes more positive with age because of lenticular aberration changes. These lenticular aberration changes may be caused by changes of the anterior and posterior lens radii [46, 47] and refractive index distribution [48], with age.

In Section 2.2, the 2004 study by Llorente *et al.* [14] on internal aberrations is summarised. This study also reports SA of the whole eye. Briefly, they measured HOA for 6.5 mm pupils in 24 myopic eyes aged 30.5 ± 3.8 yr and 22 hyperopic eyes aged 30.3 ± 5.2 yr. Shown in their Fig. 2D is the mean SA of the whole eye, with values of 0.22 ± 0.17 μm for the hyperopes and 0.10 ± 0.13 μm for the myopes.

Salmon and van de Pol [35] decided to compile aberrometry measurements from several locations in the literature dating up to 2006, with the purpose of facilitating easier comparison of results for the normal, healthy adult eye. The compilation of data results in a population of 2,560 eyes of 1,433 subjects. The sources were limited to measurements performed using the HSWFS method and for pupil sizes of at least 5 mm in diameter.

One of the most surprising findings is that the SA (Z_4^0) appeared to center around two significantly different subgroups, with averages of roughly 0.04 μm and 0.09 μm, respectively, for a 5 mm pupil. The averages of absolute Zernike coefficients are given in their Table 2. The large inter-subject variability can be seen, as the standard deviations amounted to roughly 85% of each average.

Regarding the change of SA versus age, Z_4^0 for both left and right eyes with a 5 mm pupil is presented in their Fig. 9. Rather than a linear fit, the authors obtained a better result by fitting a 2nd-order polynomial in age, to the data, with the result: $y = 0.000045 \times \text{age}^2 - 0.002038 \times \text{age} + 0.06408$. Again, a large inter-subject variability is clearly evident. In addition to the large amount of studies using the HSWFS method, the authors reference the works of Levy *et al.* [49] and Zadok *et al.* [50], who instead used the Nidek OPD Scan—the results are comparable. The reader is directed to the manuscript itself for more information. This study is referred to again in the concluding remarks of Section 2.7.

The effect of age on ocular and corneal aberrations was assessed in 2006 by Jahnke *et al.* [51] using a Tscherning aberrometer for a 6.5 mm pupil. They imaged both eyes of 49 normal subjects aged between 17 and 65 yr, with an average age of 38.6 ± 10.0 yr The subjects were split into two groups, those < 45 yr (76 eyes), having an average age of 34.6 ± 6.8 yr; and those $\geqslant 45$ yr (22 eyes), having an average age of 52.4 ± 6.9 yr.

The changes in aberrations between the two age groups are shown in their Table 3. Spherical aberration (C12) was found to increase statistically significantly,

by almost a factor of two, from 0.0738 μm in the lower age group to 0.1422 μm in the higher age group.

In 2007, Applegate *et al.* [52] published a paper on the three-dimensional relationship between HOA, pupil diameter and ageing. In this relatively large study, one eye each of 146 healthy subjects aged between 20 and 80 yr were examined. Aberrations were calculated for pupil diameters of 3, 4, 5, 6, and 7 mm. Since RMS HOA are known to increase with age [20–22, 38, 53–58], they should expect somewhat similar results in this study. Aberrations were reported as Zernikes, according to the ANSI standard. Table 7 of this manuscript includes a breakdown of aberrations for each of SA, coma, astigmatism, trefoil and tetrafoil. From this, it is possible to calculate the age-related change in aberrations. The authors calculated SA as the RMS value $\sqrt{(C_4^0)^2}$. For a 5 mm pupil, RMS SA increased from 0.065 ± 0.057 μm in the 20–29 yr age group to 0.145 ± 0.086 μm in the 70–79 yr group.

Also in 2007, Fernández de Castro *et al.* [59] measured HOA in 93 eyes of 52 subjects (52% male) with an average age of 40.9 ± 10.3 yr, of which 87 eyes were myopic and 6 hyperopic. Pupils were dilated with 1% cyclopentolate. Aberrations were measured using the HSWFS technique for 6 mm pupils. In agreement with other studies, a large inter-subject variability was found for aberration terms. It is unclear what Zernike term(s) were used to calculate SA in this study. Subjects greater than 40 years old (of which there were 58 in this study) had larger amounts of SA than younger subjects (35 in this study), with means of 0.23 ± 0.15 μm and 0.15 ± 0.14 μm, respectively. Shown in their Fig. 2 is a statistically significant correlation between age and SA, with an apparent slope of 0.004 μm/yr.

Already mentioned in Section 2.1 on the representation of SA in terms of dioptric power is the 2007 study of Radhakrishnan and Charman [6]. Although this paper deals with accommodation as well as ageing, we can use the data for 0 D accommodation stimulus to view the aberrations of the ageing unaccommodated eye. Aberrations were analysed at a fixed pupil size of 4.5 mm for 0 D stimulus to compare inter-subject values. In Fig. 2(a) of this paper, the population mean for each Zernike term is given. From the figure, we can see agreement with previous studies [7–11, 36, 41, 42, 60] showing large inter-subject variability, and also that most terms average to zero; except, for example, SA (C_4^0). The average value of

SA was 0.034 ± 0.05 μm. For this population average, 6 eyes were omitted since their pupils were smaller than 4.5 mm. In their Fig. 2(b), the values of SA (C_4^0) and total RMS for the 3rd- to 6th- order aberrations are given versus age. They found that while total RMS did not increase with age, SA became statistically significantly more positive, with a linear regression of $y = 0.0024 \times \text{age} - 0.0389$ μm.

In 2008, Goebels *et al.* [61] assessed the age-dependence of ocular, corneal and internal HOA. They measured 140 eyes of 140 subjects, ranging in age from 17–77 yr, with a mean of 39.1 ± 15 yr. The subjects were split into 6 age-dependent groups: $\leqslant 25$, $\geqslant 66$ and any ages in-between these limits, split into decades, e.g 26–35 etc.

From their Table 1, we can see that the aberrations show large inter-subject variability for the 5 mm pupil analysed. According to the authors, the only significant age-dependence found was for SA of the 26–35 yr group and the $\geqslant 56$ yr group. SA increased from a minimum of 0.04 ± 0.03 μm in the $\leqslant 25$ yr group to a maximum of 0.12 ± 0.08 μm in the 56–65 yr group, subsequently decreasing to 0.10 ± 0.06 μm for the $\geqslant 66$ yr group.

Iida *et al.* [62] assessed the effect of age on the accommodative changes in ocular aberrations in 2008. They imaged 56 eyes of 30 emmetropes, aged between 21 and 47 yr, with a mean of 31 ± 7 yr. The subjects were split into three age-dependent groups: 20–29 yr (15 subjects, 28 eyes), 30–39 yr (9 subjects, 17 eyes) and 40–49 yr (6 subjects, 11 eyes). The aberrations were determined using the iTrace for 4 mm pupils without mydriatics, and reported as Zernikes. While this study involves accommodation, we can use the results for 0 D stimulus to compare the aberrations of the ageing unaccommodated eye. We can see from their Fig. 6 that, at 0 D, SA (C_4^0) increases with age, from a value of approximately 0.011 μm in the youngest group to 0.028 μm in the middle-aged group to 0.055 μm in the oldest group.

Also assessing the accommodative changes in HOA in relation to age in 2008 were López-Gil *et al.* [63]. They imaged 60 subjects, divided into four age-dependent groups. Group A (12 subjects aged 19–29 yr; mean = 21.08 ± 2.27 yr); group B (13 subjects aged 30–39 yr; mean = 36.08 ± 1.55 yr); group C (14 subjects aged 40–49 yr; mean = 44.43 ± 3.01 yr); group D (21 subjects aged 50–60 yr; mean = 53.90 ± 2.76 yr). Aberrations were measured with the HSWFS-based irx3 aberrometer (Imagine Eyes, Orsay, France), without cycloplegia or pupil dilation.

The age-related increase in HOA found in this examination is similar to the finding of others [22, 26], in that it is more exaggerated with increasing amounts of accommodation; this effect is shown in their Fig. 2. The authors highlight the novelty of their results by saying that, to their knowledge, no other studies included all three variables of age, accommodation, and a gradient index for the crystalline lens.

In Figs. 3 & 6 of that manuscript, data for the accommodative change in SA (c_4^0) RMS are graphed, along with their linear fits. Figure 4 is for a natural pupil, while Fig. 6 is for a 4 mm pupil. The data can be summarised as follows, where y is RMS c_4^0 in µm and x is accommodation in dioptres:

Table 2: Summary data from López-Gil *et al.* [63]

group type	SA, natural pupil	SA, 4 mm pupil
(A) 19–29 yr group	$y = -0.059x - 0.006$	$y = -0.011x - 0.001$
(B) 30–39 yr group	$y = -0.054x + 0.006$	$y = -0.019x + 0.005$
(C) 40–49 yr group	$y = -0.057x - 0.005$	$y = -0.018x - 0.011$
(D) 50–59 yr group	$y = -0.078x - 0.009$	$y = -0.072x - 0.005$

In 2010, Berrio *et al.* [64] measured aberrations of the cornea and whole eye, together with tilt, for 46 eyes over a 5 mm diameter pupil using a HSWFS. Aberrations were reported as Zernikes up to 6th-order in OSA format. Subject ages ranged from 20 to 77 yr. They found that RMS higher order aberrations for the whole eye and cornea were dependent on age, with an increase of 0.0032 µm/yr and 0.0015 µm/yr, respectively. They found that, in young eyes, the internal surfaces partially compensated for the aberrations of the cornea. However, the compensation was not found in older eyes. Spherical aberration and horizontal coma of the eye increased modestly with age at the rates of 0.0011 µm/yr and 0.0017 µm/yr, respectively; these changes, they found, are not caused by changes in alignment of the optics. They explain most of the age-related increase in ocular aberrations by variations in the radii of the lens—these variations alter the shape factor of the lens and hence this geometrical alteration reduces the compensation ability of the lens.

Karimian *et al.* [65] measured HOA in 126 eyes of 63 myopes (41 female) aged between 18 and 43 yr, with an average of 26.4 ± 5.9 yr. Aberrations were measured with a Zywave II instrument (Bausch & Lomb), based on the HSWFS. Aberrations

were reported in the OSA format for 6 mm pupils—2.5% phenylephrine was used if the natural pupil was less than 6 mm. In agreement with previous studies, SA (Z_4^0) was found to be one of the most dominant aberration terms, with a mean for all subjects of -0.0642 ± 0.130 μm and a range of -0.360 to 0.280 μm. The RMS of SA (square root of the sum of Z_4^0 coefficients) was 0.12 ± 0.08 μm, with a range of 0.0 to 0.36 μm. Also in agreement with previous studies was the finding that the contribution of Zernike orders decreased successively from the 3rd-order. The authors found a significant correlation between spherical equivalent refraction and RMS SA. Interestingly, SA was found to decrease with age and, judging by their Fig. 6, the slope of SA vs age is -0.004 μm/yr. Despite the statistical significance of the decrease, the considerable scatter of data points would question its validity.

Zhang *et al.* [66] measured, in 2011, aberrations of patients screened for refractive surgery. The subjects were split into two age-dependent groups: the young group contained 120 eyes of 60 individuals aged 18–40 yr, while the middle-aged group contained 44 eyes of 22 subjects aged 41–49 yr. The aberrations were measured based on the Tscherning principle, over 6 mm pupils after dilation with tropicamide 0.1%. Their Table 2 shows that SA changed significantly between the two age groups. Judging by their Fig. 3, SA (Z_4^0) increases at a rate of approximately 0.005 μm/yr. In agreement with the work of Artal and colleagues, they found that corneal SA was partially compensated by the internal optics in the younger eye, whereas the compensation diminished in the middle-aged eye.

In 2013, Kingston and Cox [67] published a population study of SA and its relation to refractive error, age, corneal curvature and image quality in 1,124 eyes, of which 1,074 (95.5%) were myopic and 50 hyperopic. The mean age of all subjects was 31.8 yr, ranging from 19 to 45 yr. Aberrations were measured using the HSWFS-based Zywave II instrument (Bausch & Lomb) for 6 mm pupils. Mydriatic agents were not used, except if the subjects' pupils were less than 6 mm, in which case 2.5% phenylephrine and 0.5% tropicamide were used. It is unclear what Zernike term(s) were used to represent SA in this study. The authors found that SA was positive in 91% of eyes, with an overall mean of 0.018 μm. Statistical analysis showed no significant correlation of SA with amount of ametropia. The amount of SA was found to be positively correlated with age, albeit weakly—SA became more positive with increasing age. Judging by their Fig. 4, the slope of SA vs age is approximately 0.004 μm/yr. In agreement with previous studies, they found

a large inter-subject variability of SA, hence reducing the significance of its age-related change.

Fig. 4 summarises the age-related changes in SA of the middle- to old-aged eye. For each study, the pupil diameter for the original measurement, ρ_0 is given in the legends. The value of SA from each study has been scaled to a 5 mm pupil diameter for comparison, using the factor $(5/\rho_0)^4$. Also shown in this figure is the age-related change internal SA found by Alió *et al.* [25], reviewed in Section 2.2. From this visual summary, we can see a large inter-study variability; this is in addition to the inter-subject variability within each study. Furthermore, there is considerable difference in the slope of SA vs age reported by each study.

Of the studies explicitly showing a polynomial (linear or other) fit to the ageing changes in SA, we can take the average slope and the average SA value for 30 years of age. The study of Salmon and van de Pol included a large number of subjects; omitting this study to average the remaining smaller studies, the mean value of SA is 0.056 μm at 30 yr with a slope of 0.002 μm/yr, both for a 5 mm pupil. The polynomial fits of Salmon and van de Pol, and Brunnette *et al.* are shown in the figure as the purple and red traces, respectively. While the study of Salmon and van de Pol includes a large amount of eyes, the choice of a polynomial fit is questionable. This is to be questioned further in the study of Brunette *et al.*, with only 114 subjects. Although the polynomial fit may be statistically better, caution must be exercised when choosing an extra degree of freedom for fitting noisy data, as a polynomial with too many degrees of freedom will produce a good fit to noisy data.

2.5 SPHERICAL ABERRATION AND AMETROPIA

In this section, studies on the relationship between SA and refraction in the ageing eye are reviewed, and summarised in Table 3.

In 2003, Cheng *et al.* [9] published a study of aberrations in patients with different refractive errors. They decided to minimize any possible effect of age on their aberration measurements [22] by simply limiting the age distribution studied. They measured 200 eyes of 100 individuals under paralysed accommodation, for a mean pupil size of 7.58 mm. The mean age of the subjects was 26.1 ± 5.6 yr.

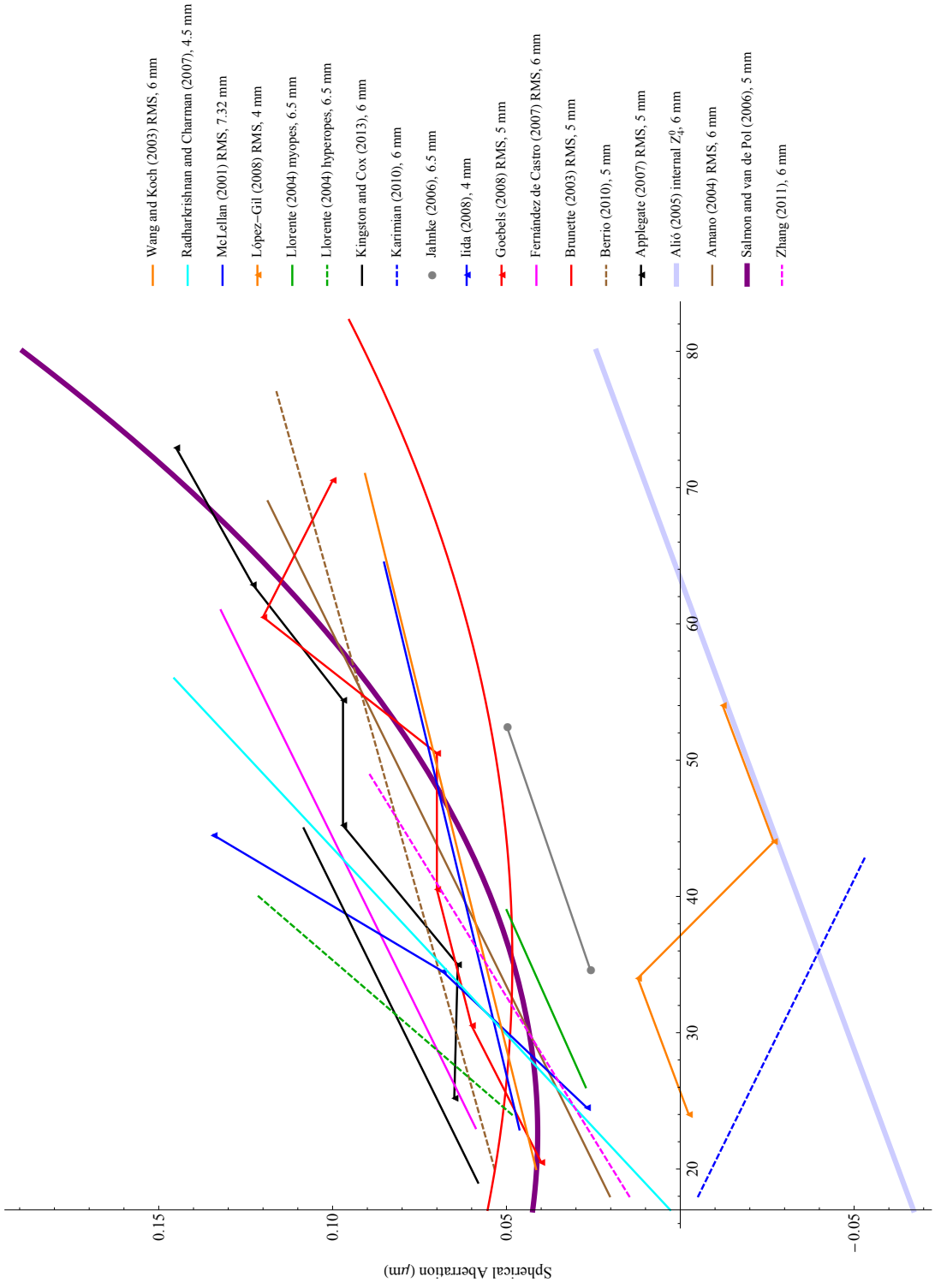

Figure 4: Summary of ageing changes in SA of mid–old age eyes. All values have been scaled to a 5 mm pupil.

They found a large inter-subject variability in the magnitude of higher-order aberrations—some of the variability may correlate with refractive error.

Since SA was not found to be correlated with degree of ametropia or astigmatism, we could average all values for (Z_4^0) in their Table 2; the average comes out as 0.0973 μm. Cheng *et al.* [9] also pay particular attention to any possible interference of their measurement technique with the results, as follows. They made measurements on emmetropic and highly-myopic patients. But, the myopic eyes were first corrected by a trial lens before they were actually measured. Since the trial lens used differed with different amounts of myopia, it is possible that the SA induced by these negative trial lenses interfered with the results. To investigate any possibility of this, they calculated the SA of they typical trial lens that was used to correct the high myopes. They found that the amount of SA produced by that lens was $< 3\%$ of the amount measured in their myopic eyes, with opposite sign. Based on this, they conclude that any SA introduced by the trial lens could not have significantly affected their results.

The 2004 study by Llorente *et al.* [14] has been mentioned in Section 2.2 and Section 2.4 with regard to internal aberrations, and the change of ocular aberrations with age. In addition, their subjects formed two groups: a hyperopic and myopic group. A more thorough description of this study is given inSection 2.2 and can be summarised as follows.

Of the eyes in the hyperopic subset, the older ones (11 eyes, >= 30 yr) displayed significantly less negative SA of the internal optics (-0.04 ± 0.07 μm) than the young group (-0.20 ± 0.14 μm). For hyperopes, this leads to a decrease in the balance of corneal aberrations by internal optics from roughly 56% to 14% with age. The older hyperopes showed significantly larger (more positive) values of internal and total SA than older myopes. Young hyperopes typically had more negative internal aberration $(-0.20 \pm 0.14$ μm) than young myopes $(-0.17 \pm 0.10$ μm), although not significantly.

In 2005, Buehren *et al.* [68] investigated aberrations in the left eye of young myopes and emmetropes. Twenty young myopes were examined, aged 19–24 yr, with a mean of 22 yr; and 20 young emmetropes, aged 19–28 yr, with a mean of 23 yr. An important note is that in this study, the individuals were of different ethnicities. Aberrations were measured with the HSWFS-based COAS wavefront

sensor (WaveFront Sciences, Inc.), and were calculated for pupils of 3 mm, 4 mm and 5 mm, reported as Zernikes according to the OSA convention.

In their Table 2, results of aberration measurements after 1 and 2 hours of far-distance reading are presented for a 5 mm pupil. Regarding ocular aberrations, for the myopes SA (Z_4^0) increased from 0.001 μm after 1 hour of reading to 0.002 μm after 2 hours; for the emmetropes SA (Z_4^0) increased from −0.003 μm after 1 hour of reading to approximately 0 after 2 hours.

Also in 2005, Zadok *et al.* [50] measured HOA in 61 myopic eyes of 36 individuals, with naturally dilated pupils of at least 6 mm. The subjects ranged in age from 18 to 43 yr, with a mean of 22 yr. To estimate repeatability, 3 measurements each were taken. Orders 3 to 8 were used in aberration analysis. Ocular HOA were examined using the OPD-Scan (NIDEK Co Ltd, Gamagori, Japan). As with the 2005 paper of Levy *et al.* [49], SA was presented as TSA (given as the square root of the sum of the squared values for C_4^0, C_6^0 and C_8^0). Total HOA had an average of 0.347 ± 0.252 μm, and TSA had an average of 0.120 ± 0.174 μm; these values were not correlated with refractive error. Large inter-subject variability can be seen from the published values, with HOA having a standard deviation of 0.25 μm on average. Also, the repeatability of HOA mesurement was found to be low.

The 2006 study of Artal *et al.* [28] on total and internal aberrations has been mentioned in Section 2.2. Briefly, 57 myopes aged 29.7 ± 7.1 yr and 16 hyperopes aged 33 ± 7.9 yr were measured with a 6 mm pupil. Judging by Fig. 5 of this manuscript, the mean value of SA was found to be 0.07 ± 0.10 μm for myopes, while hyperopes had a mean of 0.01 ± 0.11 μm.

In a paper published in 2006, Atchison *et al.* [69] began by observing that any changes in aberrations with refractive ametropia are equivocal. Some studies found that aberrations were mildly higher in myopes [16, 18, 68, 70], whereas others found no increase [7, 9, 11, 19, 50]; Llorente *et al.* [14] found in 2004 that hyperopes displayed larger amounts of aberrations than myopes.

This study examined 121 individuals (74 female) aged 17–35 in relation to myopia. The ocular and corneal aberrations of a subset of 63 eyes (58 right eyes) were measured using the HSWFS-based COAS instrument under natural pupil conditions—only one subject had a pupil that required pharmacological dilation to 5 mm. Aberrations were reported as Zernikes to 6th-order using the OSA standard.

Regarding the results of this study, only three Zernike terms had absolute means > 0.01 and differed significantly from zero: c_2^2, c_3^1, c_3^3 and c_4^0. Spherical aberration (c_4^0) averaged 0.04 ± 0.06 μm for the entire cohort, shown in their Fig. 6(a), while the emmetropes had a value of 0.06 ± 0.05 μm.

The finding that mean ocular SA was positive and significantly different from zero for the relaxed eye is in agreement with previous studies [7, 8, 71], while its independence from myopia was also found previously [9, 17]. Note that this study used the pupil centre as a reference for aberration measurements, which is different from other studies e.g those by Marcos and colleagues [72], and others [68]. As in another paper of Atchison and colleague [73], they estimated the effect of trial lens ametropia correction on aberration measurements. In this study, the aberration artefact may have been *under*estimated.

Kirwan *et al.*'s highly cited 2006 paper [30] detailed the measurement of HOA in 162 eyes of 82 children (42 female and 40 male), aged between 4 and 14 yr, with a mean of 6.7 yr. The majority of subjects were hyperopic. Aberrations were measured using the HSWFS-based Zywave II aberrometer (Bausch & Lomb) after administration of cycloplegic and mydriatic, over 6 mm pupils. The results of the aberration analysis are given in their Tables 2 & 3. Table 2 shows that the mean SA (Z_4^0) came out at -0.115 ± 0.126 μm and mean of absolute SA values was 0.171 ± 0.187 μm; 84.6% of subjects showed negative SA. In support of the findings of He *et al.*, total HOA were significantly higher in the myopes than hyperopes. Conversely, Carkeet *et al.* [74] found that myopic children had aberrations akin to emmetropic children.

Kwan, Yip and Yap [75] examined in 2009 the relationship between HOA and myopia in 116 normal myopic individuals and 26 anisometropic individuals. In this thesis, we are not interested in abnormal subjects so we occlude results for the anisometropes. One of the aims of Kwan *et al.*'s study was to use a relatively small range of subject ages, to mitigate possible error introduced by age-related changes in aberrations. The 116 normal subjects, of which 62 were female, ranged in age from 19 to 29 yr with a mean of 21.8 yr. The individuals were split up into three sub-groups depending on the degree of refractive ametropia present: non-myopes and moderate- and high-myopes. The measurements were performed with a HSWFS under natural pupil conditions, and aberrations were calculated up to 4th-order in OSA format for 5 mm pupil size. The main finding of this paper

was that the high-myopes showed significantly lower 4th-order RMS and SA RMS values than the emmetropes. This indicates that the degree of refractive ametropia is correlated with SA, but not in the expected way. Since SA is lower in the high-myopes, this would imply that SA is not a factor in myopia development. For non-, moderate- and high-myopes, the respective values of SA were 0.073 ± 0.048 µm, 0.062 ± 0.039 µm and 0.044 ± 0.035 µm.

Also in 2009, Martinez *et al.* [76] assessed the relationship between HOA in a large sample of hyperopic and emmetropic children. The children studied formed two distinctive age-related groups: one group of 771 children aged 5.7–7.9 yr (average 6.7 ± 0.4 yr); and a second group of 643 children aged 11.2–13.9 yr (average 12.6 ± 0.5 yr). The ocular aberrations were measured after cycloplegic and mydriatic agents were administered, using an instrument based on HSWFS, for 5 mm pupils. The aberrations were reported as Zernike coefficients up to the 6th-order, according to the OSA standard.

Within both age groups, the subjects were split into four sub-groups, depending on their individual amount of refractive ametropia: emmetropes, low hyperopes, moderate hyperopes and high hyperopes. For SA, $Z(4,0)$, significant differences were found between the refractive sub-groups in both the younger and older groups. In both groups, emmetropes showed less positive SA than moderate and high hyperopes. This finding of higher SA in hyperopes compared to emmetropes is consistent with previous findings [14, 15, 77].

The younger group of 771 children had a mean SA of 0.04 ± 0.06 µm, with an RMS SA of 0.06 ± 0.04 µm; whereas the older group of 643 had a mean SA of 0.06 ± 0.05 µm, with an RMS SA of 0.07 ± 0.05 µm. While the mean value of SA $Z(4,0)$ increased in all refractive groups, it was not statistically significant for the high hyperopes.

The 2010 study of Karimian *et al.* [65] is mentioned in Section 2.4 with reference to the age-related change in SA. Their findings in relation to ametropia are repeated here. The authors measured HOA in 126 eyes of 63 myopes aged 26.4 ± 5.9 yr for a 6 mm pupil, finding a significant correlation between spherical equivalent refraction and RMS spherical aberration. Interestingly, SA was found to decrease with age, but the considerable scatter of data points would question the validity of this finding.

In a large-scale 2011 study of 423 right eyes of Canadian children, Thapa *et al.* [78] analysed HOA in subjects aged 3–6 yr, with a mean of 3.89 ± 0.92 yr. The children were divided into three refraction-dependent groups: emmetropic, and low- and high-hyperopic. Aberration measurements were performed using the HSWFS principle for 5 mm pupils, and reported up to 8th-order to the OSA standard. TSA was calculated as the RMS of C_4^0, C_6^0 and C_8^0. Statistical analysis showed that TSA was significantly lower in the emmetropes than the high hyperopes. However, all other intra-group comparisons did not show different TSA. The values of TSA, in microns, for the 3 refractive groups are: emmetropes 0.044 ± 0.0303; low hyperopes 0.056 ± 0.0391; high hyperopes 0.070 ± 0.0502.

In 2012, Hartwig and Atchison [79] compiled HOA data of 24,000 individuals from Carl Zeiss Vision's European database; unfortunately, the database did not contain any information on subject age. They found that, amongst other aberration terms, SA was significantly different between myopic and hyperopic individuals. The aberrations were reported as Zernikes using the ANSI standard, and were scaled to a 4.5 mm pupil diameter. The average SA for myopes was 0.001 ± 0.056 μm, and for hyperopes was 0.035 ± 0.056 μm.

In another 2012 paper, Hashemian *et al.* [80] measured the aberrations of 2,458 eyes of 1,240 myopic individuals aged between 18 and 56 yr (mean 28.3 ± 7.32 yr), and 215 eyes of 110 hyperopic individuals aged between 20 and 64 yr (mean 37.69 ± 10.09 yr). The ocular aberrations were measured using a HSWFS for dilated pupils of 6 mm in diameter. In the myopic group, the TSA was 0.133 ± 0.112 μm, whereas the hyperopic group showed TSA of 0.202 ± 0.209 μm. The value of TSA was significantly higher in the hyperopes than the myopes, including when an age-matched analysis was performed.

In a study of the Chinese population, Li *et al.* [81] assessed the dependence of ocular aberrations on refractive ametropia in the right eye of Chinese school children. They imaged 86 children, of which 41 were male aged 7–13 yr with a mean of 10.2 ± 1.8 yr, and 45 were female aged 7–13 yr with a mean of 9.8 ± 1.9 yr. The children were split up into three groups, depending on the degree of ametropia. There were 22 emmetropic, 43 mildly myopic and 21 moderately myopic children. A HSWFS was used to measure aberrations with natural pupils; the aberrations were calculated for a pupil size of 5 mm in the OSA format. From

Fig. 2 of this manuscript, we can see that SA $C(4,0)$ is approximately 0.059 ± 0.050 μm for the emmetropes, 0.062 ± 0.051 μm for the mild myopes and 0.050 ± 0.060 μm for the moderate myopes. The authors found that RMS total HOA and SA were not significantly correlated with degree of ametropia.

Philip *et al.* [31] published a study on the correlation of internal and total aberrations with degree of ametropia in 2012. The numerical data of this study are summarised in Table 1 of Section 2.2. With regard to the correlation with ametropia, for internal aberrations, the Zernike SA term C_4^0 was found to be significantly different between the refractive error groups, being least negative in low hyperopes. It became increasingly more negative with degree of ametropia, with moderate myopes having the most negative value. For ocular aberrations, C_4^0 was also significantly different between the refractive groups. Hyperopes were found to have more positive ocular SA than emmetropes, with moderate myopes having the lowest value. All values are summarised in

Many studies have been published on the possible relationship between aberrations and refractive error. In particular, there is a question as to whether aberrations are a causal factor in refractive error development; i.e. do certain aberrations cause excess amounts of defocus as the eye grows? These studies have measured both young [16, 19, 30, 76] and adult [9, 14–16, 18, 68, 69, 75, 82, 83] populations. The results of such studies have not formed a consensus, with some showing larger aberrations (total HOA, SA or coma) in the myopic eye [16, 30, 68], and some showing no differences at all [9, 19, 69, 82]. However, one simple problem that could be avoided in future is standardisation of the measurement technique. As pointed out by Plainis and Pallikaris [84] and Atchison and Charman [73], use of trial lenses to counteract refractive ametropia before measurement can drastically affect SA measurements.

The 2013 study of Kingston and Cox [67], summarised in Section 2.4 measured aberrations of subjects aged 31.8 yr for 6 mm pupils. The amount of ametropia was not statistically correlated with SA.

A longitudinal report of HOA in 166 emmetropic right eyes was performed in 2014 by Philip *et al.* [33]. Zernike aberration coefficients were calculated up to 6th-order in OSA format, for 5 mm pupils, using the HSWFS technique after cycloplegia. Anaesthetic (1% amethocaine hydrochloride) was followed by cyclopentolate 1%

and tropicamide 1%. The purpose of this study was to compare equivalent refraction and SA ($C[4,0]$) in the 166 eyes in an initial baseline study (in the years 2004–2005) and the follow-up study (years 2009–2010). At the baseline study, average subject age was 12.63 ± 0.48 yr and in follow-up was 17.08 ± 0.67 yr. The average of all subjects' baseline value of SA ($C[4,0]$) was 0.035 ± 0.047 μm with a range of -0.070 to 0.190 μm.

The subjects were assessed to see if their equivalent refraction changed during the two measurements. 41 eyes (25%) underwent a myopic shift in refraction, with the remaining 125 showing no change. For the 41 subjects that underwent a myopic shift, SA was significantly lower (less positive) in the follow-up. At baseline and follow-up the respective values were 0.049 ± 0.062, range -0.070 to 0.280 μm; and 0.024 ± 0.050, range -0.060 to 0.130 μm. SA RMS also decreased in the follow-up. For the 125 subjects showing no change in refraction, SA was significantly higher (more positive) in the follow-up. At baseline and follow-up the respective values were 0.033 ± 0.046, range -0.050 to 0.190 μm; and 0.047 ± 0.046, range -0.060 to 0.170 μm. SA RMS also increased in the follow-up. Figure 1 of that manuscript summarises the SA findings.

A large report on 1,007 eyes (530 male) was generated in 2014 by Yazar *et al.* [85], with the aim of comparing HOA in young adults of differing visual performance. Potential age-related effects on results were reduced by including the relatively small age range of 18.3 to 22.1 yr, with a mean of 20.05 ± 0.45 yr. Pupil dilation and cycloplegic agents were not used for aberration measurements, which were measured with Bausch & Lomb's HSWFS-based Zywave, and were scaled to a 6 mm pupil. The subjects were divided into three refraction-dependent groups: myopes, 217 eyes, SA $Z(4,0)$ median (interquartile range) $= -0.242(-0.476, -0.079)$ μm; emmetropes, 476 eyes, SA $Z(4,0)$ median (interquartile range) $= -0.206(-0.361, -0.073)$ μm; hyperopes, 314 eyes, SA $Z(4,0)$ median (interquartile range) $= -0.239(-0.381, -0.097)$ μm. Subjects with higher myopia had slightly higher total HOA.

In 2015, Hashemi *et al.* [86] published the first study of HOA in an Iranian population of 904 eyes of 577 individuals, of which 62.9% were female, ranging in age from 40–64 yr, with an average of 49.5 ± 5.7 yr. Aberrations were measured for 5 mm pupils with the Zywave aberrometer (Bausch & Lomb), which is based on the HSWFS principle, without the administration of cycloplegic agent. The au-

thors found that total RMS SA (Z_4^0) was −0.161 —m, with a 95% confidence interval of −0.174 to −0.147. The authors also assessed several variables in terms of aberration analysis, including gender, age and degree of ametropia. Interestingly, SA was found to decrease with age, which is something that has not been reported previously, except by He *et al.* in 2002 [16], Brunette *et al.* in 2003 [26] who found that aberrations decreased until approximately the 4th decade of life and increased thereafter, and Karimian *et al.* in 2010 [65]. The authors report the change in SA (Z_4^0) for different age groups. All subjects were split into 5 groups. The mean value of Z_4^0 (95% confidence interval) for each age group is as follows, with SA in microns. 40–44 yr: −0.1235(−0.1484 to −.0986); 45–49 yr: −0.1491(−0.174 to −0.1243); 50–54 yr: −0.1791(−0.2031 to −0.1551); 55–59 yr: −0.1871(−0.2312 to −0.1429); ⩾ 60 yr: −0.214(−0.2988 to −0.1291). Statistical analysis of other relationships indicated that SA had significant correlation with nuclear cataract only. In terms of ametropia, SA was significantly higher in hyperopes. This relationship may have affected the age-related change in SA. Their Table 5 contains a summary of previous HOA measurements. The values for SA appear to be highly negative and show a negative trend with age, which might indicate that the SA values presented in their Table 2 have the wrong sign.

Also in 2015, Khan *et al.* [87] compared HOA in 200 eyes of 121 subjects with differing refractive errors. Subjects ranged in age from 18–40 yr, with a mean of 29.1 ± 10.6 yr, of which 129 were female. They were sub-divided into four refraction-dependent groups: low- and high-myopic, astigmatic and hyperopic. Aberrations were measured after administration of cyclopentolate, and calculated for 6 mm pupils. The authors found that the RMS of "spherical aberrations" was significantly higher in the hypermetropic group compared to the other groups, with a value of 0.30 ± 0.42 μm. The low- and high-myopes and astigmatics had respective values of 0.11 ± 0.07 μm, 0.11 ± 0.10 μm and 0.13 ± 0.09 μm. It is unclear to what these spherical aberrations refer, but it is the probably the whole cohort of spherical-like 4th-order Zernike aberrations.

As outlined at the end of Section 2.3, care must be taken when interpreting the results of cross-sectional studies on age-related changes in refraction. This is because the development of ocular growth and refractive error of the eye are not yet fully understood. For this reason, when studies compare SA between refractive groups, a large range of subject ages could compound the final conclusion. In the

summary Table 3 of this section and Table 1 of Section 2.2, we can see that there are some incongruous results. Both the 2004 study of Llorente *et al.* [14] and the 2012 study of Philip *et al.* [31] show that young- to middle-aged myopes have less positive total SA and internal SA (internal SA becomes more negative); Hartwig and Atchison [79] found similar results. This is contradicted by the 2005 and 2006 studies of Buehren *et al.* [68] and Artal *et al.* [28], saying the direct opposite. In 2003, 2012 and 2014 respectively, Cheng *et al.* [9], Li *et al.* [81] and Yazar *et al.* [85] found that SA was roughly the same between refractive groups.

Table 3: Summary of the literature on total SA in different refractive groups

Study/Method	Number of Eyes	Mean Age or Range (Years)	Z_4^0 (μm)	Pupil Dia. (mm)
Cheng *et al.* [9]/HS (2003)	200	26	0.097	7.58
Llorente *et al.* [14]/LR (2004)				
hyperopes	22	30	0.22	6.5
myopes	24	31	0.10	6.5
Buehren *et al.* [68]/HS (2005) (1 hour after reading)				
emmetropes	20	23	−0.003	5
myopes	20	22	0.001	5
Artal *et al.* [28]/HS (2006)				
hyperopes	16	33	0.01	6
myopes	57	30	0.07	6
Atchison *et al.* [69]/HS (2006)	63	17–35	0.04	5
Kirwan *et al.* [30]/HS (2006)	162	7	−0.115	6
Kwan, Yip and Yap [75]/HS (2009)	116	22	0.060	5
Martinez *et al.* [76]/HS (2009)	1542	7	0.04	5
	1286	13	0.06	5
Karimian *et al.* [65]/HS (2010)	126	26	−0.064 (−0.004/yr)	6
Hartwig and Atchison [79]/HS (2012)(review, 24000 individuals)				

Continued on next page

Table 3 – *Continued from previous page*

Study/Method	# Eyes	Age	Z_4^0	Pupil
hyperopes	—	—	0.035	4.5
myopes	—	—	0.001	4.5
Li *et al.* [81]/HS (2012)	86	10		
emmetropes	22	—	0.059	5
mild myopes	43	—	0.062	5
moderate myopes	21	—	0.060	5
Philip *et al.* [31]/HS (2012)	1350	17		
low hyperopes	706	—	0.083	5
emmetropes	394	—	0.036	5
low myopes	200	—	0.038	5
moderate myopes	50	—	0.026	5
Kingston and Cox [67]/HS (2013)	1124	32(19–45)	0.180 (0.004/yr)	6
Philip *et al.* [33]/HS (2014)				
myopic shift baseline	41	13	0.049	5
myopic shift follow-up	41	17	0.024	5
no shift baseline	125	13	0.033	5
no shift follow-up	125	17	0.047	5
Yazar *et al.* [85]/HS (2014)	1007	20		
hyperopes (median)	314	—	−0.239	6
emmetropes (median)	476	—	−0.206	6
myopes (median)	217	—	−0.242	6
Hashemi *et al.* [86]/HS (2015)	904	50	−0.161	5

[a]CA, crossed-cylinder aberroscope; CS, contrast sensitivity; DS, dynamic skiascopy; LR, Laser raytracing; PM, psychophysical methods; HS, Hartmann-Shack; TA, Tscherning aberrometer.

2.6 OTHER STUDIES ON SPHERICAL ABERRATION OF THE EYE

Studies that do not provide explicit data on age-related changes in SA are reviewed below and summarised in Table 4.

Perhaps the first commonly cited study to represent aberrations as Zernike polynomials is that of Calver *et al.* [21] who, in 1999, imaged 15 younger (mean age 24.2 ± 3 yr) and 15 older (mean age 68.0 ± 5 yr) individuals. They also used the Howland aberroscope, mentioned above. For a 4 mm pupil, SA changed from young to old by 0.019 to 0.035 μm (increase of 0.00036 μm/yr).

Published in 2001 was the highly-cited population study of Porter *et al.* [7]. For a 5 mm pupil and mean age of 41 yr for 109 subjects, they found that Zernike SA was only coefficient to have a mean significantly different from zero on average, with a value of 0.138 ± 0.103 μm.

The first population study on HOA in children was published in 2002 by Carkeet *et al.* [19]. With a mean age of 9.0 ± 0.84 yr, they found that their 273 mostly Chinese child subjects had a mean C_4^0 term (SA) of 0.0548 ± 0.0443 μm for a 5 mm pupil, after administration of cycloplegic agent. Aberrations were measured using the HSWFS-based Zywave instrument (Bausch & Lomb), and Zernike coefficients were calculated in the OSA format.

Also in 2002, Castejón-Mochón *et al.* [39] imaged 108 eyes of 59 patients with a mean age of 24 ± 3 yr. Aberrations were measured using a HSWFS under natural viewing conditions, and were calculated up to 5th-order in Noll's format. They found that SA (Z_4^0) for a 5 mm pupil was 0.008 ± 0.074 μm.

Another relatively large study of 109 subjects was performed in the same year by Guirao *et al.* [88]. With a mean age of 41 yr, average SA (Z_4^0) was significantly different from zero, with a value of 0.13 ± 0.10 μm for a 5.7 mm pupil.

The data from studies on accommodative changes in HOA can be used to provide information on the ageing eye. For example, the values for 0 D stimulus correspond to the unaccommodated eye. One such study is that published by Ninomiya *et al.* [89] in 2002, who used a HSWFS to measure aberrations of one eye each of 33 young adults, the mean age of whom was 28.7 ± 4.4 yr. In the unaccommodated eye, the average value of SA (C_4^0) came out as 0.02 ± 0.02 μm for the

4 mm zone, and 0.11 ± 0.10 μm for 6 mm. From these results, we can again see large inter-subject variability.

A final large-scale study was performed in 2002 by Thibos *et al.* [36], who imaged 100 subjects of mean age 26.1 ± 5.6 yr (range: 22–35 yr) with a 6 mm pupil; they only analysed 140 out of 200 eyes with a 7.5 mm pupil. Aberrations were measured after application of cyclopentalate 0.5% using a HSWFS, and reported in the OSA format. They found that when they averaged across the population, Zernike terms were almost zero for all higher-order modes except SA. Judging by their Fig. 6, wherein a summary of each Zernike coefficient is provided, SA (Z_4^0) appears to have an average value (of both eyes) of 0.10 ± 0.19 μm. Idiosyncrasy was highlighted where, for individual eyes, the coefficients were rarely zero for any Zernike term.

In 2003, Carkeet *et al.* [74] measured aberrations of 34 Chinese preschool children, of which 16 were female and 18 male. They ranged in age from 4.95 to 6.89 yr, with a mean of 5.91 ± 0.56 yr. The aberrations were reported as Zernikes, using the OSA standard, measured for a 5 mm pupil under cycloplegia.

In agreement with previous studies showing that 4rd-order aberrations are smaller than 3rd-order [10, 15, 41–43, 90–92], the authors found that 3rd-order terms were dominant. Spherical aberration (C_4^0) was positive, with an RMS value of 0.06 ± 0.04 μm. The results of the measured HOA are given in their Fig. 1.

He *et al.* [93] published an aberration study in 2003 on 90 eyes of 45 individuals aged between 9 and 29 yr, with a mean age of 18 yr. The first 35 Zernike aberration terms were calculated for measurements using a psychophysical raytracing technique [16, 94] with 6.32 mm pupils. Of the 45 individuals, 18 were emmetropic and 27 myopic. In agreement with previous studies, the authors found considerable inter-subject variability in wavefront aberrations for the whole eye. For all subjects, the mean *absolute* coefficient for SA (Z12) was 0.18 ± 0.13 μm. The mean (taking signs into account) of SA (Z12) was 0.06 ± 0.22 μm. Interestingly, only 33% of eyes had positive total ocular SA.

Again in 2003, a large-scale study of HOA in 102 eyes of 51 normal individuals was published by Wang *et al.* [90]. The subjects were young adults, who ranged in age from 18 to 35 yr, with a mean of 21.86 ± 4.43 yr. The aberrations were presented as Zernikes in the OSA format. In addition to Zernike SA (C_4^0), the

Zernike coefficients were used to calculate the spherical-like wavefront aberration coefficient S_4. Tables 2 & 3 of this manuscript contain values for both coefficients for three pupil diameters: 4 mm, 5 mm and 6 mm—for a 6 mm pupil diameter, SA (C_4^0) had an average of 0.09 ± 0.07 μm.

Further to this, Cheng *et al.* [71] performed another 2004 population study of accommodative changes of HOA, using a HSWFS to measure the right eye of young adults aged 21–40 yr (mean = 24.8 ± 4.0 yr). Wavefront aberrations were measured after dilation, over a 5 mm pupil. Of the 76 subjects reported for accommodative changes in aberration, 74 were used for population statistics. The aberrations were presented as Zernikes up to 6th-order, according to the OSA standard. While the main focus of this paper is on accommodation, the HOA values at 0 D stimulus can be used for information on the unaccommodated eye.

Figures 1a & 1b of Cheng *et al.* [71] respectively provide both the mean value and the mean absolute magnitude of each Zernike aberration coefficient for their 74 unaccommodated eyes. Perhaps the clearest characteristic of Fig. 1a is the large inter-subject variability within the group; moreover, all aberrations seem to average to approximately zero, apart from SA which is positive on average. These findings are concordant with data from the literature [7, 8, 36]. The mean value of SA found for the unaccommodated eye was smaller than what was reported by Porter *et al.* in 2001 [7], coming out at 0.065 ± 0.083 μm. The authors put this difference down to the lower age of subjects in the current study, since SA is known to increase with age [22, 24]. The authors point out the difficulty in comparing different studies of wave aberrations. For example, some studies are performed when the eye is in a natural viewing condition, whereas others employ cycloplegic agents to paralyze accommodation [7, 36, 39]. The various amplitudes of accommodative stimulii used in experiments, and pupil size over which the aberrations are analysed, also adversely affect attempts of direct comparison. Cheng *et al.* [71] consider that there are not yet enough data to allow confident characterisation of individual accommodative variation in ocular aberrations.

In 2004, Fujikado *et al.* [56] examined one eye each of 66 normal individuals ranging in age from 4 to 69 yr, with a mean of 37.4 ± 15.4 yr. A HSWFS was used to measure both ocular and corneal aberrations over a 4 mm pupil. For total ocular HOA, the authors discovered a significant age-related correlation of SA, coma-like aberrations and total HOA.

From Figs. 1 & 2 of this paper, we can see that the corneal spherical-like aberrations (4th-order aberrations) are larger than total spherical-like in the younger, whereas the opposite is true in older eyes; the two values are equal at approximately 40 years of age. This could imply that the spherical-like aberrations of the lens increase with age and hence disrupt any partial compensation of corneal aberrations present in the younger eye. This effect, combined with other aberration increases, leads to a sharp increase of total HOA after approximately 50 years of age. For the 4 mm pupil, provided in Fig. 1 is a linear fit to the data points for both total and corneal spherical-like aberrations. From this, it is possible to deduce the linear age-related change in internal spherical-like aberrations. The fit for total spherical-like aberrations is given as: $y = 0.0012 \times \text{age} + 0.0107$; the units are not specified but are likely in microns.

Atchison wrote a comprehensive review paper in 2005 containing over 300 references [95]. While the reader is directed to that paper for full information, some of the main points are excerpted below.

On average, the value of SA (c_4^0) is approximately 0.10 ± 0.10 μm for a pupil diameter of 6 mm [8, 10, 90]. While this value is positive for the unaccommodated eye, SA decreases, tending towards negative values, with accommodation [15, 71, 89, 96–105].

While the majority of studies show an age-related increase in total HOA throughout adulthood [20–22, 44, 56, 106], Brunette *et al.* [26], in a study involving a large spectrum of ages, concluded that total and component HOA, including SA, become smaller until about 40 years of age, thenceforth they increase. Some studies found an age-related increase in SA throughout the adult age [13, 20–22, 44], while another found up to three-fold increase in RMS aberrations from the 20 year old eye to the 70 year old eye with a 5.9 mm pupil [20].

Regarding aberrations of the lens, several studies have found that the SA of the lens tends to positive (less negative) values [13, 20]. Interestingly, Kuroda *et al.* [107] discovered that, when compared to normal eyes, mild nuclear and cortical cataract were correlated with atypical values of SA, for a 6 mm pupil. Sachdev *et al.* [108] discovered that eyes with nuclear cataracts showed high levels of positive SA.

As pointed out in this review paper by Atchison [95], care must be taken when comparing the results of different studies, as all investigators may not have used

the same notation for the Zernike coefficients—e.g. standard normalised coefficients. For example, Kuroda *et al.* [107] omitted the normalisation terms.

Levy *et al.* [49] measured aberrations in 70 eyes of 35 subjects with supernormal vision, for a natural pupil with a diameter greater than 6 mm. The subjects ranged in age from 18 to 51 yr, with a mean of 24.3 ± 7.7 yr. In Table 2 of that manuscript, average values are provided for, amongst others: average RMS values for ocular total HOA and TSA (given as the square root of the sum of the squared values for C_4^0, C_6^0 and C_8^0). The HOA mean value was 0.334 ± 0.192 μm, while TSA was 0.110 ± 0.077 μm. Also provided in that table are summary values of Li Wang and Koch [10] and Yan Wang *et al.* [90].

As with previous studies [7, 10, 39], inter-subject variability became apparent in this study—the standard deviation of HOA was as large as 0.192 μm. Interestingly, the TSA was found to have the lowest variance. As this study measured ocular aberrations from 3rd- to 8th-orders, whereas previous studies have used 3rd- to 6th-orders. It is known that truncating the Zernike coefficents at different orders affects the computed coefficients; however, the magnitude of the 7th- and 8th-orders are probably small, as it has been shown that successively higher orders (higher than 3rd) have successively lower RMS values, for the human eye [10, 90].

This study did not find a statistically significant correlation between any of the aberrations and age. The authors cite the 2003 work of Li Wang and Koch [10], who found a weak correlation between HOA, SA and coma with age. In addition to the weak correlation, age was found to account for only 10% of the overall changes.

The aberration profiles of very young subjects were measured in 2005 by Wang and Candy [109], who imaged the right eye of 17 infants aged 5 to 7 weeks, and their parents. A pupil size of 3 mm was used for the infants' aberration analysis, while 4.5 mm was used for the adults'. Aberration measurements were also performed with the COAS system and given in the OSA format. Figure 3 of this manuscript shows the mean for each Zernike coefficient. From this figure, we can see that the infants had a mean SA Z_4^0 value of approximately 0.03 ± 0.01 μm, whereas the adults had a mean of approximately 0.06 ± 0.04 μm.

Using a Tscherning aberrometer, Jankov *et al.* [110] examined the effect of two mydriatic agents on ocular wavefront error—phenylephrine and cyclopentolate. They imaged 151 (72 left and 79 right) eyes of 81 myopic subjects, of whom 38

were female and 43 male, aged 18–57 yr, with a mean of 33 ± 9 yr. The subjects were imaged prior to refractive surgery; hence, the amount of myopia in some subjects was considerable. The effect on wavefront error was assessed by measuring aberrations for pupil diameters of 4 and 7 mm, and reported as Zernikes up to 6th-order using the OSA standard.

Perhaps the most surprising result of this paper is that the authors observed a change in sign of SA when using phenylephrine and cyclopentolate, seen in their Fig. 5. For phenylephrine, the SA was found to be negative, whereas for cyclopentolate, it was positive. After administration of cyclopentolate, SA for the 7 mm pupil was found to be 0.098 ± 0.148 μm, which is in agreement with the literature showing that, for a 6 mm pupil, SA is between 0.1 and 0.15 μm [5, 7, 10, 71, 102]. The value that was found after administering phenylephrine was -0.026 ± 0.189 μm. Since the SA of the human eye is known to shift towards negative values with accommodation, the authors postulate that the phenylephrine renders the eye in a slightly accommodated state. This study does not give values of SA without the use of either drug; furthermore, since a relatively large range of subject ages was examined, the results may not be of use in characterising the ageing eye.

The effect of race on HOA was assessed in 2006 by Nakano *et al.* [111], who imaged 384 eyes of 192 Asian subjects and 264 eyes of 132 non-Asians. The average age for Asians was 32.78 ± 7.69 yr and for non-Asians was 30.93 ± 7.98 yr. Aberrations were measured using the OPD-Scan (NIDEK Co Ltd, Gamagori, Japan), for 6 mm pupils. It is unclear what Zernike term(s) were used to calculate SA in this manuscript, but it was found to be similar in both groups. However, the age difference between the two groups was statistically significant, so this may have confounded the results. For Asians, mean SA was 0.172 ± 0.293 μm, while for non-Asians it was 0.192 ± 0.341 μm.

The aberration profiles of 166 Chinese myopic right eyes were assessed in 2006 by Wei *et al.* [112], for a 6 mm dilated pupil; mean subject age was 32.1 ± 6.2 yr. Aberrations were measured using the HSWFS-based Bausch & Lomb Zywave. On average, the total RMS for HOA (3rd- to 5th-order) came out at 0.49 ± 0.16 μm. In agreement with previous studies [10, 15, 41–43, 74, 90–92], 3rd-order RMS was largest of the aberrations, followed by 4th-order RMS. SA was found to be the dominant individual aberration, with an average of 0.23 ± 0.14 μm. SA was found

to be significantly correlated with age, whereas total RMS was not. Total RMS was also not significantly correlated with myopia.

The relationship between HOA and intraocular pressure was examined in 2007 by Qu *et al.* [113], who imaged 70 myopic subjects aged 18–37 yr (mean = 25.7 yr). Aberrations were measured using a HSWFS, specifically a wavefront aberration supported corneal ablation wavefront analyser (Complete Ophthalmic Analysis System, Carl Zeiss Meditec). Aberrations were reported as Zernikes up to 7th-order for 6 mm pupils, according to the OSA standard. In agreement with previous studies, SA was positive and significantly different from zero, with a mean value of $Z12 = 0.09 \pm 0.11$ μm; furthermore, ocular SA was found to correlate significantly with intraocular pressure. Interestingly, in this study, some subjects showed negative *corneal* SA, seen in their Fig. 2A. Ocular SA was found to be negative in 23% of right eyes and 24% of left eyes, seen in their Fig. 2B.

Also in 2007, Sheehan *et al.* [114], measured the on-axis properties of 60 eyes and off-axis measurements on 31 eyes. The subjects in this study ranged in age from 12 to 57 yr, with a mean of 25.7 yr; results are given for a 6 mm pupil diameter and in the OSA standard format [115]. This study again found a large inter-subject variability in aberrations of the eye. For the 60 eyes and 6 mm pupil, the mean SA coefficient for Z_4^0 was 0.00 ± 0.16 μm. While other studies have found slightly positive values in the younger eye [7, 36, 71], it is possible that the relatively small sample size in this study is responsible for the difference.

The 2008 study of Atchison and Markwell [116] reports on-axis aberrations and horizontal peripheral refraction measurements of one eye of 106 emmetropic individuals ranging in age from 19 to 70 yr. The subjects were arranged such that there were approximately 20 in each of the age groups: 18–29, 30–39, 40–49, 50–59 and 60–69. The ANSI standard was used for aberration analysis.

This study begins by referencing previous findings that that total HOA show an age-related increase [20, 22, 52, 56, 107], including changes in anterior corneal aberrations and aberrations of the internal surfaces [20, 27, 44, 45, 53]. They reference the study of Brunette *et al.* [26], finding that aberrations seemed to be minimised at the age of approximately 30 yr. Specifically, SA has been found to become more positive with age [13, 20, 22, 52]. Atchison and Markwell [116] indicate that the three-dimensional relationship between age, refractive power and aberrations may

have an influence on these aforementioned results. Of the studies investigating the effects of ammetropia on aberrations [9, 11, 16, 18, 19, 68–70], some found that myopes have larger amounts of aberrations than emmetropes. However, care must be taken when analysing these results for the same reason elucidated by Atchison and co-workers [69, 73] and referenced in Plainis and Pallikaris [84]—namely, using corrective lenses when examining myopes can lead to the erroneous overestimation of SA. The finding of Llorente *et al.* [14] in 2004 that hyoperopes showed larger amounts of aberrations than myopes was not found by Artal *et al.* in 2006 [28].

This study by Atchison and Markwell [116] shows, for a 5 mm pupil, an age-related increase of 26% in RMS of HOA over the range of ages. 4th- and 6th- order aberrations also changed significantly with age. For most individuals, SA $C(4,0)$ was positive. Statistical analysis showed that SA did not increase significantly with age, having a slope of 0.0004 μm/yr; the mean was significantly different from zero, with a value of 0.061 ± 0.062 μm, and in agreement with the literature [7, 36]

In the discussion of this manuscript, the authors point out the difference between cross-sectional and longitudinal aberration studies. The current study is a cross-sectional one, meaning that it does not take into account the changing refraction of the population with age. For example, it is known that the eye shows a hypermetropic shift with age [117–119]. If an old eye is emmetropic, it is unclear if that eye was myopic as a young eye and approached emmetropia with an age-related hypermetropic shift, or if the eye was emmetropic throughout its lifetime.

The aberration profiles of 44 British Asians (22 female, 22 male, mean age 20.73 ± 2.37 yr) and 30 Caucasians (16 female, 14 male, mean age 24.80 ± 4.40 yr) were measured in 2008 by Cerviño *et al.* [120]. The individuals were generally myopic, whose aberrations were measured using the HSWFS technique for 5 mm entrance pupil diameters. The British Asians had a mean SA (Z_4^0) value of 0.020 ± 0.042 μm, with a range of -0.052 μm to 0.135 μm. The Caucasians had a mean SA (Z_4^0) value of 0.053 ± 0.061 μm, with a range of -0.045 μm to 0.228 μm. After statistical analysis, ethnicity was found to account for 8.4% of the variance of SA, indicating that ethnicity is strongly linked to SA—British Asians had less than half the amount of SA as Caucasians. The authors also found a large inter-subject variability as

noted in previous studies. Worthy of note is the fact that the myopic nature of subjects may have affected the results.

The large-scale 2008 study of Plainis and Pallikaris [84] reports the HOA of 393 eyes of 218 individuals, under natural conditions for a 6 mm pupil, measured with the WaveLight WaveFront Analyser. The aberrations were presented as Zernikes, using the OSA standard. The subjects ranged in age from 21 to 42 yr, with an average of 33.0 ± 4.8 yr. Inter-subject variability manifested as a significant variance in all coefficients of the Zernike terms. As with other studies, the average of most Zernike terms tended towards zero, excluding SA ($c_4^0 = 0.037$ μm) and oblique trefoil ($c_3^{-3} = -0.062$). The average RMS of higher-order aberrations came out at 0.26 μm, which amounts to 0.20 D of defocus.

They found an age-related increase in higher-order RMS in individuals who were pre-presbyopic. Age-related changes were also found for coma, whereas SA was not affected. The changes in coma-like aberrations can be attributed to corneal changes, as suggested by previous studies [27, 39, 53, 121]. The lack of change in SA for the particular age-range studied (21 to 43 yr) is in agreement with previous studies which show that SA does not begin to increase until approximately 40 years of age [26, 102, 121]. This perhaps suggests that any changes in the lens structure before 40 yr do not affect SA [121], or that the cornea undergoes similar but opposite changes in terms of SA [44].

In general, they found that emmetropes had smaller individual and combined higher-order aberrations than published values for myopic eyes. As with the study of Applegate *et al.* [52], they proposed that senile pupillary miosis helps to reduce the effect of age-related increase in aberrations [21, 122, 123].

In the case of SA specifically, the average for the 199 right eyes was $c_4^0 = 0.035 \pm 0.098$ μm, whereas the 194 left eyes was $c_4^0 = 0.038 \pm 0.090$ μm. These findings are backed up by previous large-scale studies, in which average SA is non-zero and positive [35]. However, the average value of SA found is significantly smaller than that found by previous investigations [7, 10, 36, 39, 44]. The authors put this disparity down to the large percentage of eyes in the current study that contained negative SA—37% of the right eyes and 35% of the left eyes showed negative SA.

It is important to note that the results of this study were obtained in a manner different to that of other studies [26, 36, 45], as those studies used trial lenses to counteract the subjects' sphero-cylindrical error. Plainis and Pallikaris [84] refer-

ence the work of Atchison and Charman [73] who showed in 2005 that, in particular cases, SA can be artificially increased by as much as 50%.

The HOA of Indian subjects (80 male) were measured in 2008 by Prakash *et al.* [124]. They measured 412 eyes of 206 individuals aged between 18 and 34 yr, with a mean of 23.63 ± 1.99 yr. Aberrations were measured for 6 mm pupils using the Zywave instrument (Bausch & Lomb), which uses a HSWFS, and were reported up to 5th-order using the OSA standard. In agreement with previous studies, most aberration terms averaged near zero. The mean (signed) value of SA ($Z(0,4)$) was -0.007 ± 0.08 μm, with a range of -0.25 to 0.54 μm. The mean absolute value of SA was 0.057 ± 0.05 μm.

Also in 2008, Won *et al.* [125] measured HOA in 54 eyes of 27 subjects using two different instruments: the iTrace (Tracey Technologies, Texas, USA) and OPD-Scan (NIDEK, Japan). Mean subject age was 27 ± 7 yr. Aberration calculations of the two instruments were compared for 4 mm and 6 mm diameter pupils, after dilation with tropicamide 0.5%. For the 4 mm pupil size, the two instruments produced significantly different values for ocular SA ($Z(4,0)$), with the iTrace giving $Z(4,0) = 0.038 \pm 0.043$ μm and OPD-Scan giving 0.011 ± 0.039 μm. The two instruments produced similar total ocular aberrations for the 6 mm pupil, with iTrace giving $Z(4,0) = 0.164 \pm 0.161$ μm and OPD-Scan giving 0.111 ± 0.244 μm.

In 2009, Athaide *et al.* [29] examined HOA in 630 eyes of 315 subjects, of which 155 were male. Mean subject age was 31 ± 16 yr, with a range of 5–64 yr. Patients were sub-divided into four age-dependent groups: 68 aged 5–14 yr; 55 aged 15–24 yr; 116 aged 25–44 yr; and 76 aged 45–67 yr. Aberrations were measured using the LADARWave® instrument (Alcon Laboratories Inc, Orlando, FLA, USA), based on the HSWFS, up to 6th-order for 6.5 mm pupil. It is unclear whether HOA data were obtained before or after cycloplegia. Ocular SA was found to increase with age, due to the contribution of the internal optics. 50% of children showed negative SA values, with a median of 0.02 μm. The median value of SA increased to 0.26 μm in the middle-aged adult group. These results for SA are summarised in their Fig. 4, and are compared to the work of Kirwan *et al.* who, in 2006, reported that 84.6% of children had negative SA [30].

Bao *et al.* [82], in 2009, measured HOA in 75 young emmetropes aged 18–33 yr (mean: 21.7 ± 3.4 yr) and 196 young myopes aged 18–38 (mean: 25.2 ± 5.0 yr.

Corneal aberrations were measured with an ATLAS system, while ocular aberrations were obtained with a HSWFS system, for 6 mm pupils. From their Tables 2 & 3, we can see that the average SA (Z_4^0) for both eyes of the 76 emmetropes was significantly different from zero, at 0.137 ± 0.122 μm. Table 4 shows that total ocular SA for the myopes was also significantly different from zero, with a value of 0.079 ± 0.111 μm.

The aberrations of a Chinese population were measured in 2009 by Lim and Fam [126], for 70 right eyes of 18 men and 58 women, to assess ethnic differences in HOA. The individuals ranged in age from 21.97 to 52.13 yr, with a mean of 31.44 ± 6.18 yr. Aberrations were measured with a HSWFS, reported for 6 mm pupils. Mean SA ($Z(4,0)$) was 0.200 ± 0.170 μm. Their Table 2 contains a useful summary of previous HOA measurements of different ethnicities, performed using a HSWFS. The authors noted the usual trend of large inter-subject variability, and concluded that ocular aberrations in south-east Asian Chinese eyes are significantly larger than in other populations.

The on- and off-axis aberrations of 43 normal eyes of 43 individiuals (25 male), aged 19 to 66 yr, with an average age of 31.5 yr were measured in 2009 by Lundström *et al.* [127]. Aberrations were measured using a HSWFS and reported according to the ANSI standard. For a 5 mm pupil, they found on-axis SA (c_4^0) to have an average of 0.069 ± 0.054 μm.

The repeatability of the iTrace ray tracing aberrometer was assessed in 2011 by Piñero *et al.* [128], who imaged 22 eyes (4 left and 18 right) of 22 normal patients, aged 21–65 yr. The eye was examined under far and near viewing conditions, with respective focusing distances of 5 m and 40 cm, for 3 mm pupils without cycloplegia. The iTrace instrument calculates aberrations as standardised Zernikes polynomials. While the main aspect of this paper is the repeatability of the aberrometer, we can use the average data to estimate aberrations of the eye. In Table 1 of this manuscript, the average SA values are given for distance and near vision as 0.019 ± 0.012 μm and 0.017 ± 0.008 μm, respectively. It is well known that SA shows a negative trend with accommodation; however, the SA of this study did not decrease significantly between the two viewing distances. This could be due to the fact that a relatively large range of ages was studied—the large range of ages means that age-related trends in SA affect the mean value, and also may

conceal any accommodative change in SA. Furthermore, the relatively small pupil diameter of 3 mm may have affected the results, as Iida *et al.* [62] found significant differences with accommodation in SA, when using the same instrument, for 4 mm diameter pupils.

In 2012, the effects of cycloplegia, and scotopic and photopic viewing conditions on HOA were assessed by Fan *et al.* [129]. They imaged 174 eyes of 105 patients (48 male) ranging in age from 18 to 30 yr, with an average of 22 yr. The individuals examined were candidates for myopic or myopic astigmatic LASIK surgery. Aberrations were measured with the WaveScan® (AMO, Santa Clara, CA, US), which uses a HSWFS. In this study, the use of natural pupil sizes means that the pupil may have affected the SA results, and this makes direct comparison difficult. The pupil sizes for the three viewing conditions were as follows. Cycloplegic: 8.58 ± 0.54 mm; scotopic: 7.53 ± 0.69 mm; and photopic: 6.08 ± 1.14 mm.

Dilation of the pupil by pharmacological agent statistically significantly increased the value of SA (Z_4^0). Also, Z_4^0 was found to be significantly higher in the scotopic group. The values of Z_4^0 for the different viewing conditions were as follows. Cycloplegic: $Z_4^0 = 0.111 \pm 0.146$ μm; scotopic: $Z_4^0 = 0.066 \pm 0.149$ μm; and photopic: $Z_4^0 = 0.043 \pm 0.106$ μm.

Hashemian *et al.* [130] carried out a large study of 2,390 Iranian myopic eyes (1,641 female) in 2012. The subjects were divided into two age-dependent groups: $<$ 30 yr and $>$ 30 yr. Aberrations were calculated for 6 mm pupils using the Zywave instrument, based on the HSWFS, after pupil dilation with tropicamide 0.5%. Males and females were found to have statistically similar aberration profiles. It is unclear to what TSA refers in this paper, but the value for the younger group is 0.13 μm, while the older group is 0.17 μm.

The aberration profiles of Mexicans were examined in 2013 by Tepichín-Rodríguez *et al.* [131], who measured HOA in 71 eyes of 38 males. Mean subject age was 25 yr, and the eyes were untreated. Aberrations were measured for 6 mm pupils, and were reported as Zernikes in ANSI form. In line with other studies, most aberration coefficients were found to average to approximately zero, and 3rd-order terms contributed most to the RMS wavefront error. The mean value of SA ($Z(0,4)$) was -0.018 ± 0.117 μm, with a range of -0.502 μm to 0.502 μm. The mean absolute value (ignoring signs) was 0.081 ± 0.086 μm.

In 2014, Dias-Santos *et al.* [132] conducted a study on 74 eyes of 38 children. The children were split up into two groups depending on their type of amblyopia ("lazy eye"), with one control group with normal visual development. The children were fully examined after administration of cyclopentolate 1%. Aberrations were measured using an OPD-Scan III (NIDEK, Japan) for a 6 mm pupil. The mean age of all subjects was 9.8 yr (range: 5–16 yr), of which 23 were male. Although the subjects were split into 3 groups, the authors did not find any statistically significant difference in SA among the groups. For this reason, we can combine all SA value to give an overall Zernike SA mean of 0.11 ± 0.18 μm.

Also in 2014, Hiraoka *et al.* [133] determined the effect of cycloplegia on aberrations in the right eyes of 28 myopic children aged 3–12 yr, with a mean of 7.25 ± 2.55 yr. The measured aberrations were reported as Zernikes measured up to 6th-order on a 6 mm pupil.

Their Table 1 gives the changes in each Zernike component, before and after administration of the cycloplegic. Spherical aberration (C_4^0) showed a significant increase from 0.033 ± 0.015 μm to 0.050 ± 0.015 μm. The authors investigated whether this change in SA was significantly correlated with patient age, refractive ametropia and change in ametropia (caused by administering the cycloplegic agent), but it was found not to be. In agreement with the work of Artal and colleagues, the authors found that corneal aberrations were compensated (at least in part) by the internal optics; also, large inter-subject variability in aberrations was found.

The observation that cycloplegic agents affect HOA has been found previously by Carkeet *et al.* [134], albeit the subjects were of a different age. Hiraoka *et al.* say that, before their study [133], only one other study has investigated the effect of cyclopentolate on HOA in children—Kirwan *et al.* found in 2006 that there was scarcely any effect on HOA in children aged 4–14 yr. Regarding adults, Jankov *et al.* [110] found no significant effect of cycloplegia on HOA, in 2006.

Monochromatic HOA were studied in an Arab population for the first time in 2016 by Prakash *et al.* [135], who measured HOA in two groups with different ethnicities and statistically similar ages and refractive errors. Group 1 contained 200 Arab individuals (112 female) with a mean age of 29.6 ± 8.5 yr, and group 2 contained 200 South-Asian individuals (126 female) with a mean age of 30.2 ± 8.9 yr. Aberrations were measured using the HSWFS-based iDesign instrument (AMO,

Santa Ana, CA, USA) without pupil dilation, and reported for 6 mm pupils according to the ANSI standard. The signed and absolute means of SA (Z_4^0) were not significantly different between the two ethnicities, and SA was significantly different from zero. The means of SA (Z_4^0) for both groups were as follows. Group 1: signed $= 0.066 \pm 0.17$ μm, absolute $= 0.123 \pm 0.14$ μm; group 2: signed $= 0.047 \pm 0.17$ μm, absolute $= 0.130 \pm 0.12$ μm.

Table 4: Summary of the literature on total SA

Study/Method	Number of Eyes	Mean Age or Range (Years)	Ocular Z_4^0 (μm)	Pupil Dia. (mm)
Calver et al. [21]/CA (1999)	15	24	0.095	6
	15	68	0.175	6
Porter et al. [7]/HS (2001)	218	42	0.138	5.7
Carkeet *et al.* [19]/HS (2002)	546	9	0.055	5
Castejón-Mochón *et al.* [39]/HS (2002)	108	24	0.008	5
Guirao *et al.* [88]/HS (2002)	109	41	0.13	5.7
Ninomiya *et al.* [89]/HS (2002)	33	29	0.02	4
	33	29	0.11	6
Thibos et al. [36]/HS (2002)	200	26	0.120	6
Carkeet *et al.* [74]/HS (2003)	67	6	0.06	5
He et al. [93]/PM (2003)	90	18	0.060	6.3
Wang *et al.* [90]/DS (2003)	102	22	0.09	6
Cheng *et al.* [71]/HS (2004)	74	25	0.065	5
Atchison [95] (review) (2005)	—	—	0.10	6
Wang and Candy [109]/HS (2005)	17	5–7 wk	0.03	3
Jankov *et al.* [110]/TA (2006)				
after cyclopentolate	151	33	0.098	7
after phenylephrine	151	33	−0.026	7

Continued on next page

Table 4 – *Continued from previous page*

Study/Method	# Eyes	Age	Z_4^0	Pupil
Nakano *et al.* [111]/DS (2006)				
Asian	384	33	0.172	6
non-Asian	264	31	0.192	6
Wei *et al.* [112]/HS (2006)	166	32	0.23	6
Qu *et al.* [113]/HS (2007)	140	26	0.09	6
Sheehan *et al.* [114]/HS (2007)	60	26	0.00	6
Atchison and Markwell [116]/HS (2008)	106	19–70	0.061	5
Cerviño *et al.* [120]/HS (2008)				
British Asian	44	21	0.020	5
Caucasian	30	25	0.053	5
Plainis and Pallikaris [84]/TA (2008)	393	33	0.037	6
Prakash *et al.* [124]/HS (2008)	412	24	−0.007	6
Won *et al.* [125]/LR (2008)	54	27	0.164	6
Won *et al.* [125]/DS (2008)	54	27	0.111	6
Bao *et al.* [82]/HS (2009)				
emmetropes	150	22	0.137	6
myopes	392	25	0.079	6
Lim and Fam [126]/HS (2009)	70	31	0.200	6
Lundström *et al.* [127]/HS (2009)	43	32	0.069	5
Piñero *et al.* [128]/LR (2011)	22	21–65	0.019	3
Fan *et al.* [129]/HS (2012)				
cycloplegic	174	22	0.111	8.58
scotopic	174	22	0.066	7.53
photopic	174	22	0.043	6.08
Tepichín-Rodríguez *et al.* [131]/DS (2013)	71	25	−0.018	6

Continued on next page

Table 4 – *Continued from previous page*

Study/Method	# Eyes	Age	Z_4^0	Pupil
Dias-Santos *et al.* [132]/DS (2014)	74	10	0.11	6
Hiraoka *et al.* [133]/HS (2014)	28	7	0.033	6
after cycloplegia			0.050	5
Prakash *et al.* [135]/HS (2016)				
Arab	400	30	0.066	6
south-Asian	400	30	0.047	6

[a]CA, crossed-cylinder aberroscope; CS, contrast sensitivity; DS, dynamic skiascopy; LR, Laser raytracing; PM, psychophysical methods; HS, Hartmann-Shack; TA, Tscherning aberrometer.

2.7 CONCLUDING REMARKS

The figures and tables of the preceding sections summarise, as expected, that there is no exact answer for SA of the human eye. From the summary of Fig. 4 in Section 2.4, the average value of SA at 30 years of age is 0.056 µm, with a slope of 0.002 µm/yr; both for a 5 mm pupil—this average omits the large study of Salmon and van de Pol.

In addition to the large inter-subject variability outlined in the review above, the figures highlight also a large inter-study variability. There are many factors that can affect the results of a study, the most obvious of which are subject age, gender, ethnicity, ametropia and medication; instrument used; and measurement protocol. While there are no definitive answers on the correlation between some of these factors and SA, their possible effects are not to be ignored. Furthermore, the vast majority of studies are cross-sectional, so the typical age-related changes in ocular biometry cannot be fully understood. For example, a young myopic eye might grow to be an emmetropic eye in old age. Hence, emmetropic young eyes might not correspond to emmetropic old eyes, and cross-sectional studies on the age-related changes of SA in emmetropic eyes might not represent the true SA trend. To mitigate some of these confounding effects, the 2006 compilation study of Salmon and van de Pol, described above, could be used [35]. In this study, data were collected from 10 studies that measured HOA using a HSWFS

in a total of 2560 eyes. They provide a polynomial fit for SA vs age, shown as the thick purple line in Figs. 3 & 4. The polynomial fit was calculated as $y = 0.000045 \times \text{age}^2 - 0.002038 \times \text{age} + 0.06408$. We will be using this polynomial fit, together with the data average of Section 2.4—which excludes Salmon and van de Pol, mentioned in the preceding paragraph—as the basis for constructing a generic ageing eye model in Chapter 6.

3

METHODS

3.1 THE DIFFERENTIAL RAY EQUATION AND THE CALCULUS OF VARIATIONS

3.1.1 *Introduction*

We start by first defining the ray equation, and subsequently show its derivation using both the *eikonal equation* and *the calculus of variations*. The ray equation of light rays in a medium of gradient index is given by:

$$\frac{d}{ds}\left(n\frac{d\mathbf{r}}{ds}\right) = \nabla n,$$

where $\mathbf{r}(s)$ denotes the position vector of a point P on a ray, s is the length of arc of the ray and $n = n(\mathbf{r})$ is the refractive index distribution. This nomenclature is shown schematically in Fig. 5.

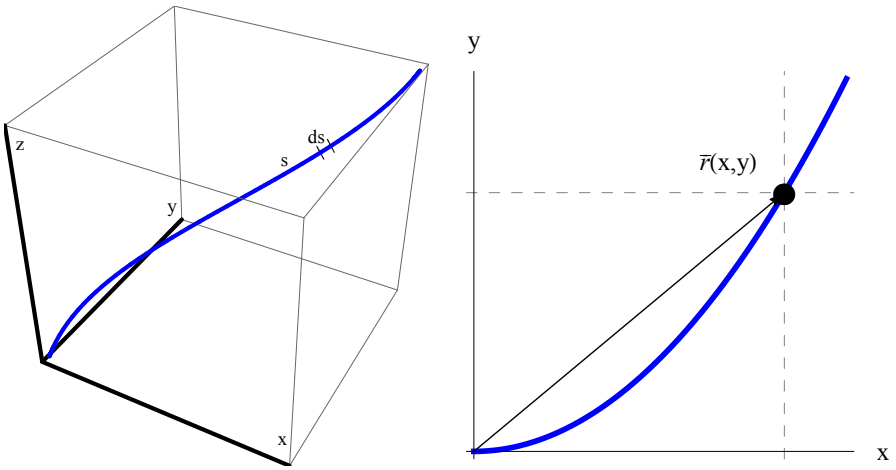

(a) Ray trajectory in 3D, showing arc s.

(b) Ray trajectory in 2D, showing the position vector **r**.

Figure 5: Schematic diagrams of the ray trajectory.

In three dimensions, the ray equation takes the form:

$$\frac{d}{ds}\left(n\frac{dx}{ds}\right) = \frac{\partial n}{\partial x}, \quad \frac{d}{ds}\left(n\frac{dy}{ds}\right) = \frac{\partial n}{\partial y}, \quad \frac{d}{ds}\left(n\frac{dz}{ds}\right) = \frac{\partial n}{\partial z}.$$

3.1.2 *The Ray Equation from the Eikonal and Maxwell's Equations*

The following derivation relies heavily on the work of Born and Wolf [136].

In a nonconducting isotropic medium, we consider a general time-harmonic field

$$\mathbf{E}(\mathbf{r}, t) = \mathbf{E}_0(\mathbf{r})e^{-i\omega t}, \tag{1}$$

$$\mathbf{H}(\mathbf{r}, t) = \mathbf{H}_0(\mathbf{r})e^{-i\omega t}, \tag{2}$$

where $\mathbf{E}_0$ and $\mathbf{H}_0$ denote complex vector functions of positions representing electric and magnetic fields, and will satisfy Maxwell's equations in their time-independent form. In free space, the charge density (ρ) and current density $(\mathbf{j})$ both equal to zero; hence, Maxwell's equations are

$$\nabla \times \mathbf{H}_0 + ik_0\epsilon\mathbf{E}_0 = 0, \tag{3}$$

$$\nabla \times \mathbf{E}_0 - ik_0\mu\mathbf{H}_0 = 0, \tag{4}$$

$$\nabla \cdot \epsilon\mathbf{E}_0 = 0, \tag{5}$$

$$\nabla \cdot \mu\mathbf{H}_0 = 0. \tag{6}$$

In regions sufficiently far away from a source $(r \gg \lambda_0)$, more general types of fields may be represented in the form

$$\mathbf{E}_0 = \mathbf{e}(\mathbf{r})e^{-ik_0S(\mathbf{r})}, \qquad \mathbf{H}_0 = \mathbf{h}(\mathbf{r})e^{-ik_0S(\mathbf{r})}, \tag{7}$$

where the *optical path* $S(\mathbf{r})$ is a real scalar function of position. The vectors $\mathbf{e}(\mathbf{r})$ and $\mathbf{h}(\mathbf{r})$ are also functions of position, and can be complex—complex $\mathbf{e}$ and $\mathbf{h}$ are required for the consideration of all possible polarisation states; real $\mathbf{e}$ and $\mathbf{h}$ correspond to linearly polarised fields. For small λ_0, it will be shown that S satisfies a differential equation independent of the amplitude vectors $\mathbf{e}$ and $\mathbf{h}$. Noting that $\mathbf{h}$ is a vector and the natural exponential function is a scalar, we can use the vector calculus identity for the product of a scalar (ψ) and a vector $(\mathbf{A})$

$$\nabla \times (\psi\mathbf{A}) = \psi\nabla \times \mathbf{A} + \nabla\psi \times \mathbf{A}$$

to find the curl of $\mathbf{H}_0$ in Eq. 7 above, giving

$$\nabla \times \mathbf{H}_0 = (\nabla \times \mathbf{h} + ik_0 \nabla S \times \mathbf{h})\, e^{-ik_0 S}.$$

Next, we find the divergence of $\mu\mathbf{H}_0$ by noting that we twice apply the identity

$$\nabla \cdot (\psi \mathbf{A}) = \mathbf{A} \cdot \nabla\psi + \psi \nabla \cdot \mathbf{A}$$

to give

$$\nabla \cdot \mu\mathbf{H}_0 = (\mu \nabla \cdot \mathbf{h} + \mathbf{h} \cdot \nabla\mu + ik_0 \mu \mathbf{h} \cdot \nabla S)\, e^{-ik_0 S},$$

with analogous expressions for $\nabla \times \mathbf{E}_0$ and $\nabla \cdot \epsilon\mathbf{E}_0$. We can hence transform Eqs. 3–6 to

$$\begin{aligned}
\nabla S \times \mathbf{h} + \epsilon \mathbf{e} &= \frac{i}{k_0} \nabla \times \mathbf{h}, \\
\nabla S \times \mathbf{e} - \mu \mathbf{h} &= \frac{i}{k_0} \nabla \times \mathbf{e}, \\
\mathbf{e} \cdot \nabla S &= \frac{i}{k_0} (\mathbf{e} \cdot \nabla \ln \epsilon + \nabla \cdot \mathbf{e}), \\
\mathbf{h} \cdot \nabla S &= \frac{i}{k_0} (\mathbf{h} \cdot \nabla \ln \mu + \nabla \cdot \mathbf{h}).
\end{aligned}$$

We are interested in the case of very small λ_0; hence k_0 is very large, and the right-hand side may be neglected, provided the multiplicative factors of i/k_0 are not exceedingly large. The equations then reduce to

$$\nabla S \times \mathbf{h} + \epsilon \mathbf{e} = 0, \tag{8}$$

$$\nabla S \times \mathbf{e} - \mu \mathbf{h} = 0, \tag{9}$$

$$\mathbf{e} \cdot \nabla S = 0, \tag{10}$$

$$\mathbf{h} \cdot \nabla S = 0. \tag{11}$$

Rearranging Eq. 9 for $\mathbf{h}$ and substituting into Eq. 8 gives

$$\nabla S \times \left(\frac{1}{\mu} \nabla S \times \mathbf{e} \right) + \epsilon \mathbf{e} = 0.$$

Recalling the vector triple product:

$$\mathbf{A} \times (\mathbf{B} \times \mathbf{C}) = (\mathbf{A} \cdot \mathbf{C})\, \mathbf{B} - (\mathbf{A} \cdot \mathbf{B})\, \mathbf{C},$$

the LHS of the equation above becomes:

$$\nabla S \times \left(\frac{1}{\mu}\nabla S \times \mathbf{e}\right) = \frac{1}{\mu}\left[(\nabla S \cdot \mathbf{e})\nabla S - (\nabla S)^2\mathbf{e}\right];$$

hence we have

$$\frac{1}{\mu}\left[(\mathbf{e}\cdot\nabla S)\nabla S - \mathbf{e}(\nabla S)^2\right] + \epsilon\mathbf{e} = 0.$$

The first term above vanishes in accordance with Eq. 10 to give

$$(\nabla S)^2 = n^2,$$

where $n = \sqrt{\epsilon\mu}$ is the refractive index. This equation is stated fully as

$$\left(\frac{\partial S}{\partial x}\right)^2 + \left(\frac{\partial S}{\partial y}\right)^2 + \left(\frac{\partial S}{\partial z}\right)^2 = n^2(x, y, z).$$

This is known as the *eikonal equation*, and forms the basis of geometrical optics. The scalar S is the *eikonal*, where surfaces of constant $S(\mathbf{r})$ are the *geometrical wavefronts*.

Here we have derived the eikonal using the first-order Maxwell's equations, but it may also be derived from the second-order wave equation, which itself is derived from Maxwell's equations. To do this, we begin with Maxwell's equations in free space

$$\nabla \times \mathbf{H} - \frac{1}{c}\dot{\mathbf{D}} = 0, \tag{12}$$

$$\nabla \times \mathbf{E} + \frac{1}{c}\dot{\mathbf{B}} = 0, \tag{13}$$

$$\nabla \cdot \mathbf{D} = 0, \tag{14}$$

$$\nabla \cdot \mathbf{B} = 0, \tag{15}$$

and we also note the constitutive relations

$$\mathbf{j} = \sigma\mathbf{E}, \tag{16}$$

$$\mathbf{D} = \epsilon\mathbf{E}, \tag{17}$$

$$\mathbf{B} = \mu\mathbf{H}. \tag{18}$$

We substitute Eq. 18 into Eq. 13, divide by μ and take the curl, to give

$$\nabla \times \left(\frac{1}{\mu}\nabla \times \mathbf{E}\right) + \frac{1}{c}\nabla \times \dot{\mathbf{H}} = 0. \tag{19}$$

Next, take the time derivative of Eq. 12, use the constitutive relation of Eq. 17, and replace $\nabla \times \dot{\mathbf{H}}$ using Eq. 19 to give

$$\nabla \times \left(\frac{1}{\mu}\nabla \times \mathbf{E}\right) + \frac{\epsilon}{c^2}\ddot{\mathbf{E}} = 0. \tag{20}$$

Using the vector identity

$$\nabla \times (\psi \mathbf{A}) = \psi \nabla \times \mathbf{A} + \nabla\psi \times \mathbf{A},$$

followed by

$$\nabla \times (\nabla \times \mathbf{A}) = \nabla(\nabla \cdot \mathbf{A}) - \nabla^2 \mathbf{A},$$

we can expand $\nabla \times \left(\frac{1}{\mu}\nabla \times \mathbf{E}\right)$ to transform Eq. 20 into

$$\nabla^2 \mathbf{E} - \frac{\epsilon\mu}{c^2}\ddot{\mathbf{E}} + (\nabla \ln \mu) \times \nabla \times \mathbf{E} - \nabla(\nabla \cdot \mathbf{E}) = 0, \tag{21}$$

noting that

$$-\nabla \ln \mu = \nabla \ln\left(\frac{1}{\mu}\right) = \mu\nabla\left(\frac{1}{\mu}\right).$$

Using the constitutive relation of Eq. 17 again, together with Eq. 14 and the vector calculus identity

$$\nabla \cdot (\psi \mathbf{A}) = \mathbf{A} \cdot \nabla\psi + \psi\nabla \cdot \mathbf{A},$$

we find that

$$\epsilon\nabla \cdot \mathbf{E} + \mathbf{E} \cdot \nabla\epsilon = 0.$$

Rearranging, we find that

$$\nabla \cdot \mathbf{E} = -\frac{1}{\epsilon}\mathbf{E} \cdot \nabla\epsilon = -\mathbf{E} \cdot \nabla \ln \epsilon.$$

We substitute this into Eq. 21 to give the wave equation of motion

$$\nabla^2 \mathbf{E} - \frac{\epsilon\mu}{c^2}\ddot{\mathbf{E}} + (\nabla \ln \mu) \times \nabla \times \mathbf{E} + \nabla(\mathbf{E} \cdot \nabla \ln \epsilon) = 0, \tag{22}$$

with a similar equation found for $\mathbf{H}$ alone. If the medium is homogeneous, the equation reduces to

$$\nabla^2\mathbf{E} - \frac{\epsilon\mu}{c^2}\ddot{\mathbf{E}} = 0.$$

Finally, we can substitute Eqs. 1, 2 and 7 into Eq. 22 to find the expression

$$\mathbf{K}(\mathbf{e}, S, n) + \frac{1}{ik_0}\mathbf{L}(\mathbf{e}, S, n, \mu) + \frac{1}{(ik_0)^2}\mathbf{M}(\mathbf{e}, \epsilon, \mu) = 0,$$

where

$$\begin{aligned}
\mathbf{K}(\mathbf{e}, S, n) &= (n^2 - (\nabla S)^2)\mathbf{e}, \\
\mathbf{L}(\mathbf{e}, S, n, \mu) &= (\nabla S \cdot \nabla \ln \mu - \nabla^2 S)\mathbf{e} - 2(\mathbf{e} \cdot \nabla \ln n)\nabla S - 2(\nabla S \cdot \nabla)\mathbf{e}, \\
\mathbf{M}(\mathbf{e}, \epsilon, \mu) &= \nabla \times \mathbf{e} \times \nabla \ln \mu - \nabla^2\mathbf{e} - \nabla(\mathbf{e} \cdot \nabla \ln \epsilon).
\end{aligned}$$

Since we are interested in large k_0, only $\mathbf{K}$ is retained; thus $\mathbf{K} = 0$ and we again have the eikonal equation

$$(\nabla S)^2 = n^2.$$

As a consequence of the eikonal equation, we can define a unit vector $\mathbf{s}$

$$\mathbf{s} = \frac{\nabla S}{n} = \frac{\nabla S}{|\nabla S|}.$$

We have seen that $\mathbf{r}(s)$ denotes the position vector of a point P on a ray, as a function of the arc length s along the ray. Hence, $d\mathbf{r}/ds = \mathbf{s}$ and we can write

$$n\frac{d\mathbf{r}}{ds} = \nabla S. \tag{23}$$

Equation 23 above defines the path of light rays in terms of the scalar function S. However, we would like to define the ray paths as a function of refractive index $n(\mathbf{r})$; we can do this by deriving the differential ray equation as follows.

Taking the derivative of Eq. 23 with respect to s we obtain

$$\frac{d}{ds}\left(n\frac{d\mathbf{r}}{ds}\right) = \frac{d}{ds}(\nabla S).$$

Applying the chain rule:

$$\frac{d}{ds} = \frac{d\mathbf{r}}{ds}\frac{d}{d\mathbf{r}} = \frac{d\mathbf{r}}{ds}\nabla$$

to the right-hand side of the equation above, we have

$$\begin{aligned}\frac{d}{ds}\left(n\frac{d\mathbf{r}}{ds}\right) &= \frac{d\mathbf{r}}{ds}\cdot\nabla(\nabla S),\\ &= \frac{1}{n}\nabla S\cdot\nabla(\nabla S),\end{aligned}$$

where we used Eq. 23 in the last line. Next, we note from the chain rule that

$$\nabla(\nabla S)^2 = 2\nabla S\cdot\nabla(\nabla S),$$

hence we can simplify the right-hand side of the above to give

$$\begin{aligned}\frac{d}{ds}\left(n\frac{d\mathbf{r}}{ds}\right) &= \frac{1}{2n}\nabla(\nabla S)^2\\ &= \frac{1}{2n}\nabla n^2,\end{aligned}$$

where $(\nabla S)^2 = n^2$ is given by the definition of the eikonal equation. Finally, noting the calculus relation $\nabla n^2 = 2n\nabla n$, we arrive at the equation

$$\frac{d}{ds}\left(n\frac{d\mathbf{r}}{ds}\right) = \nabla n.$$

This is the differential equation of light rays in a gradient index medium. In the case of a homogeneous medium, n does not depend on the spatial co-ordinates; hence, $\nabla n = 0$ and the equation reduces to

$$\frac{d^2\mathbf{r}}{ds^2} = 0,$$

from which $\mathbf{r} = s\mathbf{a} + \mathbf{b}$. We therefore see that, in homogeneous media, light travels in straight lines.

In the next section, we will derive the differential ray equation using the calculus of variations.

3.1.3 *The Ray Equation from the Calculus of Variations*

The field of calculus deals with functions and exercises involved in finding the maxima or minima of a particular function. Such points of interest are called *extrema*, and we recall that the existence of an extremum depends on a particular

variable, or set of variables. However, the calculus of variations deals with *functionals*, which are functions of functions of variables—the functional itself can also depend directly upon the variable(s) in question. Functionals have maxima and minima that therefore depend on a function, and not just on variables alone; the functions for which this situation occurs are called *extremals*.

To illustrate the difference between the two fields of study in two-dimensional space, we first consider the very familiar function notation $y = y(x)$ in the cartesian plane, with y as the ordinate and x as the abscissa. This arbitrary function will have extrema depending on the variable x. Next, we consider two points in the (x, y) plane joined by the arbitrary curve $y = y(x)$. We can calculate the length of this curve and its associated maxima/minima, by noting that the length of the curve depends on the *whole* path of the function $y(x)$, and not just the variable x alone. Hence, we see that the extrema of the functional are obtained for a particular function $y(x)$, called the extremal. Problems in the calculus of variations are hence associated with finding such extremals.

The above problem belongs to a famous family of problems that involve, in general, minimising the path between two points. The most familiar case of constant "potential" has the solution of a straight line—we shall see shortly what is the meaning of this potential and also the trivial straight-line solution. Perhaps the most famous problem is known as the *brachistochrone problem* and was one of the earliest posed in the calculus of variations. The problem involves minimising the time taken for a particle to slide, without friction, along a path under the influence of gravity by selecting the appropriate path. Historically, the problem was originally erroneously solved by Johann Bernoulli. After posing the problem in *Acta Eruditorum* in June, 1696, five mathematicians responded with solutions, among which were and Isaac Newton and Jakob Bernoulli (Johann's brother). Newton stayed up all night to find the solution and mailed it in the following post, or so the story goes. Jakob Bernoulli, not to be outdone, posed a more difficult version of the problem; the solution of which helped to develop mew methods subsequently refined and termed the *calculus of variations* by Leonhard Euler. David Hilbert did much to modernise the subject [137], with books written by him and Richard Courant on the subject, both independently and collaboratively [138, 139].

In an attempt to first put some plain English on the subject, we consider a string C linking two points (the shortest distance between which is a straight line). In this example, stretching the string by an amount perpendicular to the line joining

the two points will result in a longer path. We see that the new 'stretched' string is basically the original string, plus a new function (which we call η) that has a value of zero at the endpoints themselves, and has its maximum somewhere in between the two. This arbitrary 'variation' function results in a 'varied' curve C' between the points. The amount of variation depends on how much the string is stretched; we denote this amount of stretch by a small parameter ϵ. To summarise, we stretch the string by an amount ϵ, giving a new function $\epsilon\eta$, which we add to the original function; this function $\epsilon\eta$ disappears at the endpoints. Next, we point out that we do not know our original function C, since this is found by minimising the integral of the path between the two endpoints. We see that increasing ϵ increases the length of the curve. Conversely, we can say that the shortest path will be obtained when ϵ vanishes; we call this the *first variation*. Hence, if we take the integral of the path between the two endpoints along the curve C', take the derivative with respect to ϵ and equate ϵ to zero (the first variation vanishes), we will be left with the extremum of the path; that is, the derivative will equal to zero, and we are left with the *vanishing of the first variation*. This basic, hand-waving reasoning will form the basis of the calculus of variations to the level that we require. Henceforth, the formal notation will be adopted.

In the three-dimensional space (x, y, z), let $F(x, y, z, x', y')$ be a given function with continuous first- and second- partial derivatives, where the prime denotes differentiation with respect to z; and let C be any curve $x = x(z)$, $y = y(z)$ defined parametrically as a function of z. The integral

$$I = \int_{z_1}^{z_2} F(x, y, z, x', y')\, dz$$

is seen to depend on the curve C; that is, it is a function of the two functions $x(z)$ and $y(z)$—it is a functional. The fundamental problem of the calculus of variations is [138]:

Among all the functions that are defined and continuous and possess continuous first and second derivatives in the interval $z_1 \leqslant z \leqslant z_2$*, and for which the boundary points* $P_1[x_1 = x(z_1), y_1 = y(z_1), z_1]$ *and* $P_2[x_2 = x(z_2), y_2 = y(z_2), z_2]$ *are prescribed find the one for which the functional* I *has the least possible value (or the greatest possible value).*

The conditions that the extremal C must satisfy are determined by the aforementioned process of linear variation, for which we choose the function $\eta(z)$ vanishing at the endpoints z_1 and z_2 such that

$$\eta(z_1) = \eta(z_2) = 0.$$

We form the varied curve C′ by replacing x with $x + \epsilon\eta$, where ϵ is a small parameter defining the extent of variation. The integral I becomes a function of ϵ such that

$$I(\epsilon) = \int_{z_1}^{z_2} F(x + \epsilon\eta, y, z, x' + \epsilon\eta', y')\, dz\,.$$

Next, we differentiate the above expression with respect to ϵ. Using the chain rule for partial derivatives

$$\frac{dF}{d\epsilon} = \frac{\partial F}{\partial x}\frac{dx}{d\epsilon} + \frac{\partial F}{\partial x'}\frac{dx'}{d\epsilon},$$

we have the expression

$$(\delta I)_x = \left(\frac{dI}{d\epsilon}\right)_{\epsilon=0} = \int_{z_1}^{z_2} \left(\frac{\partial F}{\partial x}\eta + \frac{\partial F}{\partial x'}\eta'\right) dz \tag{24}$$

called *the first variation*. The condition for an extremum necessitates vanishing of the first variation, i.e. $(\delta I)_x = 0$. Using integration by parts

$$\int u\, dv = uv - \int v\, du,$$

we can transform the second term above to give

$$\int_{z_1}^{z_2} \frac{\partial F}{\partial x'}\eta'\, dz = \frac{\partial F}{\partial x'}\eta\Big|_{z_1}^{z_2} - \int_{z_1}^{z_2} \eta\frac{d}{dz}\frac{\partial F}{\partial x'}\, dz.$$

Noting that the function η vanishes at the endpoints z_1 and z_2, the first part on the right-hand side disappears. Hence, Eq. 24 becomes, adopting Lagrange's notation for the partial derivatives,

$$(\delta I)_x = \int_{z_1}^{z_2} \left(F_x - \frac{d}{dz}F_{x'}\right)\eta\, dz\,.$$

We obtain a similar expression for y by introducing a variation therein. Since we chose an arbitrary (i.e. non-zero) function η in the region $z_1 \leqslant z \leqslant z_2$, and as

a consequence of the above equation and the condition $(\delta I)_x = 0$, the term in parenthesis above must equal zero and so we arrive at *Euler's equations*

$$F_x - \frac{d}{dz}F_{x'} = 0,$$
$$F_y - \frac{d}{dz}F_{y'} = 0.$$

If the function F does not depend explicitly on the independent variable z, we can simplify it as follows. In Leibniz's notation we take the total derivative of the x-component of F with respect to z

$$\frac{dF}{dz} = \frac{\partial F}{\partial x}\frac{dx}{dz} + \frac{\partial F}{\partial x'}\frac{dx'}{dz} + \frac{\partial F}{\partial z},$$

and rearrange to give

$$\frac{\partial F}{\partial x}\frac{dx}{dz} = \frac{dF}{dz} - \frac{\partial F}{\partial x'}\frac{dx'}{dz} - \frac{\partial F}{\partial z}. \tag{25}$$

Multiplying Euler's equation

$$\frac{\partial F}{\partial x} - \frac{d}{dz}\left(\frac{\partial F}{\partial x'}\right) = 0$$

by dx/dz gives

$$\frac{\partial F}{\partial x}\frac{dx}{dz} - \frac{d}{dz}\left(\frac{\partial F}{\partial x'}\right)\frac{dx}{dz} = 0.$$

Substituting Eq. 25 into the above then gives

$$\frac{dF}{dz} - \frac{\partial F}{\partial x'}\frac{dx'}{dz} - \frac{\partial F}{\partial z} - \frac{d}{dz}\left(\frac{\partial F}{\partial x'}\right)\frac{dx}{dz} = 0.$$

As stated, the function F does not depend explicitly on z; hence $\partial F/\partial z = 0$ and we can tidy the above equation to give

$$\frac{dF}{dz} - \frac{\partial F}{\partial x'}\frac{d}{dz}x' - \frac{d}{dz}\left(\frac{\partial F}{\partial x'}\right)x' = 0.$$

The second and third components above are the expansion of the chain rule, which allows us to tidy the whole expression to give, after factorising,

$$\frac{d}{dz}\left(F - \frac{\partial F}{\partial x'}x'\right) = 0,$$

whence

$$F - \frac{\partial F}{\partial x'} x' = \gamma, \tag{26}$$

where γ is the constant of integration. Equation 26 is known as the *Beltrami identity*, and greatly simplifies solutions in the case of non-explicit dependence on z. Noting that $F = F(x, x')$, we can consider x' as calculated from the above equation, say $x' = dx/dz = f(x, \gamma)$; we can solve the equation

$$\frac{dz}{dx} = \frac{1}{f(x, \gamma)}$$

to give $z = g(x, \gamma) + \alpha$, where α is another constant of integration; that is, z is expressed as a function of x, γ and α. We can finally solve this simplified expression for x to find the function $x(z, \gamma, \alpha)$. Hence, we can use a simple integration to find the general solution of Euler's differential equation.

3.1.3.1 *Solution of the Beltrami identity; example: light rays in a homogeneous medium*

We can highlight the use of the Beltrami identity by considering the relatively straightforward example of light rays in the x, y-plane in a homogeneous medium, i.e. the refractive index n is a constant. According to Fermat's principle, the path length of light rays is an extremum; that is, the ray path is an extremal satisfying the conditions

$$I = \int_{P_1}^{P_2} n \, ds \quad \text{and} \quad \delta I = 0.$$

Noting that $ds = \sqrt{1 + y'^2} \, dx$, we have

$$I = \int_{x_1}^{x_2} n \sqrt{1 + y'^2} \, dx.$$

This is a special case of the family of problems involving the famous Brachistochrone Problem, which involve minimising the path between two points. In the above case of a homogeneous medium, we solve the Beltrami identity and find that $dy/dx = \mathrm{constant}$, as expected—the rays travel in straight lines.

3.1.3.2 *Solution of Euler's equations; example: light rays in a gradient index medium*

In the trivial case of a homogeneous medium, we have seen that $n = \mathrm{constant}$ and the path of the light rays is found by solving the Beltrami identity. However,

in the case of a gradient index medium, the refractive index n depends on the three-dimensional spatial coordinates (x, y, z), such that the path is given by

$$I = \int_{P_1}^{P_2} n \, ds = \int_{z_1}^{z_2} n(x, y, z) \sqrt{x'^2 + y'^2 + 1} \, dz.$$

For simplicity, we again focus only on the x coordinate, for which the Euler equation associated with the above integral is

$$F_x - \frac{d}{dz} F_{x'} = 0,$$
$$\frac{\partial n}{\partial x} \sqrt{x'^2 + y'^2 + 1} - \frac{d}{dz} \frac{n x'}{\sqrt{x'^2 + y'^2 + 1}} = 0,$$

Noting that

$$\sqrt{x'^2 + y'^2 + 1} = \frac{ds}{dz} \qquad \text{and} \qquad x' = \frac{dx}{dz},$$

we can transform the last term of the equation above and rearrange to give

$$\frac{d}{ds} \left(n \frac{dx}{ds} \right) = \frac{\partial n}{\partial x}.$$

The above is combined with corresponding equations in y and z whence we again arrive at the three-dimensional ray equation

$$\frac{d}{ds} \left(n \frac{d\mathbf{r}}{ds} \right) = \nabla n.$$

3.2 THE NUMERICAL RAYTRACING METHOD

First, the differential ray tracing method is introduced. The basic concept, outlined in a 1982 paper by Sharma and coworkers [140], involves solving the differential ray equation:

$$\frac{d}{ds} \left[n(\mathbf{r}) \frac{d\mathbf{r}}{ds} \right] = \nabla n(\mathbf{r}),$$

where ds is the differential of ray arc length; $\mathbf{r}$ is the position vector of a point on the ray; and $n(\mathbf{r})$ is the refractive index as a function of $\mathbf{r}$. Derivation of this ray equation can be found in Section 3.1. With the change of variables:

$$t = \int \frac{ds}{n}; \quad dt = \frac{ds}{n},$$

the ray equation can be transformed into a second-order differential equation:

$$\frac{d^2\mathbf{r}}{dt^2} = n\nabla n.$$

The second-order equation above is divided into two first-order equations in the usual way, such that by setting a new variable $T = d\mathbf{r}/dt$, the following equations can be solved using familiar techniques, such as Runge-Kutta (RK), for example:

$$\begin{aligned} \frac{d^2R}{dt^2} &= D(R) \\ T = \frac{dR}{dt} &= n\frac{dR}{ds} \\ D = \frac{1}{2}&\left(\frac{\partial n^2}{\partial x}, \frac{\partial n^2}{\partial y}, \frac{\partial n^2}{\partial z}\right). \end{aligned}$$

Note that the bold font for vector notation has been dropped.

3.2.1 *Anterior Ray-surface Intersection and Direction Cosines*

Our raytracing problem is an initial-value one, so before we delve into the business of raytracing itself, we must find out the initial conditions of the ray:

$$R_0 = R(x_0, y_0, z_0) \text{ and } T_o = T(x_o, y_o, z_o).$$

For now, we will not concern ourselves with skew rays and so restrict our dimensions to two, in y and z. R_0 is the initial position of the ray within the lens GRIN medium. For this, we must find the ray-surface intercept.

The light rays coming from the posterior surface of the cornea and intersecting the anterior lens surface are straight lines, since the aqueous humour is a medium of constant refractive index. Finding the intercept hence involves finding the point at which a line intersects the surface of the lens. If the lens surfaces are represented by second-order polynomials in z, this simply involves solving a quadratic equation. However, our use of a cubic surface makes an analytical solution somewhat more difficult. This is because the usual method of solving cubic equations by Cardano's method involves complex numbers [141]. This is fine when solving roots by hand or when using symbolic programming languages, such as *Mathematica*, but it is unsuitable for use in the *C* programming language, for example. To avoid the use of complex numbers, we must use the so-called *trigonometric*

method of François Viète [142]—this method performed for the purposes of raytracing through a cubic lens was recently outlined by Bahrami and Goncharov [4]. The intersection coordinates of the ray with the lens anterior surface provides the initial condition R_0 for the RK raytrace method.

Considering T above, we see that it contains the optical direction cosines; that is, it is the regular direction cosines at the point (y_0, z_0) multiplied by refractive index at that point: $T = n dR/ds$. Hence, provision of T_0 requires calculation of the direction cosines of the ray after refraction at the lens anterior surface. After calculating the intercept of the ray with the surface, the direction cosine after refraction is relatively easily calculated using a basic Snell's law routine. To convert the direction cosine into an optical direction cosine, we multiply it by n_s, which is the refractive index at the surface of the lens.

3.2.2 *The Three-dimensional Refractive Index*

From the preceding equations, we see that we require D, namely the refractive index as a function of y and z. More specifically, we require

$$1/2 \nabla n^2 = n \nabla n.$$

Recalling the definition of refractive index used in our modelling of the GRIN lens

$$n(\zeta) = n_c + (n_s - n_c)\zeta^{2P},$$

and taking an example one-dimensional derivative of n with respect to x, we have

$$\frac{d}{dx} n(\zeta) = \frac{dn}{d\zeta}\frac{d\zeta}{dx} = 2P(n_s - n_c)\zeta^{2P-1}\frac{d\zeta}{dx}.$$

Thus we see that dn/dx depends not only on the value of $d\zeta/dx$, but also on the value of ζ itself. This slightly awkward notation arises since the refractive index depends on the normalised coordinate ζ within the GRIN, and not on y or z explicitly (recall that we are only working in two dimensions). Thus, to express the refractive index as a function of y and z, we must first express ζ as a function of same.

To do this, we again note the formula for the sag of a cubic surface, but replace height ρ with y:

$$y^2 = 2\zeta^{2m+1}R_a(\zeta T_a + z) - \zeta^{2m}(1 + K_a)(\zeta T_a + z)^2 + \zeta^{2m-1}B_a(\zeta T_a + z)^3.$$

We solve for ζ in the equation above using the Newton-Raphson method. More specifically, we use Halley's method, which is essentially the same as Newton-Raphson, but includes an extra correction term. Both methods arise from a truncation of the Taylor series:

$$f(x + \delta) \simeq f(x) + f'(x)\delta + \frac{1}{2}f''(x)\delta^2 + \dots$$

Newton-Raphson involves taking the tangent to a function at an initial guess x_i. The tangent line is extended linearly to where it intersects the $y = 0$ line, and the abscissa at this intersection provides the next guess x_{i+1}. The linearity manifests itself in Newton-Raphson's choosing of only the first two terms from the right-hand side (RHS) of the Taylor series above. Finding the intercept of the tangent line with $y = 0$ means setting $f(x + \delta)$ to zero, such that

$$f(x) + f'(x)\delta = 0,$$

whence

$$\delta = -\frac{f(x)}{f'(x)}.$$

Given an initial guess x_i, the subsequent guesses are found according to

$$x_{i+1} = x_i - \frac{f(x)}{f'(x)}.$$

Halley's method follows the same procedure, except we keep a third term from the RHS side of the Taylor series, such that

$$f(x) + f'(x)\delta + \frac{1}{2}f''(x)\delta^2 = 0,$$

which is simply rearranged to give

$$\delta = -\frac{f(x)}{f'(x) + {}^1/_2 f''(x)\delta}.$$

Using the previous result for δ from Newton-Raphson above, we arrive at

$$\delta = -\frac{f(x)}{f'(x)\left(1 - \frac{f(x)f''(x)}{2f'(x)^2}\right)},$$

resulting in

$$x_{i+1} = x_i - \frac{f(x)}{f'(x)\left(1 - \frac{f(x)f''(x)}{2f'(x)^2}\right)}.$$

Halley's method converged cubically, as opposed to the quadratic convergence of Newton-Raphson. Although it converges more rapidly than Newton-Raphson, its basin of convergence (the domain of initial guesses within which the method will converge to the correct solution) will not necessarily be any larger. For guaranteed convergence, it should be complemented with the fool-proof Bisection method.

Now that we have found ζ as a function of y and z, we must find $d\zeta/dx$. To do this, we once again take the equation

$$y^2 = 2\zeta^{2m+1}R_a(\zeta T_a + z) - \zeta^{2m}(1 + K_a)(\zeta T_a + z)^2 + \zeta^{2m-1}B_a(\zeta T_a + z)^3$$

and differentiate both sides with respect to ζ. We then solve for $d\zeta/dx$. Finally, we can combine our results to produce D above.

3.2.3 *The Runge-Kutta Method*

The numerical method adopted follows the work of Sharma and coworkers. In their 1982 paper [140], they introduce a shortened version of the RK method requiring almost the same computational effort as the solution of a first-order differential equation. As argued by Press *et al.* of Numerical Recipes, basic RK methods are slightly less efficient than newer counterparts such as Richardson extrapolation, Bulirsch-Stoer and perdictor-corrector methods. However, higher-order methods have made RK competitive in many cases. RK is usually successful and is fast when function evaluations are cheap.

Using the equations from the preceding section, we are now ready to trace a ray from its initial point of intersection with the lens anterior surface to its final point at the posterior surface intersection. The RK routine is given as

$$\begin{aligned} R_{n+1} &= R_n + \Delta t\,[T_n + 1/6(A+2B)] \\ T_{n+1} &= T_n + 1/6(A+4B+C), \end{aligned}$$

$$\begin{aligned} A &= \Delta t D(R_n), \\ B &= \Delta t D(R_n + 1/2\Delta t T_n + 1/8\Delta t A), \\ C &= \Delta t D(R_n + \Delta t T_n + 1/2\Delta t B), \end{aligned}$$

where Δt is the stepsize of the RK routine. Smaller Δt gives greater accuracy, at the expense of larger computational effort. We choose Δt such that the desired raytrace accuracy is obtained. We repeatedly apply the above equations by incrementing the integer subscript until the ray exits the region of interest.

Noting that the lens GRIN has different descriptions for the anterior and posterior portions (according to the relevant cubic equation), we must divide our raytrace into these two regions of interest. The anterior and posterior portions are joined smoothly at the equatorial interface, the shape of which is given by the relevant value of the parameter m. To see this, we note the image below. Z_c is the equatorial position of the external lens contour; and, as derived in a previous manuscript of ours [143], is given by:

$$\begin{aligned} Z_c = \frac{1}{Q_p - Q_a}\Big[& T_a Q_a + T_p Q_p - 2(R_a + R_p) + \\ & \sqrt{T^2 Q_a Q_p - 4T(R_a Q_p + R_p Q_a) + 4(R_a + R_p)^2}\Big], \end{aligned}$$

where $T = T_a + T_p$ is the axial thickness of the lens. T_a and T_p are respectively defined as the anterior and posterior axial lens thicknesses relative to the centre of the lens nucleus; the *shape factor* of the lens surfaces is given by $Q = 1 + K$. To find

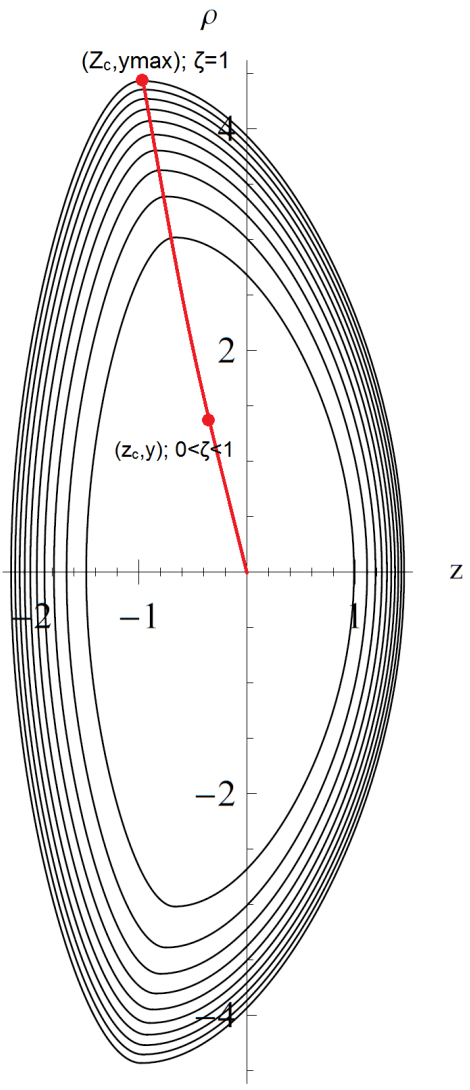

Figure 6: Schematic representation of the lens' equatorial interface.

the axial position of an internal contour as a function of ζ (i.e. $z_c(\zeta)$) we can insert the relevant scaling factor ζ to give the equation below

$$\begin{aligned} z_c(\zeta) =& \frac{1}{\zeta^{2m}(Q_p - Q_a)}\Big[\zeta T_a \zeta^{2m} Q_a + \zeta T_p \zeta^{2m} Q_p - 2\zeta^{2m+1}(R_a + R_p) + \\ & \Big(\zeta^2 T^2 \zeta^{2m} Q_a \zeta^{2m} Q_p - 4\zeta T(\zeta^{2m+1} R_a \zeta^{2m} Q_p + \\ & \zeta^{2m+1} R_p \zeta^{2m} Q_a) + 4\zeta^{4m+2}(R_a + R_p)^2\Big)^{1/2}\Big]. \end{aligned}$$

Extracting the common factor of ζ^{2m+1} from the numerator and ζ^{2m} from the denominator, we see that we are left with

$$\begin{aligned} Z_c =& \frac{\zeta^{2m+1}}{\zeta^{2m}} \frac{1}{Q_p - Q_a}\Big[T_a Q_a + T_p Q_p - 2(R_a + R_p) + \\ & \sqrt{T^2 Q_a Q_p - 4T(R_a Q_p + R_p Q_a) + 4(R_a + R_p)^2}\Big], \end{aligned}$$

which reduces to $z_c(\zeta) = \zeta Z_c$. Thus we see that the axial position of a contour scales linearly with ζ. Next, we see that the maximum height (y_0) of the lens exterior is at the equator, and is given by

$$y_0^2 = 2R_a(T_a + Z_c) - (1 + K_a)(T_a + Z_c)^2 + B_a(T_a + Z_c)^3,$$

whereas the equatorial height of an internal contour is found by introducing ζ to give

$$y(\zeta)^2 = 2R_a\zeta^{2m+1}(\zeta T_a + \zeta Z_c) - \zeta^{2m}(1 + K_a)(\zeta T_a + \zeta Z_c)^2 + \zeta^{2m-1} B_a(\zeta T_a + \zeta Z_c)^3,$$

where we can factor out ζ^{2m+2} to give

$$y(\zeta)^2 = \zeta^{2m+2} y_0^2.$$

Finally, using the above result: $z_c(\zeta) = \zeta Z_c$, we can replace ζ to solve for y as a function of z_c as follows

$$y(z_c)^2 = z_c^{2m+2}\left(\frac{y_0^2}{Z_c^{2m+2}}\right).$$

Since the quotient on the RHS is constant, we therefore see that y_c scales as z_c^{2m+2}, and this describes the shape of the equatorial interface. Thus, the following is a

description of any light ray in the anterior portion of the lens: For any given value of axial co-ordinate z, the ray will be in the anterior portion if its height y squared is less than z to the power of $2m+2$, times the maximum lens height squared, divided by the axial position of the external equator to the power of $2m+2$. This is the condition we use in our RK raytrace method. When the ray passes this equatorial interface, it will be in the posterior portion of the lens. When this happens, the raytracing equations are adjusted appropriately and the raytrace is continued.

We recall that the ray intersection with the anterior (external) surface is known with high accuracy, by virtue of the trigonometric method above. This must be the case, due to the relatively large refractive index difference at this interface—if we calculate the intersection incorrectly, then the whole raytrace will be compromised. However, we note that there is no such difference in refractive index at the equatorial interface of the lens. At this interface, the refractive index is joined smoothly, and indeed the derivative of the refractive index function at this point is zero. Therefore, we see that the ray transitions smoothly between the two regions, and exact positioning is not required. Hence, the above method is suitable.

3.2.4 *Posterior Ray-surface Intersection*

RK methods differ from other differential equation integrators in the sense that they do not provide an approximation of the solution trajectory—they only calculate the points through which the solution passes, including the direction at those points. It is this lack of an approximate trajectory that makes ray-surface intersection particularly sensitive to error in RK raytracing. It can be shown that the error in traversing a GRIN region is approximately proportional to the error associated with a single step, multiplied by the number of steps. In Sharma's method, the single-step error is proportional to Δt^5, whereas the number of steps is inversely proportional to Δt. Therefore, in a global sense, the total error associated with raytracing by Sharma's method is proportional to Δt^4, where Δt is the step length. Noting that the RK method calculates only the points through which the solution passes, the error in these points is proportional to Δt^4. In order to calculate the ray-surface intersection, we require the intermediate trajectory of the solution—hence, if the intermediate trajectory is known to error greater than the discrete points defined by the RK method, the overall solution will be less accurate than

those discrete points. That is, we wish to find the *optimal interpolant* of the solution between those points.

As the ray crosses the GRIN medium, a simple axial co-ordinate check can be initially used to indicate whether the ray has exited the region of interest. If $\mathbf{R}_l$ and $\mathbf{T}_l$ are the respective position and optical direction cosine of the ray immediately before exiting the region, then $\mathbf{R}_{l+1}$ and $\mathbf{T}_{l+1}$ are those after exiting; note that the latter two values are not necessarily calculated in this initial stage. In a 1986 paper by Sharma and Ghatak [144], those authors propose a method to use a cubic equation in t to parameterise the continuous trajectory of the ray. Say we have our parameterised interpolation polynomial $g(\tilde{t})$ of the ray trajectory; considering the z-component only, we have:

$$g(\tilde{t}) = a_0 + a_1\tilde{t} + a_1\tilde{t}^2 + a_3\tilde{t}^3,$$

where $\tilde{t} = 0, \ldots, \Delta t$. The values of the coefficients a_i can be found using the values of the function at the points l and $l+1$. Recall that points l and $l+1$ denote that the ray is within and without the GRIN medium of interest, respectively. At point l, $\tilde{t} = 0$, such that $g(0) = a_0 = \mathbf{R}_l$ and $g'(0) = a_1 = \mathbf{T}_l$. Likewise, we can find expressions for a_2 and a_3 by setting $g(\Delta t) = \mathbf{R}_{l+1}$ and $g'(\Delta t) = \mathbf{T}_{l+1}$.

Since the direction of the ray is also required, they similarly propose a method of parameterising the optical direction cosine vector $\mathbf{T}$. If $h(\tilde{t})$ is the parameterisation of the ray direction cosine $\mathbf{T}$ between the points l and $l+1$, we have:

$$h(\tilde{t}) = b_0 + b_1\tilde{t} + b_1\tilde{t}^2 + b_3\tilde{t}^3.$$

Again, we can solve for the coefficients b_i such that $h(0) = b_0 = \mathbf{T}_l$ and $h'(0) = b_1 = \mathbf{T}'_l = \mathbf{D}(\mathbf{R}_l)$. Likewise, we can find expressions for b_2 and b_3 by setting $h(\Delta t) = \mathbf{T}_{l+1}$ and $h'(\Delta t) = \mathbf{T}'_{l+1} = \mathbf{D}(\mathbf{R}_{l+1})$. This parameterisation of $\mathbf{T}$ requires one extra piece of information that is not automatically calculated in the RK raytrace; that is the derivative of the direction cosine after exiting the region of interest, $\mathbf{T}'_{l+1} = \mathbf{D}(\mathbf{R}_{l+1})$. This means that calculation of the intersection point with this method requires only one extra piece of information when compared to the actual raytrace itself; from a computation point of view, this is efficient and hence desirable.

The method for finding the ray-surface intersection point itself involves expressing the equation of the surface as a polynomial. If we take the equation for the posterior surface of our cubic model:

$$y^2 = 2R_p(T_p - z) - (1 + K_p)(T_p - z)^2 + B_p(T_p - z)^3.$$

we see that this equation is satisfied for a continuous set of co-ordinates (z, ρ) lying on the posterior surface of the lens. Conversely, the equation will not be satisfied for any points that do not lie on that surface. This perhaps becomes more illustrative if we re-arrange the equation to give:

$$y^2 - 2R_p(T_p - z) + (1 + K_p)(T_p - z)^2 - B_p(T_p - z)^3 = 0. \tag{27}$$

Note that the equation above only equals to zero for the same continuous set of co-ordinates (z, ρ) lying on the posterior surface of the lens. That is, if a particular point (z, ρ) does not lie on the surface, the equation will not equal to zero. This inequality can be used as a useful method of finding the co-ordinates of the ray-surface intersection, since we can solve the equation above using analytical or numerical techniques. In Sharma's method, the equation of the surface is parameterised as a cubic in t. Solution of this cubic equation can be performed iteratively using the Newton-Raphson method if it is treated as a transcendental equation; alternatively it can be solved analytically. Since direct analytical solution of the equation required the use of complex numbers, Sharma and Ghatak developed a convenient analytical method based on the observation that the co-efficient of the third-order term in the surface parameterisation is much smaller than the other two coefficients. This allows us to split the problem into the solution of a quadratic equation, where successively higher orders of approximation can be added for additional accuracy.

In a 1990 paper by Stone and Forbes, the method for finding an *optimal* interpolant between the RK points is discussed. Of all possible interpolants between RK points, the optimal interpolant is defined as that which is correct to the same power of Δt as the points themselves. As outlined in that manuscript, it is erroneous and wasteful of computational resources to determine the RK points to a large degree of accuracy if the intermediate trajectory is sub-optimal, since the overall error is fundamentally a combination of both. In their nomenclature, the *transfer error* is that accumulated while traversing the GRIN medium, whereas the

intersection error is that obtained while finding the intersection point of the ray with the surface. Sharma's method for finding the ray-surface intersection point is fourth-order; hence, it preserves the overall integrity of their fourth-order ray-tracing method, since the RK method is globally fourth-order also. However, to avoid dominance of the intersection error, we would like to have an intersection method accurate to the same order as the *single-step* error of the RK raytrace, i.e. Δt^5. Stone and Forbes propose such a fifth-order method requiring the same computational effort, and capable of reducing the intersection error by up to an order of magnitude.

The method proposed by Stone and Forbes is based on the interpolants discussed in 1987 by Fine [145]. The intermediate ray trajectory is determined from a quartic Hermite interpolant based on the values of:

$$\begin{gathered}\mathbf{R}_l, \\ d\mathbf{R}_l/dt = \mathbf{T}_l, \\ d^2\mathbf{R}_l/dt^2 = \mathbf{D}(\mathbf{R}_l) \\ \mathbf{R}_{l+1} \quad \text{and} \\ d\mathbf{R}_{l+1}/dt = \mathbf{T}_{l+1}.\end{gathered}$$

In Sharma's method, the intermediate optical direction cosine $\mathbf{T}$ is expressed as a cubic in t. This method required determination of one extra piece of information than what is ordinarily provided by the RK raytrace: $\mathbf{T}'_{l+1} = \mathbf{D}(\mathbf{R}_{l+1})$. This value $\mathbf{D}(\mathbf{R}_{l+1})$ is hence used in the cubic parameterisation of $\mathbf{T}$ to estimate the intermediate direction of the ray. The ray direction at the actual intersection point can then be found by inserting the relevant value of t into the cubic equation. In Stone and Forbes' method, we do not estimate $\mathbf{T}$ through evaluation of any parameterisation; hence, we do not require calculation of the gradient $\mathbf{D}(\mathbf{R}_{l+1})$. Rather, an approximation to $\mathbf{T}$ is required at only one particular point t, called t_{int}. Hence, it requires calculation of the gradient of refractive index, $\mathbf{D}$, at a point whose position depends on t_{int}. This method determines $\mathbf{T}$ to accuracy Δt^5, as opposed to Sharma's Δt^4.

The point t_{int} is found by representing the surface of interest by an equation of the form $F(x, y, z) = 0$, where the point t_{int} is found such that $\mathbf{R}(t_{int}, l)$ satisfies $F(\mathbf{R}(t_{int}, l)) = 0$. In this case, we require t_{int} to an accuracy of Δt^5 or higher. Stone

and Forbes use a method of first finding an approximation to this point, called t_{app}, whence a more correct estimate for t_{int} is obtained by using a single iteration of the Newton-Raphson method.

The quartic interpolant for ray position $\mathbf{R}$ is given by the equation:

$$\mathbf{R}(t;k) = \mathbf{R}_k + t\mathbf{T}_k + \frac{1}{2}t^2\frac{\mathbf{A}}{\Delta t} + \frac{1}{6}t^3\frac{4\mathbf{B}-\mathbf{C}-3\mathbf{A}}{\Delta t^2} + \frac{1}{24}t^4\frac{4(\mathbf{A}+\mathbf{C}-2\mathbf{B})}{\Delta t^3}. \tag{28}$$

This equation can be used to find the position of the ray an amount t from the initial point $\mathbf{R}_k$. In the case of the ray-surface intersection, the relevant value of t will be given by t_{int}. To find t_{app} first, we use the representation of the surface given by Eq. 27. We define the terms:

$$F_0 = F(\mathbf{R}_l), \tag{29}$$

$$F_1 = F(\mathbf{R}_{l+1}) \quad \text{and} \tag{30}$$

$$\dot{F}_0 = \left.\frac{dF(\mathbf{R}(t;l))}{dt}\right|_{t=0} = \nabla F(\mathbf{R}_l)\cdot\mathbf{T}_l. \tag{31}$$

We note the important point that the gradient of F is evaluated at the point $\mathbf{R}_l$ itself. The interpolant for $\mathbf{R}$ is not used here; it will, however, be used later. To see why Eq. 31 above is true, we note from Eq. 27 that $F = F(y,z)$. Using the product rule to evaluate the LHS of Eq. 31:

$$\frac{dF}{dt} = \frac{dF}{dy}\frac{dy}{dt} + \frac{dF}{dz}\frac{dz}{dt}.$$

Replacing F with its definition from Eq. 27, we see that:

$$\frac{dF}{dy} = 2y \quad \text{and} \quad \frac{dF}{dz} = 2R_p - 2(1+K_p)(T_p - z) + 3B_p(T_p - z)^2.$$

Noting that dy/dt and dz/dt are simply the y- and z-components of $\mathbf{T}$, which we denote as T_y and T_z, respectively—note that the individual components themselves do not constitute a vector and so the bold font is omitted—we can transform the equation above to give:

$$\frac{dF}{dt} = 2yT_y + (2R_p - 2(1+K_p)(T_p - z) + 3B_p(T_p - z)^2)T_z.$$

This equation is simply the dot product $\nabla F(\mathbf{R}_l)\cdot\mathbf{T}_l$; hence, we arrive at the RHS of Eq. 31. Since F_0 relates to the point $\mathbf{R}_l$ just inside the lens, and F_1 relates to the

point $\mathbf{R}_{l+1}$ just outside the lens, we can use Eqs. 29–31 to generate a Taylor series approximation to the intermediate value of F, given by:

$$F(\mathbf{R}(t;l)) = F_0 + t\dot{F}_0 - t^2 Q, \tag{32}$$

where it can be shown that Q represents a second-derivative and is given by:

$$Q = \frac{\dot{F}_0 - F_1 + \Delta t \dot{F}_0}{\Delta t^2}.$$

The value of t_{app} is found by solving for the root of the quadratic Eq. 32. If t were to equal zero or Δt, then we would simply be at the points F_0 or F_1, respectively; hence, we choose the root of the quadratic equation that lies between those two values, and this is our value for t_{app}. The quadratic can be solved directly to give:

$$t_{app} = \frac{-\dot{F}_0 \pm \sqrt{\dot{F}_0^2 + 4F_0 Q}}{-2Q}.$$

Alternatively, we can arrive at the expression in Stone and Forbes' paper by diving Eq. 32 by t^2 (which is permissible since it equals zero) and solve for t to give:

$$t_{app} = \frac{-2F_0}{\dot{F}_0 \pm \sqrt{\dot{F}_0^2 + 4F_0 Q}}.$$

Looking at Eq. 32 above, we see that it has an intercept F_0. Excluding the trivial case where $F_0 = 0$ (in this case $t = 0$ also), the quadratic has two roots. F_0 and F_1 have opposite signs, implying that the quadratic crosses the positive t-axis only once; we wish to pick this positive root. In order to have a positive root, the numerator must have the same sign as the denominator. Since the surd in the equation above must be positive (to avoid an imaginary number), we must therefore choose the $\pm$ term such that $\pm\sqrt{\dot{F}_0^2 + 4F_0 Q}$ has the same sign as $-2F_0$. This gives us the expression:

$$t_{app} = \frac{-2F_0}{\dot{F}_0 - \text{sign}(F_0)\sqrt{\dot{F}_0^2 + 4F_0 Q}},$$

where

$$\text{sign}(x) = \begin{cases} 1, & \text{if } x > 0 \\ -1, & \text{if } x < 0 \end{cases}.$$

Finally, we can take this approximate value t_{app} and use a single iteration of the Newton-Raphson method to find t_{int} according to:

$$t_{int} = t_{app} - F(\mathbf{R}(t_{app}; l)) \left[\frac{dF(\mathbf{R}(t_{app}; l))}{dt}\right]^{-1},$$

where

$$\frac{dF(\mathbf{R}(t_{app}; l))}{dt} = \nabla F(\mathbf{R}(t_{app}; l)) \cdot \frac{d\mathbf{R}(t_{app}; l)}{dt}.$$

It is important to note here that $\mathbf{R}(t_{app}; l)$ is given by the approximate form of Eq. 28. That is, we can no longer use the form of Eq. 31 to find dF/dt. To see why this is the case, we again note that the respective y- and z-components of the gradient of F are $2y$ and $2R_p - 2(1 + K_p)(T_p - z) + 3B_p(T_p - z)^2$. However, in this case, the y and z terms are not simply the y- and z- components of the vector $\mathbf{R}$; rather, they are the y- and z- components of the *approximation* to $\mathbf{R}$, given by Eq. 28. Furthermore, the derivative $d\mathbf{R}/dt$ is no longer equal to $\mathbf{T}$; rather, the derivative is given by:

$$\begin{aligned}\frac{d\mathbf{R}(t_{app}; l)}{dt} =& \frac{d}{dt}\Big(\mathbf{R}_l + t\mathbf{T}_l + \frac{1}{2}t^2\frac{\mathbf{A}}{\Delta t} + \frac{1}{6}t^3\frac{4\mathbf{B} - \mathbf{C} - 3\mathbf{A}}{\Delta t^2} + \\ & \frac{1}{24}t^4\frac{4(\mathbf{A} + \mathbf{C} - 2\mathbf{B})}{\Delta t^3}\Big)\Big|_{t=t_{app}} \qquad (33)\\ =& \mathbf{T}_l + t\frac{\mathbf{A}}{\Delta t} + \frac{1}{2}t^2\frac{4\mathbf{B} - \mathbf{C} - 3\mathbf{A}}{\Delta t^2} + \frac{1}{6}t^3\frac{4(\mathbf{A} + \mathbf{C} - 2\mathbf{B})}{\Delta t^3}. \qquad (34)\end{aligned}$$

We then take the dot product of the expression above with $\nabla F(\mathbf{R}(t_{app}; l))$ to find $dF(\mathbf{R}(t_{app}; l))/dt$. Hence, we see that the expression is different to that give in Eq. 28. However, there is one final point to note. For the intersection of the ray with the anterior surface of the lens, we can use the procedure above. However, in the anterior chamber, the ray follows a straight line. More specifically, the aqueous humour has constant refractive index. The vectors $\mathbf{A}$, $\mathbf{B}$ and $\mathbf{C}$ are directly related to the gradient of refractive index; hence, since the medium is not gradient-index, these three vectors will equal zero. As a result, Eq. 34 above reduces to the simple form $d\mathbf{R}(t_{app}; l)/dt = \mathbf{T}_l$. This means that, for the intersection of the ray with the anterior surface of the lens, the equation for $dF(\mathbf{R}(t_{app}; l))/dt$ reduces to the more convenient form of Eq. 31. Furthermore, since $\mathbf{A} = \mathbf{B} = \mathbf{C} = 0$, the approximate form of Eq. 28 reduces to:

$$\mathbf{R}(t_{int}; k) = \mathbf{R}_k + t_{int}\mathbf{T}_k,$$

where the last term on the RHS is just the definition of the differential, since it is the stepsize multiplied by the derivative.

Finally, with the value of t_{int}, we can find the position of the ray-surface intersection using Eq. 28. As we have said already, to find the direction of the ray at this point, we require one extra piece of information regarding the derivative of refractive index. This additional information is by sampling the gradient at the point

$$\mathbf{G} = \Delta t \mathbf{D}(\mathbf{R}_l + c_0 \Delta t \mathbf{T}_l + {}^1/_2 c_0^2 \Delta t \mathbf{C}),$$

where the expression for c_0 can be found in the manuscript by Stone and Forbes. With this extra term $\mathbf{G}$, we can find the optical direction cosine at the point t_{int} using the following equation:

$$\mathbf{T}(t_{int}; l) = \mathbf{T}_l + b_1 \mathbf{A} + b_2 \mathbf{B} + b_3 \mathbf{C} + b_4 \mathbf{G}, \tag{35}$$

where the coefficients b_1, b_2, b_3 and b_4 are also given by Stone and Forbes, and are not repeated here. Again, we would like to point out that the calculation of $\mathbf{T}$ simplifies in the case of the intersection of the ray with the anterior surface of the lens. As already stated, the anterior chamber is a medium of constant refractive index. Hence, $\mathbf{D}$ is zero for all points therein, and $\mathbf{A} = \mathbf{B} = \mathbf{C} = \mathbf{G} = 0$. Consequently, according to Eq. 35, $\mathbf{T}(t_{int}; l) = \mathbf{T}_l$; this means that $\mathbf{T}$ is constant (as we should expect, since the ray travels in a straight line).

3.2.4.1 *A note on polynomial interpolation*

Simply put, polynomial interpolation involves finding a polynomial that passes exactly through certain data points. The most familiar example of interpolation is *Lagrange interpolation*, where an N^{th} degree is fit to $N+1$ data points. Lagrange interpolation methods have interpolating polynomials of the general form:

$$\begin{aligned} g(x) &= \sum_{i=0}^{N} a_i x^i \\ &= a_0 + a_1 x + a_2 x^2 + a_3 x^3 + \cdots + a_N x^N \end{aligned}$$

For the interpolating polynomial to fit the data points, this means that $g(x)$ must equal the function values at the data points:

$$g(x_i) = f_i \quad i = 0, \ldots, N.$$

In the case of *Hermite interpolation*, we not only require the interpolating polynomial $g(x)$ to equal the function values at the data points, but we also require that the derivatives of the function are satisfied. That is, we develop and interpolating polynomial that equals the function and its derivatives—up to p^{th} order—at $N+1$ data points. Using Lagrange's notation for derivatives, we require that:

$$\begin{aligned} g(x_i) &= f_i \\ g^{(1)}(x_i) &= f_i^{(i)} \\ &\vdots \\ g^{(p)}(x_i) &= f_i^{(p)} \end{aligned}$$

Each expression above provides $N+1$ constraints, where $i = 0, \ldots, N$. Thus, if we have p derivatives giving $p+1$ equations of $N+1$ constraints each, we have a total of $(p+1)(N+1)$ constraints. In polynomial interpolation, to avoid over-determination in general, we must have the same number of unknowns as data points. So, to fit N constraints, we require a polynomial with the same number of coefficients; such that, including the constant term of order zero, we require a polynomial of order $N-1$. For example, four data points ($N = 4$) could be fit with a simple four-coefficient polynomial $a_0 + a_1 x + a_2 x^2 + a_3 x^3$, where the polynomial is of order $4-1 = 3$; this is a *cubic interpolant*. For our current $(p+1)(N+1)$ constraints, we hence require a polynomial of degree $(p+1)(N+1)-1$. We can set up our interpolating polynomial in the form:

$$g(x) = \sum_{i=0}^{(p+1)(N+1)-1} a_i x^i,$$

where we solve for the unknown coefficients a_i, with $i = 0, \ldots, (p+1)(N+1)-1$.

Finally, we make the simple observation that the familiar Lagrange interpolation is a special case of Hermite interpolation where no derivatives are matched (i.e $p = 0$). In the case of our ray-surface intersection problem, we must find an interpolant

that satisfies both the function values at the points $\mathbf{R}_l$ and $\mathbf{R}_{l+1}$, and the first derivatives at those points, namely $\mathbf{T}_l$ and $\mathbf{T}_{l+1}$

3.2.4.2 *A note on Sharma's use of the dimensionless quantity ϵ*

In sharma's method, after parameterisation of the ray trajectory, the value of $\tilde{t}$ for which the ray intersects a particular surface is given by:

$$\tilde{t} = u(1 + \epsilon u_1 + \epsilon^2 u_2 + \epsilon^3 u_3 + \dots),$$

where the term u with no subscript is the zeroth-order solution, and u_1, u_2, u_3,..., etc. correspond to successively higher orders of correction. The term ϵ is useful since it allows us to include the higher-order correction terms to a degree depending on ϵ. For example, if $\epsilon = 0 \implies \tilde{t} = u$, giving the zeroth-order result. If ϵ is a very small quantity, then ϵ^2, ϵ^3 and higher powers of ϵ will vanish, such that that we can include the first order correction, but successively higher orders will be included in lesser amounts. If $\epsilon = 1$, we include fully the higher-order terms.

Part II

MODELLING THE HUMAN LENS

Presented in this part is first an analytical method to describe the accommodative changes in the human crystalline lens. The method is based on the geometry-invariant lens model, in which the GRIN isoindicial contours are coupled to the external shape. This coupling means that the external surface can be used to guide the changes in the GRIN bulk, hence reducing the number of degrees of freedom required for modelling. The conic constants of the lens external surfaces were derived analytically by observing the basic physical constraints of constant lens volume and lens axial position within the eye. As a result, the changes in lens geometry are consistent with experimental findings, and the optical properties are in line with data for optical power and spherical aberration.

Subsequently, a new model is proposed for studying the age-dependent properties of the human lens, containing two GRIN power distributions (axial and radial). Together with a logarithmic formulation of the GRIN medium, three fundamental optical characteristics of the lens can be decoupled without changing the lens external shape: axial optical path length, optical power and third-order spherical aberration.

In the concluding section, the model is used with exact raytracing to reproduce age-related trends in SA from the literature, and to explore the lens paradox.

4

ACCOMMODATION OF THE HUMAN EYE

4.1 INTRODUCTION

The mechanism of accommodation in the human eye is still an area of on-going research. The most widely accepted theory is that proposed by Helmholtz in his *Handbuch der Physiologischen Optik* in 1867 [146]. This Helmholtzian theory of accommodation states that contraction of the ciliary muscle body reduces zonular and capsular tension, allowing the lens to form a steeper, more convex shape. This corresponds to the accommodated state, with an associated increase in lenticular refractive power; the accommodated state provides clear vision at near distances. For distant vision, the ciliary muscle relaxes (dilates), and as a result the lens is stretched into a thinner shape with reduced refractive power. This is the *un*accommodated state, in which the lens is kept under constant tension. Experimental support for this most commonly accepted Helmholtzian theory includes, amongst many others, an interesting paper by Shao *et al.* (2013) showing real-time imaging of accommodative changes in the anterior segment of the eye [147]. While experimental efforts show that lenticular SA becomes more negative with accomodation, it is clear that increasing surface curvatures cause more positive SA; thus the accommodative decrease in lenticular radii should produce more positive SA. We aim to investigate this apparent contradiction by looking at the lens surface and gradient index contributions to lenticular SA.

The field of ocular biometry is fast improving, with new and enhanced imaging methods capable of taking more accurate data with better sampling. While wavefront sensing continues to provide high-quality measurement of ocular wavefront aberration, the improving temporal and spatial resolution of Magnetic Resonance Imaging (MRI) [148] and Optical Coherence Tomography (OCT) [149, 150] may help with obtaining additional biometric information. The availability of these more accurate instruments for ocular biometry allows one to develop more advanced optical and physical models of the human eye; in particular, the crystalline lens.

Historically, some of the first accommodative models of the human crystalline lens were provided by Gullstrand [151] and Le Grand [152], who gave parameters for the unaccommodated and fully-accommodated lens; however, they did not provide data for intermediate accommodative amplitudes. Their four-surface lens model lacks a GRIN structure and also does not employ aspheric surfaces. This model was extended to account for the intermediate states by Blaker in his 1980 paper [153], by assuming that the GRIN lens radii, diameter and central thickness vary linearly with accommodation. In 1985, Navarro *et al.* [154] showed that the on-axis optical properties of the human eye can be reproduced using aspheric lenticular surfaces with an equivalent refractive index for the lens. The lens geometrical parameters changed logarithmically with accommodation in their model, while a parabolic adjustment to the equivalent refractive index was performed. More recently, Smith and co-workers [155] modelled the accommodating lens using a trial and error process, in which the lens dimensions were altered linearly while keeping the volume constant; this led to a change in the lens radii and asphericities. This model was based on the Liou–Brennan eye [156], which was presented only in the relaxed form; thus, the coefficients of the GRIN medium were also altered to account for accommodative effects. We can see, however, that these GRIN coefficients do not depend on surface asphericity.

It can be desirable to analyse accommodation-dependant optical properties of the human lens featuring gradient index in raytracing software such as Zemax. When starting with a set of data for the unaccommodated lens, currently one must predict what values the accommodated lens parameters will take. If, for example, the lenticular radii, conic constants and central thickness of the accommodated lens are inserted into the raytracing software, these accommodated parameters will not necessarily be optically or physically appropriate. That is, the accommodated lens will not display the correct power or SA, and it may have changed substantially in volume. The current study aims to develop an analytical method of describing the geometrical and optical changes in the lens under accommodation. In this paper, we describe an anatomically realistic, adjustable lens, which can be used as a tool for ocular modelling and understanding of accommodation.

4.2 ANALYTICAL METHOD

An equation describing the variation of refractive index n within the human lens has been proposed by Smith *et al.* [48] as:

$$n(r) = c_0 + c_p r^p,$$

where r is the normalised radius in the equatorial section, c_0 is the refractive index at the center of the lens and c_p is the difference between the refractive indices at the center and surface of the lens. The parameter p extends the applicability of this GRIN representation as it may account for some optically significant age-related changes in the GRIN structure. This equation, for the case of the geometry-invariant lens model [3], can be rewritten as:

$$n(\zeta) = n_c + (n_s - n_c)(\zeta^2)^P,$$

where ζ is the normalized distance from the lens centre, n_c and n_s are the refractive indices at the center and at the surface of the GRIN lens, respectively, and $P = p/2$.

The GRIN structure of this lens model is coupled to the shape of the external surface of the lens. This is an attractive feature for modelling the accommodative changes since it secures the optical integrity of the GRIN structure. The general outline of the GRIN medium can be visualised by looking at its iso-indicial contours, which are surfaces of constant refractive index; for example, Fig. 7 contains five iso-indicial contours with a refractive index step of 0.008. Preserving the optical integrity of the GRIN structure requires that the number of contours does not increase or decrease with accommodation. Few recent lens models [3, 157, 158] feature this coupling of GRIN structure and external lens shape. Of these recent models, we choose the geometry-invariant model [3] since it offers both a realistic GRIN distribution with the age-dependent parameter P and continuous iso-indicial surfaces. Note also that $n(\zeta)$ is a continuous function.

The external shape of the lens in this model is a conicoid of revolution with a higher-order aspheric term. The general form for a conicoid of revolution, written as a function of surface sag (z), is given by

$$\rho^2 = 2Rz - (1 + K)z^2,$$

where R is the vertex radius of curvature, K is the conic constant and ρ is the perpendicular distance (height) from the optical axis z. The addition of an aspheric cubic term transforms the surface profile into a *figuring conicoid function* [159]:

$$\rho^2 = 2Rz - (1+K)z^2 + Bz^3. \tag{36}$$

The first continuity condition states that $\rho_a(Z_c) = \rho_p(Z_c)$; where ρ_a and ρ_p are the respective heights of the anterior and posterior surface contours, and Z_c is the axial position of the lens equator. If we note that the *shape factor* of the lens surfaces is given by $Q = 1 + K$, we have the following:

$$\begin{aligned} &2R_a(T_a + Z_c) - Q_a(T_a + Z_c)^2 + B_a(T_a + Z_c)^3 = \\ &2R_p(T_p - Z_c) - Q_p(T_p - Z_c)^2 + B_p(T_p - Z_c)^3. \end{aligned} \tag{37}$$

where the subscripts a and p denote the anterior and posterior segments, respectively. As outlined in previous work by Bahrami and Goncharov [3], the constant B is chosen so that the second continuity condition $\frac{d\rho(z)}{dz}|_{Z_c} = 0$ is satisfied; i.e. the first derivative $d\rho/dz$ at the equatorial interface connecting the anterior and posterior surfaces is equal to zero, given by:

$$\begin{aligned} B_a &= \frac{2}{3}\frac{Q_a(T_a + Z_c) - R_a}{(T_a + Z_c)^2} \quad \text{and} \\ B_p &= \frac{2}{3}\frac{Q_p(T_p - Z_c) - R_p}{(T_p - Z_c)^2}. \end{aligned} \tag{38}$$

The position of the lens equator (Z_c) relative to the centre of the nucleus can thus be calculated by inserting Eq. 38 into Eq. 37 to give the following:

$$\begin{aligned} Z_c = \frac{1}{Q_p - Q_a}\Big[&T_aQ_a + T_pQ_p - 2(R_a + R_p) + \\ &\sqrt{T^2Q_aQ_p - 4T(R_aQ_p + R_pQ_a) + 4(R_a + R_p)^2}\Big], \end{aligned} \tag{39}$$

where $T = T_a + T_p$ is the axial thickness of the lens. T_a and T_p are respectively defined as the anterior and posterior axial lens thicknesses relative to the centre of the lens nucleus.

Since T_a and T_p are positive quantities, and Z_c is a negative quantity [3], the anterior and posterior axial thicknesses (sags) of the lens are given by $Z_a = T_a + Z_c$ and $Z_p = T_p - Z_c$. The anterior and posterior sags are defined from their respective

poles (vertices) to the lens *equator*, while distances T_a and T_p are defined from their respective poles to the centre of the nucleus. The centre of the nucleus is the position of peak refractive index and is defined as the origin; it is not necessarily at the same axial position as the lens equator [158, 160]. See Fig. 7 for a visualisation of the two definitions.

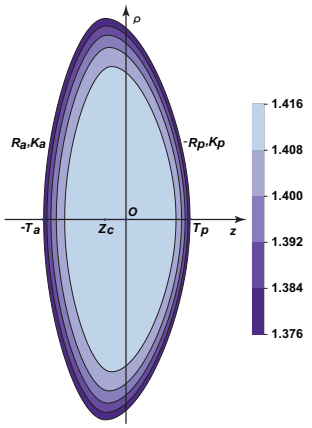

Figure 7: Visualisation of T_a, T_p and Z_c in a GRIN lens; age-related parameter $P = 2.94$.

Next, an analytical formula for the lens volume can be derived using the disc method of integral calculus for the volume of a solid of revolution:

$$V = \pi \int_{-T_a}^{Z_c} \rho_a^2(z)\,dz + \pi \int_{Z_c}^{T_p} \rho_p^2(z)\,dz, \tag{40}$$

taking note again that T_a and T_p are positive, while Z_c is negative. Since the lenticular epithelial stroma constitutes a soft condensed medium and is essentially incompressible, it seemed reasonable to assume that the volume does not change on accommodation. A recent study by Hermans *et al.* came to the same conclusion experimentally [161]. Furthermore, the relatively short timescale over which the accommodation process occurs is rather short to facilitate any volume change through passage of water/aqueous into or out of the lens material [162]. A study by Gerometta *et al.* [163] found that bovine lenticular volume increases by 8% with accommodation, and expected the human lenticular volume to increase by 3%; however, one cannot be certain of the applicability of the bovine study to the human lens. Another study by Strenk *et al.* [164] concluded that the lenticular volume increases with accommodation, but there has been considerable discussion regarding the accuracy and validity of their method [165, 166]. In any instance, we anticipate a small change in lens volume which, although non-negligible, will not drastically affect the results of our model. Any future definitive answer for the ac-

commodative change in lenticular volume can be incorporated into our analytical method.

In our present study, the constant volume condition is used as a control for the accommodated lens. The volume calculated using Eq. 40 is given below:

$$V = \frac{1}{6}\pi[5R_pZ_p^2 + 5R_aZ_a^2 - Q_pZ_p^3 - Q_aZ_a^3]. \tag{41}$$

4.3 FINDING THE CONIC CONSTANTS OF THE LENS

To demonstrate application of this analytical method, we use sample experimental data for the accommodative changes in lenticular radii and central thickness. We present an initial example using population-averaged Scheimpflug data from the work of Dubbelman *et al.* (2005) [167], which have consistently smaller error compared to data obtained with other imaging instruments, for example MRI [148, 161]. The application of these Scheimpflug data helps to ensure that the accommodative changes in radii and central thickness are anatomically realistic. The model is defined for a 30 year old lens, covering a range of accommodative amplitudes $A = 0$–8 D. In this example, the anterior and posterior radii of curvature and central lens thickness were calculated for each accommodative amplitude (in steps of 2 D, for clarity) using empirical linear equations given in Dubbelman *et al.* [167]. The change per dioptre in the anterior radius of curvature R_a, posterior radius of curvature R_p and central thickness T are:

$$\begin{aligned} R_a(A) &= R_{0a} + \Delta R_a = R_{0a} + (0.35 - 0.084R_{0a})A, \\ R_p(A) &= R_{0p} + \Delta R_p = R_{0p} + (0.37 - 0.082R_{0p})A, \\ T(A) &= T_0 + \Delta T = T_0 + (0.0436)A, \end{aligned} \tag{42}$$

where R_{0a}, R_{0p} and T_0 are the unaccommodated radii and thickness, and A is accommodative amplitude in D. Note that these equations represent the change in lenticular parameters per dioptre of stimulus. Objective accommodative response was not measured, and so these formulae may include accommodative lag.

Conic constants can only be accurately determined by imaging a relatively large diameter of the lens [159]. The accuracy in measuring the conic constants of the human lens surfaces by Scheimpflug imaging is limited by lenticular occlusion by the finite maximum size of the iris and ocular refractive distortion. Consequently,

the main motivation in our study was to find a way of predicting the conic constants of the human lens at different accommodative amplitudes, while the data for accommodative changes in the lenticular radii and central thickness were taken from the literature.

In order to develop an analytical method of finding the conic constants, we also use additional information for the accommodative changes in the anterior chamber depth (ACD) of the eye. As the lens accommodates, its anterior pole moves forward into the anterior chamber and this can be seen as a reduction in the ACD. In the same study by Dubbelman *et al.* [167], partial coherence interferometry was used to measure a change per dioptre in the anterior chamber of $\Delta ACD(A) = -0.036A$ mm for the 30 year old eye.

We use the relation above together with Eq. 42 as a basis for finding $R_a(A)$, $R_p(A)$ and $T(A)$, and $ACD(A)$ for a given accommodative amplitude. To find the anterior and posterior conic constants, we apply the following two conditions to the lens: constant volume (Eq. 41) and fixed equator position. The latter assumes that the equator of the lens does not move axially within the eye during accommodation; thus, the reduction in ACD can be seen as an increase in the anterior sag Z_a of the lens and can be expressed as:

$$Z_a(A) = Z_{0a} - \Delta ACD(A). \tag{43}$$

Finally, using Eqs. 39, 41 and 43, we can obtain the anterior and posterior conic constants as a function of accommodative amplitude:

$$K_a = \frac{\pi(T - Z_a)(R_p(T - Z_a) - R_a Z_a) - 6V_0}{\pi T Z_a^2} + \frac{5R_a}{Z_a} - 1, \quad \text{and} \tag{44}$$

$$K_p = \frac{\pi Z_a(R_a Z_a - R_p(T - Z_a)) - 6V_0}{\pi T(T - Z_a)^2} + \frac{5R_p}{T - Z_a} - 1. \tag{45}$$

Note that calculation of the initial volume V_0 requires sample data for R_{0a}, R_{0p}, K_{0a}, K_{0p} and T_0. Alternatively, if we have data for the accommodative change in K_a, we can solve Eq. 44 for Z_a, and subsequently find K_p from Eq. 45. This has physical significance since it allows us to predict, using data for K_a, the accommodative change in K_p, which is difficult to measure *in vivo*.

4.4 ANALYSIS OF LENTICULAR GEOMETRY

We define the initial lens geometry based on the recent work of Ortiz *et al.* [168]. We used the following parameters for the unaccommodated lens: $R_{0a} = 12.48$ mm, $R_{0p} = 7.25$ mm, $T_0 = 3.18$ mm, $K_{0a} = -2.57$ and $K_{0p} = -1.64$. Assuming the centre of the lens nucleus is located more posteriorly [158, 160, 169], we set $T_a = 0.6T$ and $T_p = 0.4T$, so that $T_{0a} = 1.91$ mm and $T_{0p} = 1.27$ mm.

These initial parameters allow us to calculate the geometrical features of the lens, which were derived analytically. First, the position of the lens equator with respect to the centre of the nucleus is given by Eq. 39: $Z_{0c} = -0.74$ mm. Hence, we can calculate the anterior sag $Z_{0a} = T_{0a} + Z_{0c} = 1.17$ mm, the posterior sag $Z_{0p} = T_{0p} - Z_{0c} = 2.01$ mm and the two B-coefficients: $B_{0a} = -6.93$ mm^{-1} and $B_{0p} = -1.41$ mm^{-1}. Finally, the initial volume V_0 is calculated using Eq. 41 to give $V_0 = 125.45$ mm^3. Using Eqs. 42, 4.3 and 43, we can calculate the parameters of the lens at different accommodative amplitudes, as shown in Tables 5 and 6 below for $A = 0,\ 2,\ 4,\ 6$ and 8 D. Figure 8 shows the transverse cross-section of the lens, with the anterior and posterior surfaces to the left and right, respectively—note that the lens is axisymmetric.

Table 5: Predicted changes in geometrical parameters of the lens under accommodation. All distances are in mm, with area in mm^2, and power is given in D.

A	R_a	R_p	T	Z_c	Z_a	Z_p	Eq. Diam.	Surf. Area	Refr. Power
0	12.48	7.25	3.18	−0.734	1.174	2.007	9.001	152.6	19.23
2	11.08	6.80	3.27	−0.715	1.246	2.021	8.911	150.6	20.93
4	9.687	6.35	3.35	−0.695	1.318	2.037	8.836	148.9	22.99
6	8.290	5.90	3.44	−0.675	1.390	2.052	8.774	147.6	25.58
8	6.893	5.45	3.53	−0.656	1.462	2.067	8.727	146.5	28.97

The negative value of the conic constants, seen in Table 6, can be compared with the literature [167, 168, 170, 171]. The *in vivo* study of Dubbelman *et al.* [47] reports a value of -4.5 ± 2.8 for the anterior conic of the unaccommodated 30 year old lens, and a value of -2.9 ± 3.8 for the posterior conic. Ortiz *et al.* [168] show a range in averaged asphericities of 3 subjects; from −2.57 to −0.43 for the anterior conic, and −1.64 to −0.01 for the posterior conic. For the *in vitro* lens

Table 6: Figuring and approximate conic constants of the lens surfaces, and their contribution to SA. The change in SA per dioptre is calculated as a linear fit of the SA versus accommodation for the ranges 0–2 D, 0–4 D, 0–6 D and 0–8 D.

							ΔSA (μm/D)		
A (D)	B_a (mm^{-1})	B_p (mm^{-1})	K_a	K_p	K_a^*	K_p^*	$W_{4,0}$	Z_4^0	Linear fit range (D)
0	−6.93	−1.41	−2.57	−1.64	−0.83	−1.03			
2	−6.25	−1.48	−3.79	−2.12	−2.05	−1.45	−0.0470	−0.0035	0–2
4	−5.90	−1.56	−5.32	−2.64	−3.49	−1.90	−0.0684	−0.0051	0–4
6	−5.76	−1.65	−7.03	−3.21	−5.03	−2.38	−0.0993	−0.0074	0–6
8	−5.74	−1.76	−8.87	−3.81	−6.62	−2.89	−0.1516	−0.0113	0–8

(assumed to be fully accommodated), Howcroft and Parker [172] show that both the anterior and posterior surfaces varied widely with hyperbolic, parabolic and elliptical profiles for 60 cadaver eyes. Judging by the figures presented in the work of Borja *et al* [173], the asphericity of the anterior surface ranges between −14 and +2; that of the posterior surface ranges between −2 and +2. The work of Manns *et al.* [174] produces an average of 3.27 ± 2.01 for the anterior conic, and -1.64 ± 1.85 for the posterior conic of cadaver lenses. The average *in vitro* data are difficult to interpret, since the accommodative state is not well-defined. In terms of theoretical modelling, the lens of Smith *et al.* [155] (based on Liou and Brennan's [156]) shows a decrease in anterior and posterior conic constants from −0.94 to −0.955 and 0.96 to 0.471, respectively, with 3 D accommodation. The nested shell optical model of Campbell [170] indicates that the anterior and posterior conic constants have a value of −5.00 for the 25 year old lens. The finite element model of Lanchares *et al.* [171] shows that the anterior and posterior conic constants have values of −4 and −3, respectively, in the unaccommodated eye. For their finite element model, Hermans *et al.* [175] use values of −4 and −8 for the conic constants of the anterior surface at 0 D and 8 D respectively, while using a value of −3 for the posterior conic at both accommodative amplitudes; these values are based on the work of Dubbelman and co-workers [47, 167]. The majority of these studies have shown the conic constants to be negative, with Dubbelman *et al.* [167] reporting that the

conics become more negative with accommodation; our lens example shows a similar trend.

The volume of the lens can be compared with the experimental *in vivo* data presented in the paper by Hermans *et al.* [161]. This paper indicates that the lenticular volume of five subjects between 18 and 35 years of age is in the range 150–165 mm^3. A study of 27 isolated eyes between 6–82 years old in a paper by Urs *et al.* [176] provides a regression of volume versus age, giving a volume of 172.06 ± 11.31 mm^3 for the 30 year old eye. The smaller volume given for our example could be attributed to the relatively small value for unaccommodated lens thickness, $T_0 = 3.18$ mm. A study by Koretz and co-workers suggests that the 30 year old lens thickness is in the range 3.52–3.67 mm, based on MRI and Scheimpflug imaging, respectively [177]. For this thickness range, the volume of our lens example would be 154.2–167.9 mm^3, which is in line with experimental data.

The theoretical values for surface area show the expected decreasing trend with accommodation. The surface area decrease was calculated as 3.28% over 6 D, which is comparable to the experimental MRI estimate of $4.78\% \pm 2.29\%$ over the same accommodative range (0–6 D) in the study by Hermans *et al.* [161]. This study gives values of 175.9 ± 2.8 mm^2 and 167.5 ± 2.9 mm^2 for the unaccommdated and 6 D accommodated lens, respectively. The regression formula for 27 isolated lenses provided in Urs *et al.* [176] gives a value of 170.5 ± 9.2 mm^2; usually, the isolated lenses assume the fully accommodated state. At 6 D, our model predicts a value of 147.6 mm^2; however, our initial lens is relatively thin, with a thickness of only 3.18 mm. Bringing the initial lens thickness to average values provided in Koretz *et al.* [177] of 3.52–3.67 mm would produce a surface area of 167.3–176.1 mm^2 at 6 D. Hence, the initial surface area of our model, and area decrease with accommodation, are comparable to the experimental findings.

For 30 isolated lenses aged 20–69, Urs *et al.* [178] provide a regression formula for lenticular diameter, giving a value of 9.2 ± 0.6 mm for the 30 year old lens. For the *in vivo* lens, the study of Jones *et al.* [162] gives a per-dioptre change in diameter of -0.067 ± 0.030 mm/D, corresponding to -0.402 ± 0.180 mm over 6 D. Their average unaccommodated diameter is given as 9.33 ± 0.33 mm; this represents a percentage decrease in diameter of $4.29\% \pm 1.93\%$ over 6 D. The diameter of our lens example decreases by 2.52% over the same 6 D. This decrease in diameter with accommodation, together with the initial value of 9.0 mm, is within the range of experimental data.

4.5 ANALYSIS OF LENTICULAR OPTICAL POWER AND SPHERICAL ABERRATION

It is worth noting that Eqs. 42 were generated for accommodative amplitude of the *whole* eye. Taking the cornea and lens as two refracting surfaces in a simplified schematic eye, their relative separation implies that a total *ocular* power change of 8 D requires a *lenticular* power change of approximately 10 D. An approximate thin-lens equation—differing by only 1.4% from the exact equation—was used to verify the change in lenticular power F versus accommodation [3]:

$$F = \frac{n_s - n_{aq}}{R_a} + \frac{2P}{2P-1}(n_c - n_s)\left(\frac{1}{R_a} + \frac{1}{R_p}\right) + \frac{n_s - n_{vit}}{R_p},$$

where n_{aq} and n_{vit} are the refractive indices of the aqueous and vitreous, respectively ($n_{aq} = n_{vit} = 1.336$), and the radii R_a and R_p are given in metres; P is the exponent characterising the GRIN structure of the lens. Table 5 indicates the approximate 10 D lenticular power change between the minimally and maximally accommodated states, in accordance with the 8 D total ocular power change. Note that a 30 year old subject might not be able to accommodate by 8 D, due to the onset of presbyopia. Taking into account accommodative lag and expected accommodative ability at 30 years of age, the model probably overestimates the change in lens power of the 30 year old lens.

Further validation of the method was achieved through calculation of the total lenticular SA. It is clear that an accurate model of the human crystalline lens will need to account for the trend in lenticular SA as well as the change in refractive power. Total ocular SA is known to become less positive with accommodation [15, 71, 89, 96–98, 102, 103, 155, 179–183], a trend first observed by Young in 1801 [184]; see Table 7 for a summary of recent experimental data for changes in ocular SA (Zernike coefficient Z_4^0). However, the change in lenticular SA with accommodation is not widely documented in the literature—most studies report changes in total ocular aberrations only. In general, it is difficult to disentangle the SA contribution of the human lens from that of the cornea when measuring *in vivo*. In the majority of cases, no distinction is made between the posterior corneal surface and the lens, so that the optical effects of these internal optics are considered together. In this case, the lenticular SA is found as the difference between ocular and anterior

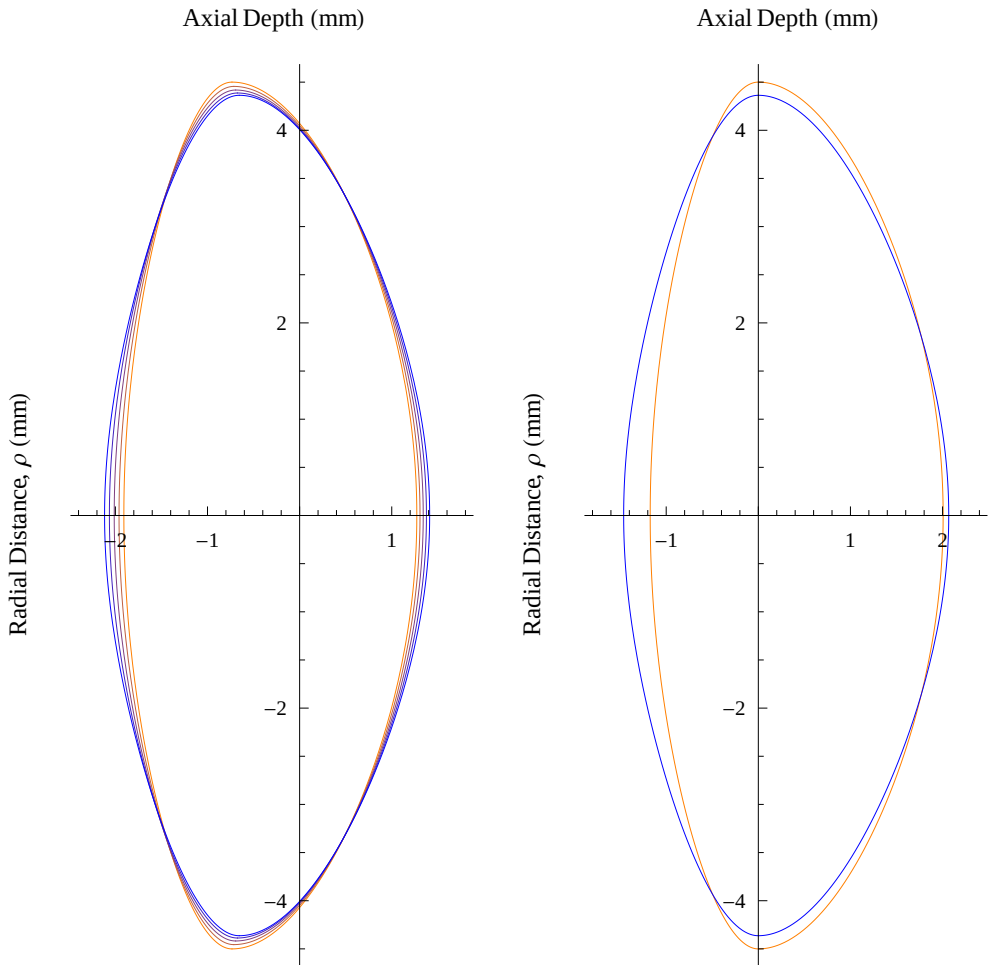

(a) Nucleus as the unmoving reference point. (b) Equator as the unmoving reference point.

Figure 8: Lens profile for ocular accommodative amplitudes from 0 D (orange) to 8 D (blue).

Table 7: Experimental changes in lenticular and ocular SA (Z_4^0) per dioptre. All data are scaled down to a 3 mm pupil diameter from their measured pupil diameters (given in mm).

Study	Measured pupil diameter	ΔSA (Z_4^0) (μm/D)	Age ± SD (Range)	# Eyes	Accommodation range (D)
† Li *et al.* [183] SRR[a]	3	−0.0043	21 ± 2.5 (19–25)	82	2.5
	5	−0.0068			
Ninomiya *et al.* [89] HS[b]	4	−0.0032	29 ± 4.4	33	3
	6	−0.0023			
López-Gil *et al.* [63] HS	4	−0.0035	21 ± 2.3 (19–29)	12	5
	4	−0.0060	36 ± 1.6 (30–39)	13	5
Cheng *et al.* [71] HS	5	−0.0056	25 ± 4 (21–40)	76	6
He *et al.* [102] SRR	6.25	−0.0035	29 ± 4.5 (24–38)	8	6

†Lenticular SA; [a]SRR, Spatially Resolved Refractometer; [b]HS, Hartmann–Shack.

corneal SA, as in the study by Li *et al.* [183]. Despite this limitation, we shall try to compare the lens model prediction with experimental data.

Before calculating the SA output of the current tool, it was first necessary to assess the contribution of conic constant to SA. According to the third-order theory applied in this paper, the SA of a surface or GRIN medium depends only on radius and conic constant. This definition is fine for surfaces which are pure conicoids of revolution, or when the pupil size is limited to the paraxial region. The solid blue curve in Fig. 10 shows the change of the SA wavefront aberration coefficient ($W_{4,0}$) calculated using the first Seidel sum (S_I) [3]:

$$W_{4,0} = \frac{1}{8} S_I.$$

The total SA of our analytical lens model was calculated from the anterior and posterior surfaces, and the GRIN structure whose profile was defined by $P = 2.94$ for the 30 year old eye, in accordance with the work of Navarro *et al.* [158]; this P-value is also within the range reported by Kasthurirangan *et al.* [185]. The corresponding iso-indicial contours are shown in Fig. 7. The lens was analysed with a collimated entrance beam in a medium with refractive index of 1.336, with $n_c = 1.416$ and $n_s = 1.376$, and a 2.66 mm iris diameter. Note that a 2.66 mm iris corresponds approximately to a 3 mm entrance pupil diameter due to typical corneal magnification of approximately 1.13 [152]. SA was calculated using the figuring conic constants K_a and K_p provided in Table 6. The SA ($W_{4,0}$) of the lens at 0 D was −0.0880 µm, and for the accommodation range of 0–2 D, a linear fit of the plot gave a slope of $\Delta W_{4,0} = -0.0677$ µm/D. This calculation is only valid for small pupil diameters. Comparison with the experimental data for pupil diameters of 3 mm and greater, in Table 7, requires an extension of the third-order theory calculation to intermediate pupil diameters.

To extend the validity of the third-order theory, we have to account for the figuring conicoid functions including the B-coefficient contribution to SA. Thus it is necessary to reconsider our description of the surface shape at intermediate pupil heights. When using only pure conicoids to represent the lens surfaces, the conic constant is responsible for the overall shape of the lens at large heights. It has been shown that the lens shape is more complex than this simple conicoid [186–188]. To provide more realistic lens shapes, we use a figuring conicoid featuring a higher-order aspheric term and B-coefficient; see Eq. 36.

The method employed in the work of Dubbelman *et al.* (2005) [167] was to fit a pure conicoid function to the experimental images of the lens surface over a 6 mm diameter; this gave an approximation to the true, highly-aspheric shape of the lens surface, with associated approximate conic constant for that surface. However, if a figuring conicoid was used, the B-coefficient would assume a certain value, and would alter the value of the approximate conic constant determined initially. The conic constants obtained using the B-coefficient are figuring conics K_a and K_p, which are suitable for use in third-order aberration analysis with small pupils.

However, to approximate the central and intermediate region of the lens, we need to modify the conic constants so that the pure conicoid of revolution more closely follows the figuring conicoid's aspheric surface. The modified values for the conic constants (K_a^* and K_p^*) can be derived by choosing ρ_1 and solving equation Eq. 36 for a corresponding sag, z_1, that defines the point (z_1, ρ_1) at which our new, pure conicoid will intersect the figuring conicoid:

$$\rho_1^2 = 2Rz_1 - (1+K)z_1^2 + Bz_1^3.$$

The approximate conic constant can be found by solving for K^* in the equation:

$$\rho_1^2 = 2Rz_1 - (1+K^*)z_1^2, \quad \text{thus:} \quad K^* = K - Bz_1.$$

Table 6 contains the figuring and approximate conic constants predicted by the current tool. Note that the approximate conics were obtained by fitting (a pure conicoid) to the lens surface at a height $\rho_1 = 2.5$ mm, which corresponds to the point M_a in Fig. 9. This height was chosen so that the internal iso-indicial contours of the GRIN structure which have not yet plateaued to the central refractive index are still suitably approximated by the pure conicoid for raytracing at 3 mm pupil diameter. For example, we can see in Fig. 9 (a) that the ray at entrance pupil height of 1.5 mm intersects the internal contour at point M_{in} at a height that is scaled down from the initial 2.5 mm height of the point M_a on the external surface. Fitting at larger heights would deteriorate the quality of the fit; thus, analysis at very large heights requires numerical raytracing.

Now, SA can be calculated for a 3 mm pupil diameter using these approximate conic constants K_a^* and K_p^*, which are provided in Table 6. The change of SA versus accommodation is given by the solid black curve in Fig. 10. From this figure, we can see that the lenticular SA predicted by the current tool—when using the

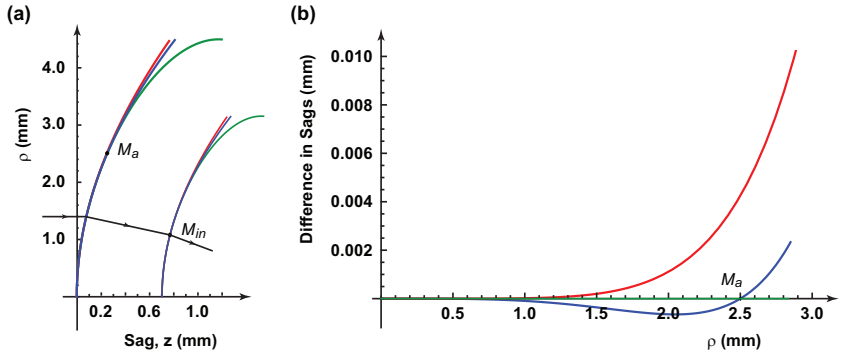

Figure 9: Fitting the figuring conicoid (green) with a pure conicoid (blue) of conic constant K_a^* at intersection point M_a, $\rho = 2.5$ mm (a). The red curve is a pure conicoid with conic constant K_a; (b): the difference in sag between green, red and blue curves for different lens heights.

approximate conics—decreases at a slower rate than with the figuring conics (blue curve). This is because the approximate conics are less negative than the figuring conics; see Table 6. Experimental data for the accommodative change in ocular and lenticular SA is provided in this Fig. 10; error bars are given where data were available. Where relevant, experimental data for SA (Zernike coefficient Z_4^0) are scaled to a 3 mm pupil. Assuming that the corneal contribution to ocular SA is constant with accommodation, the rate of change of ocular SA versus accommodation is directly related to the rate of lenticular SA change. Lenticular SA (given as internal optics) was available in the study by Li *et al.* only. The rate of change in the Zernike coefficient Z_4^0 is provided in Table 7, which is converted to $W_{4,0}$ in Fig. 10 for comparison with the third-order model prediction:

$$W_{4,0} = 6\sqrt{5}\, Z_4^0.$$

With the approximate conics, the predicted lenticular SA agrees with the well-known trend of decreasing SA with accommodation (becoming more negative). Validation of the tool was extended by analysing the decrease of SA per dioptre over a range of accommodative amplitudes. That is, the decreases in SA over the ranges 0–2 D, 0–4 D, 0–6 D and 0–8 D were each fitted with a line. The slopes of these linear fits are provided in Table 6. Given the size of the error bars and noticeable spread in experimental data [155], the decrease in Zernike Z_4^0 predicted by the current tool is in agreement with the data listed in Table 7. The predicted rate of change in SA is in line with experimental data for the available accommodative range of 0–6 D. For this range, the output of the

model shows a non-linear trend. Fitting with a second-order polynomial gives: $W_{4,0}(A) = 0.0262 - 0.0128A - 0.0145A^2$, where A is accommodation in dioptres.

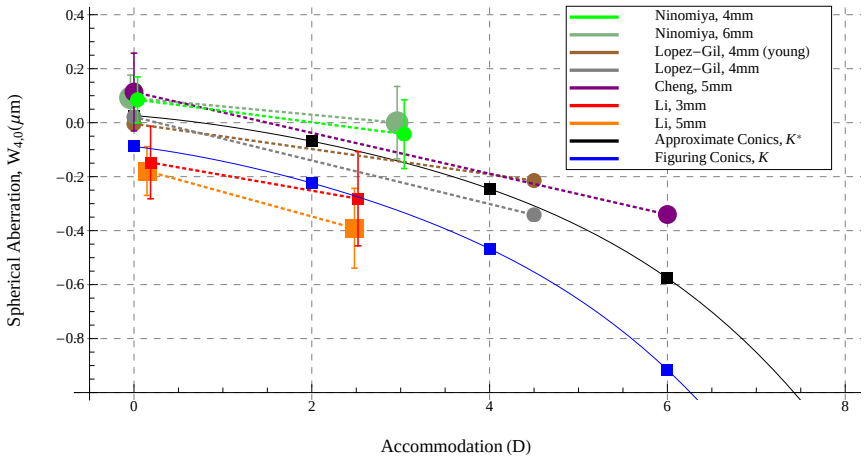

Figure 10: Change in ocular (disks) and lenticular (squares) SA; marker size indicates measured pupil diameter. All data are scaled to 3 mm pupil, and are compiled from Tables 6 & 7.

The unaccommodated lens with approximate conics shows a value of SA $(W_{4,0}) = 0.0262$ μm, which corresponds to the Zernike coefficient of primary SA: $Z_4^0 = W_{4,0}/(6\sqrt{5}) = 0.0020$ μm. This value is slightly positive, while the value obtained using the figuring conics is negative $(W_{4,0} = -0.0880$ μm); this negative value is valid for much smaller pupil diameters. Typically, the human lens shows a negative value at 0 D. Studies have found that, in general, positive corneal SA is partly cancelled by negative SA of the lens or internal optics [12, 13, 23, 25, 44, 189–193]; we stress here the generality of those results. However, a paper by Millodot and Sivak shows that the lenticular SA generally adds to that of the cornea [194]. Papers by Artal *et al.* and Glasser and Campbell show compensation in young eyes, with augmentation in older eyes [20, 24]. Furthermore, more recent papers by He *et al.* [93], and Salmon and Thibos [195] show both compensatory and additive roles of the internal optics in ocular SA production. A paper by He *et al.* shows that the lens reduces the total RMS wavefront aberration of the cornea, but individual Zernike corneal aberrations were not always compensated by the lens [196]. Kelly and co-workers also found that corneal SA was not always reduced by the lens [193].

We can see that there is large inter-subject variability in the experimental values for the SA of internal optics at 0 D; thus, we should not expect that lenticular SA is always negative. For the particular choice of initial lens geometry for this model

[168], the value of lenticular SA at 0 D is slightly positive when analysing the lens at a 3 mm pupil. More important is the trend in SA with accommodation, which is in agreement with experimental data. The approximating conics are more valid for this intermediate pupil diameter.

These approximate conics can be compared to those reported in the work of Dubbelman *et al.* (2005) [167]. Therein provided is a linear regression for the change per dioptre in conic of the lens anterior surface, as a function of the anterior conic at 0 D, K_{0a}:

$$\Delta K_a = (-0.63 - 0.07 \times K_{0a})\, A,$$

where A is accommodation in dioptres. For this, we use $K^*_{0a} = -0.83$, corresponding to an experimental $\Delta K^*_a = -4.58$ over 8 D; this can be compared with the change $\Delta K^*_a = -5.79$ predicted by the current tool, and given in Table 6.

4.6 DISCUSSION AND CONCLUSION

The modelled change in SA with accommodation is an important finding, since it represents the first clear understanding of how lenticular SA can decrease with accommodation according to Helmholtz's theory. It is widely known that increasing surface curvatures cause more positive SA, and so the accommodative decrease in lenticular radii should produce more positive SA. With this tool, we can analytically predict that the conic constants become more negative, and this in turn gives more negative SA of the lens. Our method employs the simple physical lens constraints of constant volume and fixed equator to analytically solve for the conic constants. With these conic constants, we calculate the accommodative changes in SA by raytracing through the lens GRIN medium. Since the GRIN medium follows the external surface geometry, this model takes into account both surface asphericity and GRIN structure when calculating lenticular SA.

The change in lenticular SA *in vivo* with accommodation is not widely documented in the literature, since it is difficult to disentangle the SA contribution of the human lens from that of the cornea; most studies report changes in total ocular aberrations only. Usually, the optical effect of the posterior cornea and lens are considered together. In this case, the lenticular SA is found as the difference between ocular and anterior corneal SA. In spite of this obvious limitation, we have

compared the lens model prediction with experimental data, and found that the model prediction is in agreement with the data.

With this method, it is possible to predict analytically the accommodative changes in various lenticular parameters such as surface area, equatorial diameter, refractive power and SA. We invite others to use this tool for future refinement as new data become available.

An important aspect of this new method is the constancy of lenticular volume with accommodation. With the derived formulae for figuring conic constants, it is possible to preserve the volume of the lens when modelling in raytracing software, where the specification of volume is currently not directly available. This will therefore allow modelling of a physically realistic lens in raytracing software, and give new insight into the accommodative process. If the conic constants of the lens are given as a function of accommodation, one could revisit the dependency on experimental data for accommodative changes in lenticular radii and thickness, and instead use these geometrical parameters to keep the lens volume constant. Moreover, if it is found that the lenticular volume is not constant with accommodation, one could relax the constant volume condition.

The future aim of ocular modelling is the development of a model which characterises the geometrical, optical and biomechanical properties of the ageing lens under accommodation [197]. We hope that an understanding of how the geometrical and optical properties of the lens change with accommodation will help to consolidate, in future, more information regarding the accommodation process.

5

THE AGEING CRYSTALLINE LENS

5.1 INTRODUCTION

Efforts to model the crystalline lens of the human eye are centred around faithfully representing the lens anatomically, biomechanically and optically. Anatomical and biomechanical accuracy is facilitated by the use of higher-order polynomials to describe the lens surfaces, which feature a small number of terms to prevent unnecessary complexity when fitting experimental data. The lens volume, for example, can be specified and used as an important physical constraint for modelling accommodation of the lens [143], while its growth with age is another important factor to consider. Regarding the optical properties of the lens, the GRIN nature of the lens medium has been represented analytically, with efforts to match its experimentally measured properties both qualitatively—e.g. replicating the shape of the iso-indicial contours—and quantitatively—e.g. reconstructing refractive power. The aim of this paper is to depart from geometry-invariant models and provide a representative model of the anatomy and optics of the ageing human lens.

Perhaps the most commonly used description of the refractive index from nucleus to periphery is that initially proposed by Pierscionek [2] and adopted by Smith and others [48, 158, 185]:

$$n(\zeta) = n_c + (n_s - n_c)(\zeta^2)^P, \tag{46}$$

where n_c and n_s are the refractive indices at the centre and surface of the lens, respectively; ζ is the normalised distance from lens centre to external surface; and P is an age-dependent parameter describing the steepness of the refractive index profile towards the lens periphery. In the geometry-invariant gradient index lens (GIGL) model [3], ζ has the same functional form (Eq. (46)) extending from the centre of the nucleus to all points on the lens external surface, thus resulting in invariance of geometry.

The GRIN distribution of refractive index in younger eyes has a relatively smooth increase from periphery to nucleus, and is suitably approximated by lower-order polynomials in z and r [157]. However, the older eye has a central plateau of refractive index, with a steep gradient at the periphery. To model this more abrupt distribution, higher-order polynomials have been proposed [3, 149, 158]. In addition to steepening of the axial refractive index profile with age, there is an age-related relative change in parameter P between radial and axial GRIN profiles. In the older eye, the lens iso-indicial contours approach the GIGL model. In contrast, only the sub-surface region of the younger lens has the same geometry and aspect ratio as the exterior. The internal iso-indicial contours of the young lens depart from geometrical invariance as they approach the nucleus of the lens and exhibit more rapid increase in curvature [160, 185, 198, 199]. If we consider Eq. (46), the young lens has different values of P in the axial and radial directions, respectively. This effect is perhaps most clearly demonstrated using magnetic resonance imaging (MRI) [160] and Talbot interferometry [200].

A model of the ageing human GRIN lens with different axial and radial refractive index profiles has been proposed by Bahrami *et al.* [201]. In this Adjustable Internal Structure (AIS) model, the external surfaces of the lens are conicoids of revolution. The radii of the lens surfaces control the refractive power of the lens, whereas the conic constants are used to ensure a smooth joining of anterior and posterior segments at the equator. This ties up the conics for that purpose alone, and prevents their use in aberration matching and accommodation modelling. Following on from the conclusion of Bahrami *et al.* [201], we see that it is desirable to produce a higher-order description of the iso-indicial contours of the lens. An obvious application of this is the creation of a model which, in addition to predicting optical refractive power and represent qualitatively the shape of the iso-indicial contours, can also match optical aberrations—in particular spherical aberration—of an anatomically realistic, age-dependent lens.

Similarly, the 4-variable GRIN model of Manns, de Castro and co-workers [149, 202] contains different values of P in the axial and radial directions. Also using Pierscionek's refractive index profile of Eq. (46), Manns and de Castro's model has a constant refractive index at the surfaces, which are represented by conicoids. This model is included in Table 8, in addition to the AIS model, and other recent models of the GRIN lens. The disadvantage of this model is that the surface asphericity order of 2 leads to a sharp join of the anterior and posterior lens

segments at the equator, unless one constrains the surfaces to ellipses, as done in the elliptical model of Smith *et al.* [203]. This lack of smooth join compromises the bio-mechanical structure of the lens, and the physical meaning of the lens volume is lost. Hence, the volume of the lens cannot be used as a physical parameter for modelling accommodation. Furthermore, in this model, the value of P (Eq. (46)) is a smooth function of the angle θ to the optical axis in the tangential plane, and this function is found through optimisation against experimental data. As a result, the internal structure of the lens is not explicitly defined, and therefore the optical characteristics of the GRIN bulk cannot be defined *a priori*. Consequently, developing analytical raytracing through the GRIN structure is not possible; analytical raytracing is useful as a starting point for optimisation procedures and especially for solving inverse problems. On the other hand, the functional dependence of P on θ offers a high degree of flexibility of the internal GRIN structure, where the internal iso-indicial contours might take an arbitrary shape. This flexibility is gained at the expense of stability of the optimisation process.

Both the AIS model and that of Manns and de Castro, in spite of their limitations, allow one to independently model the ageing of the GRIN profile in the axial and radial directions. Furthermore, this freedom of having two adjustable (axial and radial) GRIN profiles for the internal lens structure allows decoupling of the Optical Path Length (OPL) and refractive power of the lens, as shown later in this manuscript. In addition, one could also decouple the refractive power and SA, since the latter is primarily affected by the radial GRIN profile. The effect of radial GRIN profile on SA is seen perhaps most clearly in the 2007 paper by Goncharov and Dainty [157], where the fourth-order radial term $(n_2 r^4)$ can be used to alter SA independently of power. A sixth-order polynomial representation of the GRIN structure was adopted by Smith *et al.* [203], also allowing decoupling of power or OPL and SA. In general, if polynomials are to be used, one needs a radial profile of order at least 4 to adjust SA of the bulk independently of power. For this reason, the models of Liou and Brennan [156] and Díaz *et al.* [204] do not offer the decoupling. The axial profile of Díaz *et al.* contains trigonometric functions which can be expanded in a power series in z, resulting in an equivalent polynomial of order 3.

In principle, one can decouple the power, OPL and SA by departing from the constraint that the GRIN iso-indicial contours must be concentric with the external surface of the lens. This approach was adopted in the 2014 model of Navarro [205], where the conic constant of the GRIN bulk is different to the conic constant of the

external lens surface, resulting in a peripheral zone of zero axial thickness and constant refractive index. This approach limits the accommodative ability of the model, since the changes in the sub-surface region during accommodation have no concrete physical basis. In terms of accurately modelling the ageing of the GRIN medium, one needs to be able to adjust the structure such that the ratio between the axial and radial profile exponents (P_z and P_y) can assume not only an integer value, but any rational value. The polynomial representation of refractive index profile is not ideal because of the discrete nature of the power terms involved; since, for small ray heights, the lowest-order polynomial term is responsible for the lens optical properties. This flexibility is only available in models with decoupled axial and radial profiles, such as those of Manns, de Castro *et al.* [149, 202], the AIS model of Bahrami *et al.* [201] and the proposed AVOCADO model. For instance, in a recent paper by Pierscionek *et al.* [200], the representative examples of GRIN profile fits for the 16 year old lens have values of $P_z = 2.88$ and $P_y = 1.78$, whereas the 91 year old eye has values of $P_z = 2.40$ and $P_y = 2.53$.

In terms of matching the GRIN structure to experimental data, the stability of the optimisation process depends on the degrees of freedom in the mathematical representation of the GRIN structure. Choosing the lens external shape as a basis to confine the GRIN distribution during optimisation is probably the most sensible way to ensure optimisation convergence, because it limits the number of free parameters to the practical minimum—for example, the anterior and posterior lens radii and conic constants, and central lens thickness. Such use of the external shape to define the GRIN structure is also convenient for performing raytracing from back-to-front. This invertibility for raytracing is not available in the models of Liou and Brennan [156] or Diaz *et al.* [204], since the GRIN is not explicitly given in terms of the external lens shape parameters. Furthermore, confining the GRIN structure to the external shape is essential for modelling accommodation. In this manuscript, we show that the proposed AVOCADO model offers simplicity and flexibility to supersede existing models.

Table 8: A compilation from the literature of previous models of the human lens, including the AVOCADO model.

Geometrical properties	Smith *et al.* [203] elliptical	Liou and Brennan [156]	Navarro *et al.* 2007 [158]	Goncharov and Dainty [157]	Diaz *et al.* [204]	Manns, de Castro *et al.* [149, 202]	Navarro 2014 [205]	Sheil *et al.* [143]	AIS [201]	AVOCADO
P_z (axial) & P_y (radial) decoupled	✓	✓	—	✓	✓	✓	—	—	✓	✓
ref index max order axial	6	2	P	4	3	$P1 = P(0)$	P	2P	P_z	$P_z = 2P$
ref index max order radial	6	2	P	4	2	$P2 = P(\pi/2)$	P	2P	P_y	$P_y = {}^{2P}/_{(m+1)}$
surface asphericity order	2	2	2	2	2	2	2	3	3	3
invertibility for raytracing	✓	—	✓	✓	—	✓	✓	✓	✓	✓
analytical raytracing	—	—	—	—	—	—	—	✓	✓	✓
Structural features										
accommodation	✓	—	✓	—	—	—	—	✓	✓	✓
GRIN ageing (axial)	✓	—	✓	✓	✓	✓	✓	✓	✓	✓
GRIN ageing (radial)	✓	—	✓	✓	✓	✓	✓	✓	✓	✓
Bio-mechanical features										
volume	✓,K[†]	—	—	—	—	—	—	✓,K	✓,K	✓,K
smooth join	✓,K	—	—	✓,K	—	—	—	✓	✓,K	✓
concentricity of iso-indicial contours	✓	—	✓	✓	✓	✓	—	✓	✓	✓
Optical properties										
Power (bulk)	P_z, P_y	P_z, P_y	P_z, K	P_z, P_y	P_z, P_y	$P(\theta)$	P_z	P_z	P_z, P_y	P_z, P_y
SA (bulk)	P_y	P_y	P_z	P_y	P_y	$P(\theta)$	P_z	P_z	P_y	P_y
OPL	P_z	P_z	P_z	P_z	P_z	P_1	P_z	P_z	P_z	P_z
Decoupling of optical properties										
power and SA (bulk)	✓	—	—	✓	✓	✓	—	—	—	✓
power and OPL	✓	✓	—	✓	✓	✓	—	—	✓	✓
power and conics	✓	✓	—	✓	✓	✓	✓	✓	✓	✓

[†] The presence of conic constant K on a line indicates that K is tied to represent that feature and is not available for any other properties.
For example, in elliptical models, K must be used to ensure a smooth join at the equator, and is not available for other use.

5.2 MATHEMATICAL DESCRIPTION OF THE LENS INTERNAL ISO-INDICIAL CONTOURS

The surfaces of the new lens model are figuring conicoids [159, 188]. Representing the lens anterior surface height ρ as a function of sag z along the optical axis we have:

$$\rho^2 = x^2 + y^2 = 2R_a(T_a + z) - (1 + K_a)(T_a + z)^2 + B_a(T_a + z)^3,$$

where R_a, T_a and K_a are the radius, thickness from nucleus to pole, and conic constant of the anterior portion of the lens, respectively. The B-coefficient here is responsible for a smooth join of iso-indicial contours at the lens periphery. The equation above describes the external surface of the lens, as in the GIGL model. However, in the new model, the radii of curvature of the internal contours of the lens are not scaled linearly with the value of the dimensionless parameter ζ (in the axial direction $\zeta = -z/T_a$). In the original GIGL model, the radii must scale linearly with ζ so that the internal contours mimic the external shape of the lens, while the conic constants are left unaltered. Noting that the internal contours are represented by lower-case constants r_a, t_a, k_a and b_a, we have the following height of an internal contour:

$$\rho^2 = 2r_a(t_a + z) - (1 + k_a)(t_a + z)^2 + b_a(t_a + z)^3,$$

where the lower-case symbols can be replaced by their scaled upper-case counterparts to give the GIGL model:

$$\rho^2 = 2\zeta R_a(\zeta T_a + z) - (1 + K_a)(\zeta T_a + z)^2 + \zeta^{-1} B_a(\zeta T_a + z)^3.$$

In the new lens model, the radii are scaled non-linearly according to an appropriate power, m, of ζ. Another crucial component is that the conic constant, K, of an iso-indicial contour varies with ζ. To be more precise, the *shape factor* $Q = 1 + K$ of the surface is made to scale with ζ to the power of $2m$. This gives the following representation for an internal contour height:

$$\rho^2 = 2\zeta^{2m+1} R_a(\zeta T_a + z) - \zeta^{2m}(1 + K_a)(\zeta T_a + z)^2 + \zeta^{2m-1} B_a(\zeta T_a + z)^3, \quad (47)$$

where we introduce the new age-related parameter m. This non-uniform scaling of the contour geometry provides useful flexibility of the model, as we shall see. For values of $m > 0$, the internal contours depart from geometrical invariance, resulting in an appearance somewhat similar to the cross-section of an avocado, as seen in Fig. 11((a)). Using positive values of m enables us to describe the GRIN distribution in younger eyes, with m varying from roughly 1 to 0 as the eye ages. Eq. (47) simplifies to a geometry-invariant model for $m = 0$, shown in Fig. 11((b)). A negative value of m produces a lens with a larger value of P in the radial profile, as observed in recent studies [185, 200], and shown in Fig. 11((c)). Note that in Fig. 11, the three lenses have the same external geometry and size; only m is different ($m = 1$, 0 and -0.5).

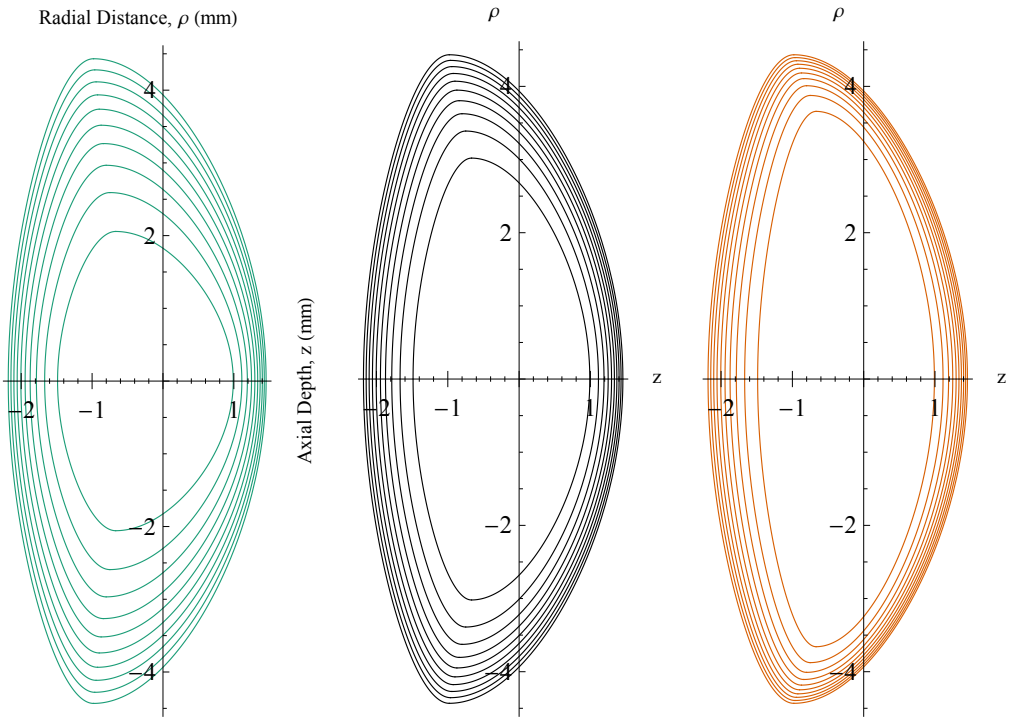

(a) $m > 0$ gives a younger lens, with an "avocado pit" in the centre.

(b) $m=0$ gives the GIGL model.

(c) $m = -0.5$ gives an effect opposite to the avocado.

Figure 11: Lenticular plots showing iso-indicial contours for young ((a)) and old ((b)). Negative m shows a bunching of contours towards the equator ((c)), a behaviour seen in recent studies [185, 200]. The three lenses have the same external geometry and parameter P representative of a 30 year old, after [47, 158, 206]: $R_a = 11.2$ mm, $R_p = 6.0$ mm, $K_a = -4.5$, $K_p = -1.1$, lens thickness $T = 3.6$ mm, $P = 3$, $n_c = 1.415$ and $n_s = 1.37$.

The new parameter m allows us to decouple the axial and radial refractive index profiles of the lens. Eq. (46) describes how the refractive index changes as a

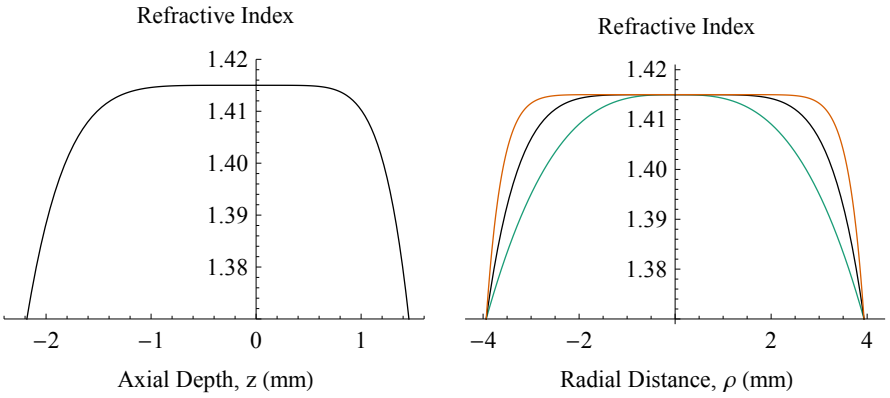

(a) Axial profiles ($\rho = 0$) are the same for all lenses.

(b) Radial profile ($z = 0$) shows the most gradual change in the younger lens (green).

Figure 12: Comparing the axial ((a)) and radial ((b)) refractive index profiles of the lenses of Fig. 11.

function of the normalised distance ζ in any direction from the nucleus within the lens. We can also look at how the index varies with distance z along the axis of the lens ($\rho = 0$); and distance ρ along the radial line $z = 0$. For the axial index profile—noting that $\Delta n = n_c - n_s$ and $\zeta = z/T_p$ for the posterior portion of the lens— Eq. (46) becomes:

$$n(\rho, z)|_{\rho=0} = n_c - \left(\Delta n / T_p^{2P}\right) z^{2P};$$

that is, the refractive index changes to the power of 2P, as in the GIGL model. For the radial profile, however, we take Eq. (47) and re-write it for the posterior surface and set $z = 0$, giving:

$$\begin{aligned} \rho^2 &= 2\zeta^{2m+1} R_p (\zeta T_p) - \zeta^{2m} (1 + K_p)(\zeta T_p)^2 + \zeta^{2m-1} B_p (\zeta T_p)^3 \\ &= \zeta^{2m+2} \left(2R_p T_p - (1 + K_p) T_p^2 + B_p T_p^3\right) \end{aligned} \tag{48}$$

The maximum height ρ_0 of the lens along the ordinate $z = 0$ occurs with $\zeta = 1$, such that Eq. (47) becomes

$$\rho_0^2 = 2R_p T_p - (1 + K_p) T_p^2 + B_p T_p^3; \tag{49}$$

thus, Eq. (48) can be simplified to express any height along this ordinate as a function of ρ_0 according to the relation $\rho^2 = \zeta^{2m+2}\rho_0^2$. This can be rearranged for ζ to give the radial profile:

$$\zeta = (\rho/\rho_0)^{\frac{1}{m+1}}. \tag{50}$$

Inserting this expression into Eq. (46) as before, we see that the refractive index now varies radially as:

$$n(\rho, z)|_{z=0} = n_c - \left(\Delta n/\rho_0^{\frac{2P}{m+1}}\right)\rho^{\frac{2P}{m+1}};$$

i.e., the refractive index decreases radially from nucleus to surface along the line $z = 0$ by the exponent $2P/(m+1)$. Comparing the exponents $2P$ and $2P/(m+1)$, we clearly see that the two refractive index profiles are decoupled; this effect is seen in Fig. 12. It is worth noting how the vertical profile of the GRIN structure affects the lens optical power; in the paraxial region, the $\rho^{2P/(m+1)}$ exponent is related to optical power by the scaling of radii: $r_p(\zeta) = \zeta^{2m+1}R_p$.

5.3 AVERAGE AND EQUIVALENT REFRACTIVE INDICES

The horizontal and vertical profiles of the GRIN can be used to account for the differences in the average refractive index (n_{av}) and the equivalent refractive index (n_{eq}) of the lens. It is well known that n_{av} and n_{eq} are two phenomena originating from simplification of the GRIN; n_{av} accounts for axial path length measurements made using OCT, and n_{eq} for the lens refractive power. A recent paper discusses the idea of separate values for n_{av} and n_{eq}, and their difference with age [199]. The average refractive index is related to the time of flight of light rays passing along the optical axis of the lens. In OCT, the information provided to the user corresponds to optical path length rather than physical distance. Thus, we can see that the measurement depends on both refractive index and physical distance. In the case of the GRIN lens, the total axial optical path is given by:

$$\mathrm{OPL} = \int_{-T_a}^{T_p} n(z)\,dz,$$

This integral can be reduced to simple multiplication with the introduction of n_{av}:

$$\mathrm{OPL} = n_{av}\Delta z, \tag{51}$$

where $\Delta z = T_a + T_p = T$, the axial thickness of the lens. The OPL for anterior and posterior lens segments is found from the sum:

$$\mathrm{OPL} = \int_{-T_a}^{0} n_c - \Delta n \left(\frac{z}{T_a}\right)^{2P} dz + \int_{0}^{T_p} n_c - \Delta n \left(\frac{z}{T_p}\right)^{2P} dz.$$

Hence, n_{av} is given by:

$$n_{av} = n_c - \Delta n/(2P+1). \tag{52}$$

In a GRIN lens, the age-dependent parameter P determines the axial behaviour of the GRIN profile, and hence n_{av}.

Similarly, n_{eq} is used to account for another property of the lens; namely, its optical refractive power. Since refractive power involves only the paraxial properties of the lens, it is convenient to replace the GRIN of the lens with a constant equivalent refractive index, n_{eq}, thus greatly simplifying raytracing through the eye model.

The thin-lens power of the AVOCADO model can be approximated when the lens is immersed in a medium of refractive index n as:

$$F_{thin} = (n_s - n)\left(\frac{1}{R_a} + \frac{1}{R_p}\right) - \frac{4P\Delta n \Delta R}{\beta R_a R_p}, \tag{53}$$

where $\Delta R = R_a + R_p$ and $\beta = 2(2m + 1 - 2P)$. As expected, the lens power now depends on m as well as P.

In terms of n_{eq}, we can also express the power of the homogeneous lens using the thick-lens equation to give:

$$F_{eq} = (n_{eq} - n)\left(\frac{1}{R_a} + \frac{1}{R_p} + \frac{T(n - n_{eq})}{R_a R_p n_{eq}}\right) = F_{thin}.$$

Hence, we can solve this quadratic equation for n_{eq}:

$$n_{eq} = \frac{1}{\beta(T - \Delta R)}\left(nT\beta - \gamma\Delta R + \sqrt{u}\right), \tag{54}$$

where $u = \gamma^2\Delta R^2 + 2nT\beta\Delta R\big((2m+1)(n-n_s) + 2P(n_c - n)\big)$ and $\gamma = n_s + 2mn_s - 2Pn_c$. This approximate formula provides a convenient way to calculate the equivalent refractive index of the AVOCADO lens model. Now we can consider a simple but illustrative example (Fig. 11), where the two lenses (Fig. 11((a)) & 11((b))) have the same external geometry and values of P, n_c and n_s, and hence n_{av}; but differ-

ent values of m. From Eqs. (53) & (54), it follows that by altering only parameter m from 0 to 1, it is possible to induce large changes of $\simeq 0.04$ in n_{eq}, and $\simeq 10$ D in the refractive power of the lens. In the GIGL model, this is not possible because $m = 0$. Figure 13 below is a plot of lens power (F) vs m for different values of P, showing that changing m from 0 to 1 induces large changes in F. Shown in this figure are the powers calculated using the thin-lens formula of Eq. (53), and exact raytracing introduced in the following section. This figure shows that while exact raytracing is preferred, Eq. (53) provides a convenient means of predicting lens power, with a typical over-estimate of approximately 0.5 D or less. A more accurate expression for lens power can be derived and used in place of this thin-lens formula [207].

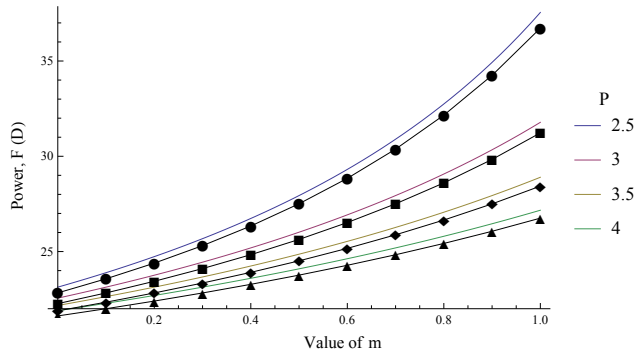

Figure 13: Lens power F vs m for different values of P, calculated using the thin-lens formula of Eq. (53) (solid lines) and exact raytracing (data points) with a ray height of 20 µm. $R_a = 11.2$ mm, $R_p = 6.0$ mm, $K_a = -4.5$, $K_p = -1.1$, lens thickness $T = 3.6$ mm, $P = 3$, $n_c = 1.415$ and $n_s = 1.37$.

It can be argued that, in the GIGL model, the extra parameter required to distinguish between n_{av} and n_{eq} could be provided by varying either n_c or n_s. While it is true that an age-related change in these parameters will alter the values of both n_{av} and n_{eq}, it changes both *simultaneously*—they cannot be decoupled in the same way as with the new parameter m. To see this, we note from Eq. (52) that n_{av} is affected if we alter either n_s, n_c, Δn or P. If we keep n_c constant, and assuming we have a value of n_{av} that we wish to match to experimental data, is there a way to alter Δn and P to keep n_{av} constant while changing n_{eq} sufficiently? It can be shown that typical values of $\Delta n = 0.04$–0.06 require a range of $P = 3.9$–6.1, resulting in a maximum change in n_{eq} of only 0.0005. Thus, this approach of decoupling n_{eq} and n_{av} does not give a satisfactory result.

Given the external shape of the lens, the GRIN medium can be optimised to account for the experimentally observed measurements of refractive power and

hence n_{eq}, as well as matching the axial OCT measurements of optical path length using n_{av}, as discussed above.

Decoupling the axial and radial refractive index profiles of the lens is an important aspect of lens modelling. For example, the 2008 study by Kasthurirangan *et al.* [185] and the 2015 study by Pierscionek *et al.* [200] show that both young (accommodated and unaccommodated) and old lenses can have larger values of P in the radial section. This result can be reproduced with the extra flexibility afforded by decoupling the axial and radial exponents in the new AVOCADO lens model. The flexibility of the new model allows the generation of a GRIN structure with any particular axial and radial refractive index profiles. The above results show that the new model is capable of producing a lens that has a larger equivalent value of P in either the axial profile ($m > 0$) or radial profile ($m < 0$).

Regarding the equivalent refractive index of the lens, n_{eq}, we emphasise the role that it plays: for a given ocular geometry (curvatures of the ocular surfaces and intraocular distances) and refractive indices of the cornea, aqueous and vitreous, n_{eq} makes up the remainder of the optical power of the eye. n_{eq} becomes particularly useful with personalised ocular modelling, where the curvatures and conic constants of the ocular surfaces can be measured, for example, and used to provide the framework on which optimization of the GRIN lens model can be based. In this type of personalised modelling, we note that it will be beneficial to use both the radius and conic constant of a surface to define the properties of the optical zone for image formation. The flexibility of the new AVOCADO lens model is important here since it allows us to use the radius and conic constant for that purpose, while the B-coefficient ensures a smooth join at the boundary.

5.4 EXACT RAYTRACING FOR POWER AND SA ANALYSIS

In addition to the simplified paraxial analysis above, we can use exact raytracing to calculate the refractive power and aberrations of the lens, by solving the differential ray equation [140, 208]. Already mentioned is the possibility of decoupling the axial optical path length and refractive power of the lens, F. We can show this by example below, where the value of P is fixed so that OPL is unchanged, but m is altered. The result is that the refractive power changes considerably, shown in Fig. 13; hence, n_{av} and n_{eq} are decoupled.

From this figure, it becomes apparent that the AVOCADO model offers an additional degree of freedom when reconstructing the internal structure of the lens. OCT measurements provide information on time-of-flight of the light through the lens, and for a given lens thickness Δz, one can determine n_{av} (Eq. (51)); also, for given values of Δn and n_c, P can be determined from Eq. (52). If one can also measure F and the external shape of the lens, the value of m can be found using exact raytracing—see Fig. 13; alternatively, the approximate value of m can be found from the thin-lens approximation (Eq. (53)). Since refractive power and time-of-flight are decoupled, as outlined above, the method is feasible as a practical way of reconstructing the GRIN profile.

Now, we can analyse SA of the lens as a function of m. From population studies of ocular aberrations, SA is the only classical (rotationally symmetric) aberration term to have an on-axis average that is significantly different from zero [36]; hence we can use the value of SA as a useful metric for verification of the model. The AVOCADO model reduces to the GIGL model for $m = 0$, which is viable in terms of SA prediction [143]. Note that SA is also strongly affected by the choice of the lens conic constants. Figure 14 shows a series plots of the LSA of the lens for different values of m, with all other lens parameters fixed, with $P = 3$. The data from numerical raytracing are shown in red, while 8th-order (even coefficients only) polynomial fits are shown in blue.

The quadratic term (ρ^2) in this polynomial fit of LSA is converted to transverse SA and then integrated to give the wavefront aberration polynomial coefficient ($W_{4,0}$) [209] for a pupil diameter of 4 mm. Assuming the system has zero defocus, this term can be converted to Zernike SA using the formula:

$$Z_4^0 = \frac{W_{4,0}}{6\sqrt{5}}.$$

Using this method, for each value of m, the corresponding plot of LSA gives us a single value Z_4^0. Figure 15 shows the change in Z_4^0 as a function of m for several values of P. Comparing Figs. 13 & 15, one can see that with increasing m, the lens becomes more powerful and its SA is more pronounced. In particular, for $m = 0.4$ and $P = 3$, $Z_4^0 = -0.0380$ µm, which is comparable to the GIGL case where $m = 0$ and $Z_4^0 = -0.0363$ µm—see Fig. 14. For values of P smaller than 3, the value of Z_4^0 becomes rapidly more negative with increasing m—see Fig. 15. It can be seen from Figs. 13 & 15 that for a given value of m, one obtains unique values of F and

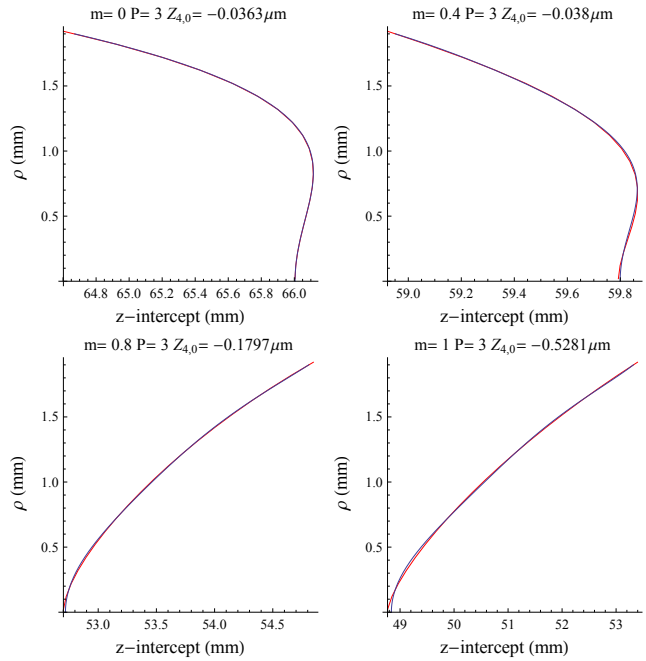

Figure 14: Plots of LSA for different values of m. $R_a = 11.2$ mm, $R_p = 6.0$ mm, $K_a = -4.5$, $K_p = -1.1$, lens thickness $T = 3.6$ mm, $P = 3$, $n_c = 1.415$ and $n_s = 1.37$. Z_4^0 is calculated for 4 mm pupil diameter.

Z_4^0. To decouple optical power (F) from third-order SA (Z_4^0) for a given value of P, we will introduce the logarithmic description of the lens core in the following section.

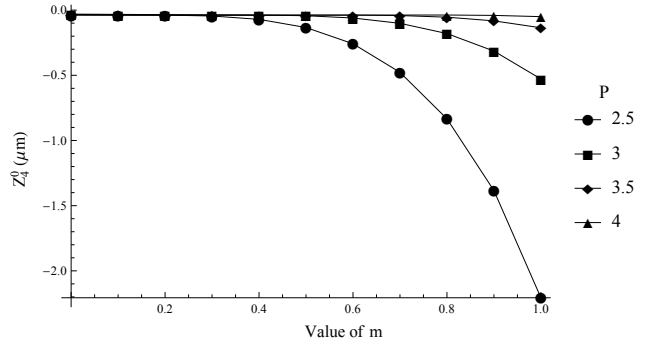

Figure 15: SA (4 mm) vs m for different values of P. $R_a = 11.2$ mm, $R_p = 6.0$ mm, $K_a = -4.5$, $K_p = -1.1$, lens thickness $T = 3.6$ mm, $n_c = 1.415$ and $n_s = 1.37$.

5.5 VOLUME AND ASPECT RATIO OF AN INTERNAL ISO-INDICIAL CONTOUR

Accommodative changes in lens radii and thickness can be accompanied with changes in conic constants to maintain constancy of volume. It can be shown that the volume of the entire lens is given by the formula:

$$V = \frac{1}{6}\pi[5R_pZ_p^2 + 5R_aZ_a^2 - (1+K_p)Z_p^3 - (1+K_a)Z_a^3],$$

where Z_a and Z_p are the respective sags, and K_a and K_p are the respective conic constants, of the anterior and posterior portions of the lens that change with accommodation [143]. This formula demonstrates the role of conic constants in volume specification. We can obtain an expression for the volume of an internal contour of the lens by taking the equation above and replacing the constants by their scaled counterparts, such that the volume as a function of the normalised distance ζ is given by:

$$v(\zeta) = \zeta^{2m+3}V. \tag{55}$$

This expression shows that the volume of any particular contour is invariant under accommodation. This could prove useful in future studies of the accommodation-related biomechanical properties of the lens internal structure.

The aspect ratio of the external shape of the lens is given by $A_0 = 2\rho_0/T$, where ρ_0 is found from Eq. (49). From Eq. (50), $\rho(\zeta) = \zeta^{m+1}\rho_0$, and since the axial thickness $t(\zeta) = \zeta T$, we see that the aspect ratio of an internal contour is given by:

$$A = \frac{2\rho(\zeta)}{t(\zeta)} = \frac{\zeta^{m+1}}{\zeta}\frac{2\rho_0}{T} = \zeta^m A_0.$$

Thus, in the limiting case as $\zeta \to 0$, the aspect ratio of the lens core vanishes ($A \to 0$). For raytracing, this is not critical, since the refractive index of the core is a smooth function of ζ. Mathematically, we can stabilise the aspect ratio A by altering the parameter m near the lens core, by introducing a dependence on the quantity ζ; hence:

$$A = \zeta^{m(\zeta)}A_0. \tag{56}$$

One can find a function for m such that, in the limiting case $\zeta \to 0$, the aspect ratio A of the core is a constant value. One such function for m is:

$$m = \left(\frac{1+w}{w}\right) m_0 \frac{\ln(\frac{1+w\zeta}{1+w})}{\ln(\zeta)}. \tag{57}$$

For this function, as we approach the core ($\zeta \to 0$), $m \to 0$ and the aspect ratio A converges to a finite value:

$$A \to A_0 \left(\frac{1}{1+w}\right)^{m_0\left(1+\frac{1}{w}\right)}. \tag{58}$$

This approach stabilises the aspect ratio of the core. Note that w can be used as a free parameter, but must be greater than -1; the AVOCADO model reduces to the GIGL model as $w \to -1$. For $w = 1$ and $m_0 = 1/2$, for example, $A \to 1/2 A_0$ as $\zeta \to 0$. As we approach the lens surface ($\zeta \to 1$), $A \to A_0$ and $m \to m_0$; hence, m becomes independent of w, and m_0 takes on the full geometrical significance of m. The parameters m_0 and w afford flexibility of the model, since they can be used to generate internal iso-indicial contours with specific aspect ratios at a given value of ζ. Note that neither m_0 nor w affect P; hence, the axial optical path length will be unaffected.

The aspect ratio of an internal core can be plotted as a function of ζ, shown in Fig. 16. This figure highlights the geometrical significance of w, as it is seen to alter both the rate of change of aspect ratio and the limiting value in the lens core, as $\zeta \to 0$. Equation (56) can be solved to find the value of w that gives a desired aspect ratio at a given iso-indicial contour depth ζ.

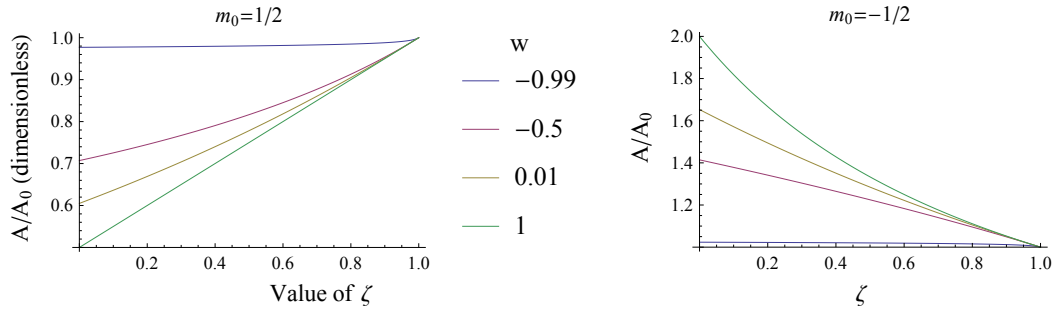

(a) $m_0 > 0$ shows a monotonically decreasing aspect ratio as the contours approach the core ($\zeta \to 0$).

(b) $m_0 < 0$ allows the aspect ratio to increase as $\zeta \to 0$.

Figure 16: The normalised aspect ratio (A/A_0) of an internal contour using Eq. (56).

Equation (57), when inserted into Eq. (47), gives the following representation for an internal iso-indicial contour:

$$\rho^2 = 2\zeta\phi R_a(\zeta T_a + z) - \phi(1 + K_a)(\zeta T_a + z)^2 + \zeta^{-1}\phi B_a(\zeta T_a + z)^3, \qquad (59)$$

where $\phi(\zeta) = \left(\frac{1+w\zeta}{1+w}\right)^{2m_0(1+1/w)}$.

Equation (59) illustrates the optical significance of parameters m and w, as follows. The radius R_a is scaled by $\zeta\phi(\zeta)$, and is directly responsible for the lens power. This effect can be seen in Fig. 17, where m produces a large change in power. Furthermore, in Eq. (59), the shape factor $(1 + K_a)$ is scaled by the factor $\phi(\zeta)$; hence, in addition to the geometrical significance of w outlined above, w has optical significance in altering SA according to this scaling of the shape factor.

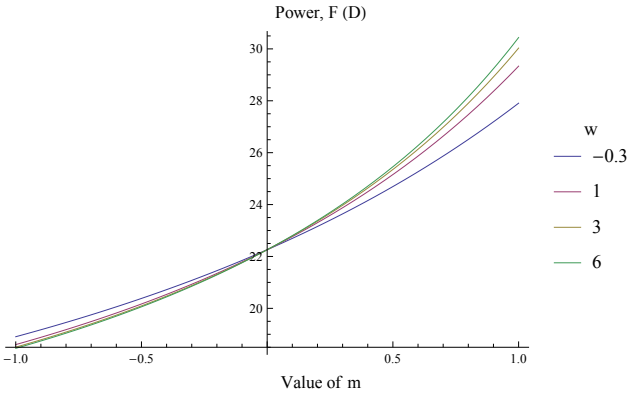

Figure 17: Plot of optical power vs m for different values of w, using the log function. $R_a = 11.2$ mm, $R_p = 6.0$ mm, $K_a = -4.5$, $K_p = -1.1$, lens thickness $T = 3.6$ mm, $P = 3$, $n_c = 1.415$ and $n_s = 1.37$. Note that $m = 0$ gives the GIGL model.

Now having an additional parameter w, we can easily decouple SA and optical power. Figure 18 is a plot of SA vs m for $P = 3$, showing that altering w affects the change of SA with m. The LSA of a selection of lenses from Fig. 18 is shown in Fig. 19. These lenses all have the same optical power $F = 28.6$ D; this can be achieved by adjusting m for a given w. As a result, each lens has a different amount of SA, while we have constant values for optical power, F; and P, which corresponds to constant axial optical path length. It is evident that SA is decoupled from both P and refractive power, and hence SA is decoupled from n_{av} and n_{eq}. Having w as an additional free parameter not only allows us to change the sign of SA, but also helps to change the higher-order SA, so that the LSA curves develop the opposite trend (bending towards the lens) at intermediate pupil heights—see

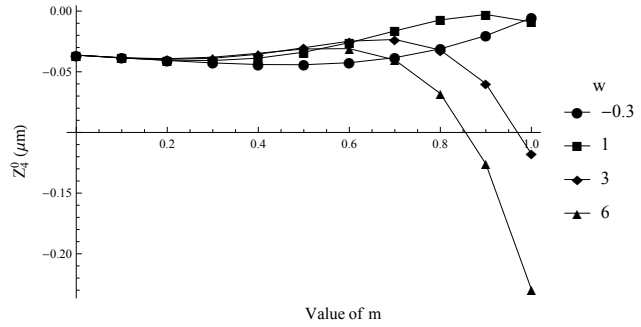

Figure 18: SA (4 mm) vs m for different values of w using the log function; $P = 3$. $R_a = 11.2$ mm, $R_p = 6.0$ mm, $K_a = -4.5$, $K_p = -1.1$, lens thickness $T = 3.6$ mm, $n_c = 1.415$ and $n_s = 1.37$.

the case of $w = -0.3$ in Fig. 19. In this case, the higher-order SA counteracts lower-order SA, and the choice of m and w will affect this SA balancing.

The logarithmic model of the lens core with P, m and w enables decoupling of three fundamental optical characteristics of the lens, to wit optical power, axial optical path length and third-order spherical aberration, without changing the external shape of the lens. On the other hand, the near-surface GRIN structure conforms to the external shape of the lens, which is necessary for accommodation modelling.

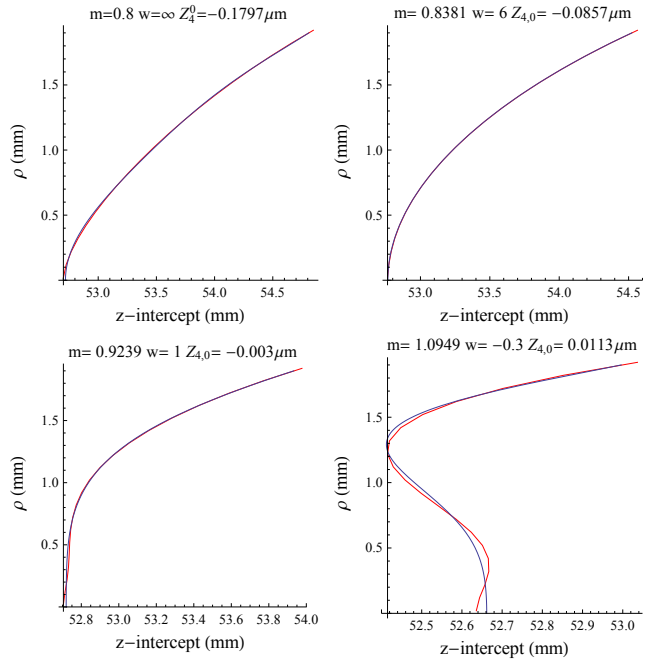

Figure 19: Plots of LSA for different values of m and w using the log function. $R_a = 11.2$ mm, $R_p = 6.0$ mm, $K_a = -4.5$, $K_p = -1.1$, lens thickness $T = 3.6$ mm, $P = 3$, $n_c = 1.415$ and $n_s = 1.37$. Z_4^0 is calculated for 4 mm pupil diameter.

5.6 DISCUSSION AND CONCLUSION

The use of a cubic profile is perhaps the simplest way to describe the lens external shape in an anatomically realistic way, while the conic constants can be used for aberration matching. The inclusion of parameter m is a convenient way to attain a particular value for the ratio $n_{av} : n_{eq}$ for a given external lens geometry. Furthermore, the age-dependence of m and P provides a useful way to account for the experimentally observed change in iso-indicial contour shape. Using the three parameters P, m and w, this new model can be used as a fundamental tool for experimental research, so that optical path, refractive power and SA measurements will allow reconstruction of the internal structure of the lens in a way that was not possible previously.

When compared to second-order conic descriptions of the lens, the cubic profile of this model imparts an anatomical accuracy to the model. With the resulting smooth equatorial join, the lens volume becomes physically meaningful and is a powerful constraint for accommodation [143]. This is essential for study by finite element methods and analysis of the accommodation-dependent properties of the ageing human eye. Therefore, we are one step closer to the ultimate goal of having a biomechanically accurate age-dependent accommodative model of the human lens, capable of predicting optical path length, refractive power and spherical aberration.

One interesting application of this core flexibility could be in the study of accommodation, where the external aspect ratio A_0 of the lens is changing. If the older eye has a stiff core in the very centre of the lens, then the aspect ratio of this *core* will not change with accommodation. Hence, we can apply Eq. (58) to the two separate accommodation states of the lens, with the condition that the aspect ratio A of the core does not change. If we wish to keep m_0 constant with accommodation, we can use this condition to solve for an accommodation-dependent value of w. Alternatively, we need not use the core in the limiting case $\zeta \to 0$; we could use any particular value of ζ—e.g. a value of $\zeta = 2/3$ might represent the lens nucleus. Together with an analysis of volume using Eq. (55), this could form the basis of a mathematical description of presbyopia.

6

FUTURE WORK AND CONCLUSIONS

6.1 FUTURE WORK

As outlined at the end of Chapter 5, the AVOCADO model can be used to alter OPL, optical power and SA independently. Furthermore, it can be combined with the approach of Chapter 4 to produce an accommodative model.

The proposed AVOCADO model includes a new description of the lens GRIN bulk. With the addition of new parameters m and w, the axial and radial GRIN profiles can be changed independently. This is a departure from the geometry-invariant model, and the aberrations are calculated using exact raytracing. To our knowledge, exact raytracing has not been performed through cubic surfaces to date. The raytracing procedure has been implemented in the C language, meaning that the code could eventually be used in Zemax raytracing software.

The combination of third-order surfaces and independence of P, m and w could prove useful for generating a combined mechanical and optical model of the lens. For example, the thickness, radii and conics of the lens external shape could be used to define the unaccommodated lens volume. The constancy of volume could be used with finite element methods to study the mechanical properties of the lens with accommodation. This finite element analysis might produce an accommodated lens with certain external radii and conic constants. Next, the lens internal bulk can be adjusted independent of the external shape to match the measured optical properties of the lens. First, P can be changed to match optical path length. Next, m and w can be used to alter optical power and spherical aberration. In this way, we would have a lens simultaneously satisfying several mechanical and optical constraints. This is not possible with any previous lens models. The AVOCADO model can be used as a practical tool for matching experimentally measured values of OPL, optical power and SA with accommodation.

Future work could involve using the AVOCADO model to account for the experimentally measured age-related change in refraction, called the lens paradox. Briefly, the lens paradox is the measured decrease (or relatively slow increase) in

refractive power of the human eye, despite the fact that the lens radii become more highly curved and hence more powerful. The paradoxical nature arises because, although the lens surfaces become more powerful, the lens power decreases. While the refractive state of the eye is relatively stable from 20–40 years [210], a hyperopic shift is observed until approximately 60 years [117–119, 211–219]. After the age of approximately 70 years, some studies found a myopic shift in refraction [117, 118, 212, 215], probably due to the formation of cataract [220–222]. This is summarised in Fig. 20.1 of *Optics of the Human Eye*, by Atchison and Smith [5], adapted in Fig. 20 below.

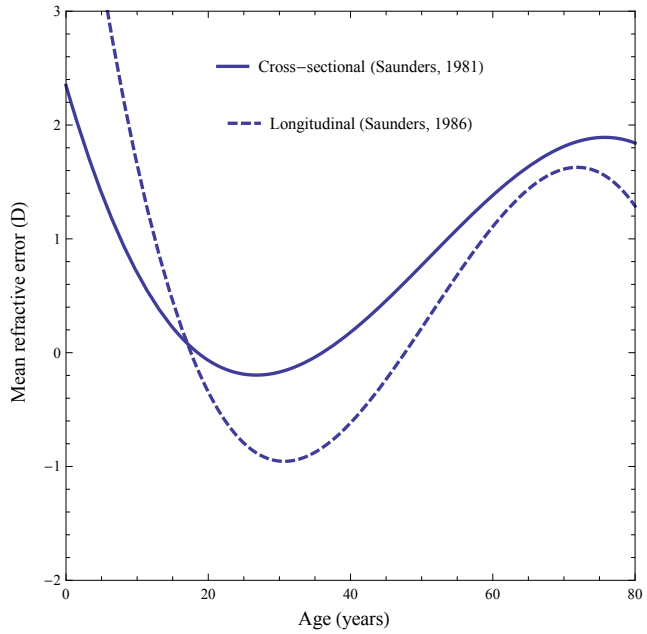

Figure 20: Cross-sectional and longitudinal data showing the age-related change in refraction, known as the lens paradox. Adapted from [5].

6.1.1 *Reconstructing the Ageing Human Eye*

As an example of the applicability and possible future use of the AVOCADO model, we present here a study on the age-related change in ocular SA.

In a 2011 paper by Tabernero *et al.* [223], the authors model, amongst other aberrations, the SA of the ageing human eye. For this modelling exercise, the authors chose to use Le Grand's original eye model as initial data for the eye [152]. The lens radii decreased, and central lens thickness increased, at the rates found exper-

imentally by Dubbelman *et al.* [47, 206]. These values, together with the decrease in lens equivalent refractive index are summarised below.

$$\begin{aligned} \Delta R_a &= -0.057 \text{ mm/yr} \\ \Delta R_p &= -0.012 \text{ mm/yr} \\ \Delta T &= +0.024 \text{ mm/yr} \\ \Delta n_{eq} &= -0.00039/\text{yr}. \end{aligned}$$

The change of the cornea with age was assumed to be negligible [27, 53]. To view the age-related change in SA, they performed a series of simulations. The first of these simulations did not incorporate any age-related changes in the lens conic constants. The authors expected to find an increase in SA with age, as reported in the literature, and discussed in Chapter 2. However, they found that SA decreased monotonically, as shown in their Fig. 6(a). This unexpected behaviour was seen as paradoxical and was termed the "spherical aberration paradox". To solve the paradox, they allowed the lens conic constants to increase with age, as found in another study of Dubbelman and van der Heijde [47]:

$$\begin{aligned} \Delta K_a &= +0.03/\text{yr} \\ \Delta K_p &= +0.07/\text{yr}. \end{aligned} \tag{60}$$

With these changes, the simulated SA increased too quickly with age. As a final fix, the authors divided the age-related changes in conic constants by 2 and re-simulated the SA. In this case, the SA increased satisfactorily with age, albeit rather slowly compared to the literature data.

The most obvious explanation for the paradoxical behaviour observed in Tabernero *et al.*'s study is the over-simplified lens model containing a homogeneous refractive index. To study the effect of a GRIN lens structure on the behaviour of ocular SA with age, we performed our own set of simulations. The simulations employed the AVOCADO lens model of Chapter 5 with age-dependent parameters P and m. The lens was initially set up in a similar manner to Tabernero's study. Instead of the relatively old Le Grand eye [152], we chose data from the 2014 study

of Rafael Navarro [205]. We chose data for the x-meridional section only. Similar to Tabernero's study, our cornea changes little with age, so its shape is given by:

$$\begin{aligned} \mathrm{Rc}_a &= 7.85 - 0.0051 \times \text{age mm} \\ \mathrm{Rc}_p &= 6.20 \text{ mm} \end{aligned}$$

The conic constant of the posterior corneal surface (Kc_p) was chosen as above from the work of Navarro. Due to the large refractive index difference at the anterior corneal surface, the anterior corneal conic constant (Kc_a) will have a considerable effect on SA of the eye. Considering the large range of values reported in the literature, Kc_a was rounded to a generic value with one significant figure; its change with age is taken from Navarro, as above. The conic constants therefore change with age according to:

$$\begin{aligned} \mathrm{Kc}_a(\text{age}) &= -0.3 - 0.0009 \times \text{age} \\ \mathrm{Kc}_p(\text{age}) &= -0.56. \end{aligned}$$

As stated, the initial ocular data were taken from Navarro's 2014 study [205], but the *age-related changes* were the same as that used by Tabernero, taken from the work of Dubbelman and van der Heijde [47]. This gives the following representation for the intraocular distances and lens radii:

$$\begin{aligned} \mathrm{T}_c &= 0.55 \\ \mathrm{T}_{cl}(\text{age}) &= 3.87 - 0.010 \times \text{age} \\ \mathrm{T}(\text{age}) &= 2.93 + 0.024 \times \text{age} \\ \mathrm{T}_a &= 0.6 \times \mathrm{T} \\ \mathrm{T}_p &= 0.4 \times \mathrm{T} \\ \mathrm{R}_a(\text{age}) &= 12.7 - 0.057 \times \text{age} \\ \mathrm{R}_p(\text{age}) &= 5.9 - 0.012 \times \text{age}, \end{aligned}$$

where T_c = corneal thickness, T_{cl} = cornea–lens thickness (anterior chamber depth), T = lens thickness, and T_a and T_p are the anterior and posterior thicknesses of the lens from nucleus to pole. Finally, as with Tabernero's initial simula-

tion, the conic constants of the lens do not change with age—the values are again taken from Navarro's 2014 study and are:

$$K_a = -4$$
$$K_p = -3.$$

The refractive indices of the cornea, aqueous and vitreous humour were taken from the 2005 paper by Escudero-Sanz and Navarro [224] for the wavelength 589.3 nm. Regarding the lens internal structure, the central and surface refractive indices of the lens were $n_c = 1.415$ and $n_s = 1.37$, respectively [225]. The value of P was taken from the 2007 study of Navarro and co-workers [158] to be:

$$P(\text{age}) = 2.85 + 1.1 \times 10^{-7} \times \text{age}^4.$$

Finally, we chose an age-related dependence for parameter m, which describes the rate of change of iso-indicial contour curvature from surface to centre. As the eye ages, we wish to have m tending towards zero, so that the older lens model approaches the GIGL model. For this, we chose the simple dependence:

$$m(\text{age}) = 8/\text{age}.$$

Parameters P and m both affect the GRIN profile in the radial direction according to the exponent $2P/(m+1)$, as shown in Section 5.2.

The particular choice of starting values for this eye produced a large amount of negative SA in the eye. Since SA is strongly coupled to conic constants, and conic constants do not affect optical power, this was remedied by simply changing the lens conic constants to more positive (less negative) values of $K_a = -3.0$ and $K_p = -2.5$.

The result of our initial SA simulation is shown as the green plot in Fig. 21. We can see in this initial simulation that SA increases with age, but decreases again after the age of about 60 years. This simple initial simulation is very promising, as it does not show Tabernero *et al.*'s observed paradoxical behaviour of SA vs age. The reason for the sensible behaviour in this simulation is the lens containing a GRIN structure—all other ocular parameters are fixed.

Regarding the choice of the GRIN structure, P was chosen in accordance with the previously published 2007 study of Navarro and co-workers [158]. The choice

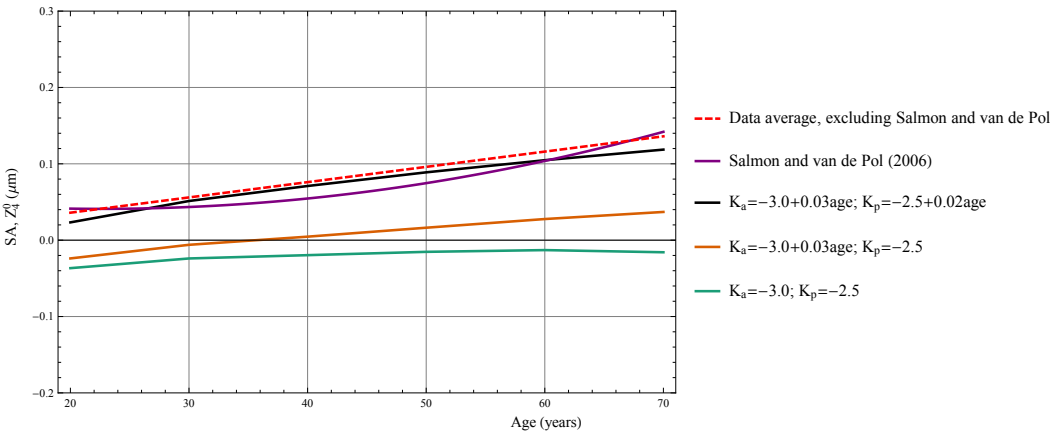

Figure 21: Simulation of SA vs age for comparison with the work of Tabernero *et al.* [223].

of $m = 8/\text{age}$ is such that it produces some very interesting results for the ocular power. Shown in Fig. 22 is the change in optical power vs age of the simulated eye (note that conic constants do not affect optical power and so the power is the same for all conic constants). From this figure, we can make two observations. First, directly comparing ages 10 and 70 years, the power of the eye decreases overall, thus accounting for the so-called "lens paradox"—this original "paradox" refers to optical power and not the "SA paradox" coined by Tabernero *et al.* [223] mentioned above. Second, the power has a minimum value at approximately 25 years of age.

Figure 22: Ocular power of the AVOCADO model vs age, with the age-dependence of $m = 8/age$.

To compare the age-related change in ocular power using the AVOCADO model to Fig. 20, we note that the data in Fig. 20 relate to *refractive error*. That is, the values refer to the correction required to restore an eye to the emmetropic state. For example, if an eye is myopic, the image will focus in front of the retina and so a negative corrective lens is required for emmetropisation. As the eye becomes

more myopic, a more negative lens is required. Hence, as the power of the eye increases (increased myopia), the correction required becomes *more negative*. Hence, the refractive power plots are to be flipped upside-down. To demonstrate how the AVOCADO model can account for the age-related shift in refraction seen in Fig. 20, a more suitable function for the age-related change in parameter m is:

$$m(age) = 0.9 - \left(\frac{age}{90}\right)^4 .$$

The constant terms in the above equation ensure that m decreases with age at a sensible rate from approximately one to zero. With the above equation for m, the resulting refractive power is shown as the red trace in Fig. 23. We can see that the refractive correction has a minimum at approximately 35 years of age; this is the first time that modelling has come close to replicating the works of Saunders [117, 118], which show a non-monotonic change in refractive error vs age; these are seen as the blue traces in Fig. 23. It is important to note again that the data in this figure correspond to *refractive error* and not *refractive power*, as in Fig. 22.

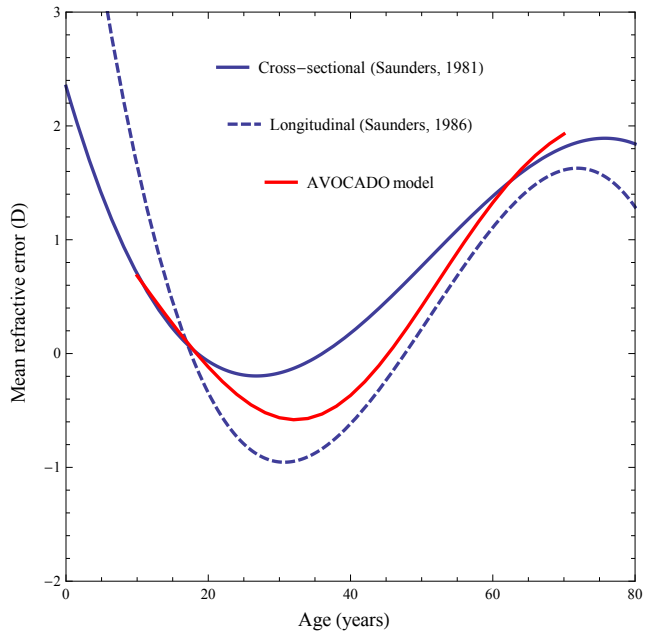

Figure 23: Simulation of ocular power vs age using the AVOCADO model, compared to the findings of Saunders [117, 118], after [5].

Summarised at the conclusion of Chapter 2 are two main age-related trends in SA. The first is the result of Salmon and van de Pol [35], who found that SA has the polynomial dependence $y = 0.000045 \times age^2 - 0.002038 \times age + 0.06408$. Second, the average of studies explicitly showing polynomial (linear or other) fits,

but excluding Salmon and van de Pol, showed that for a 5 mm pupil SA has a mean value of 0.056 μm at 30 years of age, with a slope of 0.002 μm/yr. These are shown in Fig. 21 as the purple and dashed red traces, respectively. In addition to clarifying the SA paradox, we can adjust the age-related change in lens conic constants to match these summary values of experimentally-observed age-related changes in SA.

The conic constants of the lens surfaces are very difficult to measure accurately *in vivo* [143], and hence any age-related changes are not easily recognised. For example, Tabernero *et al.* [223] initially use the age-related changes in conic constants found by Dubbelman and van der Heijde [47]. They argue that the changes were found to be non-significant; hence, they adjusted the lens conic constants vs age to match experimental data on SA from the literature. We follow the same procedure here. The orange trace in Fig. 21 is the result of changing the anterior lens conic constant by the amount +0.03/yr, in accordance with the findings of Dubbelman and van der Heijde [47]. The black trace is the result when the posterior lens conic is also increased by the amount +0.02/yr. As we can see, the black trace compares well with the experimental summary of the preceding paragraph; in particular, the value at 30 years of age and the slope agree well with the data average (dashed red trace).

Worthy of note is the observation that there are many possible configurations of the lens conic constants that can produce the same lenticular SA. While this is a problem for generic modelling, this will not be a problem with future customised modelling where, for example, the lens conic constants could be accurately measured in experiments. While the exact matching of SA vs age with the conics is not well-defined, this does not dilute the valuable finding that the AVOCADO model can explain both the power and SA paradoxes. Furthermore, until now, there has been no physical basis for the introduction of measures to explain the (optical power) lens paradox. For example, the age-related reduction in equivalent refractive index has no explanation apart from its ability to reduce the optical power of the lens. The AVOCADO model, containing a physically relevant change in parameter m with age, produces optical power that follows the correct trend; the physical relevance comes from the age-related change in iso-indicial contour shape. As a result, m is useful not only in qualitatively reproducing the features of the ageing eye, but also in quantitatively accounting for optical power and hence equivalent refractive index.

Also worthy of note is the age-related increase in lens conic constants required to produce a lens whose SA increases with age. This is opposite to the trend observed in the accommodating eye, where the conics decrease, resulting in an accommodative decrease in SA. Conceptually, this contradicts the observation that the ageing eye is similar to the accommodating eye. While it is true that the central thickness increases and radii decrease in both cases, the processes are similar in this regard only. One particular difference is that the lens diameter decreases with accommodation, whereas it increases with age. The mechanisms of accommodation and ageing are not yet fully understood, but the following could be considered. When the lens accommodates, the zonular forces are reduced and the elastic capsule forms the accommodated lens shape. In this case, the reduction of stretching effort on the capsule allows the lens conics to decrease, resulting in a negative change in SA. On the contrary, the ageing unaccommodated eye grows in volume and so there will be a larger stretching force on the elastic capsule. Perhaps this stretching causes the age-related increase in conic constants and hence SA.

6.1.2 *Aetiology of Age-related Changes in Ocular Properties*

The following is a brief discussion of the 2004 paper titled "Myopic versus hyperopic eyes: axial length, corneal shape and optical aberrations", by Llorente *et al.* [14], and how the AVOCADO model could explain some of the results therein.

First, we summarise some initial findings with the AVOCADO model:

- For a given lens geometry, increasing the value of m increases the power.
- For a given accommodative change in lens geometry, increasing m increases the change in lens power per dioptre of accommodation. That is, a younger eye with higher m will show a greater increase in power for a certain change in lens geometry.
- For a given lens geometry (say corresponding to zero dioptres), increasing m makes SA more negative (less positive).
- Increasing m also causes a greater accommodative change in SA
- Younger eye = larger m = higher power = higher accommodative change in power = less positive (more negative) SA = higher accommodative change in SA

- Older eye = smaller m = lower power = lower accommodative change in power = more positive SA = lower accommodative change in SA

The 2004 paper of Llorente *et al.* [14] outlines the measurement of corneal and total ocular aberrations versus age. The internal aberrations were estimated by subtracting corneal from total aberrations. The study found that for myopes, internal SA does not increase significantly with age. Only hyperopes followed the classic trend of increasing internal SA (this trend is also seen in the 2014 study by Philip *et al.* [33]; see Fig. 3 in Section 2.3). This means that, for hyperopes, the compensation of corneal SA with internal SA was present only in young eyes, while the increasing internal SA with age meant that the overall SA became more positive with age. Note that the study only included a relatively small range of ages (23–40 years). Also stated in this study is the finding that accommodation amplitudes have been found to be significantly lower in young hyperopes compared to young emmetropes aged 20 yr. They cite Spierer and Shalev [226] who found that hyperopes required reading glasses at an earlier age, and the hyperopes' lower amplitude of accommodation might be indicative of earlier onset of presbyopia.

According to our findings with the AVOCADO model, this would mean that hyperopes might have a lower value of m compared to emmetropes (and also myopes), since a lower m means a smaller accommodative change in power. For hyperopes, a smaller m would also mean that those eyes have more positive (less negative) SA compared to emmetropes (and myopes). Figure 2D from Llorente *et al.* [14] is included in adapted form in Fig. 24, showing total, corneal and internal SA of their hyperopic and myopic subjects. We can see that the hyperopes have more positive (less negative) SA compared to the myopes. This agrees with the hypothesis that parameter m in the AVOCADO model is responsible for the differences between hyperopes and myopes.

The observation that older eyes might have larger values of m and hence a lower accommodative change in lens optical power could help to partially account for the presbyopic changes in the lens. While it is unlikely that parameter m alone can account for the full loss in accommodative ability of the ageing eye, it could perhaps supplement the loss in mechanical elasticity of the lens material. The increase in lens stiffness with age, resulting in a lack of physical lens deformation, together with the lower accommodative change in optical power, could form a major part in explaining presbyopia.

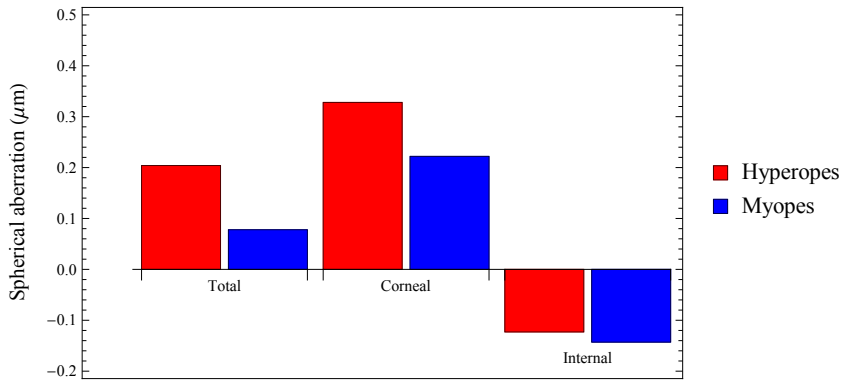

Figure 24: Total, corneal and internal SA of hyperopes and myopes. Adapted from [14].

6.2 CONCLUSION

The human eye has been studied extensively over the past century or so. More advanced measurements are becoming available, yet we are still not much closer to understanding the fundamental structure of the human lens. With more advanced data, we require more realistic models for their reconciliation.

Two fundamental scientific approaches have been undertaken to study the nature of the lens. Experimental studies measure the peculiarities of the lens and attempt to characterise the lens based on its measured behaviour. While these experimental studies are of indubitable importance, we require computational models of the human lens to formulate ideas about its true structure. The results of experimental studies are important for verifying the accuracy of these models and should not be considered second-rate, since development of a model requires some experimentally observed behaviour to imitate.

The usefulness of models lies in their ability to be manipulated to provide results for different scenarios that cannot be observed experimentally. For example, they can provide information on the aged eye, of which measurements cannot be made due to the presence of severe cataract.

Progress in modelling the human lens has been slow. Historically, the difficulty in reliably measuring the optical properties of the human eye has led to a serious lack of consistent data. Furthermore, the idiosyncratic nature of individual eyes makes averaged data less useful. Hence, personalised modelling will be required. In addition, it is not only the lack of experimental data that has hindered progress in modelling the human eye; so too has the complex nature of the lens itself. In

traditional reverse optical engineering, the optical system is optimised to produce the required output. In the case of the human eye, much the same procedure is followed; but, the human lens is not a simple homogeneous element—rather, the lens consists of a GRIN medium. We therefore see that optimization of the lens parameters becomes much more difficult. Indeed, we still do not have an accurate model of the lens GRIN bulk capable of accounting for age-related trends in experimental data and in the GRIN structure alone.

Typically, conceptual developments in modelling the lens structure will cease with the advent of a particularly clever or simple model. With this particular model, the body of literature thereafter tends to focus on optimising this model to match experimental data [227]. For example, early models of the human lens included a constant equivalent refractive index; it is testament to the difficulty of matching models with data that such simple models are still being used. On the other hand, occasionally, large progress will be made in modelling efforts. Until recently, this advancement has been hindered by two main problems. First, without a suitably simple formulation, the lens model can become over-complicated. With a disparity of data on lens structure for comparison, the lens model can quickly lose relevance. This leads us into the second problem of a lack in experimental data in general. Only within the past 10 years or so have there been publications on large-scale population studies.

It is clear that the ultimate goal in modelling the human lens is the creation of a model that is as simple as possible, yet is fully compatible with all aspects of the lens. These include anatomical, biomechanical and optical aspects. We can see from the literature that there has been a trade-off between anatomical accuracy and simplicity. Traditionally, simpler models of the lens have been used for generating personalised models. As stated above, the reason that more realistic models have not been used is because sometimes, with increasing complexity, the problem can become over-determined and the complex models quickly lose relevance. A good illustration of this trade-off is given in the 2006 paper "On the prediction of Optical Aberrations by Personalised Eye Models", by Rafael Navarro and co-workers [228]. In this paper, they generate two separate personalised models of the human lens; one model has a constant equivalent refractive index and the other has a GRIN bulk. The first model falls into the category of remaining simple while also allowing relatively easy optimisation of the lens parameters. It is relatively clear, however, that this model lacks anatomic relevance. The second model is closer to the true

nature of the lens, since it contains a GRIN; but, unfortunately, the GRIN lacks an anatomically correct structure. To remedy this, we can look at other work of Rafael Navarro and co-workers, namely the 2007 papers titled "Adaptive model of the gradient index of the human lens" [158, 169]. In this work, we can see that the GRIN has a form that is more representative of what has been measured experimentally. The conic constants of the lens surfaces could be used to provide the correct spherical aberration. We note that in the above model, the anterior and posterior surfaces join sharply at the equator. It can be argued that this is irrelevant, since the central optical zone is modelled sufficiently, and the model is attractively simple. Yet, this does not coincide with the anatomical goal of future modelling efforts. Furthermore, the same authors outline that the lens extremities will be required for modelling the far periphery of the visual field.

The next step in ocular modelling will be the provision of personalised models. Personalisation is performed where the geometrical properties of the lens are measured experimentally and are used as input for the model. The lens GRIN can then be optimised to match the experimentally determined refractive power and aberration values. From this, we can see that the 2007 work by Navarro *et al.* is not entirely suitable, since in that model, the conic constants are required for aberration and power matching. Basically, the model is lacking an extra degree of freedom. Looking for a remedy to this problem, we can turn to another paper by Rafael Navarro's, specifically the 2014 paper on an "Adaptive model of the aging emmetropic eye and its changes with accommodation" [205]. This model is an adaptation of the 2007 version, where the conic constant of the internal iso-indicial contours is different to the conic constant of the external surface. The particular advantage of this model is that the extra degree of freedom afforded by the extra conic constant allows adjustment of the GRIN internals to match the relevant values for power and SA. On the face of it, this model seems sufficient for out optical modelling purposes. However, if we consider the emerging trend—and future goal—of anatomically correct, personalised optical modelling we can see that this model is unsuitable due to the discontinuity of the lens surfaces at the equatorial join. Furthermore, the choice of different conic constants in the above model leads to a discontinuity of the internal iso-indicial contours at the anterior and posterior poles of the lens. This gives the "two thin peripheral zones with zero axial thickness and constant refractive indexes equal to that of the lens surface".

A further step in the process includes the recent 2014 model by Bahrami and co-workers on a lens with AIS [201]. This model has the great advantage of accounting for the age-related changes in internal iso-indicial contours of the GRIN bulk. If we look closely, this model is also lacking a degree of freedom, since the conic constants of the lens surfaces are required to ensure a smooth equatorial join of the anterior and posterior portions of the lens. Unfortunately, this means that the conics cannot be used for predicting aberrations. This is the first model, of which we are aware, that approximately represents both the lens anatomy and ageing GRIN medium. As an aside, the GIGL model of Bahrami and Goncharov does not account fully for age-related changes in the GRIN medium, but it does appear to be anatomically representative of the real lens. We consider that the final step in the modelling process would be to begin with such an anatomically realistic model as the AIS model, while providing one extra degree of freedom to account for both the refractive power and aberrations of the lens. This would allow for the first anatomically representative model of the lens capable of predicting age-related changes in the GRIN medium, and also able to model refractive power and spherical aberration. Such an example is the AVOCADO lens model of Chapter 5

We have to take a step back and objectively evaluate whether we are representing the human lens faithfully. With the ultimate goal of developing a simple model that can account for all experimentally-observed properties of the lens, there has been a race to apply our current over-simplified models to such data. Often, this has led to the ad-hoc placement of lens models within the human eye in a variety of different configurations e.g. with varying tilts/decentrations etc. We find that within this additional parameter space, simplified eye models are capable of accounting for certain trends, e.g. off-axis behaviour. However, we usually find that although the added complexity of the situation can account for some properties, the over-simplified lens model falls short in its ability to account for a fuller range of observations. An example of this is given in a 2015 paper by Polans *et al.* [229]. In this paper, they inserted what is, as they pointed out, essentially the Goncharov-Dainty lens model [157] into an eye, with tilt and decentration. While this helps to account for the experimentally observed off-axis behaviour of the eye, we see that, unfortunately, the lens model is still susceptible to the same pitfalls as the original Goncharov-Dainty model; the main drawback being the non-physical sharpness of the equatorial join.

In the work of Tabernero and coworkers [223, 230], the use of a constant equivalent refractive index for the lens resulted in their inability to match the theoretical and experimental data. This led to the conclusion that there exists a sort of "spherical aberration paradox" within the human eye. However, we can see that the over-simplified lens model is to blame here.

Considering the above discussion together with the problem of representing a physically realistic lens with continuous surfaces, we thought it necessary to reconsider the representation of the human lens.

Part III

APPENDIX

A

EXACT RAYTRACING CODE IN C

What follows is the exact raytracing code in the C language. It raytraces through the GRIN medium by solving the differential ray equation using Sharma's method [140]; the intersection of the ray with the posterior lens surface is found using the method of Stone and Forbes [208]—see Chapter 3 for information on the methods used.

Listing 1: Exact raytracing C code

```
//NOTE: when changing the size of dt, change the dummy array values for the memoization,
//both in their actual assignment, and in the initial size declaration in the file preamble eg
    double array[size]

/*This verison uses the trigonometric method of solving cubic equations to solve the
ray-anterior surface intersection.
It uses the method of Stone and Forbes to find the intersection of the ray with
the posterior surface of the lens. Also, within the main raytrace for() loop, I have
included a basic axial coordinate check to see if the z-position of the ray is >0, so that a more
coarse step size of dt=0.01 can be used.*/
#include<stdio.h>
#include<math.h>
#include<complex.h>
#include<time.h> // used to calculate how long the code takes
#define M_PI 3.14159265358979323846

//ARE YOU USING VALUES FOR ALPHA, BETA AND GAMMA THAT DO NOT DEPEND ON X?
//i.e. alpha=2m+1 etc.
//If so, set the value of logflag to 0. If you are using log values, set it to 1
#define logflag 0
//ARE YOU RAYTRACING THROUGH THE CORNEA?
//If so, set the value of corneaflag to 1. If you are using the lens only, set it to 0
#define corneaflag 0

double sign(double test);
double Fpost(double y, double z);
double Fpostprime(double y, double z, double Ty, double Tz);
double Ryparam(double t);
double Rzparam(double t);
double Lrzca(double dfcady,double dfcadz,double Liy,double Liz,double n1,double n2);
double Lryca(double dfcady,double dfcadz,double Liy,double Liz,double n1,double n2);
double Lrzcp(double dfcpdy,double dfcpdz,double Liy,double Liz,double n1,double n2);
double Lrycp(double dfcpdy,double dfcpdz,double Liy,double Liz,double n1,double n2);

double Lrza(double dfady,double dfadz,double Liy,double Liz,double n1,double n2);
double Lrya(double dfady,double dfadz,double Liy,double Liz,double n1,double n2);
double Lrzp(double dfpdy,double dfpdz,double Liy,double Liz,double n1,double n2);
double Lryp(double dfpdy,double dfpdz,double Liy,double Liz,double n1,double n2);

double antderiv(double z,double antX0);
double antderiv2(double z,double antX0);
double antroot(double y,double z);
```

```
double antindexfunc(double y, double z);
double postderiv(double z,double postX0);
double postderiv2(double z,double antX0);
double postroot(double y,double z);
double postindexfunc(double y, double z);

double antdndzfunc(double X, double y, double z);
double antDz(double X, double y, double z);
double antdndyfunc(double X, double y, double z);
double antDy(double X, double y, double z);
double postdndzfunc(double X, double y, double z);
double postDz(double X, double y, double z);
double postdndyfunc(double X, double y, double z);
double postDy(double X, double y, double z);

double antRz(int i);
double antRy(int i);
double antTz(int i);
double antTy(int i);
double antaz(int i);
double antay(int i);
double antbz(int i);
double antby(int i);
double antcz(int i);
double antcy(int i);
double postRz (int i);
double postRy (int i);
double postTz (int i);
double postTy (int i);
double postaz (int i);
double postay (int i);
double postbz (int i);
double postby (int i);
double postcz (int i);
double postcy (int i);

double Rym,Rzm,Tym,Tzm,Ay,Az,By,Bz,Cy,Cz;
double nair = 1.0,ncornea = 1.3777,naqueous = 1.336,nvitreous = 1.336, ns = 1.37, nc = 1.415;
double dt = 0.001;
double w, p, tr;
#define maxarray round(10./dt)

//corneal parameters
double Tc = 0.55,Tcl = 3.05,Rca = 7.72,Rcp = 6.5,Kca = -0.26,Kcp = -0.1;
//lens parameters
double m,Ra,Rp,T,Ta,Tp,Ka,Kp,Zc,Ba,Bp;
double alpha,beta,gamma;
double zsb,ysb,Liy,Liz;
double zroot[1000],antXroot[10000000],antfunc[10000000],antRzarray[10000000],antRyarray[10000000],
    antTzarray[10000000],antTyarray[10000000],antazarray[10000000],antayarray[10000000],antbzarray
    [10000000],antbyarray[10000000],antczarray[10000000],antcyarray[10000000];
double postXroot[10000000],postfunc[10000000],postRzarray[10000000],postRyarray[10000000],
    postTzarray[10000000],postTyarray[10000000],postazarray[10000000],postayarray[10000000],
    postbzarray[10000000],postbyarray[10000000],postczarray[10000000],postcyarray[10000000];

int main(void)
{       clock_t launch = clock();
        double age=30;
        double y0min=0.02, y0max=2.0,y0sample=0.1;
        double mmin=0.0, mmax=1.0, msample=0.2;
```

```
        for(m=mmin;m<=mmax;m+=msample){
        double pmin=2.5, pmax=4.0, psample=0.5;
        for(p=pmin;p<=pmax;p+=psample){
        //double wmin=0.2, wmax=6.01, wsample=2.0;
        //for(w=wmin;w<=wmax;w+=wsample){

        if(logflag==0)printf("age: %f\t m: %f\t p: %f\n",age,m,p);
        else printf("age: %f\t m: %f\t w: %f\n",age,m,w);

        for(double y0=y0min;y0<=y0max;y0+=y0sample){
        //Lenticular parameters
        tr=0.6; //tr is the axial position of the lens nucleus
        Ra = 12.9 - 0.057*age;
        Rp = 6.5 - 0.017*age;
        T = 2.93 + 0.0236*age;
        Ta = tr*T;
        Tp = (1.0-tr)*T;
        Ka = -5.4 + 0.03*age;
        Kp=-1.1;

        Zc=(2.*Ra + 2.*Rp - sqrt(4.*pow(Ra,2) + 4.*pow(Rp,2) - 4.*(1. + Ka)*Rp*T +(1. + Ka)*(1. +
            Kp)*pow(T,2) - 4.*Ra*(-2.*Rp + (1. +Kp)*T)) - Ta - Ka*Ta - Tp - Kp*Tp)/(Ka - Kp);
        Ba=(2.*(-Ra + (1. + Ka)*(Ta + Zc)))/(3.*pow(Ta + Zc,2));
        Bp=(2.*(-Rp + (1. + Kp)*(Tp - Zc)))/(3.*pow(Tp - Zc,2));
        double ymaxsquared=2.*Ra*(Ta + Zc) - (1. + Ka)*pow(Ta + Zc,2) + Ba*pow(Ta + Zc,3);

/*********************************************************************/
//corneal raytrace
        //analytical solution for intersection of ray with anterior cornea for on-axis beam
        zsb = (Rca-1.*Ta-1.*Kca*Ta-1.*Tc-1.*Kca*Tc-1.*Tcl-1.*Kca*Tcl-1.*sqrt(pow(Rca,2)-1.*pow(y0
            ,2)-1.*Kca*pow(y0,2)))/(1.+Kca);
        ysb = y0;

        //define z and y cosines
        Liz = 1.;
        Liy = 0.;
        double dfcady = 2.0*ysb;
        double dfcadz = -2.0*Rca + 2.0*(1.0 + Kca)*(Ta + Tc + Tcl + zsb);
        double Lry = Lryca(dfcady, dfcadz, Liy, Liz, nair, ncornea); //Refraction
        double Lrz = Lrzca(dfcady, dfcadz, Liy, Liz, nair, ncornea);
        double mr= Lry/Lrz;

        //analytical solution for intersection of ray with posterior cornea
        double zsa=(0.5*(2.*Rcp-2.*Ta-2.*Kcp*Ta-2.*Tcl-2.*Kcp*Tcl-2.*mr*ysb+2.*pow(mr,2)*zsb-1.*
            sqrt(pow(-2.*Rcp+2.*Ta+2.*Kcp*Ta+2.*Tcl+2.*Kcp*Tcl+2.*mr*ysb-2.*pow(mr,2)*zsb,2)
            -4.*(1.+Kcp+pow(mr,2))*(-2.*Rcp*Ta+     pow(Ta,2)+Kcp*pow(Ta,2)-2.*Rcp*Tcl+2.*Ta*Tcl
            +2.*Kcp*Ta*Tcl+pow(Tcl,2)+Kcp*pow(Tcl,2)+pow(ysb,2)-2.*mr*ysb*zsb+pow(mr,2)*pow(zsb,2)
            ))))/(1.+Kcp+pow(mr,2));
        double ysa= mr*zsa + (ysb - mr*zsb);
        ysb=ysa;
        zsb=zsa;

        Liy = Lry;
        Liz = Lrz;
        double dfcpdy = 2.0*ysb;
        double dfcpdz = -2.0*Rcp + 2.0*(1.0 + Kcp)*(Ta + Tcl + zsb);
        Lry = Lrycp(dfcpdy, dfcpdz, Liy, Liz, ncornea, naqueous);
        Lrz = Lrzcp(dfcpdy, dfcpdz, Liy, Liz, ncornea, naqueous);
        mr = Lry/Lrz;
```

```
/*************************************************************************/
// lens
//Anterior lens ray-surface intersection
                                //THE FOLLOWING ARE FOR USE WITHOUT THE CORNEA
                                if(corneaflag==0){
                                ysb=y0;
                                mr=0.;
                                Liz=Lrz=1.;
                                Liy=Lry=0.;}
/*The trigonometric method for solving cubic equations. For use with the cornea, I want to solve
    the equation of the line: y-y1=m(x-x1) with the anterior surface: sqrt(2Rz-(1+K)z^2+Bz^3).
    This gives the formula:
(m(x-x1)+y1)^2==2Rz-(1+K)z^2+Bz^3.
In our case, the equation comes out as:
(mr(z - zsb) + ysb)^2 - 2Ra(Ta + z) + (1 + Ka) (Ta + z)^2 - Ba(Ta + z)^3==0.
I want to solve the equation above for z, using the trigonometric method. For this, I need the
    coefficients of the different powers of z in the cubic equation above. I can use mathematica
    to do this using the Coefficient[] function. */
        double a0=-2.*Ra*Ta + pow(Ta,2) + Ka*pow(Ta,2) - Ba*pow(Ta,3) + pow(ysb,2) - 2.*mr*ysb*zsb
            + pow(mr,2)*pow(zsb,2);
        double a1=2.*(-1.*Ra + Ta + Ka*Ta  + mr*ysb - pow(mr,2)*zsb) - 3.*Ba*pow(Ta,2);
        double a2=1. + Ka + pow(mr,2) - 3.*Ba*Ta;
        double a3=-Ba;

        double beta0=(2.*pow(a2,3) - 9.*a1*a2*a3 + 27.*a0*pow(a3,2))/(27.*pow(a3,3));
        double beta1=(-pow(a2,2) + 3.*a1*a3)/(3.*pow(a3,2));

        double zeta=2.*sqrt(-beta1/3.)*cos((2.*M_PI)/3.- acos((3.*sqrt(3.)*beta0*sqrt(-(1./beta1)))
            /(2.*beta1))/3.);
        zsa=zeta-a2/(3.*a3);
        ysa=ysb+mr*(zsa-zsb);

        double dfady=2.*ysa;
        double dfadz=-2.*Ra + 2.*(1. + Ka)*(Ta + zsa) - 3.*Ba*pow(Ta + zsa,2);
        Liy = Lry;
        Liz = Lrz;
        Lry = Lrya(dfady, dfadz, Liy, Liz, naqueous, ns); //Refract
        Lrz = Lrza(dfady, dfadz, Liy, Liz, naqueous, ns);

        ysb=ysa;
        zsb=zsa;
        Liy = Lry;
        Liz = Lrz;

        for(int inc = 0; inc < round(4./dt); inc++){
                antRzarray[inc] = antRyarray[inc] = antTzarray[inc] = antTyarray[inc] = antazarray[
                    inc] =  antayarray[inc] =
                        antbzarray[inc] = antbyarray[inc] = antczarray[inc] = antcyarray[inc] =
                            -1000;
        }
        for (int inc = round (0.5/dt); inc < round (8./dt); inc++){
                postRzarray[inc] = postRyarray[inc] = postTzarray[inc] = postTyarray[inc] =
                    postazarray[inc] =
                postayarray[inc] = postbzarray[inc] = postbyarray[inc] = postczarray[inc] =
                    postcyarray[inc] = -1000;
        }

        /*This is the iterative routine for solving the differential equation*/
        int flag = 0;//to tell if the ray has entered the posterior section
        int outside;//to tell the point at which the ray exits the lens
```

```
for (int q = 1; q < 100000000000; q++){
        outside = q;

        //if the ray is in the anterior section and has not crossed equatorial region
        if (flag == 0&& (antRz(q) > antroot(antRy(q), antRz(q))*Zc||antRz(q)>=0)){
                flag = 1;//set flag to 1 as the ray will henceforth be in the posterior
                //once the ray has crossed the equator, the anterior values are passed to
                    the posterior array to start the posterior raytrace
        postRzarray[q] = antRz(q-1);
        postRyarray[q] = antRy(q-1);
        postTzarray[q] = antTz(q-1);
        postTyarray[q] = antTy(q-1);
}
        //else if the ray is in the posterior section and has exited the lens
        else if(flag==1&&pow(postRy(q),2)>2.*Rp*(Tp - postRz(q))-(1.+Kp)*pow(Tp-postRz(q)
            ,2)+Bp*pow(Tp - postRz(q),3)){
                outside = q;//store the point at which the ray exits the lens, for the
                    interpolant method of Stone and Forbes
                break ;
        }
}
//Assign the position and direction cosines of the ray before and after exiting the lens
Rym = postRy(outside - 1);
double Rym1 = postRy(outside);
Rzm = postRz(outside - 1);
double Rzm1 = postRz(outside);

Tym = postTy(outside - 1);
double Tym1 = postTy(outside);
Tzm = postTz(outside - 1);
double Tzm1 = postTz(outside);

//Code for the Stone and Forbes method
double Fm=Fpost(Rym,Rzm);
double Fm1=Fpost(Rym1,Rzm1);
double Fprimem=Fpostprime(Rym,Rzm,Tym,Tzm);
double Fprimem1=Fpostprime(Rym1,Rzm1,Tym1,Tzm1);
double F0=Fm;
double F1=Fm1;
double F0dot=Fprimem;
double Q=(F0-F1+dt*F0dot)/pow(dt,2);
double tapp=-2.0*F0/(F0dot-sign(F0)*sqrt(pow(F0dot,2)+4.0*F0*Q));

Ay = postay(outside - 1);
Az = postaz(outside - 1);
By = postby(outside - 1);
Bz = postbz(outside - 1);
Cy = postcy(outside - 1);
Cz = postcz(outside - 1);

/*For the single iteration of Netwon-Raphson method required for Stone and Forbes' method,
    I need to find the value of (dF(R))/dt, EVALUATED AT R(tapp,l), WHERE R(tapp,l) IS
    APPROIXMATED BY EQUATION 13:
(dF(R))/dt=\[Del]F.(dR/dt).
In two dimensions, this is:
dF/dydR/dt+dF/dzdR/dt.
Find the derivative of F wrt y and z, and evaluate using the parameterised function for R.
    The y-derivatieve comes out as 2y*/
double dFdy=2.0*Ryparam(tapp);
```

```
        //z-derivative is 2 Rp-2(1+Kp)(Tp-z)+3 Bp(Tp-z)^2, where z is given by the parametric eqn
            13
        double dFdz = 2.*Rp - 2.*(1. + Kp)*(Tp - Rzparam(tapp)) + 3.*Bp*pow(Tp - Rzparam(tapp),2);

        /*dR/dt is just the derivative of the parameterised function for R. Do each one separately.
             The derivative of the y-component with respect to t comes out as:
        Tym+tAy/dt+1/2t^2 (4By-Cy-3Ay)/dt^2+1/6t^3((4(Ay+Cy-2By))/dt^3).
        A similar equation is found for z*/
        double dRydt=Tym+ (Ay*tapp)/dt + ((-3.*Ay + 4.*By - Cy)*pow(tapp,2))/(2.*pow(dt,2)) + (2.*(
            Ay - 2.*By + Cy)*pow(tapp,3))/(3.*pow(dt,3));
        double dRzdt=Tzm+ (Az*tapp)/dt + ((-3.*Az + 4.*Bz - Cz)*pow(tapp,2))/(2.*pow(dt,2)) + (2.*(
            Az - 2.*Bz + Cz)*pow(tapp,3))/(3.*pow(dt,3));

        /*now, calculate (dF(R))/dt=dF/dySubscript[dR, y]/dt and dF/dzSubscript[dR, z]/dt*/
        double dFRydt = dFdy * dRydt;
        double dFRzdt = dFdz * dRzdt;
        /*Finally, I have to add the two components*/
        double dFRdt = dFRydt + dFRzdt;

        double tint=tapp - Fpost(Ryparam(tapp),Rzparam(tapp))*1.0/(dFRdt);

        ysa = Ryparam(tint);
        zsa = Rzparam(tint);

        double tau=tint/dt;
        double c0=0.75 - 0.25*sqrt(9. + (16.*tau)/(-3. + tau));

        double Gy= dt*postDy(postroot((Rym + c0*dt*Tym + 0.5*pow(c0,2)*dt*Cy),(Rzm + c0*dt*Tzm+0.5*
            pow(c0,2)*dt*Cz)),(Rym + c0*dt*Tym +0.5*pow(c0,2)*dt*Cy),(Rzm+ c0*dt*Tzm + 0.5*pow(c0
            ,2)*dt*Cz));
        double Gz = dt*postDz(postroot((Rym + c0*dt*Tym + 0.5*pow(c0,2)*dt*Cy),(Rzm + c0*dt*Tzm
            +0.5*pow(c0,2)*dt*Cz)),(Rym + c0*dt*Tym +0.5*pow(c0,2)*dt*Cy),(Rzm+ c0*dt*Tzm + 0.5*
            pow(c0,2)*dt*Cz));

        double b1=(1./12.)*(2.*c0- 3.)*(tau- 3.)*(c0*(4.*pow(tau,2)- 9.*tau + 6.)-3.*tau*pow(tau -
            1.,2));
        double b2=(2.*pow(tau,3)*(c0-1.)*(3.*tau*(pow(tau,2)+13.) - 4.*(5.*pow(tau,2)+6.)))/(3.*(
            tau*(3.*tau-4.)+(3. - 2.*tau)*(3. - 2.*c0)));
        double b3=(pow(tau,2)*(c0*(4.*tau-3.)+tau*(2.-3.*tau)))/(6.*(c0-1.));
        double b4=(1./12.)*tau*(tau-1.)*pow(tau-3.,2)*(2.*c0-3.);
        double Ty=Tym+Ay*b1 + b2*By + b3*Cy + b4*Gy;
        double Tz=Tzm+Az*b1 + b2*Bz + b3*Cz + b4*Gz;

        double dfpdz = 2.*Rp - 2.*(1. + Kp)*(Tp - 1.*zsa) + 3.*Bp*pow(Tp - 1.*zsa,2);
        double dfpdy = 2.*ysa;

        Liy = Ty/ns;
        Liz = Tz/ns;
        Lry = Lryp(dfpdy, dfpdz, Liy, Liz, ns, nvitreous);//Refract
        Lrz = Lrzp(dfpdy, dfpdz, Liy, Liz, ns, nvitreous);
        mr = Lry/Lrz;

        double abz = (Tc+Tcl+T) -ysa/mr + (zsa - Tp);//The z-position of the ray intersection with
            the optical axis, used for longitudinal aberration calculation
        double focal,paraxial_BFL;
        //for the paraxial ray, calculate the focal length and power
        if(y0==y0min){
                focal = -y0/mr;
                double power = -nvitreous*1000.*mr/y0;
        }
```

```
        //Here, we can calculate the equivalent refractive index (neq) of the lens
        //ONLY if corneaflag==0
        if(corneaflag==0&&y0==y0min){
                //introduce some dummy variables to tidy up the equation for neq
                double na=y0*(T*naqueous+T*nvitreous-nvitreous*Ra-naqueous*Rp)+nvitreous*Ra*Rp*mr;
                double nb=y0*(T-Ra-Rp);
                //equivalent refractive index
                double neq=(na-sqrt(pow(na,2)-4.0*T*y0*naqueous*nvitreous*nb))/(2.0*nb);
        }
}}}
        clock_t done = clock();
        double length = (done - launch);
        // print out how long the programme took to run
        printf("\nThe programme took %.2lf milliseconds seconds to complete\n\n", length);
}
/*****************************************************************************
End of main()
*****************************************************************************/

//a simple function to return the sign of a particular number
double sign(double test) {
        return (test > 0) - (test < 0);
}
//this is the posterior surface of the lens, represented as the equation F(x,y,z)=0.
//Used in Stone and Forbes' method
double Fpost(double y, double z){
        //return pow(y,2) - 2.*Rp*(Tp - 1.*z) + (1. + Kp)*pow(Tp - 1.*z,2) - 1.*Bp*pow(Tp - 1.*z,3)
            ;
        return pow(y,2) - 2.*Rp*(Tp - z) + (1. + Kp)*pow(Tp - z,2) - Bp*pow(Tp - z,3);
}
//this is the derivative of the anterior surface of the lens, represented as the equation F(x,y,z)
    =0.
//Used in Stone and Forbes' method
double Fpostprime(double y, double z, double Ty, double Tz){
        return -2*Rp*Tz + 2*Ty*y + 2*(1 + Kp)*Tz*(Tp - z) - 3*Bp*Tz*pow(Tp - z,2);
}
/*These are the parameterised descriptions of the ray position; they just say that
the values of y and z can be given as the parametric equation in t:*/
double Ryparam(double t){
        return Rym + t*Tym + (Ay*pow(t,2))/(2.*dt) + ((-3*Ay + 4*By - Cy)*pow(t,3))/(6.*pow(dt,2))
            + ((Ay - 2*By + Cy)*pow(t,4))/(6.*pow(dt,3));
}
double Rzparam(double t){
        return Rzm + t*Tzm + (Az*pow(t,2))/(2.*dt) + ((-3*Az + 4*Bz - Cz)*pow(t,3))/(6.*pow(dt,2))
            + ((Az - 2*Bz + Cz)*pow(t,4))/(6.*pow(dt,3));
}
//The following are the equations for refraction
double Lrzca(double dfcady,double dfcadz,double Liy,double Liz,double n1,double n2){
        return (dfcadz*(-1.*sqrt(1. - (1.*(1. - 1.*pow((-1.*dfcady*Liy)/sqrt(pow(dfcady,2) + pow(
            dfcadz,2)) - (1.*dfcadz*Liz)/sqrt(pow(dfcady,2) + pow(dfcadz,2)),2))*pow(n1,2))/pow(n2
            ,2)) + (((-1.*dfcady*Liy)/sqrt(pow(dfcady,2) + pow(dfcadz,2)) - (1.*dfcadz*Liz)/sqrt(
            pow(dfcady,2) + pow(dfcadz,2)))*n1)/n2))/sqrt(pow(dfcady,2) + pow(dfcadz,2)) + (Liz*n1
            )/n2;
}
double Lryca(double dfcady,double dfcadz,double Liy,double Liz,double n1,double n2){
        return (dfcady*(-1.*sqrt(1.-(1.*(1.-1.*pow((-1.*dfcady*Liy)/sqrt(pow(dfcady,2)+pow(dfcadz
            ,2))-(1.*dfcadz*Liz)/sqrt(pow(dfcady,2)+pow(dfcadz,2)),2))*pow(n1,2))/pow(n2,2))
            +(((-1.*dfcady*Liy)/sqrt(pow(dfcady,2)+pow(dfcadz,2))-(1.*dfcadz*Liz)/sqrt(pow(dfcady
            ,2)+pow(dfcadz,2)))*n1)/n2))/sqrt(pow(dfcady,2)+pow(dfcadz,2))+(Liy*n1)/n2;
}
```

```
double Lrzcp(double dfcpdy,double dfcpdz,double Liy,double Liz,double n1,double n2){
        return (dfcpdz*(-1.*sqrt(1.-(1.*(1.-1.*pow((-1.*dfcpdy*Liy)/sqrt(pow(dfcpdy,2)+pow(dfcpdz
            ,2))-(1.*dfcpdz*Liz)/sqrt(pow(dfcpdy,2)+pow(dfcpdz,2)),2))*pow(n1,2))/pow(n2,2))
            +(((-1.*dfcpdy*Liy)/sqrt(pow(dfcpdy,2)+pow(dfcpdz,2))-(1.*dfcpdz*Liz)/sqrt(pow(dfcpdy
            ,2)+pow(dfcpdz,2)))*n1)/n2))/sqrt(pow(dfcpdy,2)+pow(dfcpdz,2))+(Liz*n1)/n2;
}
double Lrycp(double dfcpdy,double dfcpdz,double Liy,double Liz,double n1,double n2){
        return (dfcpdy*(-1.*sqrt(1.-(1.*(1.-1.*pow((-1.*dfcpdy*Liy)/sqrt(pow(dfcpdy,2)+pow(dfcpdz
            ,2))-(1.*dfcpdz*Liz)/sqrt(pow(dfcpdy,2)+pow(dfcpdz,2)),2))*pow(n1,2))/pow(n2,2))
            +(((-1.*dfcpdy*Liy)/sqrt(pow(dfcpdy,2)+pow(dfcpdz,2))-(1.*dfcpdz*Liz)/sqrt(pow(dfcpdy
            ,2)+pow(dfcpdz,2)))*n1)/n2))/sqrt(pow(dfcpdy,2)+pow(dfcpdz,2))+(Liy*n1)/n2;
}
double Lrza(double dfady,double dfadz,double Liy,double Liz,double n1,double n2){
        return (Liz*n1)/n2+(dfadz*(-1.*sqrt(1. - (1.*(1. - 1.*pow((-1.*dfady*Liy)/sqrt(pow(dfady,2)
             + pow(dfadz,2)) - (1.*dfadz*Liz)/sqrt(pow(dfady,2) + pow(dfadz,2)),2))*pow(n1,2))/pow
            (n2,2)) + (((-1.*dfady*Liy)/sqrt(pow(dfady,2) + pow(dfadz,2)) - (1.*dfadz*Liz)/sqrt(
            pow(dfady,2) + pow(dfadz,2)))*n1)/n2))/sqrt(pow(dfady,2) + pow(dfadz,2));
}
double Lrya(double dfady,double dfadz,double Liy,double Liz,double n1,double n2){
        return (dfady*(-sqrt(1.-((1.-pow(-((dfady*Liy)/sqrt(pow(dfady,2)+pow(dfadz,2)))-(dfadz*Liz)
            /sqrt(pow(dfady,2) +pow(dfadz,2)),2))*pow(n1,2))/pow(n2,2)) + ((-((dfady*Liy)/sqrt(pow
            (dfady,2) + pow(dfadz,2))) - (dfadz*Liz)/sqrt(pow(dfady,2) + pow(dfadz,2)))*n1)/n2))/
            sqrt(pow(dfady,2) + pow(dfadz,2)) + (Liy*n1)/n2;
}
double Lrzp(double dfpdy,double dfpdz,double Liy,double Liz,double n1,double n2){
        return (-1.*dfpdz*(-1.*sqrt(1. - (1.*(1. - 1.*pow((dfpdy*Liy)/sqrt(pow(dfpdy,2) + pow(dfpdz
            ,2)) + (dfpdz*Liz)/sqrt(pow(dfpdy,2) + pow(dfpdz,2)),2))*pow(n1,2))/pow(n2,2)) + (((
            dfpdy*Liy)/sqrt(pow(dfpdy,2) + pow(dfpdz,2)) + (dfpdz*Liz)/sqrt(pow(dfpdy,2) + pow(
            dfpdz,2)))*n1)/n2))/sqrt(pow(dfpdy,2) + pow(dfpdz,2)) + (Liz*n1)/n2;
}
double Lryp(double dfpdy,double dfpdz,double Liy,double Liz,double n1,double n2){
        return (-1.*dfpdy*(-1.*sqrt(1. - (1.*(1. - 1.*pow((dfpdy*Liy)/sqrt(pow(dfpdy,2) + pow(dfpdz
            ,2)) + (dfpdz*Liz)/sqrt(pow(dfpdy,2) + pow(dfpdz,2)),2))*pow(n1,2))/pow(n2,2)) +(((
            dfpdy*Liy)/sqrt(pow(dfpdy,2) + pow(dfpdz,2)) +(dfpdz*Liz)/sqrt(pow(dfpdy,2) + pow(
            dfpdz,2)))*n1)/n2))/sqrt(pow(dfpdy,2) + pow(dfpdz,2)) + (Liy*n1)/n2;
}
/*The following are for use inside Halley's method. Noting that y and z will be given, for Halley's
     method we require that the function:
f(X)= -y^2 + 2 Ra X^\[Alpha] (X Ta + z) - (1 + Ka) X^\[Beta] (X Ta + z)^2 + Ba X^\[Gamma] (X Ta + z
    )^3 == 0
In Halley's method, we also require both f'(X) and f''(X). These are calculated by taking the
    derivative of both sides of the equation above with respect to X in mathematica*/
double antderiv(double z,double antX0){
        if(logflag==0){
        //Derivatives for : \[Alpha][X_] := 2 m + 1; \[Beta][X_] := 2 m ; \[Gamma][X_] := 2 m - 1;
        return 2.*Ra*Ta*pow (antX0, 1. + 2.*m) + 2.*(1. + 2.*m)*Ra*pow (antX0, 2.*m)*(Ta*antX0 + z)
             - 2.*(1. + Ka)*Ta*pow (antX0, 2.*m)*(Ta*antX0 + z) - 2.*(1. + Ka)*m*pow (antX0, -1. +
             2.*m)*pow (Ta*antX0 + z, 2) + 3.*Ba*Ta*pow (antX0, -1. + 2.*m)*pow (Ta*antX0 + z, 2)
            + Ba*(-1. + 2.*m)*pow (antX0, -2. + 2.*m)*pow (Ta*antX0 + z, 3);
        }else{
        /*the following is for  \[Alpha] = 2(1 + w)/w (m Log[(1 + w X)/(1 + w)])/Log[X] + 1;
        \[Beta] = 2(1 + w)/w (m Log[(1 + w X)/(1 + w)])/Log[X];
        \[Gamma] = 2(1 + w)/w (m Log[(1 + w X)/(1 + w)])/Log[X] - 1;*/
        return 2.*Ra*Ta*antX0*pow((1. + w*antX0)/(1. + w),(2.*m*(1. + w))/w) + 2.*Ra*pow((1. + w*
            antX0)/(1. + w),(2.*m*(1. + w))/w)*(Ta*antX0 + z) - 2.*(1. + Ka)*Ta*pow((1. + w*antX0)
            /(1. + w),(2.*m*(1. + w))/w)*(Ta*antX0 + z) + 4.*m*Ra*antX0*pow((1. + w*antX0)/(1. + w
            ),-1. + (2.*m*(1. + w))/w)*(Ta*antX0 + z) +(3.*Ba*Ta*pow((1. + w*antX0)/(1. + w),(2.*m
            *(1. + w))/w)*pow(Ta*antX0 + z,2))/antX0 - 2.*(1. + Ka)*m*pow((1. + w*antX0)/(1. + w)
            ,-1. + (2.*m*(1. + w))/w)*pow(Ta*antX0 + z,2) - (1.*Ba*pow((1. + w*antX0)/(1. + w)
```

```
            ,(2.*m*(1. + w))/w)*pow(Ta*antX0 + z,3))/pow(antX0,2) + (2.*Ba*m*pow((1. + w*antX0)
            /(1. + w),-1. + (2.*m*(1. + w))/w)*pow(Ta*antX0 + z,3))/antX0;
        }}
//second derivative used for Halley's method
double antderiv2(double z,double antX0){
        if(logflag==0){
        //Derivatives for : \[Alpha][X_] := 2 m + 1; \[Beta][X_] := 2 m ; \[Gamma][X_] := 2 m - 1;
        return 4.*(1. + 2.*m)*Ra*Ta*pow (antX0, 2.*m) - 2.*(1. + Ka)*pow (Ta, 2)*pow (antX0, 2.*m)
            + 4.*m*(1. + 2.*m)*Ra*pow (antX0, -1. + 2.*m)*(Ta*antX0 + z) -8.*(1. + Ka)*m*Ta*pow (
            antX0, -1. + 2.*m)*(Ta*antX0 + z) + 6.*Ba*pow (Ta, 2)*pow (antX0, -1. + 2.*m)*(Ta*
            antX0 + z) - 2.*(1. + Ka)*m*(-1. + 2.*m)*pow (antX0, -2. + 2.*m)*pow (Ta*antX0 + z, 2)
             + 6.*Ba*(-1. + 2.*m)*Ta*pow (antX0, -2. + 2.*m)*pow (Ta*antX0 + z, 2) + Ba*(-2. + 2.*
            m)*(-1. + 2.*m)*pow (antX0, -3. + 2.*m)*pow (Ta*antX0 + z, 3);
        }else{
        /*the following is for  \[Alpha] = 2(1 + w)/w (m Log[(1 + w X)/(1 + w)])/Log[X] + 1;
        \[Beta] = 2(1 + w)/w (m Log[(1 + w X)/(1 + w)])/Log[X];
        \[Gamma] = 2(1 + w)/w (m Log[(1 + w X)/(1 + w)])/Log[X] - 1;*/
        return 4.*Ra*Ta*pow((1. + w*antX0)/(1. + w),(2.*m*(1. + w))/w) - 2.*(1. + Ka)*pow(Ta,2)*pow
            ((1. + w*antX0)/(1. + w),(2.*m*(1. + w))/w) + 8.*m*Ra*Ta*antX0*pow((1. + w*antX0)/(1.
            + w),-1. + (2.*m*(1. + w))/w) + (6.*Ba*pow(Ta,2)*pow((1. + w*antX0)/(1. + w),(2.*m*(1.
             + w))/w)*(Ta*antX0 + z))/antX0 +(4.*m*Ra*w*(-1. + (2.*m*(1. + w))/w)*antX0*pow((1. +
            w*antX0)/(1. + w),-2. + (2.*m*(1. + w))/w)*(Ta*antX0 + z))/(1. + w) + 8.*m*Ra*pow((1.
            + w*antX0)/(1. + w),-1. + (2.*m*(1. + w))/w)*(Ta*antX0 + z) - 8.*(1. + Ka)*m*Ta*pow
            ((1. + w*antX0)/(1. + w),-1. + (2.*m*(1. + w))/w)*(Ta*antX0 + z) - (6.*Ba*Ta*pow((1. +
             w*antX0)/(1. + w),(2.*m*(1. + w))/w)*pow(Ta*antX0 + z,2))/pow(antX0,2) - (2.*(1. + Ka
            )*m*w*(-1. + (2.*m*(1. + w))/w)*pow((1. + w*antX0)/(1. + w),-2. + (2.*m*(1. + w))/w)*
            pow(Ta*antX0 + z,2))/(1. + w) + (12.*Ba*m*Ta*pow((1. + w*antX0)/(1. + w),-1. + (2.*m
            *(1. + w))/w)*pow(Ta*antX0 + z,2))/antX0 + (2.*Ba*pow((1. + w*antX0)/(1. + w),(2.*m
            *(1. + w))/w)*pow(Ta*antX0 + z,3))/pow(antX0,3) +
   (2.*Ba*m*w*(-1. + (2.*m*(1. + w))/w)*pow((1. + w*antX0)/(1. + w),-2. + (2.*m*(1. + w))/w)*pow(Ta
       *antX0 + z,3))/((1. + w)*antX0)- (4.*Ba*m*pow((1. + w*antX0)/(1. + w),-1. + (2.*m*(1. + w))
       /w)*pow(Ta*antX0 + z,3))/pow(antX0,2);
        }}
//Halley's method
double antroot(double y,double z){
        antXroot[0] = -z/Ta + pow(10,-10);
        int j = 0;
        double antdiff = 1000.;
        while (antdiff>0.00001) {
        if(logflag==0){
                alpha=2.*m+1.;
                beta=2.*m;
                gamma=2.*m-1.;
                antfunc[j]=-pow(y,2)+2.*Ra*pow (antXroot[j],alpha)*(antXroot[j]*Ta+z)-(1.+Ka)*pow (
                    antXroot[j],beta)*pow (antXroot[j]*Ta+z,2)+Ba*pow(antXroot[j],gamma)*pow(
                    antXroot[j]*Ta+z,3);
                double halley = (1. - (antfunc[j]*antderiv2(z, antXroot[j]))/(2.*pow(antderiv(z,
                    antXroot[j]),2)));
                antXroot[j+1]=antXroot[j]-antfunc[j]/(antderiv(z,antXroot[j])*halley);
                antdiff=fabs(antXroot[j+1]-antXroot[j]);
                j++;
        }else{
                double Xj=antXroot[j];
                antfunc[j]=-pow(y,2) + 2.*Ra*Xj*pow((1. + w*Xj)/(1. + w),(2.*m*(1. + w))/w)*(Ta*Xj
                    + z) - (1. + Ka)*pow((1. + w*Xj)/(1. + w),(2.*m*(1. + w))/w)*pow(Ta*Xj + z,2)
                    + (Ba*pow((1. + w*Xj)/(1. + w),(2.*m*(1. + w))/w)*pow(Ta*Xj + z,3))/Xj;
                double halley = (1. - (antfunc[j]*antderiv2(z, Xj))/(2.*pow(antderiv(z, Xj),2)));
                antXroot[j+1]=Xj-antfunc[j]/(antderiv(z,Xj)*halley);
                antdiff=fabs(antXroot[j+1]-Xj);
                j++;
```

```
        }
        }       return antXroot[j];
}
//The refractive index function n=nc+(ns-nc)X^(2p)
double antindexfunc(double y, double z){
        return nc + (ns-nc)*pow(antroot(y,z),2.*p);
}
double postderiv(double z,double postX0){
        if(logflag==0){
        //Derivatives for : \[Alpha][X_] := 2 m + 1; \[Beta][X_] := 2 m ; \[Gamma][X_] := 2 m - 1;
        return 2.*Rp*Tp*pow (postX0, 1. + 2.*m) + 2.*(1. + 2.*m)*Rp*pow (postX0, 2.*m)*(Tp*postX0 -
             1.*z) - 2.*(1. + Kp)*Tp*pow (postX0, 2.*m)*(Tp*postX0 - 1.*z) - 2.*(1. + Kp)*m*pow (
            postX0, -1. + 2.*m)*pow (Tp*postX0 - 1.*z, 2) + 3.*Bp*Tp*pow (postX0, -1. + 2.*m)*pow
            (Tp*postX0 - 1.*z, 2) + Bp*(-1. + 2.*m)*pow (postX0, -2. + 2.*m)*pow (Tp*postX0 - 1.*z
            , 3);
        }else{
        /*the following is for  \[Alpha] = 2(1 + w)/w (m Log[(1 + w X)/(1 + w)])/Log[X] + 1;
        \[Beta] = 2(1 + w)/w (m Log[(1 + w X)/(1 + w)])/Log[X];
        \[Gamma] = 2(1 + w)/w (m Log[(1 + w X)/(1 + w)])/Log[X] - 1;*/
        return 2.*Rp*Tp*postX0*pow((1. + w*postX0)/(1. + w),(2.*m*(1. + w))/w) + 2.*Rp*pow((1. + w*
            postX0)/(1. + w),(2.*m*(1. + w))/w)*(Tp*postX0 - 1.*z) - 2.*(1. + Kp)*Tp*pow((1. + w*
            postX0)/(1. + w),(2.*m*(1. + w))/w)*(Tp*postX0 - 1.*z) + 4.*m*Rp*postX0*pow((1. + w*
            postX0)/(1. + w),-1. + (2.*m*(1. + w))/w)*(Tp*postX0 - 1.*z) + (3.*Bp*Tp*pow((1. + w*
            postX0)/(1. + w),(2.*m*(1. + w))/w)*pow(Tp*postX0 - 1.*z,2))/postX0 - 2.*(1. + Kp)*m*
            pow((1. + w*postX0)/(1. + w),-1. + (2.*m*(1. + w))/w)*pow(Tp*postX0 - 1.*z,2) - (1.*Bp
            *pow((1. + w*postX0)/(1. + w),(2.*m*(1. + w))/w)*pow(Tp*postX0 - 1.*z,3))/pow(postX0
            ,2) + (2.*Bp*m*pow((1. + w*postX0)/(1. + w),-1. + (2.*m*(1. + w))/w)*pow(Tp*postX0 -
            1.*z,3))/postX0;
        }}
double postderiv2(double z,double postX0){
        if(logflag==0){
        //Derivatives for : \[Alpha][X_] := 2 m + 1; \[Beta][X_] := 2 m ; \[Gamma][X_] := 2 m - 1;
        return 4.*(1. + 2.*m)*Rp*Tp*pow(postX0,2.*m) - 2.*(1. + Kp)*pow(Tp,2)*pow(postX0,2.*m) +
            4.*m*(1. + 2.*m)*Rp*pow(postX0,-1. + 2.*m)*(Tp*postX0 - 1.*z) - 8.*(1. + Kp)*m*Tp*pow(
            postX0,-1. + 2.*m)*(Tp*postX0 - 1.*z) + 6.*Bp*pow(Tp,2)*pow(postX0,-1. + 2.*m)*(Tp*
            postX0 - 1.*z) - 2.*(1. + Kp)*m*(-1. + 2.*m)*pow(postX0,-2. + 2.*m)*pow(Tp*postX0 -
            1.*z,2) + 6.*Bp*(-1. + 2.*m)*Tp*pow(postX0,-2. + 2.*m)*pow(Tp*postX0 - 1.*z,2) + Bp
            *(-2. + 2.*m)*(-1. + 2.*m)*pow(postX0,-3. + 2.*m)*pow(Tp*postX0 - 1.*z,3);
        }else{
        /*the following is for  \[Alpha] = 2(1 + w)/w (m Log[(1 + w X)/(1 + w)])/Log[X] + 1;
        \[Beta] = 2(1 + w)/w (m Log[(1 + w X)/(1 + w)])/Log[X];
        \[Gamma] = 2(1 + w)/w (m Log[(1 + w X)/(1 + w)])/Log[X] - 1;*/
        return 4.*Rp*Tp*pow((1. + w*postX0)/(1. + w),(2.*m*(1. + w))/w) - 2.*(1. + Kp)*pow(Tp,2)*
            pow((1. + w*postX0)/(1. + w),(2.*m*(1. + w))/w) + 8.*m*Rp*Tp*postX0*pow((1. + w*postX0
            )/(1. + w),-1. + (2.*m*(1. + w))/w) + (6.*Bp*pow(Tp,2)*pow((1. + w*postX0)/(1. + w)
            ,(2.*m*(1. + w))/w)*(Tp*postX0 - 1.*z))/postX0 + (4.*m*Rp*w*(-1. + (2.*m*(1. + w))/w)*
            postX0*pow((1. + w*postX0)/(1. + w),-2. + (2.*m*(1. + w))/w)*(Tp*postX0 - 1.*z))/(1. +
             w) + 8.*m*Rp*pow((1. + w*postX0)/(1. + w),-1. + (2.*m*(1. + w))/w)*(Tp*postX0 - 1.*z)
             - 8.*(1. + Kp)*m*Tp*pow((1. + w*postX0)/(1. + w),-1. + (2.*m*(1. + w))/w)*(Tp*postX0
            - 1.*z) - (6.*Bp*Tp*pow((1. + w*postX0)/(1. + w),(2.*m*(1. + w))/w)*pow(Tp*postX0 -
            1.*z,2))/pow(postX0,2) - (2.*(1. + Kp)*m*w*(-1. + (2.*m*(1. + w))/w)*pow((1. + w*
            postX0)/(1. + w),-2. + (2.*m*(1. + w))/w)*pow(Tp*postX0 - 1.*z,2))/(1. + w) +(12.*Bp*m
            *Tp*pow((1. + w*postX0)/(1. + w),-1. + (2.*m*(1. + w))/w)*pow(Tp*postX0 - 1.*z,2))/
            postX0 + (2.*Bp*pow((1. + w*postX0)/(1. + w),(2.*m*(1. + w))/w)*pow(Tp*postX0 - 1.*z
            ,3))/pow(postX0,3) + (2.*Bp*m*w*(-1. + (2.*m*(1. + w))/w)*pow((1. + w*postX0)/(1. + w)
            ,-2. + (2.*m*(1. + w))/w)*pow(Tp*postX0 - 1.*z,3))/((1. + w)*postX0) - (4.*Bp*m*pow
            ((1. + w*postX0)/(1. + w),-1. + (2.*m*(1. + w))/w)*pow(Tp*postX0 - 1.*z,3))/pow(postX0
            ,2);
        }}
double postroot(double y,double z){
```

```
        postXroot[0] = fabs(z/Tp) + 0.1*((Tp - fabs(z))/Tp);
        int j = 0;
        double postdiff = 1000.;
        while (postdiff>0.0001){
        if(logflag==0){
                alpha=2.*m+1.;
                beta=2.*m;
                gamma=2.*m-1.;
                postfunc[j]=-1.*pow(y,2) + 2.*Rp*pow(postXroot[j],alpha)*(-1.*z + Tp*postXroot[j])
                    -1.*(1. + Kp)*pow(postXroot[j],beta)*pow(-1.*z + Tp*postXroot[j],2) + Bp*pow(
                    postXroot[j],gamma)*pow(-1.*z + Tp*postXroot[j],3);
                double halley = (1. - (postfunc[j]*postderiv2(z, postXroot[j]))/(2.*pow(postderiv(z
                    , postXroot[j]),2)));
                postXroot[j+1]=postXroot[j]-postfunc[j]/(postderiv(z,postXroot[j])*halley);
                postdiff=fabs(postXroot[j+1]-postXroot[j]);
                j++;
        }else{
                double Xj=postXroot[j];
                postfunc[j]=-1.*pow(y,2) + 2.*Rp*Xj*pow((1. + w*Xj)/(1. + w),(2.*m*(1. + w))/w)*(Tp
                    *Xj - 1.*z) - 1.*(1. + Kp)*pow((1. + w*Xj)/(1. + w),(2.*m*(1. + w))/w)*pow(Tp*
                    Xj - 1.*z,2) +(Bp*pow((1. + w*Xj)/(1. + w),(2.*m*(1. + w))/w)*pow(Tp*Xj - 1.*z
                    ,3))/Xj;
                double halley = (1. - (postfunc[j]*postderiv2(z, Xj))/(2.*pow(postderiv(z, Xj),2)))
                    ;
                postXroot[j+1]=Xj-postfunc[j]/(postderiv(z,Xj)*halley);
                postdiff=fabs(postXroot[j+1]-Xj);
                j++;
        }
        }       return postXroot[j];
}
double postindexfunc(double y, double z){
        return nc + (ns-nc)*pow(postroot(y,z),2.*p);
}
//Derivative of n with respect to z, for use in the Runge-Kutta method
double antdndzfunc(double X, double y, double z){
        if(logflag==0){
                alpha=2.*m+1.;
                beta=2.*m;
                gamma=2.*m-1.;
                return (2.*(-nc+ns)*p*pow(X,-1.+2.*p)*(-2.*Ra*pow(X,alpha)+2.*(1.+Ka)*pow(X,beta)*(
                    Ta*X+z)-3.*Ba*pow(X,gamma)*pow(Ta*X+z,2)))/(2.*Ra*pow(X,-1.+alpha)*z*alpha+2.*
                    Ra*Ta*pow(X,alpha)*(1.+alpha)-(1.+Ka)*pow(X,-1.+beta)*z*(Ta*X+z)*beta-(1.+Ka)*
                    Ta*pow(X,beta)*(Ta*X+z)*(2+beta)+Ba*pow(X,-1.+gamma)*z*pow(Ta*X+z,2)*gamma+Ba*
                    Ta*pow(X,gamma)*pow(Ta*X+z,2)*(3.+gamma));
        }else{
                return (2.*(-1.*nc + ns)*p*pow(X,-1. + 2.*p)*(-2.*Ra*X*pow((1. + w*X)/(1. + w),(2.*
                    m*(1. + w))/w) + 2.*(1. + Ka)*pow((1. + w*X)/(1. + w),(2.*m*(1. + w))/w)*(Ta*X
                     + z) - (3.*Ba*pow((1. + w*X)/(1. + w),(2.*m*(1. + w))/w)*pow(Ta*X + z,2))/X))
                    /(2.*Ra*Ta*X*pow((1. + w*X)/(1. + w),(2.*m*(1. + w))/w) + 2.*Ra*pow((1. + w*X)
                    /(1. + w),(2.*m*(1. + w))/w)*(Ta*X + z) - 2.*(1. + Ka)*Ta*pow((1. + w*X)/(1. +
                     w),(2.*m*(1. + w))/w)*(Ta*X + z) + (4.*m*Ra*(1. + w)*X*pow((1. + w*X)/(1. + w
                    ),(2.*m*(1. + w))/w)*(Ta*X + z))/(1. + w*X) +(3.*Ba*Ta*pow((1. + w*X)/(1. + w)
                    ,(2.*m*(1. + w))/w)*pow(Ta*X + z,2))/X - (2.*(1. + Ka)*m*(1. + w)*pow((1. + w*
                    X)/(1. + w),(2.*m*(1. + w))/w)*pow(Ta*X + z,2))/(1. + w*X) - (1.*Ba*pow((1. +
                    w*X)/(1. + w),(2.*m*(1. + w))/w)*pow(Ta*X + z,3))/pow(X,2) + (2.*Ba*m*(1. + w)
                    *pow((1. + w*X)/(1. + w),(2.*m*(1. + w))/w)*pow(Ta*X + z,3))/(X*(1. + w*X)));
        }}
double antDz(double X, double y, double z){
        return antindexfunc(y, z)*antdndzfunc(X, y, z);
}
```

```
double antdndyfunc(double X, double y, double z){
        if(logflag==0){
                alpha=2.*m+1.;
                beta=2.*m;
                gamma=2.*m-1.;
                return (4.*(-nc + ns)*p*pow(X,2.*p)*y)/(2.*Ra*pow(X,alpha)*(z*alpha + Ta*X*(1. +
                    alpha)) +(Ta*X + z)*((-1. - Ka)*pow(X,beta)*(z*beta + Ta*X*(2. + beta)) + Ba*
                    pow(X,gamma)*(Ta*X + z)*(z*gamma + Ta*X*(3. + gamma))));
        }else{
                return (4.*(-1.*nc + ns)*p*pow(X,1. + 2.*p)*(1. + w*X)*y)/(pow((1. + w*X)/(1. + w)
                    ,(2.*m*(1. + w))/w)*(2.*Ta*(2.*Ra + Ta*(-1. - 1.*Ka + Ba*Ta))*pow(X,3)*(1. + (
                    m + w + m*w)*X) + (2.*Ra + Ta*(-2. - 2.*Ka + 3.*Ba*Ta))*pow(X,2)*(1. + w*X +
                    2.*m*(1. + w)*X)*z - 2.*m*(1. + Ka - 3.*Ba*Ta)*(1. + w)*pow(X,2)*pow(z,2) + Ba
                    *(-1. - 1.*w*X + 2.*m*(1. + w)*X)*pow(z,3)));
        }}
double antDy(double X, double y, double z){
        return antindexfunc(y, z)*antdndyfunc(X, y, z);
}
double postdndzfunc(double X, double y, double z){
        if(logflag==0){
                alpha=2.*m+1.;
                beta=2.*m;
                gamma=2.*m-1.;
                return (2.*(-1.*nc + ns)*p*pow(X,-1. + 2.*p)*(-2.*Rp*pow(X,alpha) + 2.*(1. + Kp)*
                    pow(X,beta)*(Tp*X - 1.*z) - 3.*Bp*pow(X,gamma)*pow(-1.*Tp*X + z,2)))/(2.*Rp*
                    pow(X,-1. + alpha)*z*alpha - 2.*Rp*Tp*pow(X,alpha)*(1. + alpha) - 1.*(1. + Kp)
                    *pow(X,-1. + beta)*(Tp*X - 1.*z)*z*beta + (1. + Kp)*Tp*pow(X,beta)*(Tp*X - 1.*
                    z)*(2. + beta) + Bp*pow(X,-1. + gamma)*z*pow(-1.*Tp*X + z,2)*gamma - 1.*Bp*Tp*
                    pow(X,gamma)*pow(-1.*Tp*X + z,2)*(3. + gamma));
        }else{
                return (2.*(-1.*nc + ns)*p*pow(X,-1. + 2.*p)*(2.*Rp*X*pow((1. + w*X)/(1. + w),(2.*m
                    *(1. + w))/w) - 2.*(1. + Kp)*pow((1. + w*X)/(1. + w),(2.*m*(1. + w))/w)*(Tp*X
                    - 1.*z) + (3.*Bp*pow((1. + w*X)/(1. + w),(2.*m*(1. + w))/w)*pow(-1.*Tp*X + z
                    ,2))/X))/(2.*Rp*Tp*X*pow((1. + w*X)/(1. + w),(2.*m*(1. + w))/w) + 2.*Rp*pow
                    ((1. + w*X)/(1. + w),(2.*m*(1. + w))/w)*(Tp*X - 1.*z) - 2.*(1. + Kp)*Tp*pow
                    ((1. + w*X)/(1. + w),(2.*m*(1. + w))/w)*(Tp*X - 1.*z) + (4.*m*Rp*(1. + w)*X*
                    pow((1. + w*X)/(1. + w),(2.*m*(1. + w))/w)*(Tp*X - 1.*z))/(1. + w*X) + (2.*Bp*
                    m*(1. + w)*pow((1. + w*X)/(1. + w),(2.*m*(1. + w))/w)*pow(Tp*X - 1.*z,3))/(X
                    *(1. + w*X)) + (3.*Bp*Tp*pow((1. + w*X)/(1. + w),(2.*m*(1. + w))/w)*pow(-1.*Tp
                    *X + z,2))/X - (2.*(1. + Kp)*m*(1. + w)*pow((1. + w*X)/(1. + w),(2.*m*(1. + w)
                    )/w)*pow(-1.*Tp*X + z,2))/(1. + w*X) + (Bp*pow((1. + w*X)/(1. + w),(2.*m*(1. +
                     w))/w)*pow(-1.*Tp*X + z,3))/pow(X,2));
        }}
double postDz(double X, double y, double z){
        return postindexfunc(y, z)*postdndzfunc(X, y, z);
}
double postdndyfunc(double X, double y, double z){
        if(logflag==0){
                alpha=2.*m+1.;
                beta=2.*m;
                gamma=2.*m-1.;
                return (4.*(-1.*nc + ns)*p*pow(X,2.*p)*y)/   (2.*Rp*pow(X,alpha)*(-1.*z*alpha + Tp*
                    X*(1. + alpha)) + (Tp*X - 1.*z)*((-1. - 1.*Kp)*pow(X,beta)*(-1.*z*beta + Tp*X
                    *(2. + beta)) + Bp*pow(X,gamma)*(Tp*X - 1.*z)*(-1.*z*gamma + Tp*X*(3. + gamma)
                    )));
                }else{
                return (4.*(-1.*nc + ns)*p*pow(X,1. + 2.*p)*(1. + w*X)*y)/(pow((1. + w*X)/(1. + w)
                    ,(2.*m*(1. + w))/w)*(2.*Tp*(2.*Rp + Tp*(-1. - 1.*Kp + Bp*Tp))*pow(X,3)*(1. + (
                    m + w + m*w)*X) - 1.*(2.*Rp + Tp*(-2. - 2.*Kp + 3.*Bp*Tp))*pow(X,2)*(1. + w*X
```

```
                    + 2.*m*(1. + w)*X)*z - 2.*m*(1. + Kp - 3.*Bp*Tp)*(1. + w)*pow(X,2)*pow(z,2) +
                    Bp*(1. + w*X - 2.*m*(1. + w)*X)*pow(z,3)));
            }}
double postDy(double X, double y, double z){
        return postindexfunc(y, z)*postdndyfunc(X, y, z);
}
//The Runge-Kutta method
//The following use "memoization". From Wikipedia: "In computing, memoization is an optimization
    technique used primarily to speed up computer programs by storing the results of expensive
    function calls and returning the cached result when the same inputs occur again."
double antRz(int i){
        if(i == 0){
                return zsb;
        }else{
                //if the array does not contain the dummy value of -1000, then it has a valid
                    number, so return it.
                if (antRzarray[i] != -1000){
                        return antRzarray[i];
                }
                //if the array contains the pre-assigned dummy value, the proper value must be
                    calculated
                else{
                        antRzarray[i] = antRz(i-1) + dt*(antTz(i-1) + (1./6.)*(antaz(i-1) + 2.*
                            antbz(i-1)));
                        return antRzarray[i];
                }}}
double antRy(int i){
        if(i==0){
                return ysb;
        }else{
                if (antRyarray[i]!= -1000){
                        return antRyarray[i];
                }else{
                        antRyarray[i]=antRy(i-1)+dt*(antTy(i-1)+(1./6.)*(antay(i-1)+2.*antby(i-1)))
                            ;
                        return antRyarray[i];
                }}}
double antTz(int i){
        if(i == 0){
        return ns*Liz;
        }else{
                if (antTzarray[i] != -1000){
                        return antTzarray[i];
                }else{
                        antTzarray[i]=antTz(i-1)+ (1./6.)*(antaz(i-1) + 4.*antbz(i-1) + antcz(i-1))
                            ;
                        return antTzarray[i];
                }}}
double antTy(int i){
        if(i==0){
                return ns*Liy;
        }else{
                if (antTyarray[i]!=-1000){
                        return antTyarray[i];
                }else{
                        antTyarray[i]=antTy(i-1)+(1./6.)*(antay(i-1)+4.*antby(i-1)+antcy(i-1));
                        return antTyarray[i];
                }}}
double antaz(int i){
        if (antazarray[i] != -1000){
```

```
                        return antazarray[i];
        }else{
                antazarray[i] = dt*(antDz(antroot(antRy(i), antRz(i)), antRy(i), antRz(i)));
                return antazarray[i];
        }}
double antay(int i){
        if (antayarray[i] != -1000){
                return antayarray[i];
        }else {
                antayarray[i] = dt*(antDy(antroot(antRy(i), antRz(i)), antRy(i),antRz(i)));
                return antayarray[i];
  }}
double antbz(int i){
        if (antbzarray[i] != -1000){
                        return antbzarray[i];
        }else{
                antbzarray[i] = dt*(antDz(antroot(antRy(i)+ 0.5*dt*antTy(i) + 0.125*dt*antay(i),
                    antRz(i)+ 0.5*dt*antTz(i) + 0.125*dt*antaz(i)), antRy(i)+ 0.5*dt*antTy(i) +
                    0.125*dt*antay(i),antRz(i)+ 0.5*dt*antTz(i) + 0.125*dt*antaz(i)));
                return antbzarray[i];
        }}
double antby(int i){
        if (antbyarray[i]!=-1000){
                return antbyarray[i];
        }else{
                antbyarray[i] = dt*(antDy(antroot(antRy(i)+0.5*dt*antTy(i)+0.125*dt*antay(i),antRz(
                    i)+0.5*dt*antTz(i)+0.125*dt*antaz(i)),antRy(i)+0.5*dt*antTy(i)+0.125*dt*antay(
                    i),antRz(i)+0.5*dt*antTz(i)+0.125*dt*antaz(i)));
                return antbyarray[i];
        }}
double antcz(int i){
        if (antczarray[i] != -1000){
                        return antczarray[i];
        }else{
                antczarray[i] = dt*(antDz(antroot(antRy(i)+ dt*antTy(i) + 0.5*dt*antby(i),antRz(i)+
                     dt*antTz(i) + 0.5*dt*antbz(i)), antRy(i)+ dt*antTy(i) + 0.5*dt*antby(i),antRz
                    (i)+ dt*antTz(i) + 0.5*dt*antbz(i)));
                return antczarray[i];
        }}
double antcy(int i){
        if (antcyarray[i]!=-1000){
                return antcyarray[i];
        }else{
                antcyarray[i]=dt*(antDy(antroot(antRy(i)+dt*antTy(i)+0.5*dt*antby(i),antRz(i)+dt*
                    antTz(i)+0.5*dt*antbz(i)),antRy(i)+dt*antTy(i)+0.5*dt*antby(i),antRz(i)+dt*
                    antTz(i)+0.5*dt*antbz(i)));
                return antcyarray[i];
        }}
double postRz(int i){
        if(i==0){
                return zsb;
        }else{
                if (postRzarray[i]!=-1000){
                        return postRzarray[i];
                }else{
                        postRzarray[i]=postRz(i-1)+dt*(postTz(i-1)+(1./6.)*(postaz(i-1)+2.*postbz(i
                            -1)));
                        return postRzarray[i];
                }}}
double postRy(int i){
```

```
        if(i==0){
                return ysb;
        }else{
                if (postRyarray[i]!=-1000){
                        return postRyarray[i];
                }else{
                        postRyarray[i]=postRy(i-1)+dt*(postTy(i-1)+(1./6.)*(postay(i-1)+2.*postby(i
                            -1)));
                        return postRyarray[i];
                }}}
double postTz(int i){
        if(i==0){
                return ns*Liz;
        }else{
                if (postTzarray[i]!=-1000){
                        return postTzarray[i];
                }else{
                        postTzarray[i]=postTz(i-1)+(1./6.)*(postaz(i-1)+4.*postbz(i-1)+postcz(i-1))
                            ;
                        return postTzarray[i];
                }}}
double postTy(int i){
        if(i==0){
                return ns*Liy;
        }else{
                if (postTyarray[i]!=-1000){
                        return postTyarray[i];
                }else{
                        postTyarray[i]=postTy(i-1)+(1./6.)*(postay(i-1)+4.*postby(i-1)+postcy(i-1))
                            ;
                        return postTyarray[i];
                }}}
double postaz(int i){
        if (postazarray[i]!=-1000){
                return postazarray[i];
        }else{
                postazarray[i]=dt*(postDz(postroot(postRy(i),postRz(i)),postRy(i),postRz(i)));
                return postazarray[i];
        }}
double postay(int i){
        if (postayarray[i]!=-1000){
                return postayarray[i];
        }else{
                postayarray[i]=dt*(postDy(postroot(postRy(i),postRz(i)),postRy(i),postRz(i)));
                return postayarray[i];
        }}
double postbz(int i){
        if (postbzarray[i]!=-1000){
                return postbzarray[i];
        }else{
                postbzarray[i]=dt*(postDz(postroot(postRy(i)+0.5*dt*postTy(i)+0.125*dt*postay(i),
                    postRz(i)+0.5*dt*postTz(i)+0.125*dt*postaz(i)),postRy(i)+0.5*dt*postTy(i)
                    +0.125*dt*postay(i),postRz(i)+0.5*dt*postTz(i)+0.125*dt*postaz(i)));
                return postbzarray[i];
        }}
double postby(int i){
        if (postbyarray[i]!=-1000){
                return postbyarray[i];
        }else{
```

```
                postbyarray[i]=dt*(postDy(postroot(postRy(i)+0.5*dt*postTy(i)+0.125*dt*postay(i),
                    postRz(i)+0.5*dt*postTz(i)+0.125*dt*postaz(i)),postRy(i)+0.5*dt*postTy(i)
                    +0.125*dt*postay(i),postRz(i)+0.5*dt*postTz(i)+0.125*dt*postaz(i)));
                return postbyarray[i];
        }}
double postcz(int i){
        if (postczarray[i]!=-1000){
                return postczarray[i];
        }else{
                postczarray[i]=dt*(postDz(postroot(postRy(i)+dt*postTy(i)+0.5*dt*postby(i),postRz(i
                    )+dt*postTz(i)+0.5*dt*postbz(i)),postRy(i)+dt*postTy(i)+0.5*dt*postby(i),
                    postRz(i)+dt*postTz(i)+0.5*dt*postbz(i)));
                return postczarray[i];
        }}
double postcy(int i){
        if (postcyarray[i]!=-1000){
                return postcyarray[i];
        }else{
                postcyarray[i]=dt*(postDy(postroot(postRy(i)+dt*postTy(i)+0.5*dt*postby(i),postRz(i
                    )+dt*postTz(i)+0.5*dt*postbz(i)),postRy(i)+dt*postTy(i)+0.5*dt*postby(i),
                    postRz(i)+dt*postTz(i)+0.5*dt*postbz(i)));
                return postcyarray[i];
        }}
```

BIBLIOGRAPHY

[1] G. Smith, "Schematic eyes: history, description and applications," Clinical and Experimental Optometry **78**, 176–189 (1995).

[2] B. K. Pierscionek, "Presbyopia: effect of refractive index," Clinical & Experimental Optometry **73**, 23–30 (1990).

[3] M. Bahrami and A. V. Goncharov, "Geometry-invariant gradient refractive index lens: analytical ray tracing," Journal of Biomedical Optics **17**, 055001–1 – 055001–9 (2012).

[4] M. Bahrami and A. V. Goncharov, "Geometry-invariant grin lens: finite ray tracing," Opt. Express **22**, 27797–27810 (2014).

[5] D. A. Atchison and G. Smith, *Optics of the human eye* (Butterworth-Heinemann, Oxford, 2000).

[6] H. Radhakrishnan and W. N. Charman, "Age-related changes in ocular aberrations with accommodation," Journal of Vision **7**, 1–21 (2007).

[7] J. Porter, A. Guirao, I. G. Cox, and D. R. Williams, "Monochromatic aberrations of the human eye in a large population," Journal of the Optical Society of America A **18**, 1793–1803 (2001).

[8] L. N. Thibos, A. Bradley, and X. Hong, "A statistical model of the aberration structure of normal, well-corrected eyes," Ophthalmic and Physiological Optics **22**, 427–433 (2002).

[9] X. Cheng, A. Bradley, X. Hong, and L. N. Thibos, "Relationship between refractive error and monochromatic aberrations of the eye," Optometry and vision science **80**, 43–49 (2003).

[10] L. Wang and D. D. Koch, "Ocular higher-order aberrations in individuals screened for refractive surgery," Journal of Cataract & Refractive Surgery **29**, 1896–1903 (2003).

[11] M. V. Netto, R. Ambrósio, T. T. Shen, and S. E. Wilson, "Wavefront analysis in normal refractive surgery candidates," Journal of refractive surgery **21**, 332–338 (2005).

[12] A. Tomlinson, R. P. Hemenger, and R. Garriott, "Method for estimating the spheric aberration of the human crystalline lens in vivo." Investigative Ophthalmology & Visual Science **34**, 621–629 (1993).

[13] G. Smith, M. J. Cox, R. Calver, and L. F. Garner, "The spherical aberration of the crystalline lens of the human eye," Vision Research **41**, 235–243 (2001).

[14] L. Llorente, S. Barbero, D. Cano, C. Dorronsoro, and S. Marcos, "Myopic versus hyperopic eyes: axial length, corneal shape and optical aberrations," Journal of Vision **4** (2004).

[15] M. J. Collins, C. F. Wildsoet, and D. A. Atchison, "Monochromatic aberrations and myopia," Vision Research **35**, 1157–1163 (1995).

[16] J. C. He, P. Sun, R. Held, F. Thorn, X. Sun, and J. E. Gwiazda, "Wavefront aberrations in eyes of emmetropic and moderately myopic school children and young adults," Vision Research **42**, 1063 – 1070 (2002).

[17] S. Marcos, S. Barbero, and L. Llorente, "The sources of optical aberrations in myopic eyes [arvo abstract]," in "Investigative Ophthalmology & Visual Science," , vol. 43 (2002), vol. 43, p. 1510.

[18] M.-P. Paquin, H. Hamam, and P. Simonet, "Objective measurement of optical aberrations in myopic eyes," Optometry & Vision Science **79**, 285–291 (2002).

[19] A. Carkeet, H. D. Luo, L. Tong, S. M. Saw, and D. T. Tan, "Refractive error and monochromatic aberrations in singaporean children," Vision Research **42**, 1809 – 1824 (2002).

[20] P. Artal, E. Berrio, A. Guirao, and P. Piers, "Contribution of the cornea and internal surfaces to the change of ocular aberrations with age," Journal of the Optical Society of America A **19**, 137–143 (2002).

[21] R. I. Calver, M. J. Cox, and D. B. Elliott, "Effect of aging on the monochromatic aberrations of the human eye," Journal of the Optical Society of America A **16**, 2069–2078 (1999).

[22] J. S. McLellan, S. Marcos, and S. A. Burns, "Age-related changes in monochromatic wave aberrations of the human eye," Investigative Ophthalmology & Visual Science **42**, 1390–1395 (2001).

[23] P. Artal and A. Guirao, "Contributions of the cornea and the lens to the aberrations of the human eye," Optics Letters **23**, 1713–1715 (1998).

[24] A. Glasser and M. C. Campbell, "Presbyopia and the optical changes in the human crystalline lens with age," Vision Research **38**, 209–229 (1998).

[25] J. L. Alió, P. Schimchak, H. P. Negri, and R. Montés-Micó, "Crystalline lens optical dysfunction through aging," Ophthalmology **112**, 2022–2029 (2005).

[26] I. Brunette, J. M. Bueno, M. Parent, H. Hamam, and P. Simonet, "Monochromatic aberrations as a function of age, from childhood to advanced age," Investigative Ophthalmology & Visual Science **44**, 5438–5446 (2003).

[27] T. Oshika, S. D. Klyce, R. A. Applegate, and H. C. Howland, "Changes in corneal wavefront aberrations with aging," Investigative Ophthalmology & Visual Science **40**, 1351–1355 (1999).

[28] P. Artal, A. Benito, and J. Tabernero, "The human eye is an example of robust optical design," Journal of Vision **6**, 1–7 (2006).

[29] H. V. Z. Athaide, M. Campos, and C. Costa, "Study of ocular aberrations with age," Arquivos brasileiros de oftalmologia **72**, 617–621 (2009).

[30] C. Kirwan, M. O'Keefe, and H. Soeldner, "Higher-order aberrations in children," American Journal of Ophthalmology **141**, 67–70 (2006).

[31] K. Philip, A. Martinez, A. Ho, F. Conrad, J. Ale, P. Mitchell, and P. Sankaridurg, "Total ocular, anterior corneal and lenticular higher order aberrations in hyperopic, myopic and emmetropic eyes," Vision Research **52**, 31 – 37 (2012).

[32] J.-A. Little, S. J. McCullough, K. M. M. Breslin, and K. J. Saunders, "Higher order ocular aberrations and their relation to refractive error and ocular biometry in childrenhigher order ocular aberrations in children," Investigative Ophthalmology & Visual Science **55**, 4791–4800 (2014).

[33] K. Philip, P. Sankaridurg, B. Holden, A. Ho, and P. Mitchell, "Influence of higher order aberrations and retinal image quality in myopisation of emmetropic eyes," Vision Research **105**, 233–243 (2014).

[34] G. Papamastorakis, S. Panagopoulou, M. K. Tsilimbaris, I. G. Pallikaris, and S. Plainis, "Ocular higher-order aberrations in a school children population," Journal of Optometry **8**, 93–100 (2015).

[35] T. O. Salmon and C. van de Pol, "Normal-eye zernike coefficients and root-mean-square wavefront errors," Journal of Cataract & Refractive Surgery **32**, 2064–2074 (2006).

[36] L. N. Thibos, X. Hong, A. Bradley, and X. Cheng, "Statistical variation of aberration structure and image quality in a normal population of healthy eyes," Journal of the Optical Society of America A **19**, 2329–2348 (2002).

[37] H. C. Howland, "High order wave aberration of eyes," Ophthalmic and Physiological Optics **22**, 434–439 (2002).

[38] A. Guirao, C. González, M. Redondo, E. Geraghty, S. Norrby, and P. Artal, "Average optical performance of the human eye as a function of age in a normal population," Investigative Ophthalmology & Visual Science **40**, 203–213 (1999).

[39] J. F. Castejón-Mochón, N. López-Gil, A. Benito, and P. Artal, "Ocular wavefront aberration statistics in a normal young population," Vision Research **42**, 1611–1617 (2002).

[40] R. Sperduto, D. Seigel, J. Roberts, and M. Rowland, "Prevalence of myopia in the United States," Archives of Ophthalmology **101**, 405–407 (1983).

[41] M. Smirnov, "Measurement of the wave aberration of the human eye," Biofizika **6**, 687–703 (1961).

[42] H. C. Howland and B. Howland, "A subjective method for the measurement of monochromatic aberrations of the eye," Journal of the Optical Society of America **67**, 1508–1518 (1977).

[43] G. Walsh, W. N. Charman, and H. C. Howland, "Objective technique for the determination of monochromatic aberrations of the human eye," Journal of the Optical Society of America A **1**, 987–992 (1984).

[44] S. Amano, Y. Amano, S. Yamagami, T. Miyai, K. Miyata, T. Samejima, and T. Oshika, "Age-related changes in corneal and ocular higher-order wavefront aberrations," American Journal of Ophthalmology **137**, 988–992 (2004).

[45] L. Wang, E. Dai, D. D. Koch, and A. Nathoo, "Optical aberrations of the human anterior cornea," Journal of Cataract & Refractive Surgery **29**, 1514–1521 (2003).

[46] N. Brown, "The change in lens curvature with age," Experimental Eye Research **19**, 175–183 (1974).

[47] M. Dubbelman and G. van der Heijde, "The shape of the aging human lens: curvature, equivalent refractive index and the lens paradox," Vision Research **41**, 1867–1877 (2001).

[48] G. Smith, D. A. Atchison, and B. K. Pierscionek, "Modeling the power of the aging human eye," Journal of the Optical Society of America A **9**, 2111–2117 (1992).

[49] Y. Levy, O. Segal, I. Avni, and D. Zadok, "Ocular higher-order aberrations in eyes with supernormal vision," American Journal of Ophthalmology **139**, 225–228 (2005).

[50] D. Zadok, Y. Levy, O. Segal, Y. Barkana, Y. Morad, and I. Avni, "Ocular higher-order aberrations in myopia and skiascopic wavefront repeatability," Journal of Cataract & Refractive Surgery **31**, 1128–1132 (2005).

[51] M. Jahnke, C. Wirbelauer, and D. Pham, "Einfluss des alters auf die optischen aberrationen des menschlichen auges (influence of age on optical aberrations of the human eye)," Der Ophthalmologe **103**, 596–604 (2006).

[52] R. A. Applegate, I. William J. Donnelly, J. D. Marsack, D. E. Koenig, and K. Pesudovs, "Three-dimensional relationship between high-order root-mean-square wavefront error, pupil diameter, and aging," J. Opt. Soc. Am. A **24**, 578–587 (2007).

[53] A. Guirao, M. Redondo, and P. Artal, "Optical aberrations of the human cornea as a function of age," Journal of the Optical Society of America A **17**, 1697–1702 (2000).

[54] P. Artal, M. Ferro, I. Miranda, and R. Navarro, "Effects of aging in retinal image quality," Journal of the Optical Society of America A **10**, 1656–1662 (1993).

[55] H. S. Ginis, S. Plainis, and A. Pallikaris, "Variability of wavefront aberration measurements in small pupil sizes using a clinical shack-hartmann aberrometer," BMC Ophthalmology **4**, 1 (2004).

[56] T. Fujikado, T. Kuroda, S. Ninomiya, N. Maeda, Y. Tano, T. Oshika, Y. Hirohara, and T. Mihashi, "Age-related changes in ocular and corneal aberrations," American Journal of Ophthalmology **138**, 143–146 (2004).

[57] W. N. Charman, "Wavefront aberration of the eye: A review." Optometry & Vision Science **68**, – (1991).

[58] D. Whitaker and D. Elliott, "Simulating age-related optical changes in the human eye," Documenta Ophthalmologica **82**, 307–316 (1992).

[59] L. E. Fernández de Castro, H. P. Sandoval, L. R. Bartholomew, D. T. Vroman, and K. D. Solomon, "High-order aberrations and preoperative associated factors," Acta Ophthalmologica Scandinavica **85**, 106–110 (2007).

[60] G. Walsh and W. N. Charman, "Measurement of the axial wavefront aberration of the human eye," Ophthalmic and Physiological Optics **5**, 23–31 (1985).

[61] S. Goebels, G. Auffarth, and M. Holzer, "Lokalisation und altersabhängige verteilung von aberrationen des auges (localization and age relations of ocular aberrations)," Der Ophthalmologe **105**, 825–831 (2008).

[62] Y. Iida, K. Shimizu, M. Ito, and M. Suzuki, "Influence of age on ocular wavefront aberration changes with accommodation," Journal of refractive surgery **24**, 696–701 (2008).

[63] N. López-Gil, V. Fernández-Sánchez, R. Legras, R. Montés-Micó, F. Lara, and J. L. Nguyen-Khoa, "Accommodation-related changes in monochromatic aberrations of the human eye as a function of age," Investigative Ophthalmology & Visual Science **49**, 1736–1743 (2008).

[64] E. Berrio, J. Tabernero, and P. Artal, "Optical aberrations and alignment of the eye with age," Journal of Vision **10**, 34 (2010).

[65] F. Karimian, S. Feizi, and A. Doozande, "Higher-order aberrations in myopic eyes," Journal of Ophthalmic & Vision Research **5**, 3–9 (2010).

[66] F.-J. Zhang, Z. Zhou, F.-L. Yu, Z.-L. Lu, T. Li, and M.-M. Wang, "Comparison of age-related changes between corneal and ocular aberration in young and mid-age myopic patients," International journal of ophthalmology **4**, 286–292 (2011).

[67] A. C. Kingston and I. G. Cox, "Population spherical aberration: associations with ametropia, age, corneal curvature, and image quality," Clinical ophthalmology (Auckland, NZ) **7**, 933 (2013).

[68] T. Buehren, M. J. Collins, and L. G. Carney, "Near work induced wavefront aberrations in myopia," Vision Research **45**, 1297–1312 (2005).

[69] D. A. Atchison, K. L. Schmid, and N. Pritchard, "Neural and optical limits to visual performance in myopia," Vision Research **46**, 3707–3722 (2006).

[70] S. Marcos, E. Moreno-Barriuso, L. Llorente, R. Navarro, and S. Barbero, "Do myopic eyes suffer from large amounts of aberration?" VIII International Congress on Myopia pp. 118–121 (2000).

[71] H. Cheng, J. K. Barnett, A. S. Vilupuru, J. D. Marsack, S. Kasthurirangan, R. A. Applegate, and A. Roorda, "A population study on changes in wave aberrations with accomodation," Journal of Vision **4**, 272–280 (2004).

[72] S. Barbero, S. Marcos, and J. Merayo-Lloves, "Corneal and total optical aberrations in a unilateral aphakic patient," Journal of Cataract & Refractive Surgery **28**, 1594–1600 (2002).

[73] D. A. Atchison and W. N. Charman, "Influences of reference plane and direction of measurement on eye aberration measurement," J. Opt. Soc. Am. A **22**, 2589–2597 (2005).

[74] A. Carkeet, S.-W. Leo, B.-K. Khoo, and K.-G. A. Eong, "Modulation transfer functions in children: Pupil size dependence and meridional anisotropy," Investigative Ophthalmology & Visual Science **44**, 3248–3256 (2003).

[75] W. C. Kwan, S. P. Yip, and M. K. Yap, "Monochromatic aberrations of the human eye and myopia," Clinical and Experimental Optometry **92**, 304–312 (2009).

[76] A. A. Martinez, P. R. Sankaridurg, T. J. Naduvilath, and P. Mitchell, "Monochromatic aberrations in hyperopic and emmetropic children," Journal of Vision **9**, 23 (2009).

[77] A. Carkeet, S.-M. Saw, G. Gazzard, W. Tang, and D. T. H. Tan, "Repeatability of iolmaster biometry in children," Optometry & Vision Science **81**, 829–834 (2004).

[78] D. Thapa, A. Fleck, V. Lakshminarayanan, and W. R. Bobier, "Ocular wavefront aberration and refractive error in pre-school children," Journal of Modern Optics **58**, 1681–1689 (2011).

[79] A. Hartwig and D. A. Atchison, "Analysis of higher-order aberrations in a large clinical populationhigher-order aberrations," Investigative Ophthalmology & Visual Science **53**, 7862–7870 (2012).

[80] S. J. Hashemian, M. Soleimani, A. Foroutan, M. Joshaghani, M. J. Ghaempanah, M. E. Jafari, and M. Yaseri, "Ocular higher-order aberrations and mesopic pupil size in individuals screened for refractive surgery," International Journal of Ophthalmology **5**, 222–225 (2012).

[81] T. Li, X. Zhou, Z. Chen, X. Zhou, R. Chu, and M. R. Hoffman, "Relationship between ocular wavefront aberrations and refractive error in chinese school children," Clinical and Experimental Optometry **95**, 399–403 (2012).

[82] J. Bao, R. Le, J. Wu, Y. Shen, F. Lu, and J. C. He, "Higher-order wavefront aberrations for populations of young emmetropes and myopes," Journal of Optometry **2**, 51–58 (2009).

[83] H. Radhakrishnan, S. Pardhan, R. I. Calver, and D. J. O'Leary, "Effect of positive and negative defocus on contrast sensitivity in myopes and nonmyopes," Vision Research **44**, 1869–1878 (2004).

[84] S. Plainis and I. Pallikaris, "Ocular monochromatic aberration statistics in a large emmetropic population," Journal of Modern Optics **55**, 759–772 (2008).

[85] S. Yazar, A. W. Hewitt, H. Forward, C. M. McKnight, A. Tan, J. A. Mountain, and D. A. Mackey, "Comparison of monochromatic aberrations in young adults with different visual acuity and refractive errors," Journal of Cataract & Refractive Surgery **40**, 441–449 (2014).

[86] H. Hashemi, M. Khabazkhoob, E. Jafarzadehpur, A. Yekta, M. H. Emamian, M. Shariati, and A. Fotouhi, "Higher order aberrations in a normal adult population," Journal of Current Ophthalmology **27**, 115–124 (2015).

[87] M. S. Khan, S. Humayun, A. Fawad, M. Ishaq, S. Arzoo, and F. Mashhadi, "Comparison of higher order aberrations in patients with various refractive errors," Pakistan Journal of Medical Sciences **31**, 812–815 (2015).

[88] A. Guirao, J. Porter, D. R. Williams, and I. G. Cox, "Calculated impact of higher-order monochromatic aberrations on retinal image quality in a population of human eyes: erratum," J. Opt. Soc. Am. A **19**, 620–628 (2002).

[89] S. Ninomiya, T. Fujikado, T. Kuroda, N. Maeda, Y. Tano, T. Oshika, Y. Hirohara, and T. Mihashi, "Changes of ocular aberration with accommodation," American Journal of Ophthalmology **134**, 924–926 (2002).

[90] Y. Wang, K. Zhao, Y. Jin, Y. Niu, and T. Zuo, "Changes of higher order aberration with various pupil sizes in the myopic eye," Journal of refractive surgery **19**, S270–S274 (2003).

[91] G. van den Brink, "Measurements of the geometrical aberrations of the eye," Vision Research **2**, 233–244 (1962).

[92] M. C. Campbell, E. M. Harrison, and P. Simonet, "Psychophysical measurement of the blur on the retina due to optical aberrations of the eye," Vision Research **30**, 1587–1602 (1990).

[93] J. C. He, J. Gwiazda, F. Thorn, and R. Held, "Wave-front aberrations in the anterior corneal surface and the whole eye," Journal of the Optical Society of America A **20**, 1155–1163 (2003).

[94] J. C. He, S. Marcos, R. H. Webb, and S. A. Burns, "Measurement of the wave-front aberration of the eye by a fast psychophysical procedure," Journal of the Optical Society of America A **15**, 2449–2456 (1998).

[95] D. A. Atchison, "Recent advances in measurement of monochromatic aberrations of human eyes," Clinical and Experimental Optometry **88**, 5–27 (2005).

[96] D. A. Atchison, M. J. Collins, C. F. Wildsoet, J. Christensen, and M. D. Waterworth, "Measurement of monochromatic ocular aberrations of human eyes

as a function of accommodation by the howland aberroscope technique," Vision Research **35**, 313–323 (1995).

[97] T. Jenkins, "Aberrations of the eye and their effects on vision: 1. spherical aberration," The British journal of physiological optics **20**, 59 (1963).

[98] M. Koomen, R. Tousey, and R. Scolnik, "The spherical aberration of the eye," Journal of the Optical Society of America **39**, 370–372 (1949).

[99] A. Ivanoff, "About the spherical aberration of the eye," Journal of the Optical Society of America **46**, 901–903 (1956).

[100] H. Schober, H. Munker, and F. Zolleis, "Die aberrations des menschlichen auges und ihre messung," Optica Acta **15**, 47–57 (1968).

[101] F. Berny, "Etude de la formation des images retiniennes et determination de l'aberration de sphericite de l'oeil humain," Vision Research **9**, 977 – 990 (1969).

[102] J. He, S. Burns, and S. Marcos, "Monochromatic aberrations in the accommodated human eye," Vision Research **40**, 41–48 (2000).

[103] C. Hazel, M. Cox, and N. Strang, "Wavefront aberration and its relationship to the accommodative stimulus-response function in myopic subjects," Optometry & Vision Science **80**, 151–158 (2003).

[104] S. Panagopoulou, S. Plainsis, S. MacRae, and I. Pallikaris, "The implications of pupil size and accommodation dynamics on customized wavefront-guided refractive surgery," in "Wavefront Customized Visual Correction: The Quest for Super Vision II," , R. Krueger, R. Applegate, and S. MacRae, eds. (SLACK Incorporated, Thorofare, 2004), chap. 14, pp. 121–124.

[105] V. Katsanevaki, S. Panagopoulou, S. Plainsis, H. Ginis, and I. Pallikaris, "Accommodation dynamics and its implication on customized corrections," in "Wavefront Customized Visual Correction: The Quest for Super Vision II," , R. Krueger, R. Applegate, and S. MacRae, eds. (SLACK Incorporated, Thorofare, 2004), chap. 13, pp. 115–119.

[106] T. Kuroda, T. Fujikado, N. Maeda, T. Oshika, Y. Hirohara, and T. Mihashi, "Wavefront analysis in eyes with nuclear or cortical cataract," American Journal of Ophthalmology **134**, 1–9 (2002).

[107] T. Kuroda, T. Fujikado, S. Ninomiya, N. Maeda, Y. Hirohara, and T. Mihashi, "Effect of aging on ocular light scatter and higher order aberrations," Journal of refractive surgery **18**, S598 (2002).

[108] N. Sachdev, S. E. Ormonde, T. Sherwin, and C. N. McGhee, "Higher-order aberrations of lenticular opacities," Journal of Cataract & Refractive Surgery **30**, 1642–1648 (2004).

[109] J. Wang and T. R. Candy, "Higher order monochromatic aberrations of the human infant eye," Journal of Vision **5**, 6 (2005).

[110] M. R. Jankov, H. P. Iseli, M. Bueeler, P. Schor, T. Seiler, and M. Mrochen, "The effect of phenylephrine and cyclopentolate on objective wavefront measurements," Journal of refractive surgery **22**, 472–481 (2006).

[111] E. Nakano, H. Bains, K. Nakano, C. Nakano, W. Portellinha, M. Oliveira, and L. Alvarenga, "Wavefront analysis in asian-brazilians," Journal of Refractive Surgery **22**, S1024–S1026 (2006).

[112] R. H. Wei, L. Lim, W. K. Chan, and D. T. H. Tan, "Higher order ocular aberrations in eyes with myopia in a chinese population," Journal of refractive surgery **22**, 695–702 (2006).

[113] J. Qu, F. Lu, J. Wu, Q. Wang, C. Xu, X. Zhou, and J. C. He, "Wavefront aberration and its association with intraocular pressure and central corneal thickness in myopic eyes," Journal of Cataract & Refractive Surgery **33**, 1447–1454 (2007).

[114] M. T. Sheehan, A. V. Goncharov, V. M. O'Dwyer, V. Toal, and C. Dainty, "Population study of the variation in monochromatic aberrations of the normal human eye over the central visual field," Opt. Express **15**, 7367–7380 (2007).

[115] L. Thibos, R. A. Applegate, J. T. Schwiegerling, and R. Webb, "Standards for reporting the optical aberrations of eyes," in "Vision Science and its Applications," (Optical Society of America, 2000), p. SuC1.

[116] D. A. Atchison and E. L. Markwell, "Aberrations of emmetropic subjects at different ages," Vision Research **48**, 2224–2231 (2008).

[117] H. Saunders, "Age-dependence of human refractive errors," Ophthalmic and Physiological Optics **1**, 159–174 (1981).

[118] H. Saunders, "A longitudinal study of the age-dependence of human ocular refraction—i. age-dependent changes in the equivalent sphere," Ophthalmic and Physiological Optics **6**, 39–46 (1986).

[119] F. Slataper, "Age norms of refraction and vision," Archives of Ophthalmology **43**, 466–481 (1950).

[120] A. Cerviño, S. L. Hosking, T. Ferrer-Blasco, R. Montes-Mico, and J. M. Gonzalez-Meijome, "A pilot study on the differences in wavefront aberrations between two ethnic groups of young generally myopic subjects," Ophthalmic and Physiological Optics **28**, 532–537 (2008).

[121] L. Wang, R. M. Santaella, M. Booth, and D. D. Koch, "Higher-order aberrations from the internal optics of the eye," Journal of Cataract & Refractive Surgery **31**, 1512–1519 (2005).

[122] W. N. Charman, "The Charles F. Prentice award lecture 2005: Optics of the human eye: Progress and problems," Optometry & Vision Science **83**, 335–345 (2006).

[123] B. Winn, D. Whitaker, D. Elliott, and N. Phillips, "Factors affecting light-adapted pupil size in normal human subjects," Investigative Ophthalmology & Visual Science **35**, 1132–1137 (1994).

[124] G. Prakash, N. Sharma, V. Choudhary, and J. S. Titiyal, "Higher-order aberrations in young refractive surgery candidates in india: Establishment of normal values and comparison with white and chinese asian populations," Journal of Cataract & Refractive Surgery **34**, 1306–1311 (2008).

[125] J. B. Won, S. W. Kim, E. K. Kim, B. J. Ha, and T.-i. Kim, "Comparison of internal and total optical aberrations for 2 aberrometers: itrace and opd scan," Korean Journal of Ophthalmology : KJO **22**, 210–213 (2008).

[126] K. L. Lim and H. B. Fam, "Ethnic differences in higher-order aberrations: Spherical aberration in the south east asian chinese eye," Journal of Cataract & Refractive Surgery **35**, 2144–2148 (2009).

[127] L. Lundström, J. Gustafsson, and P. Unsbo, "Population distribution of wavefront aberrations in the peripheral human eye," J. Opt. Soc. Am. A **26**, 2192–2198 (2009).

[128] D. P. Piñero, P. J. Sánchez-Pérez, and J. L. Alió, "Repeatability of measurements obtained with a ray tracing aberrometer," Optometry & Vision Science **88**, 1099–1105 (2011).

[129] R. Fan, T. He, Y. Qiu, Y.-L. Di, S.-y. Xu, and Y.-y. Li, "Comparison of wavefront aberrations under cycloplegic, scotopic and photopic conditions using wavescan," Arquivos Brasileiros de Oftalmologia **75**, 116–121 (2012).

[130] S. J. Hashemian, M. Soleimani, A. Foroutan, M. Joshaghani, M. J. Ghaempanah, M. E. Jafari, and H. Nikoueinejad, "The relationship between ocular higher-order aberrations and mesopic pupil size with age and gender in iranian myopic candidates," Iranian Journal of Ophthalmology **24**, 38–44 (2012).

[131] E. Tepichín-Rodríguez, A. S. Cruz Felix, E. López-Olazagasti, and S. Balderas-Mata, "Emmetropic eyes: objective performance and clinical reference," Proc. SPIE **8785**, 8785G5–8785G5–7 (2013).

[132] A. Dias-Santos, R. Rosa, J. Ferreira, J. P. Cunha, C. Brito, A. Paixão, and A. Toscano, "Higher order aberrations in amblyopic children and their role in refractory amblyopia," Revista Brasileira de Oftalmologia **73**, 358–362 (2014).

[133] T. Hiraoka, K. Miyata, Y. Nakamura, M. Ogata, F. Okamoto, and T. Oshika, "Influence of cycloplegia with topical cyclopentolate on higher-order aberrations in myopic children," Eye **28**, 581–586 (2014).

[134] A. Carkeet, S. Velaedan, Y. K. Tan, D. Y. J. Lee, and D. T. H. Tan, "Higher order ocular aberrations after cycloplegic and non-cycloplegic pupil dilation," Journal of refractive surgery **19**, 316–322 (2003).

[135] G. Prakash, D. Srivastava, S. Choudhuri, and R. Bacero, "Comparison of ocular monochromatic higher-order aberrations in normal refractive surgery candidates of arab and south asian origin," Middle East Afr J Ophthalmol **23**, 115–121 (2016).

[136] M. Born and E. Wolf, *Principles of Optics* (Cambridge University Press, 1999), 7th ed.

[137] D. Hilbert, *David Hilbert's Lectures on the foundations of Mathematics and Physics, 1891–1933* (Springer-Verlag, 2004).

[138] R. Courant and F. John, *Introduction to Calculus and Analysis II/2* (Springer-Verlag, 1989).

[139] R. Courant and D. Hilbert, *Methods of Mathematical Physics, Vol. 1* (Interscience Publishers, Inc., 1953).

[140] A. Sharma, D. V. Kumar, and A. K. Ghatak, "Tracing rays through graded-index media: a new method," Appl. Opt. **21**, 984–987 (1982).

[141] N. Jacobson, *Basic Algebra* (Dover, 2009), 2nd ed.

[142] R. W. D. Nickalls, "Viète, descartes and the cubic equation," Mathematical Gazette **90**, 203–208 (2006).

[143] C. J. Sheil, M. Bahrami, and A. V. Goncharov, "An analytical method for predicting the geometrical and optical properties of the human lens under accommodation," Biomed. Opt. Express **5**, 1649–1663 (2014).

[144] A. Sharma and A. K. Ghatak, "Ray tracing in gradient-index lenses: computation of ray–surface intersection," Appl. Opt. **25**, 3409–3412 (1986).

[145] J. Fine, "Interpolants for Runge-Kutta-Nyström methods," Computing **39**, 27–42 (1987).

[146] H. von Helmholtz, *Handbuch der Physiologischen Optik* (Leopold Voss, 1867).

[147] Y. Shao, A. Tao, H. Jiang, M. Shen, J. Zhong, F. Lu, and J. Wang, "Simultaneous real-time imaging of the ocular anterior segment including the ciliary muscle during accommodation," Biomedical Optics Express **4**, 466–480 (2013).

[148] K. Richdale, L. T. Sinnott, M. A. Bullimore, P. A. Wassenaar, P. Schmalbrock, C.-Y. Kao, S. Patz, D. O. Mutti, A. Glasser, and K. Zadnik, "Quantification of age-related and per diopter accommodative changes of the lens and ciliary muscle in the emmetropic human eye," Investigative Ophthalmology & Visual Science **54**, 1095–1105 (2013).

[149] A. de Castro, S. Ortiz, E. Gambra, D. Siedlecki, and S. Marcos, "Three-dimensional reconstruction of the crystalline lens gradient index distribution from OCT imaging," Optics Express **18**, 21905–21917 (2010).

[150] A. de Castro, J. Birkenfeld, B. Maceo, F. Manns, E. Arrieta, J.-M. Parel, and S. Marcos, "Influence of shape and gradient refractive index in the accommodative changes of spherical aberration in nonhuman primate crystalline lenses," Investigative Ophthalmology & Visual Science **54**, 6197–6207 (2013).

[151] A. Gullstrand, *Appendix IV of Treatise on Physiological Optics*, vol. 1 (Dover Phoenix Editions, 2005).

[152] Y. Le Grand and S. G. El Hage, *Physiological Optics* (Springer-Verlag, 1980).

[153] J. W. Blaker, "Toward an adaptive model of the human eye," Journal of the Optical Society of America **70**, 220–223 (1980).

[154] R. Navarro, J. Santamaría, and J. Bescós, "Accommodation-dependent model of the human eye with aspherics," Journal of the Optical Society of America A **2**, 1273–1280 (1985).

[155] G. Smith, P. Bedggood, R. Ashman, M. Daaboul, and A. Metha, "Exploring ocular aberrations with a schematic human eye model," Optometry & Vision Science **85**, 330–340 (2008).

[156] H.-L. Liou and N. A. Brennan, "Anatomically accurate, finite model eye for optical modeling," Journal of the Optical Society of America A **14**, 1684–1695 (1997).

[157] A. V. Goncharov and C. Dainty, "Wide-field schematic eye models with gradient-index lens," Journal of the Optical Society of America A **24**, 2157–2174 (2007).

[158] R. Navarro, F. Palos, and L. González, "Adaptive model of the gradient index of the human lens. i. formulation and model of aging ex vivo lenses," Journal of the Optical Society of America A **24**, 2175–2185 (2007).

[159] G. Smith, "The optical properties of the crystalline lens and their significance." Clinical & Experimental Optometry **86**, 3–18 (2003).

[160] C. Jones, D. Atchison, R. Meder, and J. Pope, "Refractive index distribution and optical properties of the isolated human lens measured using magnetic resonance imaging (MRI)," Vision Research **45**, 2352–2366 (2005).

[161] E. A. Hermans, P. J. W. Pouwels, M. Dubbelman, J. P. A. Kuijer, R. G. L. van der Heijde, and R. M. Heethaar, "Constant volume of the human lens and decrease in surface area of the capsular bag during accommodation: An MRI and scheimpflug study," Investigative Ophthalmology & Visual Science **50**, 281–289 (2009).

[162] C. E. Jones, D. A. Atchison, and J. M. Pope, "Changes in lens dimensions and refractive index with age and accommodation," Optometry & Vision Science **84**, 990–995 (2007).

[163] R. Gerometta, A. C. Zamudio, D. P. Escobar, and O. A. Candia, "Volume change of the ocular lens during accommodation," American Journal of Physiology - Cell Physiology **293**, C797–C804 (2007).

[164] S. A. Strenk, L. M. Strenk, J. L. Semmlow, and J. K. DeMarco, "Magnetic resonance imaging study of the effects of age and accommodation on the human lens cross-sectional area," Investigative Ophthalmology & Visual Science **45**, 539–545 (2004).

[165] S. J. Judge and H. J. Burd, "The MRI data of strenk et al. do not suggest lens compression in the unaccommodated state (e-letter)," Investigative Ophthalmology & Visual Science **45**, 539 (2004).

[166] R. A. Schachar, "The change in intralenticular pressure during human accommodation (e-letter)," Investigative Ophthalmology & Visual Science **45**, 539 (2004).

[167] M. Dubbelman, G. V. der Heijde, and H. Weeber, "Change in shape of the aging human crystalline lens with accommodation," Vision Research **45**, 117–132 (2005).

[168] S. Ortiz, P. Pérez-Merino, E. Gambra, A. de Castro, and S. Marcos, "In vivo human crystalline lens topography," Biomedical Optics Express **3**, 2471–2488 (2012).

[169] R. Navarro, F. Palos, and L. M. González, "Adaptive model of the gradient index of the human lens. ii. optics of the accommodating aging lens," Journal of the Optical Society of America A **24**, 2911–2920 (2007).

[170] C. E. Campbell, "Nested shell optical model of the lens of the human eye," Journal of the Optical Society of America A **27**, 2432–2441 (2010).

[171] E. Lanchares, R. Navarro, and B. Calvo, "Hyperelastic modelling of the crystalline lens: Accommodation and presbyopia," Journal of Optometry **5**, 110–120 (2012).

[172] M. J. Howcroft and J. A. Parker, "Aspheric curvatures for the human lens," Vision Research **17**, 1217–1213 (1977).

[173] D. Borja, D. Siedlecki, A. de Castro, S. Uhlhorn, S. Ortiz, E. Arrieta, J.-M. Parel, S. Marcos, and F. Manns, "Distortions of the posterior surface in optical coherence tomography images of the isolated crystalline lens: effect of the lens index gradient," Biomedical Optics Express **1**, 1331–1340 (2010).

[174] F. Manns, V. Fernandez, S. Zipper, S. Sandadi, M. Hamaoui, A. Ho, and J.-M. Parel, "Radius of curvature and asphericity of the anterior and posterior surface of human cadaver crystalline lenses," Experimental Eye Research **78**, 39–51 (2004).

[175] E. Hermans, M. Dubbelman, G. van der Heijde, and R. Heethaar, "Estimating the external force acting on the human eye lens during accommodation by finite element modelling," Vision Research **46**, 3642–3650 (2006).

[176] R. Urs, F. Manns, A. Ho, D. Borja, A. Amelinckx, J. Smith, R. Jain, R. Augusteyn, and J.-M. Parel, "Shape of the isolated ex-vivo human crystalline lens," Vision Research **49**, 74–83 (2009).

[177] J. F. Koretz, S. A. Strenk, L. M. Strenk, and J. L. Semmlow, "Scheimpflug and high-resolution magnetic resonance imaging of the anterior segment: a comparative study," Journal of the Optical Society of America A **21**, 346–354 (2004).

[178] R. Urs, A. Ho, F. Manns, and J.-M. Parel, "Age-dependent fourier model of the shape of the isolated ex vivo human crystalline lens," Vision Research **50**, 1041–1047 (2010).

[179] A. Ivanoff, "On the influence of accommodation on spherical aberration in the human eye, an attempt to interpret night myopia," Journal of the Optical Society of America **37**, 730–731 (1947).

[180] S. Plainis, H. S. Ginis, and A. Pallikaris, "The effect of ocular aberrations on steady-state errors of accommodative response," Journal of Vision **5**, 466–477 (2005).

[181] Y. Wang, Z.-Q. Wang, H.-Q. Guo, Y. Wang, and T. Zuo, "Wavefront aberrations in the accommodated human eye based on individual eye model," Optik - International Journal for Light and Electron Optics **118**, 271–277 (2007).

[182] E. Gambra, L. Sawides, C. Dorronsoro, and S. Marcos, "Accommodative lag and fluctuations when optical aberrations are manipulated," Journal of Vision **9**, 1–15 (2009).

[183] Y.-J. Li, J. A. Choi, H. Kim, S.-Y. Yu, and C.-K. Joo, "Changes in ocular wavefront aberrations and retinal image quality with objective accommodation," Journal of Cataract & Refractive Surgery **37**, 835–841 (2011).

[184] T. Young, "On the mechanism of the eye," Philosophical Transactions of the Royal Society of London **91**, 23–88 (1801).

[185] S. Kasthurirangan, E. L. Markwell, D. A. Atchison, and J. M. Pope, "In vivo study of changes in refractive index distribution in the human crystalline lens with age and accommodation," Investigative Ophthalmology & Visual Science **49**, 2531–2540 (2008).

[186] G. Smith, D. A. Atchison, D. R. Iskander, C. E. Jones, and J. M. Pope, "Mathematical models for describing the shape of the in vitro unstretched human crystalline lens," Vision Research **49**, 2442–2452 (2009).

[187] H. T. Kasprzak, "New approximation for the whole profile of the human crystalline lens," Ophthalmic & Physiological Optics **20**, 31–43 (2000).

[188] S. Giovanzana, R. A. Schachar, S. Talu, R. D. Kirby, E. Yan, and B. K. Pierscionek, "Evaluation of equations for describing the human crystalline lens," Journal of Modern Optics **60**, 406–413 (2013).

[189] S. G. El Hage and F. Berny, "Contribution of the crystalline lens to the spherical aberration of the eye," Journal of the Optical Society of America **63**, 205–211 (1973).

[190] J. Sivak and R. Kreuzer, "Spherical aberration of the crystalline lens," Vision Research **23**, 59–70 (1983).

[191] T. Salmon and L. Thibos, "Relative contribution of the cornea and internal optics to the aberrations of the eye," Optometry & Vision Science **75**, 235 (1998).

[192] P. Artal, A. Guirao, E. Berrio, and D. R. Williams, "Compensation of corneal aberrations by the internal optics in the human eye," Journal of Vision **1**, 1–8 (2001).

[193] J. E. Kelly, T. Mihashi, and H. C. Howland, "Compensation of corneal horizontal/vertical astigmatism, lateral coma, and spherical aberration by internal optics of the eye," Journal of Vision **4**, 262–271 (2004).

[194] M. Millodot and J. Sivak, "Contribution of the cornea and lens to the spherical aberration of the eye," Vision Research **19**, 685–687 (1979).

[195] T. O. Salmon and L. N. Thibos, "Videokeratoscope-line-of-sight misalignment and its effect on measurements of corneal and internal ocular aberrations," Journal of the Optical Society of America A **19**, 657–669 (2002).

[196] J. He, E. Ong, J. Gwiazda, R. Held, and F. Thorn, "Wave-front aberrations in the cornea and the whole eye," Investigative Ophthalmology & Visual Science **41**, S105 (2000).

[197] H. Burd, S. Judge, and J. Cross, "Numerical modelling of the accommodating lens," Vision Research **42**, 2235–2251 (2002).

[198] B. K. Pierscionek, "Refractive index contours in the human lens," Exp. Eye Res. **64**, 887–893 (1997).

[199] W. N. Charman and D. A. Atchison, "Age-dependence of the average and equivalent refractive indices of the crystalline lens," Biomedical Optics Express **5**, 31–39 (2014).

[200] B. Pierscionek, M. Bahrami, M. Hoshino, K. Uesugi, J. Regini, and N. Yagi, "The eye lens: age-related trends and individual variations in refractive index and shape parameters," Oncotarget **6**, 1–13 (2015).

[201] M. Bahrami, A. V. Goncharov, and B. K. Pierscionek, "Adjustable internal structure for reconstructing gradient index profile of crystalline lens," Opt. Lett. **39**, 1310–1313 (2014).

[202] F. Manns, A. Ho, D. Borja, and J.-M. Parel, "Comparison of uniform and gradient paraxial models of the crystalline lens," Invest. Ophthalmol. Vis. Sci. **51 (E-Abstract)**, 789–789 (2010).

[203] G. Smith, B. K. Pierscionek, and D. A. Atchison, "The optical modelling of the human lens," Ophthalmic and Physiological Optics **11**, 359–369 (1991).

[204] J. A. Díaz, C. Pizarro, and J. Arasa, "Single dispersive gradient-index profile for the aging human lens," J. Opt. Soc. Am. A **25**, 250–261 (2008).

[205] R. Navarro, "Adaptive model of the aging emmetropic eye and its changes with accommodation," Journal of Vision **14**, 21 (2014).

[206] M. Dubbelman, G. van der Heijde, and H. Weeber, "The thickness of the aging human lens obtained from corrected scheimpflug images." Optom. Vis. Sci. **78**, 411–416 (2001).

[207] Alexander V. Goncharov and Conor J. Sheil, Applied Optics Group, National University of Ireland, Galway, are preparing a manuscript on raytracing through GRIN media defined as an infinite number of thin shells with a known shape.

[208] B. D. Stone and G. W. Forbes, "Optimal interpolants for runge–kutta ray tracing in inhomogeneous media," J. Opt. Soc. Am. A **7**, 248–254 (1990).

[209] J. C. Wyant and K. Creath, "Basic wavefront aberration theory for optical metrology," in "Applied Optics and Optical Engineering," , vol. 11, R. R. Shannon and J. C. Wyant, eds. (1992), vol. 11, p. 2.

[210] T. Grosvenor, "Changes in spherical refraction during the adult years," in "Refractive anomalies. Research and clinical applications," , T. Grosvenor and M. Flom, eds. (Butterworth-Heinemann, Boston, 1991), pp. 131–145.

[211] D. A. Atchison, E. L. Markwell, S. Kasthurirangan, J. M. Pope, G. Smith, and P. G. Swann, "Age-related changes in optical and biometric characteristics of emmetropic eyes," Journal of Vision **8**, 1–20 (2008).

[212] K. Attebo, R. Q. Ivers, and P. Mitchell, "Refractive errors in an older population: The blue mountains eye study," Ophthalmology **106**, 1066–1072 (1999).

[213] J. Katz, K. West, S. K. Khatry, S. C. LeClerq, E. K. Pradhan, M. Thapa, S. R. Shrestha, and H. R. Taylor, "Prevalence and risk factors for trachoma in Sarlahi district, Nepal." British Journal of Ophthalmology **80**, 1037–1041 (1996).

[214] C. Shufelt, S. Fraser-Bell, M. Ying-Lai, M. Torres, R. Varma, and the Los Angeles Latino Eye Study Group, "Refractive error, ocular biometry, and lens opalescence in an adult population: The Los Angeles latino eye study," Investigative Ophthalmology & Visual Science **46**, 4450–4460 (2005).

[215] Q. Wang, B. E. Klein, R. Klein, and S. E. Moss, "Refractive status in the beaver dam eye study." Investigative Ophthalmology & Visual Science **35**, 4344–7 (1994).

[216] M. Wensor, C. McCarty, and H. Taylor, "Pevalence and risk factors of myopia in Victoria, Australia," Archives of Ophthalmology **117**, 658–663 (1999).

[217] S. Wickremasinghe, P. J. Foster, D. Uranchimeg, P. S. Lee, J. G. Devereux, P. H. Alsbirk, D. Machin, G. J. Johnson, and J. Baasanhu, "Ocular biometry and refraction in Mongolian adults," Investigative Ophthalmology & Visual Science **45**, 776–783 (2004).

[218] T. Y. Wong, P. J. Foster, T. P. Ng, J. M. Tielsch, G. J. Johnson, and S. K. L. Seah, "Variations in ocular biometry in an adult Chinese population in Singapore: The tanjong pagar survey," Investigative Ophthalmology & Visual Science **42**, 73–80 (2001).

[219] S.-Y. Wu, B. Nemesure, M. C. Leske, and for the Barbados Eye Study Group, "Refractive errors in a black adult population: The Barbados eye study," Investigative Ophthalmology & Visual Science **40**, 2179–2184 (1999).

[220] N. A. Brown and A. R. Hill, "Cataract: the relation between myopia and cataract morphology." British Journal of Ophthalmology **71**, 405–414 (1987).

[221] R. Lim, P. Mitchell, and R. G. Cumming, "Refractive associations with cataract: the blue mountains eye study," Investigative Ophthalmology & Visual Science **40**, 3021 (1999).

[222] C. Younan, P. Mitchell, R. G. Cumming, E. Rochtchina, and J. J. Wang, "Myopia and incident cataract and cataract surgery: The blue mountains eye study," Investigative Ophthalmology & Visual Science **43**, 3625 (2002).

[223] J. Tabernero, E. Berrio, and P. Artal, "Modeling the mechanism of compensation of aberrations in the human eye for accommodation and aging," J. Opt. Soc. Am. A **28**, 1889–1895 (2011).

[224] I. Escudero-Sanz and R. Navarro, "Off-axis aberrations of a wide-angle schematic eye model," Journal of the Optical Society of America A **16**, 1881–1891 (1999).

[225] C. J. Sheil and A. V. Goncharov, "Accommodating volume-constant age-dependent optical (AVOCADO) model of the crystalline GRIN lens," Biomed. Opt. Express **7**, 1985–1999 (2016).

[226] A. Spierer and B. Shalev, "Presbyopia among normal individuals," Graefe's Archive for Clinical and Experimental Ophthalmology **241**, 101–105 (2003).

[227] R. Navarro, "The optical design of the human eye: a critical review," Journal of Optometry **2**, 3–18 (2009).

[228] R. Navarro, L. González, and J. L. Hernández-Matamoros, "On the prediction of optical aberrations by personalized eye models," Optometry & Vision Science **83**, – (2006).

[229] J. Polans, B. Jaeken, R. P. McNabb, P. Artal, and J. A. Izatt, "Wide-field optical model of the human eye with asymmetrically tilted and decentered lens that reproduces measured ocular aberrations," Optica **2**, 124–134 (2015).

[230] J. Tabernero, A. Benito, E. Alcón, and P. Artal, "Mechanism of compensation of aberrations in the human eye," J. Opt. Soc. Am. A **24**, 3274–3283 (2007).

COLOPHON

This document was typeset using the typographical look-and-feel `classicthesis` developed by André Miede. The style was inspired by Robert Bringhurst's seminal book on typography "*The Elements of Typographic Style*". `classicthesis` is available for both LaTeX and LyX:

http://code.google.com/p/classicthesis/

Happy users of `classicthesis` usually send a real postcard to the author, a collection of postcards received so far is featured here:

http://postcards.miede.de/

DECLARATION

I hereby declare that this thesis has not been submitted in whole or in part to any other university as an exercise for a degree. In addition, I declare that, except where reference is made in the text, this thesis is entirely my own work.

Galway, June 2016

Conor J. Sheil